



Université
de Toulouse

THÈSE

En vue de l'obtention du

DOCTORAT DE L'UNIVERSITÉ DE TOULOUSE

Délivré par l'Université Toulouse III Paul Sabatier (UT3 Paul Sabatier)

Discipline ou spécialité : Chimie moléculaire – CO 046

Présentée et soutenue le 9 juillet 2014 par

Cristina MATTIOLI

Design, synthesis and study of molecules for graphene functionalization.

JURY

André-Jean Attias	<i>Professeur, Université Pierre et Marie Curie (Paris)</i>	<i>Rapporteur</i>
Marc Sallé	<i>Professeur, Université d'Angers</i>	<i>Rapporteur</i>
Rémi Chauvin	<i>Professeur, Université Paul Sabatier (Toulouse)</i>	<i>Examineur</i>
Stéphane Campidelli	<i>Chercheur, CEA-Saclay</i>	<i>Examineur</i>
Alain Pénicaud	<i>Directeur de Recherche, CRPP (Bordeaux)</i>	<i>Examineur</i>
Andrea Secchi	<i>Professeur, Università degli Studi di Parma (Italie)</i>	<i>Examineur</i>
André Gourdon	<i>Directeur de Recherche, CEMES-CNRS</i>	<i>Directeur de thèse</i>

Ecole doctorale : *Sciences de la matière*

Unité de recherche : *CEMES-CNRS (UPR 8011)*

Directeur de Thèse : *Dr André Gourdon*

Rapporteurs : *Prof. André-Jean Attias et Prof. Marc Sallé*

Acknowledgments

After more than three years spent at the laboratory CEMES, I would like to thank all the people that contributed directly or indirectly to the work described in this manuscript.

In a first place, I would like to thank my thesis supervisor, Dr. André Gourdon, who allowed me to work in his research group on a cutting edge and stimulating project. He has my gratitude for giving me the freedom to work on my own ideas, being at the same time ready to guide and provide precious advices. I would like to thank also the director of the laboratory, Dr. Alain Claverie, for giving me the possibility to work in a pleasant environment.

The next thanks goes to the commission for accepting to evaluate my work: the two “rapporteurs” Prof. Marc Sallé and Prof. André-Jean Attias, and the other “commissaires”: Prof. Rémi Chauvin, who agreed to be the president, Dr. Alain Pénicaud, Dr. Stéphane Campidelli and Prof. Andrea Secchi. I would like to express a sincere gratitude for the observations made during the thesis discussion.

During the course of my thesis, I had the occasion to work and discuss with many experts of different disciplines. Firstly, I would like to thank Dr. Laurent Simon and his entire group at the Institut de Science des Matériaux de Mulhouse (in particular Dr. Marion Cranney and Maya Nair) for studying by STM some of the synthesized molecules. I am grateful to them for always taking the time to answer my numerous questions. I thank as well Prof. M. Yu (Harbin Institut of Technology, China) for starting the studies in UHV of some other derivatives. I would like to thank Dr. Fabrice Charra at the IRAMIS-CEA in Saclay for introducing me the technique of STM at the solid/liquid interface.

I would like to thank Dr. Erik Dujardin in the Nanosciences Group at CEMES, and in particular Dr. Miguel Rubio-Roy and Dr. Olivier Couturaud for preparing and studying by Raman and transport measurements graphene samples functionalized by some of my molecules. I thank them also for the discussions that allowed me to understand different aspects of this complex subject. In this context, I would like to thank Dr. Pascal Puech, who kindly helped me to understand further some aspects of the Raman characterizations.

My next thanks goes to the chemists of GNS. In particular, Christine Viala has all my gratitude for transmitting me her knowledge about the vacuum-techniques and for the everyday help that she has always provided. I would also like to thank her for the nice jams and for her support, especially during the last phase of the thesis.

I thank Prof. Jean-Pierre Launay, for helping me to get a better insight into my subject, through the discussions about molecular orbitals. I would like to thank as well Dr. Jaques Bonvoisin, Dr. Claire Kammerer and Prof. Gwenael Rapenne, for their kindness and help in many occasions.

My gratitude goes also to the different past and present non-permanent students: starting from those that received and helped me to start my work (and life) in this new town: Adeline Pujol, Dr. Gregory Franc and Gurunath Kargal. The former students: Roman Stefak and Romain Garbage. The present students: the “new Italian” Chiara Venturini and Agnes Sirven, to whom I wish all my wishes for their last year. Finally the present and past post-docs: Dr. Tung Than Dang, Dr. Marios Markoulides and Dr. Hung Nguyen Than. My gratitude goes also to Hiromi Nagashima, the internship student from NAIST (Nara, Japan) with whom I had the occasion to work with. I thank her for the nice moments we shared in the lab., as well as for teaching me how to roll Sushi and other Japanese dishes.

I would like to thank all Group Nanosciences. In particular, I am grateful to Dr. Veronique Langlais and Dr. Olivier Guillermet, who replied many questions about STM, as well to Gregory Seine who assisted me during the tries at the liquid STM at the CEMES.

I would like to thank all the PhD students and post-docs of the CEMES I could meet during these years for the joyful environment. In particular, Alessandro, Audrey, Julien, Lorraine, Marc, Marie, Maxime...

I would like to thank all the common services at CEMES (administration, informatics, safety and infrastructures) for rendering possible the working of the lab., as well as the common services at University Paul Sabatier (NMR, Mass, IR-Raman, HPLC and Electrochemistry) for providing the analysis of the chemical compounds.

The financial support of ANR Blanc program, ANR-2010-BLAN-1017-ChimiGraphN is gratefully acknowledged.

I would like to thank all the new friends I met in Toulouse: Adeline, Angela, Antoine, Florence, Jonathan, Laure, Mathieu, Nicolas, Rémi as well as Dan, Sebastian and the little Jeanne, for all the support and the fun moments that we could share in Toulouse during these years.

I would also like to thank all my friends in Italy who came and see me here and who I know I can always count on: Cinzia, Daniela, Isabella, Miriam, Monica, Sara, Valentina B. and Valentina C., as well as my friends Camilla, Elisa and Merina. I express my gratitude also to the University of Parma and my entire former group, who gave me a formation in Chemistry, allowing to face this experience.

I would like to thank all my family for always supporting me, even if I was far, and for coming to visit me in many occasions. I would also like to thank the family of Renaud for welcoming me and for their support. My final big “thank you” goes to Renaud who is at my side every day.

List of abbreviations

Ac ₂ O	Acetic Anhydride
AFM	Atomic Force Microscopy
DCI	Direct Chemical Ionization
DDQ	2,3-dichloro-5,6-dicyano-1,4-benzoquinone
DCTB	Trans-2-[3-(4-tert-Butylphenyl)-2-methyl-2-propenylidene]malononitrile
Et ₃ N	Triethylamine
Et ₂ NH	Diethylamine
Et ₂ O	Diethylether
EtOAc	Ethyl Acetate
ESI	Electrospray Ionization
G/SiC	Epitaxial Graphene on Silicon Carbide
G/SiO ₂	Mechanically Exfoliated Graphene on Oxidized Silicon
HBC	Hexabenzocoronene
HBB	Hexabiphenylbenzene
HPLC	High Pressure Liquid Chromatography
HOPG	Highly Oriented Pyrolytic Graphite
HR-MS	High Resolution Mass Spectrometry
(iPr) ₂ NH	Di-isopropylamine
MALDI	Matrix Assisted Laser Desorption Ionization
MeOH	Methanol
MS	Mass Spectrometry
PAH	Polycyclic Aromatic Hydrocarbons
RT	Room Temperature
STM	Scanning Tunneling Microscopy
SFC	Supercritical Fluid Chromatography
THF	Tetrahydrofuran
TLC	Thin Layer Chromatography
TMS	Trimethylsilyl
TMSA	Trimethylsilyl Acetylene
TOF	Time of Flight
UHV	Ultra High Vacuum
wt/wt	In weight

Table of contents

General introduction	1
References	3
Chapter 1	
State of the art and general objectives	5
1.1 Control in 2D of graphene functionalization	5
1.1.1 Motivation	5
1.1.2 State of the art.....	5
1.2 Objective of the project.....	8
1.3 Functionalization of epitaxial graphene/SiC (0001).....	10
1.3.1 Non-covalent functionalization	10
1.3.2 Covalent functionalization.....	15
1.4 Presentation of the proposed strategies	20
1.5 References.....	21
PART I	
Synthesis of molecules for non-covalent functionalization of graphene	23
References	25
Chapter 2	
Synthesis and studies of the self-assembling behaviour of a tetrathiafulvalene derivative	27
2.1 Introduction	27
2.2 Objective	28
2.3 Different contributions to the work.....	28
2.4 Molecular design	29
2.5 Results and discussion.....	29
2.5.1 Synthesis	29
2.5.2 STM Studies	31
2.6 Conclusions.....	35
2.7 References.....	36
Chapter 3	
Synthesis of a hexaphenanthrocoronene derivative	37
3.1 Introduction	37
3.1.1 Polycyclic Aromatic Hydrocarbons (PAHs).....	37
3.2 Objective	41
3.3 Molecular design	42
3.4 Results and discussion.....	43

3.4.1	Retrosynthetic analysis.....	43
3.4.2	Synthesis	43
3.5	Conclusions.....	58
3.6	References.....	60

Part II

Synthesis of molecules for covalent functionalization of graphene.....	63
References	64

Chapter 4

Synthesis of molecules for covalent functionalization of graphene by radicalar addition	65	
4.1	Introduction	65
4.2	Objective	65
4.3	Molecular design	66
4.3.1	Choice of the reactive group	66
4.3.2	Self-assembling strategies	67
4.3.3	Design.....	67
4.4	Molecules with linear geometry	69
4.4.1	Retrosynthetic analysis of the linear derivative Br1 (4.1).....	69
4.4.2	Synthesis of the linear derivative Br1.....	70
4.4.3	Characterization of the linear derivative Br1.....	72
4.4.4	Retrosynthetic analysis for the linear derivative Br2 (4.2).....	73
4.4.5	Synthesis of the linear derivative Br2.....	74
4.4.6	Characterization of the linear derivative Br2.....	75
4.5	Molecule with C3 symmetry	76
4.5.1	Retrosynthetic analysis of the derivative TBr (4.3).....	76
4.5.2	Synthesis of the derivative TBr	76
4.5.3	Characterization of the derivative TBr.....	77
4.6	Conclusions.....	78
4.7	References.....	79

Chapter 5

Synthesis of anthracene derivatives for covalent functionalization of graphene byDiels-Alder reaction	81	
5.1	Reactivity of carbon nanomaterials as dienophiles.....	81
5.2	Objective	82
5.3	Molecular design	83
5.4	Anthracene derivative A1 (5.1).....	84
5.4.1	Rethrosynthetic analysis for A1	84
5.4.2	Synthesis of A1	84

5.4.3	Characterization of A1.....	87
5.5	Anthracene derivative A2 (5.2).....	88
5.5.1	Retrosynthetic analysis or A2	88
5.6	Synthesis of A2 (5.2).....	89
5.6.1	Synthesis of the self-assembling groups 5.10, 5.11 and 5.13.....	89
5.6.2	Coupling of the self-assembling groups to the anthracene core.....	93
5.6.3	Deprotection of the methyl-esters	95
5.7	Characterization of A2	96
5.8	Conclusions.....	97
5.9	References.....	98

Chapter 6

Synthesis and study of maleimide derivatives for covalent functionalization of graphene by Diels-Alder reaction..... 101

6.1	Reactivity of carbon nanomaterials as dienes	101
6.2	Objective	101
6.3	Molecular design	102
6.4	Alkyl-chains functionalized maleimide derivative M1(6.1).....	103
6.4.1	Retrosynthetic analysis for M1.....	103
6.4.2	Synthesis of M1	104
6.4.3	Characterization of M1.....	107
6.5	C3-symmetry maleimide derivative M2(6.2).....	109
6.5.1	Retrosynthetic analysis for M2.....	109
6.5.2	Synthesis of M2	110
6.5.3	Characterization of M2.....	115
6.6	Isophthalic-acid N-functionalized maleimide derivative M3(6.3).....	116
6.6.1	Synthesis of M3	116
6.7	Conclusions.....	116
6.8	Tests of reactivity at the solid/liquid interface	117
6.8.1	Objective	117
6.8.2	Different contributions to the work	117
6.8.3	Molecular design.....	118
6.8.4	Synthesis of MF(6.15).....	118
6.8.5	Characterization of MF.....	120
6.8.6	Experimental procedure for graphene functionalization.....	120
6.8.7	Characterization techniques	121
6.8.8	Results and discussion	124
6.8.9	Conclusions	133
6.9	References.....	135

General conclusions.....	137
Experimental procedures	
Generalities	143
Chemicals	143
Analytical tools and devices	143
Chapter 2: TTC ₁₂ -TTF (2.1).....	145
Chapter 3: Hexaphenanthrocoronene (3.1)	146
Chapter 4: Radicalar precursors	150
Precursor Br1 (4.1):.....	150
Precursor Br2 (4.2):.....	151
Precursor TBr (4.3):	152
Chapter 5: Anthracene derivatives	153
Anthracene A1(5.1):	153
Anthracene A2 (5.1):	153
Chapter 6: Maleimide derivatives.....	161
Maleimide M1 (6.1):	161
Maleimide M2 (6.2):	163
Maleimide M3 (6.3):	167
Maleimide MF (6.15):.....	167
Appendice A1	
Scanning Tunnelling Microscopy	169
Appendice A2	
The surfaces.....	173
Appendice A3	
Résumé.....	179

General introduction

Graphene is a two-dimensional carbon allotrope in which the atoms are hybridized sp^2 and arranged in a honeycomb lattice. Experimental studies of its properties have become possible only very recently¹, upon the first establishment of an easy isolation procedure for graphene from graphite by mechanical exfoliation by a scotch tape techniqueⁱ.

The name “graphene” includes a variety of materials characterized by subtle differences in the chemical and physical properties, depending on the different procedures employed for the production², i.e. epitaxial growth, chemical vapour deposition, mechanical exfoliation in solution, reduction of graphite oxide... However, all the “graphenes” are characterized by unique properties such as enhanced electrical conductivity, optical transparency, mechanical strength and thermal conductivity. Because of these unique properties, applications spanning over many fields, ranging from protective coatings to sensors or even flexible and transparent electronics, are envisioned. Such a potential explains the recent interest devoted to the material in both fundamental and applied researches, which results from a synergy between public and private organizations^{2,3}.

In order to employ graphene for such applications, three main issues have to be addressed. Firstly, the *production strategies* should be improved and standardised in order to guarantee quantities of material adapted to industrial applications^{4,5, 6}. Secondly, reliable and reproducible methods should be developed, allowing not only the manipulation on large scale and integration of graphene into functional devices (i. e. *processability*), but also the fine tuning of the material’s properties. In particular, the *electronic properties* have to be adapted to the different devices’ requisites². One example consists in the possibility of opening a gap into the valence and conduction bands such as to transform graphene into a semiconductor and be able to implement it in a future generation of transistors.

Chemical functionalization schemes are considered among the promising approaches able to face all the described matters⁷. Despite the inertness of graphene, connected to its extended π -conjugated aromatic structure, many possibilities of functionalization have already been explored and shown to be viable, relying both on non-covalent or covalent strategies. If

ⁱ Attempts to grow graphene on other single crystal surfaces have been ongoing since the 1970’s, but strong interactions with the surface on which it was grown always prevented the true properties of graphene being measured experimentally.

many advances have been reached, still a number of issues need to be addressed, in order to get a better understanding and control over graphene functionalization and, thus, properties.

The present thesis is set in this context. In particular, the question of graphene functionalization is approached through the perspective of supramolecular chemistry on surface, employing STM (Scanning Tunnelling Microscopy) as a tool for characterization and mean for activation of chemical reactivity. The general objective is to reach a spatial control over the sites of functionalization of the surface at an atomic level. The acquirement of this ability would furnish a mean of tuning precisely the material's electronic properties.

The work has essentially been focused on the synthesis of molecules for the functionalization of graphene. Some of the synthesized derivatives are being tested on the surface, in collaboration with different groups in France and China.

Chapter 1 reports the state of the art of graphene *non-covalent* and *covalent* functionalization as well as the strategies so far employed in order to achieve a *spatial control* over the functionalization pattern. Finally, the general objective of the thesis is presented.

The first chapter is followed by two sections, **Part I** and **Part II**, consisting in two and three chapters respectively:

Part I deals with the synthesis and study of molecules for the *non-covalent* functionalization of graphene surfaces:

Chapter 2 describes the synthesis and self-assembling STM-studies of a tetrathiafulvalene derivative.

Chapter 3 describes the synthesis of an extended poly-aromatic hydrocarbon, derived from hexabenzocoronene and named as "hexaphenanthrocoronene".

Part II deals with the synthesis and study of molecules for the *covalent* functionalization of graphene surfaces:

Chapter 4 describes the synthesis of brominated precursors designed to self-assemble on graphene and react with it after the generation of the corresponding radical species.

Chapter 5 describes the synthesis of anthracene derivatives designed to self-assemble on graphene and to react with it as dienes by Diels-Alder reaction.

Chapter 6 describes the synthesis of maleimide derivatives designed to self-assemble and to react with graphene as dienophiles by Diels-Alder reaction. A Raman study on the reactivity at the solid/liquid interface of a particular fluorinated maleimide is also reported.

References

- ¹ Novoselov, K. S., Geim, A. K., Morozov, S. V., Jiang, D., Zhang, Y., Dubonos, S. V., Grigorieva, I. V., Firsov, A. A., *Science*, **2004**, *306*, 666-669
- ² Novoselov, K. S., Falko, V. I., Colombo, L., Gellert, P. R., Schwab, M. G., Kim, K., *Nature*, **2012**, *490*, 192-200.
- ³ The Graphene Flagship's target for 2020 is directing the research from laboratories to actual innovation, <http://graphene-flagship.eu/>.
- ⁴ Roll to roll production of a 30 inches² (0.5 m²) graphene film. Bae, S., Kim, H., Lee, Y., Xu, X., Park, J.-S., Zheng, Y., Balakrishnan, J., Lei, T., Kim, H. R., Song, Y. H., Kim, Y.-J., Kim, K. S., Özyilmaz, B., Ahn, J.-H., Hong, B. H., Iijima, S., *Nature Nanotec.*, **2010**, *5*, 574-578.
- ⁵ Wafer-scale growth of single-crystal monolayer graphene on a reusable substrate, Lee, J.-H., Lee, E. K., Joo, W.-J., Jang, Y., Kim, B.-S., Lim, J. Y., Choi, S.-H., Ahn, S. J., Ahn, J. R., Park, M.-H., Yang, C.-W., Choi, B. L., Hwang, S.-W., Whang, D., *Science*, **2014**, *344*, 6181, 286-289.
- ⁶ It is now possible to produce batches of liquid exfoliated graphene with volumes up to 300 litres. Paton, K. R., Varrla, E., Backes, C., Smith, R. J., Khan, U., O'Neill, A., Boland, C., Lotya, M., Istrate, O. M., King, P., Higgins, T., Barwich, S., May, P., Puczkarski, P., Ahmed, I., Moebius, M., Pettersson, H., Long, E., Coelho, J., O'Brien, S. E., McGuire, E. K., Sanchez, B. M., Duesberg, G. S., McEvoy, N., Pennycook, T. J., Downing, C., Crossley, A., Nicolosi, V., Coleman, J. N., *Nat. Mat.*, **2014**, DOI: 10.1038/nmat3944.
- ⁷ Georgakilas, V., Otyepka, M., Bourlinos, A. B., Chandra, V., Kim, N., Kemp, C. K., Hobza, P., Zboril, R., Kim, K. S., *Chem. Rev.*, **2012**, *112*, 6156-6214.

Chapter 1

State of the art and general objectives

1.1 Control in 2D of graphene functionalization

1.1.1 Motivation

The possibility of readily producing graphene on a laboratory scale, has prompted many studies aimed at controlling its properties by chemical functionalization¹. Different strategies have been explored, showing the possibility of a fine tuning of both chemical and electronic material's properties. For example, the controlled local modification of graphene surface chemistry has already demonstrated to be useful for the templating of subsequent chemistry at a nanometric level, allowing an easy integration of graphene with other materials². Another interesting application is the controlled modification of electronic properties, such as the controlled opening of a band-gap into graphene energetic levels, which is necessary for the employment of graphene in advanced optical and electronic devices³. If the random chemical modification of graphene has already been proven interesting towards this goal⁴, a spatially controlled functionalization would offer the possibility to reach a finer tuning on the band-gap opening, through the creation of alternating functionalized and not-functionalized areas, leading to a possible control of quantum confinement effects⁵.

In this chapter, we firstly introduce a brief *state of the art* on the most pertinent methodologies employed so far to get a 2D spatial control of graphene covalent and non-covalent functionalization. Examples relative to supported graphene are included, without classifying them depending on the substrate. We then present the general *objectives of the thesis* in terms of spatial control of graphene functionalization. We then focus the attention mainly on the functionalization of epitaxial graphene supported on silicon carbide (0001), which has been chosen as substrate for our studies (see **Appendix A2**). We introduce a *state of the art* on the molecular interactions employed in the literature in order to get self-assembled monolayers on graphene on silicon carbide (0001) and the covalent chemistry that has been developed on this kind of material. In the final part of the chapter, we introduce *the particular strategies that we have selected* in the context of the project.

1.1.2 State of the art

So far, different methods have been proposed in order to achieve a spatial control on graphene functionalization, both through covalent and non-covalent strategies. In the following,

the approaches are classified in “*top-down*” or “*bottom-up*”, accordingly to the different methods applied in order to get a precisely spatially organized functionalization. In particular, in our classification, “*top-down*” methods are characterized by an external type of control: a random chemical functionalization process is followed by a spatially controlled de-functionalization, i. e. lithographic methods. “*Bottom-up*” methods are, instead, characterized by an internal type of control: the system (the molecules or the surface) is opportunely “programmed” such as to afford an ordered patterning process (i. e. template adsorption methods).

1.1.2.1 “Top-down” methods

Lithographic mask

The group of J. Tour applied a multiple-steps procedure in order to get a 2D control on the sites of graphene functionalization⁶, with optical lithographic resolution ($\sim 1 \mu\text{m}$). The procedure consisted in creating defined patterns on a glass-supported graphene surface, by photolithographic techniques. The graphene regions left free from functionalization were subsequently modified by controlled hydrogenation. After removal of the mask, the sample was further functionalized by reaction with aryl-radicals deriving from aryl diazonium-salts decomposition. The authors showed that in the applied conditions (acetonitrile, at room temperature, for 20 hours) the aryl-functionalization was selective to the previously partially hydrogenated regions.

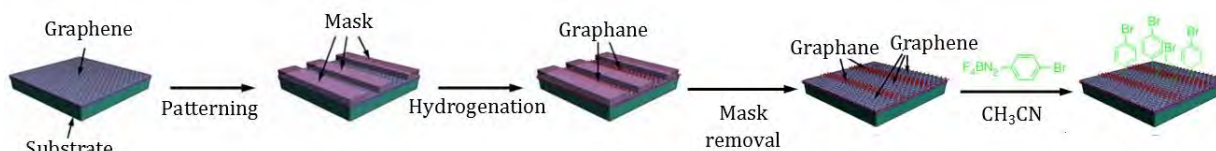


Figure 1.1: Multiple-steps procedure for controlling graphene aryl functionalization (from reference 6).

STM nano-lithography

The method consists in employing the STM tip to defunctionalize in a controlled way previously randomly functionalized areas of the surface, such as to create controlled patterns. By this methodology a resolution higher than with other lithographic techniques can be reached, at nanometer instead of micrometer scale. The defunctionalization process consists in applying high sample biases and tunnel currents to the tip (higher than those employed for imaging), in order to favor the molecular desorption.

The technique has been employed both to induce aryl moieties⁴ and hydrogen⁷ desorption, allowing to create nanopatterns at the sub-5 nm length scale.

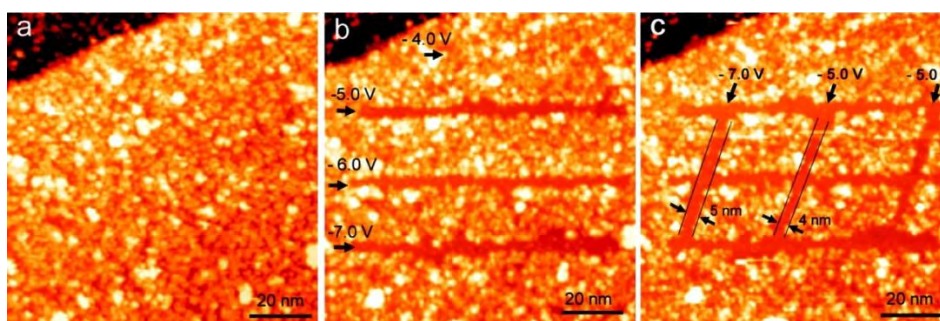


Figure 1.2 : a) STM image of the chemically nitroaryl-modified graphene before nanopatterning; b,c) STM images after bias-dependent nanopatterning procedures (from reference 4).

The same concept was applied to the patterning of a self-assembled monolayer of 3,4,9,10-perylene-tetracarboxylic dianhydride (PTCDA) on epitaxial graphene on SiC(0001)⁸. The as-recovered pristine graphene areas (generally of 4-5 nm in diameter) could successively be employed as a chemical template for driving the adsorption of a subsequently evaporated *N,N'*-dioctyl-3,4,9,10-perylene-tetracarboxylic di-imide (PTDCI-C₈).

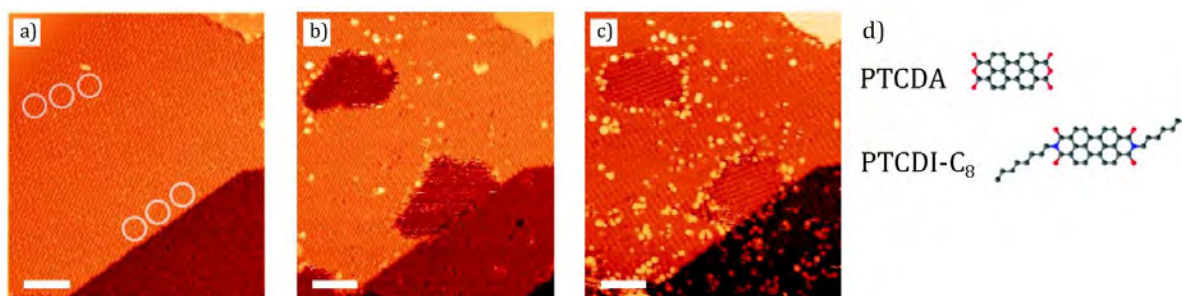


Figure 1.3: Formation of heteromolecular nanopatterns: a) PTCDA deposition and monolayer formation on epitaxial graphene on SiC(0001); b) Lithographic patterning by STM tip ($U_t = -4.6$ V, $I_t = 0.5$ nA); c). Deposition of PTDCI-C₈ to form the heteromolecular monolayer; d) Schematic representation of PTCDA and PTDCI-C₈. $U_t = -1.8$ V, $I_t = 0.02$ nA, scale bars are 10 nm (from reference 8).

Force-Accelerated graphene printing

A complementary approach, where the adsorption of the chemical species is spatially controlled by an atomic force microscope (AFM) has also been suggested. The group of A. B. Braunschweig⁹ demonstrated the possibility of controlling the functionalization of single layer CVD-graphene surfaces taking advantage of the possibility of promoting Diels-Alder cycloadditions between cyclopentadiene derivatives and CVD-graphene by exerting a force in localized areas by means of an array of elastomeric tips mounted onto the piezoelectric actuators of an atomic force microscope. Even if the spatial resolution did not reach molecular levels, the interest of this approach is that it could be employed to selectively pattern large graphene areas (~ 1 cm²).

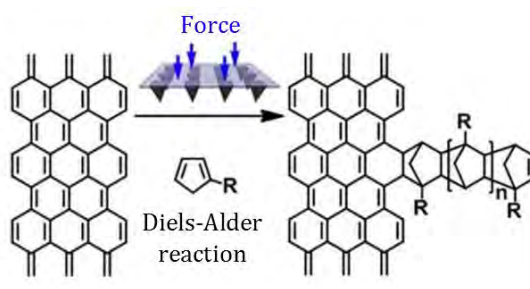


Figure 1.4 : Diels-Alder reaction between cyclopentadiene derivatives and graphene activated by the force applied through an AFM tips array (from reference 9).

1.1.2.2 “Bottom-up” methods

Templated adsorption on moiré superlattices

A moiré superlattice¹⁰ is an interference figure appearing in STM images when graphene is grown on a substrate, characterized by a commensurable crystalline lattice. The presence of the substrate can determine local variations both on the electronic (i.e. doping) and geometrical (i.e. buckling) characteristics of the graphene layer. The resulting “non-flat” surface landscape can, in some cases, template the chemi-sorption of atoms (like hydrogen, on G/Ir(111)⁵) in particular positions or drive the organization of molecules in specific geometries (like 1D lines of 2,4'-bis(terpyridine) on G/Ru(0001), **Figure 1.7**)¹¹.

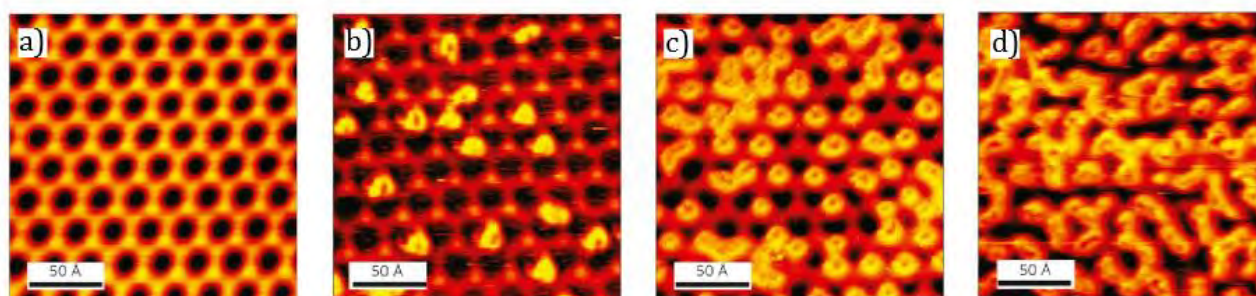


Figure 1.5 : a) Moiré pattern of G/Ir(111); b, c, d) STM images of graphene exposed to atomic hydrogen for 15, 30, 50 seconds respectively. The images show the evolution of the hydrogen structures along the bright parts of the Moiré pattern with increasing hydrogen dose (from reference 5).

Adsorption templated by a self-assembled monolayer

The deposition of atomic layer oxide nanostructure (ZnO or Al₂O₃) was templated with a sub-10 nm resolution by a pre-formed self-assembled monolayer of (10,12-pentacosadiynoic acid) PCDA² on an epitaxial graphene on SiC(0001) surface .

1.2 Objective of the project

If the methods described in **section 1.1** of this chapter allow to get a control on the graphene functionalization at “large” scale (micro or nanometric scale), no solutions have still

been proposed, allowing to exercise a control on the precise sites of functionalization of graphene at a single molecular or atomic level.

The approach proposed in the project in which this thesis work is set, is to resort to self-assembly on surface in order to achieve a spatially controlled organization of the “active” groups on graphene.

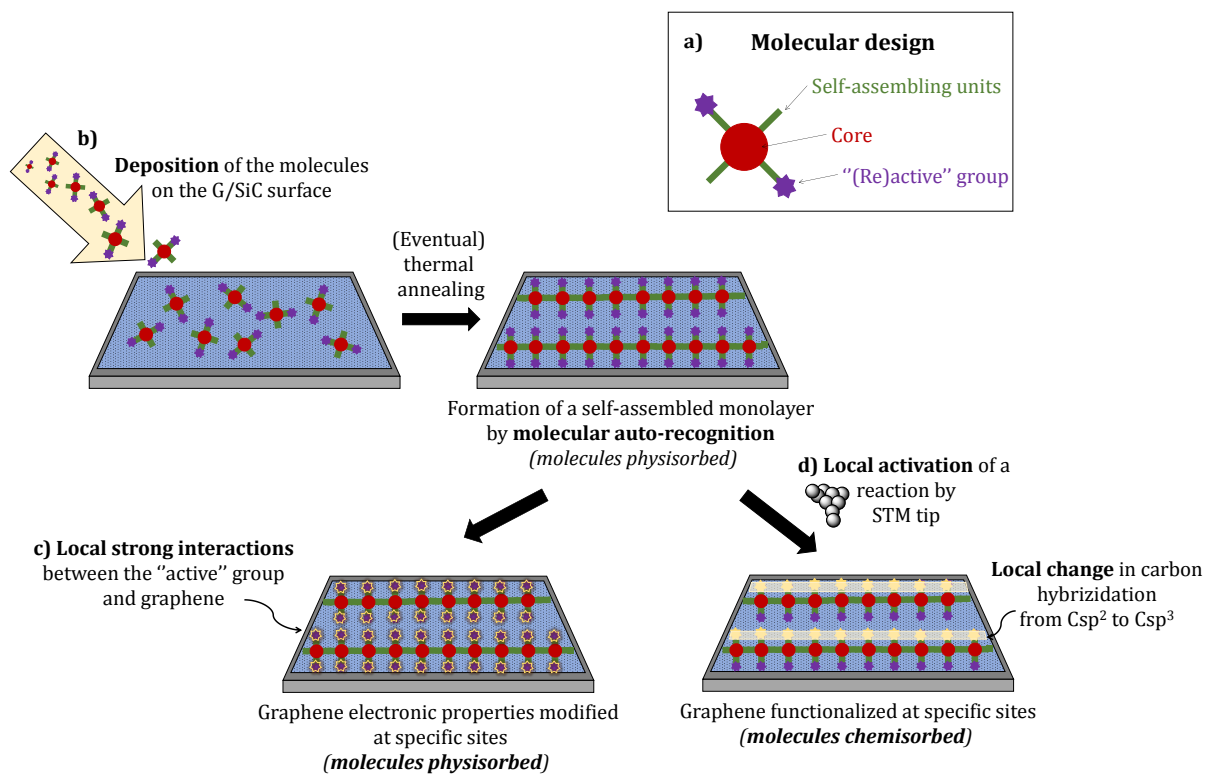


Figure 1.6: General objective of the project.

The molecular “active” functional groups are meant to interact with graphene either by *strong non-covalent* interactions or by a *chemical reaction*, leading to the formation of a covalent bond. Their geometrical organization on the surface should be driven by the self-recognition on the surface of complementary units. The extended self-assembled molecular organization is also devised to prevent the molecular diffusion on the surface, which, in general, is quite important on graphene/SiC(0001) even at low temperatures (see **Appendix A2**).

In the case of covalent functionalization, in order to be able to choose with precision the sites of chemisorption of the molecules, the chemical reaction has to be activated by means of a Scanning Tunneling Microscope (STM) tip manipulation, which allows exercising a high deal of energy in an atomic resolved area (see **Appendix A1**). Ultra-High Vacuum (UHV) conditions allow to work on a single molecular scale in a perfectly clean environment.

Among the different supported graphenes (CVD, epitaxial on Iridium...) we choose to employ epitaxial graphene on silicon carbide (0001) (graphene/SiC(0001) for our studies (see **Appendix A2**).

In order to accomplish the described objective, the first step consists in devising an appropriate molecular design, taking into consideration what is already known in the literature about self-assembly on graphene/SiC (0001) and the reactivity of this kind of surface.

1.3 Functionalization of epitaxial graphene/SiC (0001)

1.3.1 Non-covalent functionalization

Non-covalent functionalization procedures allow modifying graphene properties, while preserving the conjugated π -structure.

The physisorption of non-polar gases as hydrogen, or alkali metals, like potassium and lithium has been amply studied. This ability makes graphene an interesting substrate for storage or sensing applications. Some other non-covalent functionalization strategies have been proven useful in modulating some graphene electronic properties, such as charge carrier concentration (doping level), through charge transfer between the molecules and graphene (the most studied case is the adsorption of 2,3,5,6-Tetrafluoro-7,7,8,8-tetracyanoquinodimethane, F4-TCNQ¹²).

A finer tuning of graphene properties could be achieved by a more precise modulation of the *geometries* of the obtained monolayers¹³.

The possibility of achieving self-assembled monolayers with a controlled geometry has been demonstrated on different types of graphene (epitaxial, CVD, mechanically exfoliated) both in Ultra High Vacuum (UHV) conditions and at the solid/liquid interphase, at room or low temperature¹⁴, STM being the first tool of choice for the characterization. In this introduction we will consider the self-assembly phenomena in UHV environment.

Due to the different characteristics of the graphene layers supported on various substrates, the self-assembly process vary depending on the *type of graphene* considered. Two situations can be found: 1) graphene is strongly interacting with the substrate (i. e. is strongly electronically and/or geometrically perturbed by the presence of the particular substrate (for eg. a metal, like epitaxial graphene on Ru(0001)¹⁵); or 2) graphene is weakly interacting with the substrate (i. e. not perturbed, for ex. epitaxial graphene on SiC(0001) (see **Appendix A2**).

In the first case, at low molecular coverage, molecular diffusion is spatially constrained due to the inhomogeneous environment determined by the graphene-metal interactions, defining a moiré superlattice¹⁰. In this context, the molecules-graphene interactions influence highly the structure of the self-assembled monolayers obtained. One example is reported in **Figure 1.7**.

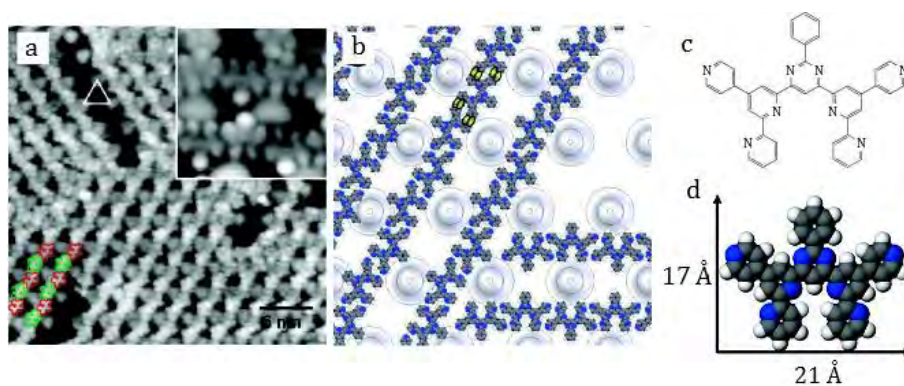


Figure 1.7 : a) STM image of an adlayer of 2,4'-bis(terpyridine) (2,4'-BTP) molecules on G/Ru(0001). Inset: detail of the structure; b) True scale model of 2,4'-BTP molecules on graphene; c) Schematic drawing of the 2,4'-BTP molecule studied and d) model with lateral dimensions (from reference 11).

In the case of graphene weakly interacting with the substrate (for ex. G/SiC(0001)), the surface landscape is extremely flat, both from an electronic and a geometrical point of view. As a first consequence, molecular diffusion generally is important even at low temperature (77K) and in order to get a stable monolayer, it is necessary to opportunely engineer the intermolecular interactions in 2D^{16,17,18,19}, such as to completely cover the whole surface and block the diffusion by steric hindrance. The self-assembled structures obtained on graphene/SiC(0001) are more similar to those obtained on the “inert” HOPG. The same kind of intermolecular interactions is involved in driving the organization of the self-assembled structures. Notwithstanding the similarities, molecules seem to be much strongly absorbed on HOPG, than on G/SiC(0001) surfaces, in UHV conditions. One effect is that, even at low temperature, the possibility to find monolayers self-assembled in registry with graphene symmetry is less frequent than what is known for HOPG. The reason can be ascribed to a difference in the polarizability of the two surfaces, determining a different strength of the involved dispersive interactions²⁰. This characteristic has been proven to determine also differences in the geometry of the resulting self-assembled structures in UHV²⁰.

Hereafter a selection of the most significative self-assembled monolayers obtained on epitaxial graphene/SiC(0001) so far is presented. In our report, we will put an accent specifically on the description of the interactions involved in the organization of the monolayer on general carbon surfaces, as well as to the structure of the obtained monolayer and insert specific examples illustrating the state of the art of epitaxial graphene on SiC(0001) functionalization.

The interactions can be classified in two categories, depending if they are involved in the promotion of *adsorption* on the surface or rather are employed to drive the *molecular organization* on the surface

1.3.1.1 Molecular interactions *with* graphene: favouring adsorption

Among the literature examples, two types of interactions are mainly employed in order to drive molecular adsorption on carbon surfaces: π - π and CH- π interactions.

π - π interactions

According to a model proposed by Hunter C. A. and Sanders J. K. M., two contributions are at interplay determining the directionality and strength of π - π interactions.

The main contribution, determining the final geometry of the interaction is an electrostatic attraction between the negatively charged π -electron cloud of one conjugated system and the positively charged σ -framework of a neighbouring molecule²¹. The second contribution, determining partially the magnitude of the π - π interactions is attributed in the model to a van der Waals attractive dispersive contribution. Two resulting configurations are possible: edge-on (a) and face-to-face (b) (**Figure 1.8**).

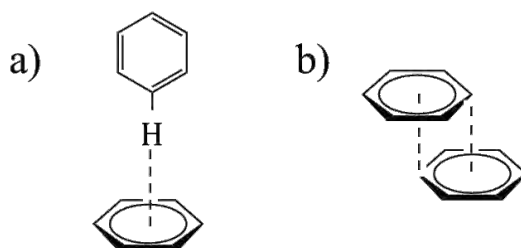


Figure 1.8 : a) edge-on and b) face-on configuration for π - π interactions.

In the *edge-on* configuration (a), the interaction appears between a hydrogen atom of one ring and the centre of another ring, in a perpendicular direction. In the *face-to-face* configuration (b), the two rings systems are disposed in a parallel geometry, separated by 3.5 Å: the interaction, in this case, is between the corner of one ring and the centre of another. The energy can vary between 0 and 500 meV per couple of benzene rings.

Due to the high affinity of G/SiC(0001) to polyaromatic molecules, the most studied systems present a rigid and extended polyaromatic core, such as perylene derivatives, like PTCDA (perylene-3,4,9,10-tetracarboxylic dianhydride)²² and its imide derivatives, PTCDI²³. An example on hexadecafluoro copper phthalocyanine (F16CuPc)²⁴ is also reported.

CH- π interactions

The interaction between HOPG and alkyl chains was amply studied^{25,26} (**Figure 1.9a**) and the considerations can be extended to the any type of graphene. CH- π interactions are classified as a weak type of hydrogen bond and appear between the H atoms of the alkyl chains and the π -

electrons of the carbon lattice. The adsorption of n-alkanes is favored by the commensurability between the graphitic lattice along the $\langle 100 \rangle$ direction ($a=0.251$ nm) and the distance between two methylenic units of the alkyl chain ($b=0.246$ nm), with a stabilization energy estimated to be about 64 meV per methylene group.

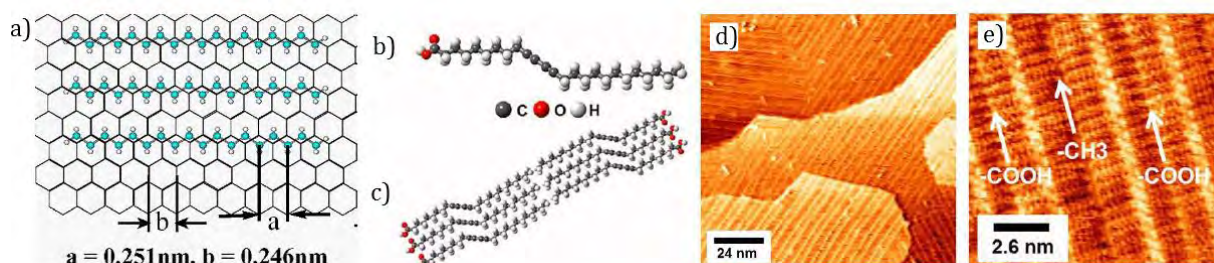


Figure 1.9 : a) Schematic representation of CH- π interactions between alkyl chains and graphitic substrates (blue=C, white=H); b) Molecular structure of 10,12-pentacosadiynoic acid (PCDA); c) Schematic of the molecular assembly of PCDA; d) Large scale UHV STM image of PCDA on G/SiC(0001): PCDA self-assembles into monolayer domains consisting of 1D stripes on the graphene surface; e) Molecularly resolved UHV STM image: the bright protrusions are the diacetylene groups.

One interesting example, was reported by M. Hersam and consist in the PCDA (10,12-pentacosadiynoic acid) system²⁷. PCDA assembles in ordered 1D structures on G/SiC(0001) in UHV conditions, at room temperature, forming structures covering uniformly the surface, without interruption at the atomic step edges and following the underlying lattice symmetry, thanks to the favorable CH- π interactions established between the CH of the alkyl chains and the graphene aromatic backbone.

1.3.1.2 Molecular interactions *on* graphene: driving self-assembly

Dispersive interactions between alkyl chains

Together with driving the molecular adsorption, the van der Waals dispersive interactions between alkyl chains can contribute to determine the geometry and stability of self-assembled supramolecular structures on carbon surfaces (both on HOPG and graphene in UHV or at the solid/liquid interphase²⁸). Alkane chains tend, in fact, to pack in a parallel fashion, with a distance of 4.1 Å. The stabilization energy has been calculated²⁶ to be of the order of 20-25 meV per pair of facing methylene groups (**Figure 1.9a**).

A representative example is the case of the derivative DHH-PTCDI (N, N'-bis-(1-hexylheptyl) perylene-3,4:9,10-bis (dicarboximide))²³: the formation of a self-assembled brick-wall structure on G/SiC(0001) in UHV was observed at room temperature, driven by dispersive forces between the swallow tail hexyl-chains.

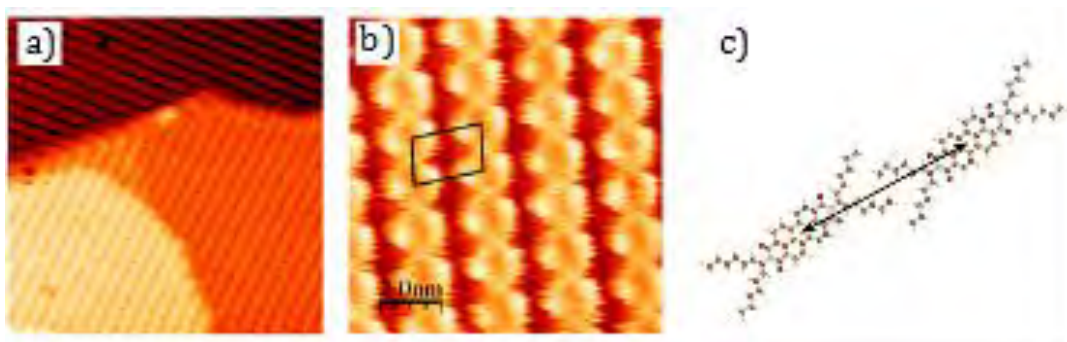


Figure 1.10 : Formation of a brick-wall structure of DHH-PTCDI on G/SiC(0001) driven by alkyl chains interdigitation.

Hydrogen bond interactions

Hydrogen bond interactions are considered as a special kind of dipole-dipole interactions between a proton donor (D) and a proton acceptor (A). The proton donor is a group where a hydrogen atom is born by an electronegative atom (such as nitrogen or oxygen), while the acceptor is generally an electronegative atom (such nitrogen, oxygen, fluorine). Depending on the atoms involved, the strength can vary between 40 and 1200 meV/mol. The interactions are highly directional and different geometries can be found. If arrays of hydrogen bonds are opportunely engineered, such as to drive the establishment of favorable secondary interactions, the strength can be extremely high.

A characteristic example of self-assembled monolayer which organization is driven by H-bonds is the PTCDAs (perylene-3,4,9,10-tetracarboxylic dianhydride)²² system: on epitaxial G/SiC(0001), at room temperature, an herringbone structure originating as a consequence of the hydrogen bond interactions O---H established between the aromatic C-H and the carbonyl or anhydride oxygens was observed by STM.

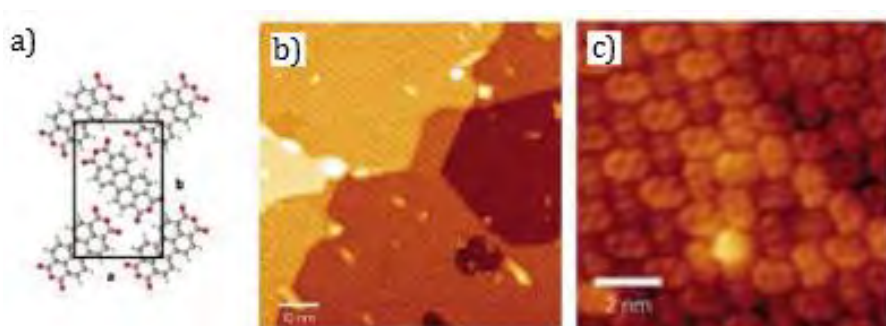


Figure 1.11 : Formation of a herringbone structure of PTCDAs on G/SiC(0001) driven by hydrogen bonds.

Another interesting case is represented by the formation of a bimolecular nanoporous molecular array on G/SiC(0001) in UHV at room temperature, which organization is driven by hydrogen bonds²⁹. The two constituent components, PTCDI and melamine, are interacting by

multiple hydrogen bonds and form a self-assembled monolayer that follows the symmetry of the underlying substrate lattice.

π - π interactions

The self-assembly of 2 and 3-TBT (2,5-dialkoxy-phenylene-thienylene-based oligomers) derivatives functionalized with octyl chains was studied on G/SiC(0001) at 77K in UHV conditions¹⁹. In particular, the supramolecular organization, leading to the formation of lines on the surface, was driven by the establishment of π - π intermolecular interactions between the terminal thiophene moieties of the molecules, strong enough to afford a continuous conjugated path along the supra-molecular aggregates.

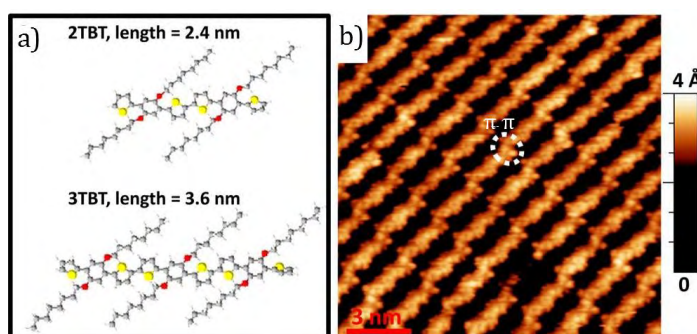


Figure 1.12 : Formation of a linear structures of 2 and 3-TBT on G/SiC(0001) driven by π - π interactions.

1.3.2 Covalent functionalization

The covalent chemistry of graphene can benefit from the studies conducted on the functionalization of fullerenes and carbon nanotubes. However, graphene basal plane is endowed with a much lower chemical reactivity compared to the other sp^2 conjugated carbon allotropes. A model for this behavior has taken into account a particular value characterizing the carbon atoms orbitals, named as “*pyramidalization angle*” and defined as the angle between the sp^2 and p_z carbon orbitals. Going from fullerene to carbon nanotubes and graphene, the angle value diminishes from the typical value of 11.64° for fullerene C60³⁰, to $4.70 - 7.49$ for SWCNTs (varying depending on the particular bond)³¹, until 0° for graphene basal plane³⁰ (**Figure 13**). The larger reactivity characterizing the most strained carbon centers (i.e. fullerenes and some carbon nanotubes bonds) is the result of the attempts to release the strain through the formation of sp^3 centers. On the contrary, pristine graphene basal plane has in theory no strain (except at edges, wrinkles and some strained areas determined by the substrate): therefore, the tendency for sp^3 hybridization is low and this makes the material intrinsically chemically more inert (see also **Chapter 5**).

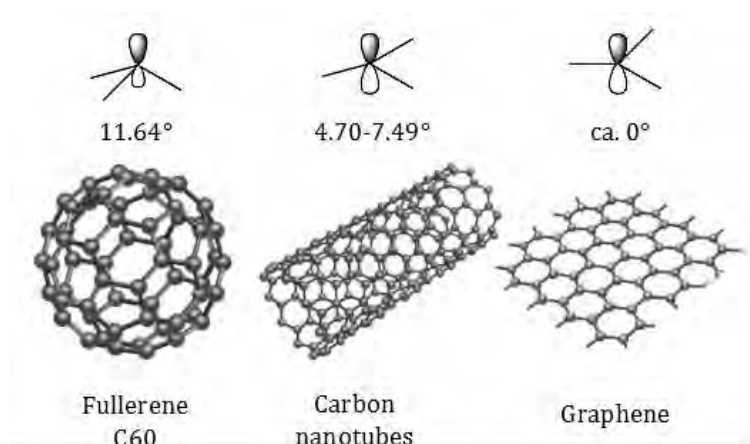


Figure 13: Degree of strain as p-orbital axis vector.

The introduction of oxygen functionalities, such as hydroxyl, epoxy and carboxylic acid groups on graphene basal plane by chemical oxidation procedures³², allows to increase the material reactivity. These groups can, in fact, eventually be functionalized and permit to insert a variety of molecular functions on the graphene surface. Despite the interest connected to the possibility of chemical functionalization, the electronic quality of the partially oxidized graphene is lowered by the presence of oxygenated defects, rendering the material not adequate for the most sophisticated applications. Moreover, the density and chemical structure of the defects cannot be controlled and even reduction procedures are not able to restore completely the conjugated carbon structure.

Another strategy allowing to increase basal plane graphene reactivity, without, in this case, damaging the sp^2 conjugated carbon lattice, consists in introducing excess negative charge on the graphene sheets, by producing the graphene layers by a liquid phase exfoliation of intercalation compounds of alkaline metals (like potassium³³) or alkaline-metals alloy (like sodium-potassium alloy³⁴). The obtained graphene is highly electron rich and thus activated towards electrophilic attacks³⁴.

Despite the interest connected to these methodologies, the dimensions of the flakes that can be produced by chemical exfoliation are still quite small. Therefore, the chemical modification of basal plane CVD and epitaxial graphene, which, instead can be grown over larger areas, arises a great interest, as a mean to locally introduce defects and tune the electronic properties, in a more controlled fashion, than employing the rather harsh conditions described above.

The chemical reactivity of graphene is related to the particular *substrate* serving as support³⁵. In particular, the substrate influence can be summarized in a series of parameters, such as:

- substrate-induced *graphene buckling*, determined by the substrate local morphology and influencing the level of the carbon atoms strain, thus the ease in changing from sp^2 to sp^3 hybridization upon covalent functionalization;
- different *graphene flexibility* determined by the different strength of surface-substrate interactions;
- local *electronic inhomogeneities*, determining local variations of the doping level³⁶, thus local reactivity differences (for ex. in electron-transfer chemistries, such as diazonium's³⁷).

A layer number dependence on the chemical reactivity is also observed³⁷, i.e. an higher reactivity of monolayer than multilayer graphene on substrates. This observation can be explained by geometrical and electronic considerations. In fact, the top-layer on a graphene bi- or multi-layer is more flat and less flexible than a monolayer directly in contact with a substrate; moreover it is less influenced by the local electronic and geometrical landscape of the substrate.

In this introduction, the attention will be focused mainly on examples of functionalization of epitaxial graphene/SiC (0001). However, most of the cited procedures, have found application in the functionalization of other kinds of graphene. For a general survey, some reviews are available¹.

Due to the important chemical inertia, most of the applied strategies considered the employment of highly reactive intermediates, such as radical derivatives. This has put forward difficulties in controlling the reaction kinetics and grafting density, together with the formed coating composition, due to the adsorption of byproducts, deriving from side reactions. In order to get a larger control, other strategies based on cycloaddition reactions have more recently been described³⁸.

1.3.2.1 Radicalar chemistry

Hydrogen radicals

High energy hydrogen radicals generated in a specific source^{39,40} can chemisorb on epitaxial G/SiC(0001) surfaces in UHV conditions. In particular, it has been shown that for low hydrogen doses a dimer adsorption configuration is thermodynamically favored, dictated by the possibility of absorbing on only one graphene face, due to the presence of the SiC substrate (instead of both as for not-supported graphene). Moreover, the formation of stable hydrogen clusters with patterns following the surface buckling induced by the underlying carbon buffer-layer³⁹ has been observed.

Nitrene radicals

Nitrene radicals generated from azido-trimethylsilane⁴¹ are reactive with epitaxial graphene/SiC(0001). The functionalization procedure has been shown not to be very efficient due to the low stability of the nitrene radical and its tendency to decompose.

Aryl radicals derived from the spontaneous reduction of aryl-diazonium salts

Some aryl-diazonium salts (for ex. 4-nitrophenyl diazonium tetrafluoroborate⁴²) have been shown to spontaneously decompose in the presence of epitaxial graphene at relatively low temperature (i.e. room temperature⁴²), to generate an aryl-radical reactive with graphene. In order to favor the covalent reaction over the physisorption, it is opportune carefully control the reaction conditions³⁰ (ex. diazonium salt type, presence of surfactants, temperature, time...).

The reaction mechanism involves³⁷ (**Figure 14**): 1) electron transfer reaction to a preadsorbed aryl diazonium ion, 2) release of nitrogen, to yield a reactive aryl radical, 3) reaction between the aryl radical and the graphene surface. The covalent reaction determines the changing of the interested carbon hybridization from sp^2 to sp^3 , and its displacement out of the plane (ca. 0.7 Å). Due to the high reactivity of the radicals, in general a distribution of products is obtained, derived in large part from radicals-auto-polymerization processes.

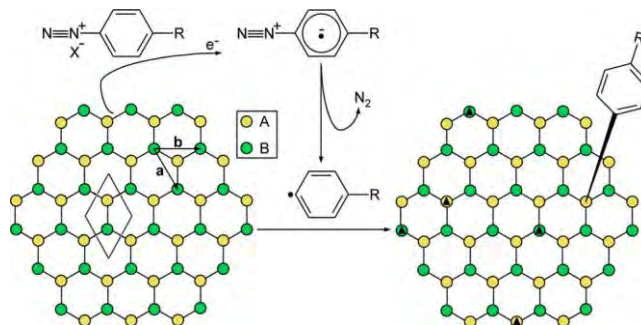


Figure 14 : Schematic illustration of the spontaneous reduction and graphing of a diazonium salt with R functional group and X⁻ counterion to a graphene sheet. Some lattice positions are (in theory) thermodynamically favoured for the attack (marked with a black triangle). (From reference 37).

Electrochemically generated radicals

This strategy of radical generation appears interesting, offering the possibility of control in the grafted molecule concentration thanks to a variation in the time of the electrochemical treatment. Two examples are reported in the literature:

- **α-naphthylmethyl radicals** electrochemically generated from the Kolbe oxidation of α-naphthylacetate by employing an epitaxial graphene wafer as working electrode⁴³. The reversibility of the reaction by electrochemical reduction is also been shown to be viable.

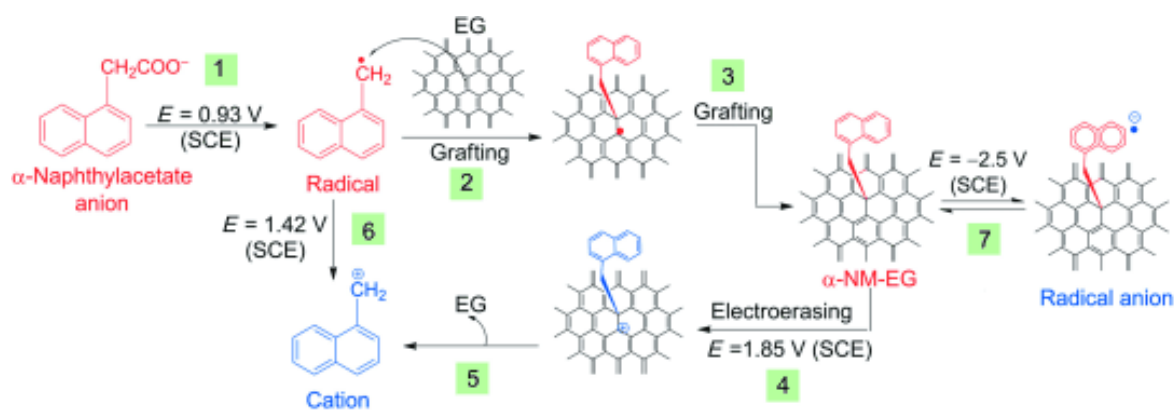


Figure 15 : Reversible electrochemically activated grafting of α -naphthylmethyl radicals (from reference 44).

- **aryl radicals** derived from decomposition of fluorinated aryl iodonium salts⁴⁴. The electron injection from graphene results in the one-electron reduction and dissociation of the iodonium salt, to yield a radical reactive with graphene. The reduction potential of iodonium compounds is higher compared to that of the analogous diazonium salts. Therefore, the radical formation is not spontaneous on graphene and can be controlled by electrochemistry.

1.3.2.2 Cycloadditions

Diels-Alder

The group of R. Haddon has reported on the reactivity of epitaxial graphene/SiC(0001)³⁸ in Diels-Alder cycloaddition with the dienophile maleic anhydride and the diene 2,3-dimethoxy-1,3-butadiene. In particular, it was observed that graphene/SiC(0001) was reactive at relatively mild temperatures: 70°C in p-xylene for maleic anhydride and 50°C in pure 2,3-dimethoxy-1,3-butadiene. The reactivity was proved also for two other reactants, tetracyanoethylene and 9-methylanthracene, respectively at room temperature and 130°C in 1,4-dioxane or p-xylene, on HOPG or exfoliated graphene (mechanically exfoliated or in solution).

A debate based on some experimental observations (on different kind of graphenes, like CVD) and DFT⁴⁵ calculations is ongoing, aiming at establishing whether the reactivity interests only graphene edges and defects or the entire basal plane. The questions arise in first place by the difficulties of characterization of the formation of the sp^3 carbonsⁱ (see **Chapter 6, section 6.8.6**) and secondly from the fact that the calculations did not take into account the eventual presence of a substrate³⁵ (ripples, doping...), that can bear important differences to graphene reactivity.

ⁱ The standard NMR or mass spectroscopy techniques are not viable.

1.4 Presentation of the proposed strategies

Taking advantage of the literature analysis, our target molecules have been designed such as to present the following general characteristics:

- *Polyaromatic core* to favor the adsorption of the molecules on graphene ;
- *Self-assembling groups* to direct the molecular organization on the surface;
- *“Active” group*, giving a strong non-covalent or covalent interaction with graphene.

The details of the different molecular design choices will be described in the dedicated chapters (**Chapters 2, 3, 4, 5, 6**).

In particular, **Chapters 2** and **3** are devoted to the solutions proposed for the non-covalent functionalization of graphene: in this case the aim is to drive the formation of a self-assembled monolayer with a controlled geometry, such as to leave some regions of the surface not functionalized. The local variation of energy potential should provide a controllable tuning of some electronic-properties. In this context, a tetrathiofulvalene and a “super-hexabenzocoronene” derivatives have been synthesized.

The **Chapters 4, 5** and **6** are dedicated to the description of the strategies proposed for the covalent controlled functionalization: the main objective in this case, is still to drive the chemical modification of the surface only in selected areas, but this time the modification of the electronic properties should be stronger, as a consequence of a covalent reaction. In this context, brominated precursors have been synthesized to be precursors of radicalar species, while functionalized maleimides and anthracenes have been proposed, in order to investigate their as Diels-Alder reactivity with graphene.

1.5 References

- ¹ a) Georgakilas, V., Otyepka, M., Bourlinos, A. B., Chandra, V., Kim, N., Kemp, C. K., Hobza, P., Zboril, R., Kim, K. S., *Chem. Rev.*, **2012**, *112*, 6156-6214; b) Chua, C. K., Pumera, M., *Chem. Soc. Rev.*, **2013**, *42*, 3222-3233; c) Park, J., Yan, M., *Acc. Chem. Res.*, **2013**, *46*, 1, 181-189.
- ² Alaboson, J. M. P., Sham, C. H., Kewalramani, S., Emery, J. D., Johns, J. E., Deshpande, A., Chien, T. Y., Bedzyk, M. J., Elam, J. W., Pellin, M. J., Hersam, M. C., *Nano Lett.*, **2013**, *13*, 12, 5763-5770.
- ³ Novoselov, K. S., Falko, V. I., Colombo, L., Gellert, P. R., Schwab, M. G., Kim, K., *Nature*, **2012**, *490*, 192-200.
- ⁴ Hossain, Z., Walsh, M. A., Hersam, M. C., *J. Am. Chem. Soc.*, **2010**, *132*, 43, 15399-15403.
- ⁵ Balog, R., Jørgensen, B., Nilsson, L., Andersen, M., Rienks, E., Bianchi, M., Fanetti, M., Lægsgaard, E., Baraldi, A., Lizzit, S., Slijivancanin, Z., Besenbacher, F., Hammer, B., Pedersen, T. G., Hofmann, P., Hornekær, L., *Nature Mat.*, **2010**, *9*, 315-319.
- ⁶ Sun, Z, Pint, C. L., Marcano, D. C., Zhang, C., Yao, J., Ruan, G., Yan, Z., Zhu, Y., Hauge, R. H., Tour, J. M., *Nature Comm.*, **2011**, *2*, 559, 1-5.
- ⁷ Sessi, P., Guest, J. R., Bode, M., Guisinger, N. P., *Nano Lett.*, **2009**, *9*, 12, 4343-4347.
- ⁸ Wang, Q. H., Hersam, M. C., *Nano Lett.*, **2011**, *11*, 589-593.
- ⁹ Bian, S., Scott, A. M., Cao, Y., Liang, Y., Osuna, S., Houk, K. N., Braunschweig, A. B., *J. Am. Chem. Soc.*, **2013**, *135*, 9240-9243.
- ¹⁰ van den Brink, J., *Nature Mat.*, **2010**, *9*, 291-292.
- ¹¹ Roos, M., Künzel, D., Uhl, B., Huang, H. H., Brandao Alves, O., Hoster, H. E., Gross, A., Behm, R. J., *J. Am. Chem. Soc.*, **2011**, *133*, 9208-9211.
- ¹² Chen, W., Chen, S., Qi, D. C., Gao, X. Y., Wee, A. T. S., *J. Am. Chem. Soc.*, **2007**, *129*, 10418-10422.
- ¹³ MacLeod, J. M., Rosei, F., *Small*, **2013**, DOI: 10.1002/sml.201301982.
- ¹⁴ Li, B., Tahara, K., Adisoejoso, J., Vanderlinden, W., Mali, K. S., De Gendt, S., Tobe, Y., De Feyter, S., *ACS Nano*, **2013**, *7*, 12, 10764-10772.
- ¹⁵ Roos, M., Künzel, D., Uhl, B., Huang, H. H., Brandao Alves, O., Hoster, H. E., Gross, A., Behm, R. J., *J. Am. Chem. Soc.*, **2011**, *133*, 9208-9211.
- ¹⁶ Wang, Q. H., Hersam, M. C., *Nat. Chem.*, **2009**, *1*, 206-211.
- ¹⁷ Yang, H., Mayne, A. J., Comtet, G., Dujardin, G., Kuk, Y., Sonnet, Ph., Stauffer, L., Nagarajan, S., Gourdon, A., *Phys. Chem. Chem. Phys.*, **2013**, *15*, 4939-4946.
- ¹⁸ Karmel, H. J., Chien, T.-Y., Demers-Carpentier, V., Garramone, J. J., Hersam, M. C., *J. Phys. Chem. Lett.*, **2014**, *5*, 270-274.
- ¹⁹ Shokri, R., Lacour, M.-A., Jarrosson, T., Lère-Porte, J.-P., Serein-Spirau, F., Miqueu, K., Sotiropoulos, J.-M., Vonau, F., Aubel, D., Cranney, M., Reiter, G., Simon, L., *J. Am. Chem. Soc.*, **2013**, *135*, 5693-5698.
- ²⁰ Shokri, R., Vonau, F., Cranney, M., Aubel, D., Narladkar, A., Isare, B., Bouteiller, L., Simon, L., Reiter, G., *J. Phys. Chem. C*, **2012**, *116*, 21594-21600.
- ²¹ Hunter, C. A., Sanders, J. K. M., *J. Am. Chem. Soc.*, **1990**, *112*, 5525-5534.

- ²² Wang, Q. H., Hersam, M. C., *Nat. Chem.*, **2009**, *1*, 206-211.
- ²³ Yang, H., Mayne, A. J., Comtet, G., Dujardin, G., Kuk, Y., Sonnet, Ph., Stauffer, L., Nagarajan, S., Gourdon, A., *Phys. Chem. Chem. Phys.*, **2013**, *15*, 4939-4946.
- ²⁴ Wang, Y.-L., Ren, J., Song, C.-L., Jiang, Y.-P., Wang, L.-L., He, K., Chen, X., Jia, J.-F., Meng, S., Kaxiras, E., Xue, Q.-K., Ma, X.-C., *Phys. Rev. B*, **2010**, *82*, 245420, 1-5.
- ²⁵ Groszek, A. J., *Proc. R. Soc. London. Ser. A*, **1970**, *314*, 1519, 473-498.
- ²⁶ Bléger, D., Kreher, D., Mathevet, F., Attias, A.-J., Schull, G., Huard, A., Douillard, L., Fiorini-Debuischert, C., Charra, F., *Angew. Chem. Int. Ed.*, **2007**, *46*, 7404-7407.
- ²⁷ Deshpande, A., Sham, C.-H., Alaboson, J. M. P., Mullin, J. M., Schatz, G. C., Hersam, M. C., *J. Am. Chem. Soc.*, **2012**, *134*, 40, 16759–16764.
- ²⁸ Li, B., Tahara, K., Adisoejoso, J., Vanderlinden, W., Mali, K. S., De Gendt, S., Tobe, Y., De Feyter, S., *ACS Nano*, **2013**, *7*, 12, 10764-10772.
- ²⁹ Karmel, H. J., Chien, T.-Y., Demers-Carpentier, V., Garramone, J. J., Hersam, M. C., *J. Phys. Chem. Lett.*, **2014**, *5*, 270-274.
- ³⁰ Koehler, F. M., Stark, W. J., *Acc. Chem. Res.*, **2013**, *46*, 10, 2297-2306.
- ³¹ Li, J., Jia, G., Zhang, Y., *Chem. Eur. J.*, **2007**, *13*, 6430-6436.
- ³² Park, S., Ruoff, R. S., *Nature Nanotech.*, **2009**, *4*, 217-224.
- ³³ Catheline, A., Vallés, C., Drummond, C., Ortolani, L., Morandi, V., Marcaccio, M., Iurlo, M., Paolucci, F., Pénicaud, A., *Chem. Comm.*, **2011**, *47*, 5470-5472.
- ³⁴ Englert, J. M., Dotzer, C., Yang, G., Schmid, M., Papp, C., Gottfried, J. M., Steinrück, H. P., Spiecker, E., Hauke, F., Hirsch, A., *Nature Chem.*, **2011**, *3*, 279-286.
- ³⁵ Boukhvalov, D. W., *RSC Adv.*, **2013**, *3*, 7150–7159.
- ³⁶ Kittel, Charles. *Introduction to Solid State Physics*, 7th Edition. Wiley.
- ³⁷ Paulus, G. L. C., Wang, Q. H., Strano, M. S., *Acc. Chem. Res.*, **2013**, *46*, 1, 160-170.
- ³⁸ Sarkar, S., Bekyarova, E., Niyogi, S., Haddon, R. C., *J. Am. Chem. Soc.*, **2011**, *133*, 3324–3327.
- ³⁹ Balog, R., Jørgensen, B., Wells, J., Lægsgaard, E., Hofmann, P., Besenbacher, F., Hornekær, L., *J. Am. Chem. Soc.*, **2009**, *131*, 8744–8745.
- ⁴⁰ Guisinger, N. P., Rutter, G. M., Crain, J. N., First, P. N., Stroscio, J. A., *Nano Lett.*, **2009**, *9*, 4, 1462-1466.
- ⁴¹ Choi, J., Kim, K., Kim, B., Lee, H., Kim, S., *J. Phys. Chem. C Lett.*, **2009**, *113*, 9433-9435.
- ⁴² Bekyarova, E., Itkis, M. E., Ramesh, P., Berger, C., Sprinkle, M., de Heer, W. A., Haddon, R. C., *J. Am. Chem. Soc.*, **2009**, *131*, 1336-1337.
- ⁴³ Chan, C. K., Beechem, T. E., Ohta, T., Brumbach, M. T., Wheeler, D. R., Stevenson, K. J., *J. Phys. Chem. C.*, **2013**, *117*, 12038-12044.
- ⁴⁴ Sarkar, S., Bekyarova, E., Haddon, R. C., *Angew. Chem. Int. Ed.*, **2012**, *51*, 4901 –4904.
- ⁴⁵ a) Cao, Y., Osuna, S., Liang, Y., Haddon, R. C., Houk, K. N., *J. Am. Chem. Soc.*, **2013**, *135*, 17643-17649; b) Denis, P. A., *Chem. Eur. J.*, **2013**, *19*, 15719-15725.

PART I

Synthesis of molecules for non-covalent functionalization of graphene

As already introduced in **Chapter 1**, the possibility of absorbing different chemical species on graphene resorting to non-covalent interactions (mainly cation- π , π - π or CH- π , see **Chapter 1, section 1.3.1.1**) paves the way to the employment of the material in many applications¹. Concerning the case of epitaxial graphene/SiC(0001), the general objective of the non-covalent chemical modification can be summarized to 1) change graphene's properties (i.e. electronic properties) or 2) to introduce new functionalities, i.e. exploiting the material as a support.

In the first case (1), in order to achieve a modification on graphene's electronic structure, the interaction between the molecules and graphene has to be strong, for example by formation of a charge-transfer complex. In this case, the doping level can be varied. The charge transfer interaction between different electron donors and acceptors and epitaxial graphene/SiC(0001) has been studied. Examples of electron donors are perylene-3,4,9,10-tetracarboxylic dianhydride (PTCDA)² and its imide derivative PTCDI³ molecules and of electron-acceptors, hexadecafluoro copper phthalocyanine⁴.

As already introduced in **Chapter 1**, all these molecules are forming stable self-assembled monolayers on graphene/SiC(0001). In the aim of modify graphene electronic properties, it can also be interesting to study the interaction between a single molecule and graphene. Considering the high molecular diffusivity on graphene/SiC(0001), the necessity of forming a self-assembled layer all over the surface is imposed in order to limit the molecular diffusion. A possible strategy in order to keep the molecules isolated consists in designing their structure in order that in the self-assembled system it is guaranteed the presence of pores, for example by introducing at their periphery insulating alkyl chains. Once known the single molecule interaction with the material, it would be in principle possible to tune the different modifications eventually brought to the electronic properties of the material, by controlling exactly the periodic organization of the self-assembled structures obtained on the surface.

In some other cases (2) the interaction between the molecules and graphene is weaker, i.e. no charge-transfer occurs. In this context, graphene can be considered as an inert substrate and can be employed as a support for many applications, like sensoristics, or as a template for the building of new structures. As an example of recent application, the templating character of graphene/SiC(0001) has been explored as a mean to drive the organization of molecular wires, by opportunely programming the supramolecular organization on the surface of molecular entities⁵.

The role of supramolecular chemistry on surface becomes thus important from two point of views: 1) as a method allowing the spatially controlled organization of functional groups over the surface with reproducible and controllable patterns, over large areas; 2) as a mean to induce the molecular organization with specific patterns, that would not be possible to obtain by other ways. If many examples of self-assembled monolayers have appeared in the literature, a full control over the molecular self-assembly in Ultra High Vacuum (UHV) (as well as at the solid/liquid interphase) has still to be attained. It appears, thus, very interesting to expand the number of molecules studied and investigate their interaction with graphene/SiC(0001), such to acquire the ability to get a fine control on the organization on surface and/or entity of charge transfer interaction by designing properly the molecular structure.

In the **Part I** of the manuscript we describe the design and synthesis of molecules for the non-covalent functionalization of epitaxial graphene/SiC. The molecular design have been developed taking into account the different aspects related to the constraints imposed by the UHV-experiments and the nature of the surface, such as the requisites for stability of the molecular structure in the UHV-sublimation phase and the necessity to afford strong interactions with graphene (π - π or CH- π).

The molecular structure can be schematized as following (**Figure I.1**):

1. *Core* interacting with graphene (possibly leading to n or p-doping);
2. *Self-assembling units*.

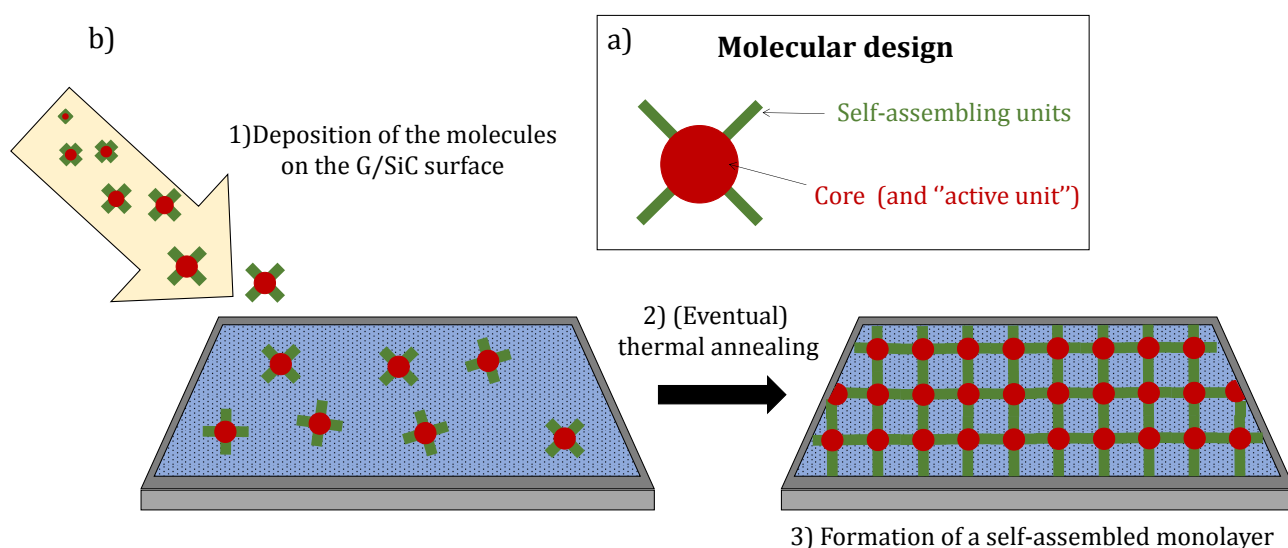


Figure I.1: a) Schematic molecular structure of the molecules we have devised for the non-covalent functionalization of epitaxial graphene/SiC; b) different steps of the formation of a self-assembled monolayer on the surface: 1) deposition in UHV (by sublimation) and absorption on the surface, 2) (eventual) thermal annealing in order to favour the organization of the molecules in periodic structures (3).

The cores we have chosen are a tetrathiafulvalene (TTF) and hexaphenanthrocoronene derivative, devised in order to study their self-assembling behaviour and electron donating properties on epitaxial graphene on SiC(0001). We have functionalized them by alkyl chains, as elements driving the molecular organisation on the surface.

The synthesis of the two molecules and an STM study of the synthesized tetrathiafulvalene derivative are presented in the following **Chapter 2** and **Chapter 3**.

References

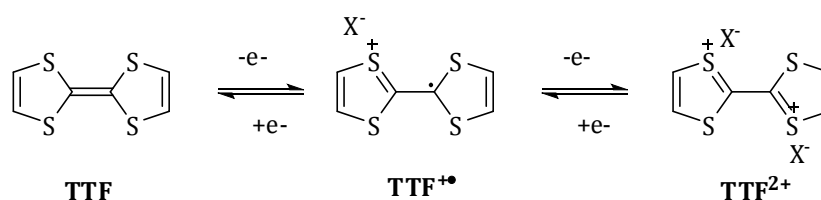
- ¹ Georgakilas, V., Otyepka, M., Bourlinos, A. B., Chandra, V., Kim, N., Kemp, C. K., Hobza, P., Zboril, R., Kim, K. S., *Chem. Rev.*, **2012**, *112*, 6156-6214.
- ² Wang, Q. H., Hersam, M. C., *Nat. Chem.*, **2009**, *1*, 206-211.
- ³ Yang, H., Mayne, A. J., Comtet, G., Dujardin, G., Kuk, Y., Sonnet, Ph., Stauffer, L., Nagarajan, S., Gourdon, A., *Phys. Chem. Chem. Phys.*, **2013**, *15*, 4939-4946.
- ⁴ Wang, Y.-L., Ren, J., Song, C.-L., Jiang, Y.-P., Wang, L.-L., He, K., Chen, X., Jia, J.-F., Meng, S., Kaxiras, E., Xue, Q.-K., Ma, X.-C., *Phys. Rev. B*, **2010**, *82*, 245420, 1-5.
- ⁵ Shokri, R., Lacour, M.-A., Jarrosson, T., Lère-Porte, J.-P., Serein-Spirau, F., Miqueu, K., Sotiropoulos, J.-M., Vonau, F., Aubel, D., Cranney, M., Reiter, G., Simon, L., *J. Am. Chem. Soc.*, **2013**, *135*, 5693-5698.

Chapter 2

Synthesis and studies of the self-assembling behaviour of a tetrathiafulvalene derivative

2.1 Introduction

Tetrathiafulvalene^{1,2} (TTF) is a non-aromatic 14- π -electrons molecule, characterized by interesting electron donor properties: the molecule possesses three stable redox states (**Scheme 2.1**), that can be reached within relatively low potential values ($E^{1/2} = 0.37$, $E^{2/2} = 0.67$ vs SCE in CH_2Cl_2 ³). The driving force for the oxidation is the attainment of some degree of aromaticity in the formation of the radical cation $\text{TTF}^{+\bullet}$ and full aromaticity in the dication salt TTF^{2+} upon loss of two electrons, together by the stabilization of both the positive charge and radicals by the lone pairs on the sulphur atoms.



Scheme 2.1 : Reversible oxidation of the TTF core.

The TTF core can be functionalized in many different ways, allowing the tuning of its electronic behaviour and imparting new properties. The versatility of the chemistry reflects in the high number of possible applications in which the TTF building-block is employed^{1,2}: catalysts for radical-polar crossover reactions (where the TTF core acts as a reducing reagent); redox-active supramolecular systems: chemical sensors, redox switchable ligands, molecular shuttles and switches; liquid crystals; covalent donor-acceptor systems to be employed in non-linear optic materials; magnetic materials; electrically conducting materials.

Among the class of conducting materials, TTFs appear to be interesting candidates as building-blocks for the creation of self-assembled molecular wires. The conduction along the wires is guaranteed by the simultaneous presence of alternating neutral TTF and its radical cation $\text{TTF}^{+\bullet}$. Different lateral substituents have been inserted in order to enhance the π - π and S \cdots S interactions among the cores over long distances and thus increase the molecular conductivity. The mostly employed substituents favouring this type of supra-molecular organization in bulk crystals are hydrogen-bond donor-acceptors, like carboxylic derivatives⁴, or thio-alkyl chains⁵.

Recently, some strategies have also been developed in order to build TTF nanowires already on a substrate, based on the possibility of TTF amide-functionalized derivatives to self-assemble at the solvent/HOPG interphase. The driving force to organize the molecules in π - π stacked wires, by prompting the cores to lie perpendicular to the surface, is in this case the formation of hydrogen bonds between lateral amide units⁶.

However, this type of edge-on organization represents an exception to the commonly observed structures of self-assembled monolayers of TTF on HOPG at the solid/liquid interphase. In general, in fact, the most favourable conformation for the TTF cores is lying planar on the surface, favoured by the establishment of π - π interactions with the underlying graphite^{i,7,8}. The substitution pattern and the solvent contribute, instead, to determine the characteristics of the packing inside the monolayer.

When the cores are lying flat on the surface, a charge transfer with graphene can be measured, determining a n-doping of the material^{ii,9,10}.

2.2 Objective

Due to the interest of TTF derivatives for the development of different devices, and in particular electronic conducting wires, much effort has been and is devoted to understanding the factors governing the molecular packing on surfaces. If many information are now available concerning a solid/liquid environment, there's a lack of knowledge about the self-assembling behaviour of this kind of molecules in UHV.

In this chapter we report the synthesis and an STM-study of the self-assembling behaviour of a tetra-alkyl-thio derivative, on epitaxial graphene/SiC(0001) and HOPG. We show the possibility of tuning the molecular interactions with the carbon surface by varying the environment where the self-assembling process takes place (UHV or in the presence of solvent). An original self-assembling behaviour is observed in UHV, leading to the generation of extended molecular wires over the surface, thanks to the combination of *weak* molecule-molecule and molecule-substrate interactions.

2.3 Different contributions to the work

The synthesis of the molecule has been carried out following a procedure kindly provided by M. Sallè (University of Angers, France).

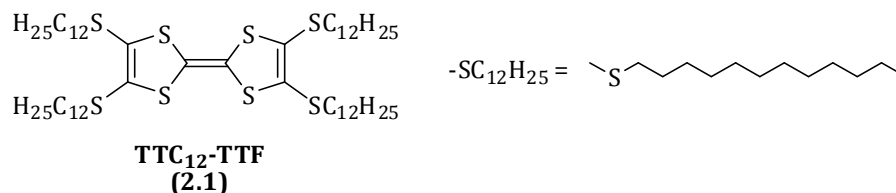
The STM-studies in UHV and at the liquid/solid interphase have been carried out by the group of L. Simon at the IS2M in Mulhouse (France). I participated in the initial screening of the

ⁱ Solutions 10⁻³M in the solvents phenyloctane or 1-octanol.

ⁱⁱ The charge transfer has been estimated by XPS to be of the order of $\sim 10^{12}$ electrons/cm² (from reference 9).

conditions and in recording the first preliminary images at the solid/liquid interphase on HOPG and G/SiC(0001).

2.4 Molecular design



Scheme 2.2 : Molecular structure of TTC₁₂-TTF (2.1).

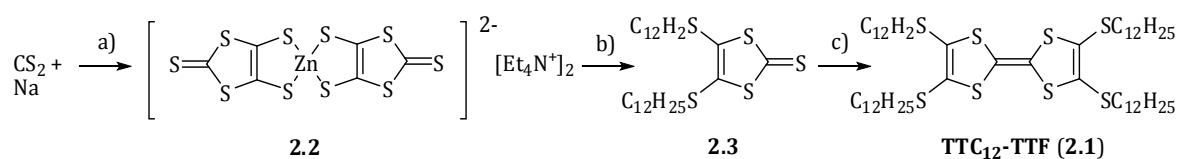
The molecule we selected is characterized by a tetrathiofulvalene (TTF) core, functionalized with four thio-alkyl-chains of length -C₁₂H₂₅. In reason of this characteristic, the molecule is named all throughout the text as “TTC₁₂-TTF”, where 12 is number of carbon atoms constituting the chains. The presence of the long alkyl chains is a way to 1) allow a flat molecular adsorption of the cores on the graphene surface, as it has already been observed at the liquid/solid interface⁷; 2) drive the organization of the TTFs in a “porous” monolayer, where the cores are separated, thus providing the possibility of investigate their electronic interaction with graphene.

The introduction of the thio-alkyl chains determines a variation in the electron donor properties of this derivative. In particular for TTC₁₂-TTF, two oxidation potentials have been measured⁷: E_{1/2}¹ = 0.61 V, E_{1/2}² = 0.96 V vs SCE in CHCl₂.

2.5 Results and discussion

2.5.1 Synthesis

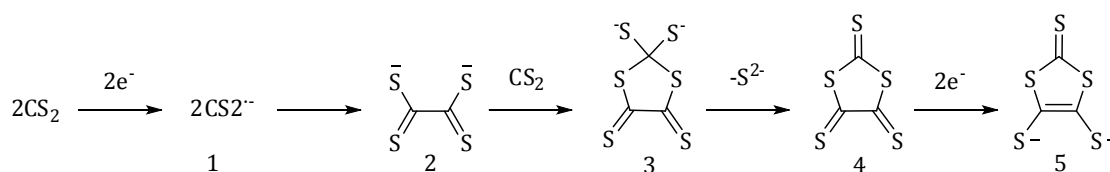
The derivative TTC₁₂-TTF (2.1) was synthesized from the 4,5-ethylenedithio-1,3-dithiole-2-thione precursor 2.3 obtained from the salt 2.2, which can be obtained from the reduction of carbon disulphide¹¹ (Scheme 2.3).



Scheme 2.3 : Synthesis of the derivative TTC₁₂-TTF (2.1) : a) i) DMF dry, 0-25°C, 19h ; ii) ZnCl₂, NH₃ aq. (28%), 30 mins.; iii) TEAB, H₂O, 18h, 25°C, 27% ; b) C₁₂H₂₅Br, Acetone, 60°C, 18h, 100% ; c) P(OEt)₃ dry, 130°, 6h, 32%.

Step a)

The TTF core precursor **2.2** was obtained by a one-pot procedure based on the reduction of carbon disulphide by metallic sodium¹¹. Carbon disulphide was reacted with sodium in DMF at room temperature (25°C), to afford the sodium salt of **5** (**Scheme 2.4**). After destroying the eventual residual of sodium by adding 2-propanol and methanol, a solution of ZnCl₂ in aqueous ammonia was added, to afford the precursor **2.2**, after precipitation as tetraethyl ammonium bromide salt. After some washing procedures (with water, 2-propanol and diethyl ether) the compound **2.2** was pure enough to be employed in the following step of the synthesis. The zinc salt **2.2** is highly stable and the (unoptimized) yield was estimated to be 27%.



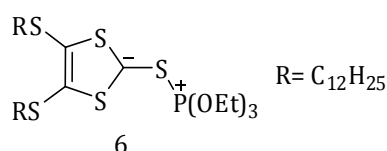
Scheme 2.4 : Mechanism of formation of the 4,5-ethylenedithio-1,3-dithiole-2-thione by reduction of CS₂ (from reference 11).

Step b)

The thiolic functions of **2.2** were alkylated with -C₁₂H₂₅ chains, in a S_N2 reaction with 1-bromododecane, conducted in acetone, at reflux (60°C) for 18 hours. The product **2.3** could be isolated as a yellow solid after chromatographic purification on silica with hexane as eluent, with a quantitative yield.

Step c)

The precursor **2.3** was homo-coupled in order to yield the TTC₁₂-TTF (**2.1**) in a reaction conducted in triethylphosphite, at 130°C for 6 hours. A description of the mechanism can be found in a paper by McCullough *et al.*¹² and is based on the formation of a zwitterionic intermediate between triethylphosphite and the precursor **2.2** (**Scheme 2.5**). The product could be recovered as an orange solid after precipitation from methanol and further purified by column chromatography on silica, employing petroleum ether : dichloromethane 9 : 1 as eluent, with a 32% yield.



Scheme 2.5 : Zwitterionic intermediate originated by the reaction between **2.2** and P(OEt)₃.

The characterizations were conform to those reported in the literature for the product TTC₁₂-TTF.

2.5.2 STM Studies

2.5.2.1 Self-assembly studies in UHV on G/SiC(0001)

The molecules were deposited on G/ SiC(0001) surface held at room temperature by UHV-sublimation at temperatures ranging from 420 to 490 K. The imaging was performed at 77K at a 10^{-11} mbar range, with Pt/Ir tips. Some representative images are reported in **Figure 2.3** and **2.2**.

The **TTC₁₂-TTF (2.1)** molecules are forming in UHV on epitaxial graphene/SiC(0001) a tightly packed monolayer (**Figure 2.2**), continuous over the graphene step edges (**Figure 2.2c** and **d**). By analysis of the height profiles and the core-to-core distances in the pictures, it can be assumed that the molecules adopt an edge-on conformation, where the cores lie perpendicularly to the surface, being forced to form π - π stacked 1D aggregates by the interactions between the alkyl-chains. This effect has been denominated « fastener effect » by Inokuchi *et al.*⁵ (**Figure 2.1**) who observed it for the first time in the 1980's in bulk crystals of TTC_n-TTF molecules functionalized with long alkyl chains (i.e. $7 < n < 14$).

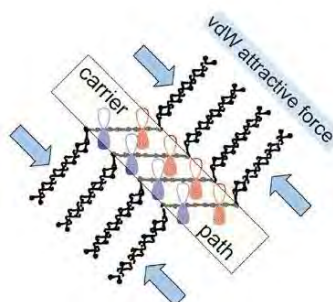


Figure 2.1 : Schematic representation of the alkyl-chains induced « fastener effect » (from reference 13).

The van der Waals attractive intermolecular interactions between the alkyl chains enforce the central π -segments to form wires characterized by small interplanar distances, which in our case are measured by STM to be smaller than 5 Å. In particular, the TTF cores are able to assume a «chair» or a «boat conformation» (**Figure 2.3**) with S...S and π - π interactions between the C₆S₈ cores of adjacent molecules. Due to the close proximity of the π -cores, a 1D conduction along the rows is expected¹⁵.

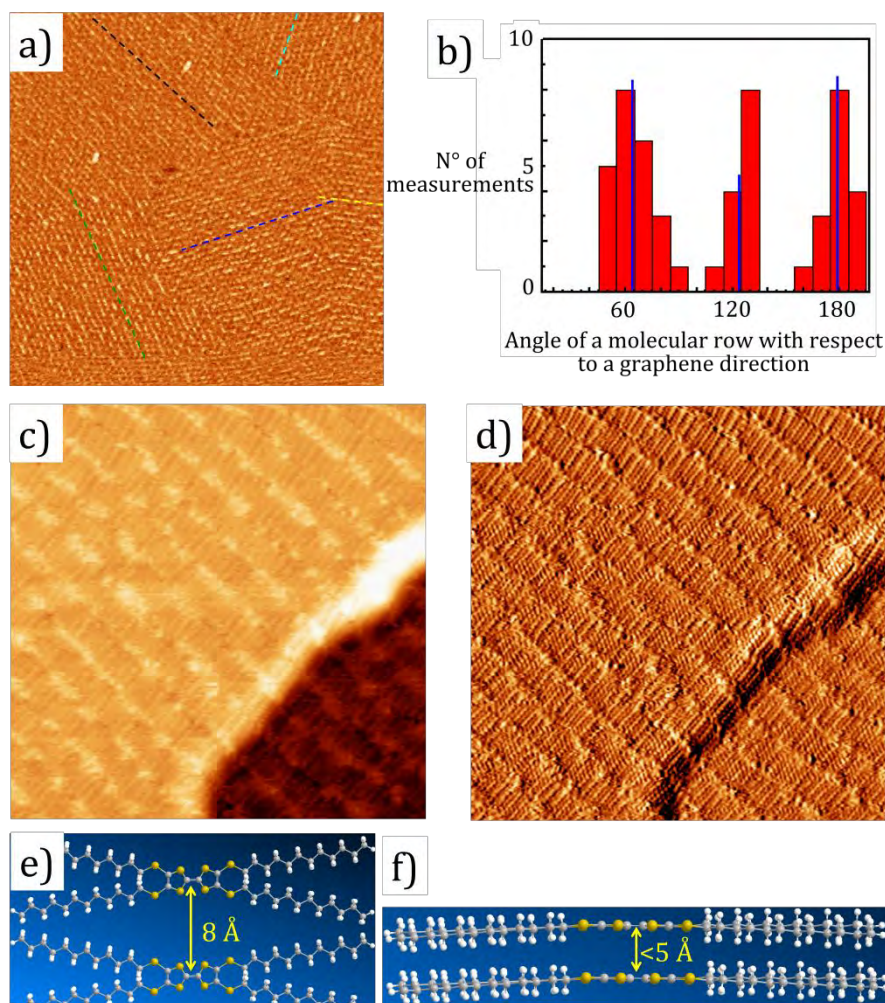


Figure 2.2ⁱⁱⁱ : a) STM topographic image of TTC₁₂-TTF molecules on epitaxial graphene/SiC(0001) in UHV. The molecules form domains of parallel rows with different orientations, as indicated by the coloured lines ($U_t = -2$ V, 100×100 nm²); b) Distribution of the measured angles of the molecular rows respect to one of the graphene directions. The mean values of the angles are $64^\circ \pm 4^\circ$, $124^\circ \pm 4^\circ$ and $179^\circ \pm 4^\circ$, reflecting the hexagonal symmetry of the graphene substrate and showing that the assembly of the molecules is partially guided by the underlying substrate; c) STM image ($U_t = -1.6$ V, 20×20 nm²) and d) mathematical elaboration of the image showing the continuity of the molecular layer over graphene step edges; e and f) Molecular modelling of two TTC₁₂-TTF molecules giving a distance of 8 \AA between the cores when they are lying flat, whereas a distance smaller than 5 \AA for the molecules in an edge-on conformation. The length of the molecule is 37.9 \AA and the length of a dodecylthio side chain is 15.5 \AA (estimated from ChemSketch^{iv}).

Two more observations can be made:

1) The orientations of the molecular rows are partially determined by the underlying graphene lattice, however the distribution of angles around the mean values appear to be large indicating a certain degree of flexibility of the molecular layer; (**Figure 2.2b**)

2) no perturbation of the TTC₁₂-TTF molecular orbitals is observed by Scanning Tunnelling Spectroscopy (STS): the HOMO-LUMO gap is measured by STS to be of 2.3 ± 0.1 eV, whereas

ⁱⁱⁱ The images were treated with the software WSxM (I. Horcas, R. Fernández, J.M. Gómez-Rodríguez, J. Colchero, J. Gómez-Herrero, A.M. Baro, *Rev. Sci. Instrum.*, **2007**, *78*, 013705).

^{iv} ACD/ChemSketch Freeware from ACD/Labs.

absorption-emission spectroscopy measurements of TTC₁₂-TTF in solution measure a similar optical band gap of $2.6 \pm 0.1 \text{ eV}$.

It is possible to conclude that, although the intermolecular interactions appear to be strong, the molecules-graphene interactions seems to be weak, thus probably not able to lead to a doping of graphene by charge transfer from the electron donor molecules (which, from calculations, appears to be only possible when the cores are lying flat on the surface¹⁴).

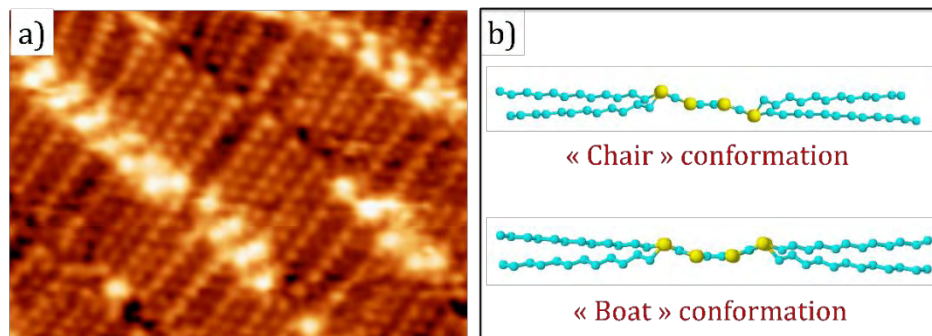


Figure 2.3 : a) STM topographic image ($U_t = -1.6 \text{ V}$, $6.4 \times 6.4 \text{ nm}^2$) clearly showing an edge-on conformation adopted by the TTC₁₂-TTF (2.1) molecules in UHV on G/SiC(0001) (only one alkyl-chain methylene unit over two can be imaged). This organization represents the first direct observation of the so called « molecular fastener»⁵ effect induced by long alkyl chains ($7 < C_n < 14$) by STM in UHV on G/SiC(0001) (a molecular model drawn to scale is superimposed); the molecules can absorb in a «chair» or in a «boat» conformation, due to the fastener effect of the alkyl chains (b). (blue = C; yellow = S).

In accordance to the low level of electronic interaction between the molecules and graphene, it is expected that the conduction properties measured in bulk crystals⁵ along the supramolecular wires are maintained in the self-assembled structures on graphene.

An interesting way to engineer 1D conducting wires over large micrometric areas has been developed, based on the combined effect of UHV conditions and weak molecular interactions with the surface. A similar result had been obtained by the group of D. Amabilino who introduced urea groups in the chains in order to modify the molecular orientation on the surface and create one-dimensional assemblies stabilized by hydrogen bonds⁶. In this case, however, the experiment was performed at the solid-liquid interphase (i.e. in the presence of a solvent) and not in UHV.

2.5.2.2 Self-assembly studies at the solid/liquid interphase on HOPG and G/SiC(0001)

In order to further confirm the fastening role of the alkyl chains, combined to the weak molecule-graphene interactions in determining the molecular adsorption geometry, we performed an STM analysis at the liquid/solid interphase, both on epitaxial graphene/SiC(0001) and HOPG.

A 4-8 μl drop of a concentrated solution (2M) of TTC_{12} -TTF in 1-phenyloctane was deposited on the G/SiC(0001) or HOPG surfaces held at room temperature. The imaging was performed at room temperature, by means of a mechanically cut Pt/Ir tip. Representative images are reported in **Figure 2.4** and **Figure 2.5**.

A highly concentrated solution was employed in order to establish if it was possible to drive an edge-on absorption conformation by fastening of the alkyl chains even in presence of a solvent, by playing on the molecular concentration. D. Amabilino, in fact, had observed a flat absorption geometry of dodecylthio-functionalized TTFs by STM before¹⁵, on HOPG at the liquid/solid interphase. The solvent employed in this study was, as well, phenyloctane and the concentration of the solution was much more diluted, 10^{-3}M . In order to investigate the role of the substrate in determining the molecular conformation on the surface, we realized STM images also on a epitaxial graphene/SiC(0001) surface.

In **Figure 2.4** the STM-images of TTC_{12} -TTF (**2.1**) in phenyloctane on G/SiC(0001) are reported. Despite the relatively important instrumental drift, causing the molecules to appear in the images as elongated features, it is possible to identify by STM a flat geometry for the TTC_{12} -TTF-cores adsorption. This observation suggests that it is not the substrate (through a different possible polarization effect) that induces the edge-on molecular conformation in UHV, but it is rather the liquid environment which stabilizes a flat core-adsorption configuration.

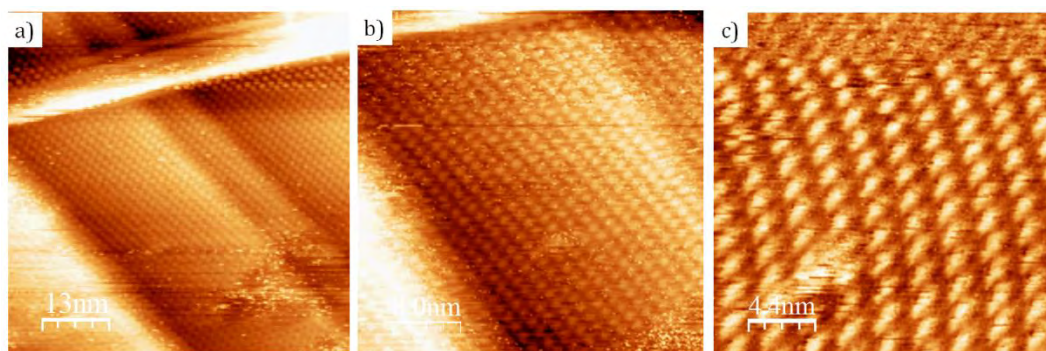


Figure 2.4 : (Preliminary) STM images of TTC_{12} -TTF (xx) on G/SiC(0001) in 1-phenyloctane: a) $U_t = -1\text{V}$, $I_t = 40\text{ pA}$, $66.4 \times 66.4\text{ nm}^2$; b) $U_t = -1\text{V}$, $I_t = 40\text{ pA}$, $40 \times 40\text{ nm}^2$; c) $U_t = -1\text{V}$, $I_t = 40\text{ pA}$, $21.9 \times 21.9\text{ nm}^2$. The molecules are lying flat on the surface.

In order to get further insight, the experience reported in reference 6 was repeated, by employing a more concentrated solution respect that reported in the published study (2M vs 10^{-3}M). The images at the phenyloctane/HOPG interface are reported in **Figure 2.5**.

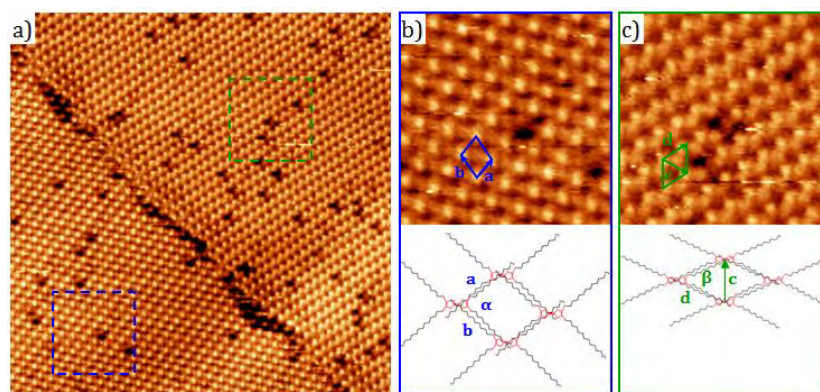


Figure 2.5 : a) STM topographic image of two domains of self-assembled **TTC₁₂-TTF (2.1)** molecules in 1-phenyloctane (2M) on HOPG ($U_t = -1.1V$ and $I_t = 7$ pA, $70 \times 70 \text{ nm}^2$); b) and c) zoom of the domains ($U_t = -1.1V$ and $I_t = 7$ pA, $15 \times 15 \text{ nm}^2$) with the corresponding molecular assembly scheme. The C_6S_8 cores of the molecules are drawn in red. The **TTC₁₂-TTF** molecules are lying flat on the substrate. Unit-cell parameters: $a = 1.54 \pm 0.04$ nm, $b = 1.87 \pm 0.18$ nm and $\alpha = 73^\circ \pm 4^\circ$; $c = 1.55 \pm 0.03$ nm, $d = 1.90 \pm 0.20$ nm and $\beta = 65^\circ \pm 2$.

Even in conditions of very high molecular concentration, it is confirmed that at the solid-liquid interphase, the obtained self-assembled systems are characterized by a totally different structure, with respect those obtained in UHV. The molecules absorb with a flat core geometry, in two configurations characterized by the same unit-cell parameters (**Figure 2.5**). The four alkyl chains give an epitaxial interaction with HOPG giving rise to a porous structure, stabilized by interaction with the solvent molecules. The « fastener effect » is not observed, likely as a consequence of the fact that the interdigitation of the alkyl-chains is made less energetically favourable, due to the presence of the 1-phenyloctane solvent.

2.6 Conclusions

A tetrathiofulvalene derivative functionalized with four $C_{12}H_{25}$ alkyl chains, **TTC₁₂-TTF**, has been synthesized by a literature procedure, with a 9% yield over three steps.

Its self-assembling properties have been studied by STM in UHV on a epitaxial graphene/SiC(0001) surface and at the solid/liquid interphase on HOPG and epitaxial graphene/SiC(0001). The studies in UHV have revealed an edge-on molecular conformation, with **TTC₁₂-TTFs** forming parallel lines tightly packed on the surface. The van der Waals interactions between the long alkyl chains force the cores to form π - π stacked aggregates between themselves, rather than interacting with graphene;. This alkyl chains-induced « fastener effect »⁵ has been observed before in bulk molecular crystals, but our observation represents the first one at molecular scale, where the « fastener effect » is induced by the combination of UHV conditions and *weak molecular interaction* with a surface. The molecular electronic structure is not perturbed upon absorption and a 1D conduction is expected along the

wires¹⁵. Graphene in vacuum appears thus to be an ideal template for the generation of extended conducting alkyl-TTF based molecular wires.

The studies at the liquid/solid interphase have allowed to investigate the different roles of the environment (UHV or liquid) and substrates (HOPG or G/SiC(0001)) in determining the molecular conformation upon adsorption. In particular, both on HOPG and G/SiC(0001), in 1-phenyloctane, a flat absorption geometry has been observed, with the TTF cores giving π - π interactions with the surface. This behaviour has been rationalized by considering the role of the solvent in stabilizing the pore-structure and preventing the alkyl chains interdigitation.

2.7 References

- ¹ Segura, J. L., Martín, N., *Angew. Chem. Int. Ed.*, **2001**, *40*, 1372-1409.
- ² Canevet, D., Sallé, M., Zhang, G., Zhang, D., Zhu, D., *Chem. Comm.*, **2009**, 2245-2269.
- ³ Garnier, J., Kennedy, A. R., Berlouis, L. E. A., Turner, A. T., Murphy, J. A., *Beilstein. J. Org. Chem.*, **2010**, *6*, 73.
- ⁴ Kobayashi, Y., Yoshioka, M., Saigo, K., Hashizume, D., Ogura, T., *J. Am. Chem. Soc.*, **2009**, *131*, 9995-10002.
- ⁵ Inokuchi, H., Saito, G., Wu, P., Seki, K., Tang, T. B., Mori, T., Imaeda, K., Enoki, T., Higuchi, Y., Inaka, K., Yasuoka, N., *Chem. Lett.* **1986**, *15* 1263-1266.
- ⁶ Puigmartí-Luis, J., Minoia, A., Uji-i, H., Rovira, C., Cornil, J., De Feyter, S., Lazzaroni, R., Amabilino, D. B., *J. Am. Chem. Soc.*, **2006**, *128*, 12602-12603.
- ⁷ Abdel-Mottaleb, M. M. S., Gomar-Nadal, E., Surin, M., Uji-i, H., Mamdouh, W., Veciana, J., Lemaur, V., Rovira, C., Cornil, J., Lazzaroni, R., Amabilino, D. B., De Feyter, S., De Schryver, F. C., *J. Mater. Chem.*, **2005**, *15*, 4601-4615.
- ⁸ Gomar-Nadal, E., Abdel-Mottaleb, M. M. S., De Feyter, S., Veciana, J., Rovira, C., Amabilino, D. A., De Schryver, F. C., *Chem. Comm.*, **2003**, 906-907.
- ⁹ Choudhury, D., Das, B., Sarma, D. D., Rao, C. N. R., *Chem. Phys. Lett.*, **2010**, *497*, 66-69.
- ¹⁰ Voggu, R., Das, B., Rout, C. S., Rao, C. N. R., *J. Phys. Condens. Matt.*, **2008**, *20*, 472204.
- ¹¹ Wawzonek, S., Heilmann, S. M., *J. Org. Chem.*, **1974**, *39*, 4, 511-514.
- ¹² McCullough, R. D., Petruska, M. A., Belot, J. A., *Tetrahedron*, **1999**, *55*, 9979-9998.
- ¹³ Saito, G., Yoshida, Y., Murofushi, H., Iwasawa, N., Hiramatsu, T., Otsuka, A., Yamochi, H., Isa, K., Mineo-Ota, E., Konno, M., Mori, T., Imaeda, K., Inokuchi, H., *Bull. Chem. Soc. Jpn.*, **2010**, *83*, 4, 335-344.
- ¹⁴ J.T. Sun, Y.H. Lu, W. Chen, Y.P. Feng, A.T.S. Wee, *Phys. Rev. B*, **2010**, *81*, 155403.
- ¹⁵ Puigmartí-Luis, J., Minoia, A., Lei, S., Geskin, V., Li, B., Lazzaroni, R., De Feyter, S., Amabilino, D. B., *Chem. Sci.*, **2011**, *2*, 1945-1951.

Chapter 3

Synthesis of a hexaphenanthrocoronene derivative

3.1 Introduction

3.1.1 Polycyclic Aromatic Hydrocarbons (PAHs)

Polycyclic Aromatic Hydrocarbons (PAHs) are defined as compounds constituted by fused aromatic rings¹. Their presence in nature is related to an incomplete combustion phenomenon of different carbon-containing materials (wood, fuel, coal, fat, tobacco...). They are considered as organic pollutants and the carcinogenicity of some compounds has already been proven.

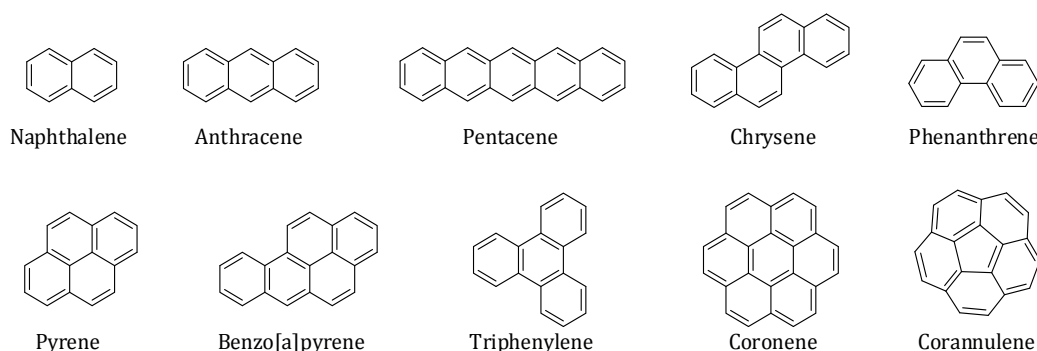


Figure 3.1: Examples of common PAHs.

3.1.1.1 Properties and applications

The attention towards this class of molecules is motivated by both theoretical curiosity and applied interests. On one side, PAHs and their functionalized derivatives have offered and still offer a nice platform for studying and further developing theories onto the “aromaticity” concept². On the other hand, the original optoelectronic and electronic properties render them good candidates for being employed in many fields of nanotechnology and materials sciences³, such as liquid crystals⁴ and organic semiconductors⁵ that could be employed, for example, in the design of new photovoltaic cells, field effect transistors, light emitting diodes³... Even the possibility of employing some PAHs to execute logic operations in molecular electronic devices has already been taken into account⁶.

A second appealing aspect is that PAHs can be considered as precursors of carbon materials such as graphene, fullerenes and carbon nanotubes⁷⁻¹¹. Bottom-up synthesis would represent a convenient alternative to currently mostly employed production strategies, offering

the advantage of an atomically precise control on the final structure, bearing an influence on the chemical and electronic properties of the materials.

3.1.1.2 Synthesis of PAHs

Since the first pioneering studies by R. Scholl, E. Clar and M. Zander, at the beginning of the last century¹², large improvements have been implemented and the synthesis of various PAHs under relatively mild conditions is now possible^{1,3}.

Among all the approaches that have been proposed, especially worth noting, considering the complexity of the structures that can be obtained, are the strategies based on aryne chemistry proposed by D. Peña, allowing the synthesis of extended cata-fused systems¹³ and the synthesis of non-planar fullerenes precursors, for which the key step is a palladium-catalysed intramolecular arylation, proposed by A. Echavarren¹⁴ (**Figure 3.2**).

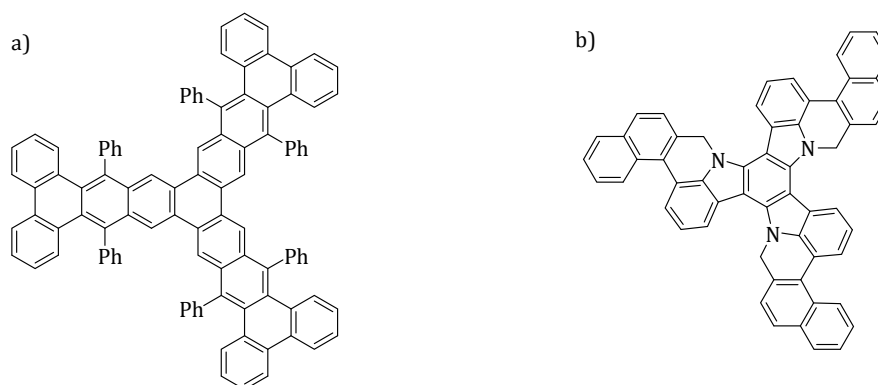


Figure 3.2: Examples of PAHs: a) substituted[16]clovophene (5.5.5)^{13b}; b) triaza analogue of truxene¹⁴.

3.1.1.3 Synthesis of hexabenzocoronene derivatives

However, the greatest impulse to the development of PAH chemistry has been offered by the group of K. Müllen, which implemented a large number of protocols leading to the synthesis of different functionalized and not-functionalized hexa-*peri*-hexabenzocoronenes (HBCs) derivatives^{1,3, 15}.

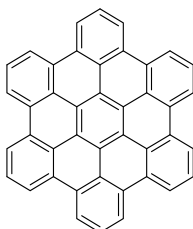
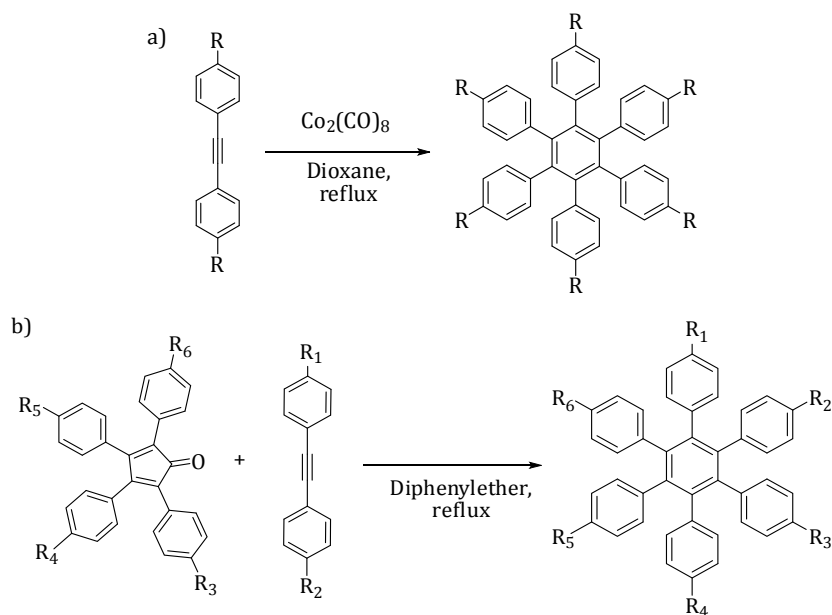


Figure 3.3: Hexa-*peri*-hexabenzocoronene

In general, the synthetic approach applied by Müllen's group can be analysed by decomposing it into two main "steps":

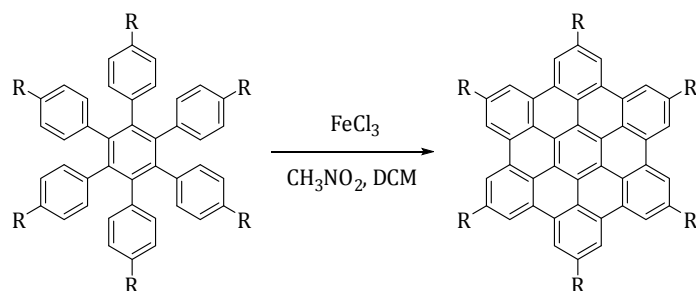
1) *Synthesis of a hexabiphenylbenzene precursor:*

A precursor with a hexabiphenylbenzene structure is synthesized by either cobalt-catalysed cyclotrimerization¹⁶ of functionalized diphenylacetylenes (**Scheme 3.1a**); or [4+2] Diels-Alder cycloaddition of tetraarylcyclopentadienones with diphenylacetylenes, followed by an in-situ decarbonylation⁴ (**b**). Normally, the choice of the cyclotrimerization method is privileged for the synthesis of D₆ symmetrical HBCs¹.



Scheme 3.1: Two alternative procedures affording hexabiphenylbenzenes: a) cobalt catalysed catalytic cyclotrimerization ($\text{R} =$ alkyl, ester, aryl, halogen...); b) Diels-Alder cycloaddition ($\text{R}_{1-6} =$ alkyl, ester, aryl, halogen...).

The hexabiphenylbenzene's geometry is planarized by an oxidative cyclodehydrogenation reaction to give the fully conjugated HBC. The reaction can be performed under Lewis acidic conditions (Scholl oxidation)¹⁷ (**Scheme 3.2**).

2) *Oxidative cyclodehydrogenation:*

Scheme 3.2: Cyclodehydrogenation reaction affording hexa-*peri*-hexabenzocoronenes ($\text{R} =$ alkyl, ester, aryl, halogen...).

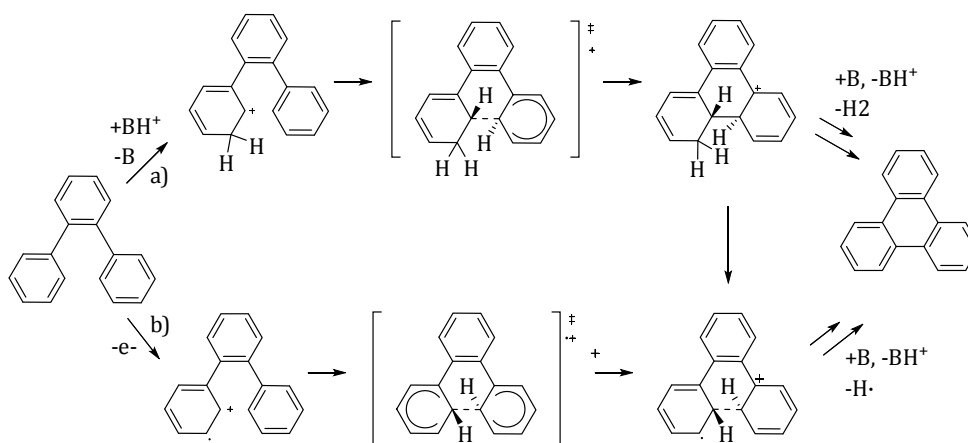
The reaction is carried out at room temperature and the most commonly employed catalytic systems for the Scholl oxidation are¹⁸:

- Copper(II) chloride/ aluminium(III) chloride ($\text{CuCl}_2/\text{Al}_2\text{Cl}_3$) in carbon disulfide at 25°C;
- Copper(II) trifluoromethanesulphonate / aluminium(III) chloride ($\text{Cu}(\text{OTf})_2/\text{Al}_2\text{Cl}_3$) in carbon disulphide at 25°C;
- Iron(III) chloride (FeCl_3) in dichloromethane/nitromethane (9:1) at 25°C.

FeCl_3 has been proven superior reagent compared to the others, suffering less from the disadvantages due to eventual chlorination, dealkylation or migration of alkyl substituents. Moreover, FeCl_3 renders unnecessary the employ of additional oxidants, its oxidation potential being high enough for the C-C bond formation³.

Another possibility, suggested by R. Rathore¹⁹, implies the utilization of 2,3-dichloro-5,6-dicyano-1,4-benzoquinone (DDQ)/ acid (for example trifluoroacetic, trifluoromethanesulfonic, methanesulfonic acid...) as oxidizing system at 0°C in dichloromethane. This methodology appears very convenient, affording highly pure cyclodehydrogenated products, not suffering from chlorination issues. The weak point consists in the possibility of oxidation only of electron rich precursors, with oxidation potential as high as 1.7 V vs SCE²⁰.

The interpretation of the oxidative cyclodehydrogenation mechanism is controversial. The reaction is assumed to occur through a stepwise cyclization process, but the debate is still centred on whether a radical cation²⁰ or arenium cation intermediate²¹ are implied (**Scheme 3.3**).



Scheme 3.3: (a) Arenium cation VS (b) radical cation o-terphenyl condensation pathways (from reference 21).

By applying different variations of the methodology described in **Scheme 3.1** and **3.2**, K. Müllen and his group managed the synthesis of different substituted and extended HBC

derivatives, even reaching the “record” of the largest PAH synthesized in solution reported in the literature: a HBC derivative constituted by 222 carbon atoms²². However, due to the low solubility of this kind of planar structures, due to the tendency to form π - π stacked aggregates, a further dimensional extension for structures synthesized in solutionⁱ seems unlikely²³.

3.1.1.4 Self-assembly of hexabenzocoronene derivatives on HOPG surfaces

Due to the high sublimation points of the HBCs derivatives, the self-assembly studies in UHV are limited to the smaller derivatives²⁴. However, a larger number of studies at the solid/liquid interface can be found in the literature²⁵. Both for the C6-symmetric HBC-C12 (**Figure 3.4a**) and the triangular shaped HBC-derivative (**Figure 3.4b**), at the liquid/HOPG interface, a *face-on* molecular conformation is observed, determined by the strong π - π interactions between the molecular cores and HOPG. The alkyl chains absorb on the surface in registry with the underlying graphite lattice. The symmetry of the final self-assembled structures depend on the molecular symmetry.

Interestingly, the HBC-C12 conformation can be switched from *face-on* to *edge-on* by previously absorbing a layer of *n*-pentacontane (n -C₅₀H₁₀₂) on the graphite surface^{25a}.

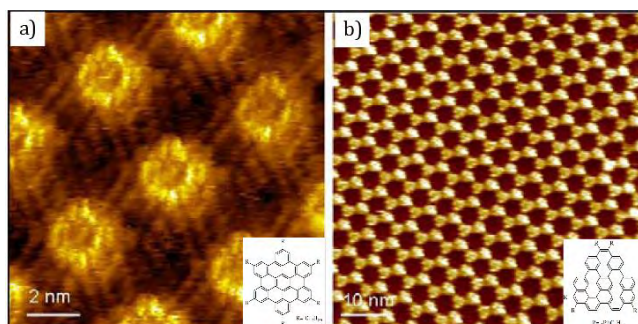


Figure 3.4: Self-assembly of HBC-C12 (a) and a triangle-shaped PAH (b) at the liquid/HOPG interface (from references 25 a and b).

3.2 Objective

Motivated by the interest of extending the study of the self-assembling properties of different hexabenzocoronene derivatives on epitaxial graphene/SiC(0001) in Ultra High Vacuum (UHV) conditions, we choose to carry out the synthesis of the derivative **hexaphenanthrocoronene 3.1** (**Figure 3.5**). The molecular structure was designed in order to keep the molecular cores isolated one from the others on the surface, thus allowing the possibility of studying the eventual single-molecule electronic interaction with graphene. The extended self-assembly is meant to stop the molecular diffusion and organize the cores on the

ⁱ Another possibility is to resort to “on-surface synthesis” techniques, see references 7-11.

surface. Being HBCs derivatives known for their electron donor properties⁴, we should be able to observe a n-doping effect on graphene/SiC(0001). The local doping should be modulated on a periodic scale, as a consequence of the organization of the electron donating cores on the surface.

3.3 Molecular design

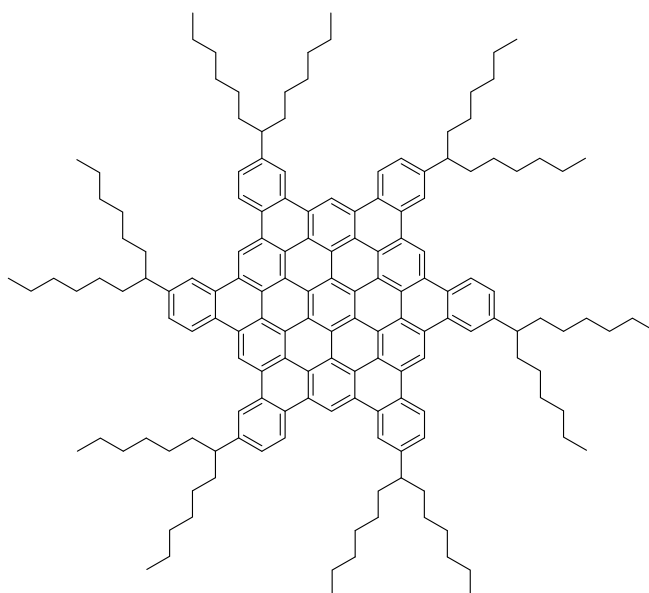
The **hexaphenanthrocoronene 3.1** that we have designed is characterized by the following structural features (**Figure 3.5**):

1) 25 fused benzene rings, for a total of 78 carbon atoms in the aromatic core. Due to the extended structure, the core is expected to give strong π - π interactions with the surface;

2) six “dove-tail” peripheral alkyl chains, completing two functions:

a) from a “chemical” perspective, they are meant to enhance the solubility of all the intermediates, “simplifying” the synthetic and purification procedures. It is in fact known that PAH derivatives are poorly soluble, due to the establishment of π - π interactions and this kind of alkyl chain tails are widely used in the literature as a way to improve their solubility¹⁵.

b) from a “physical” perspective, they are devised to drive the molecular organization on graphene by van der Waals interactions, leaving on the surface unfunctionalized pores.



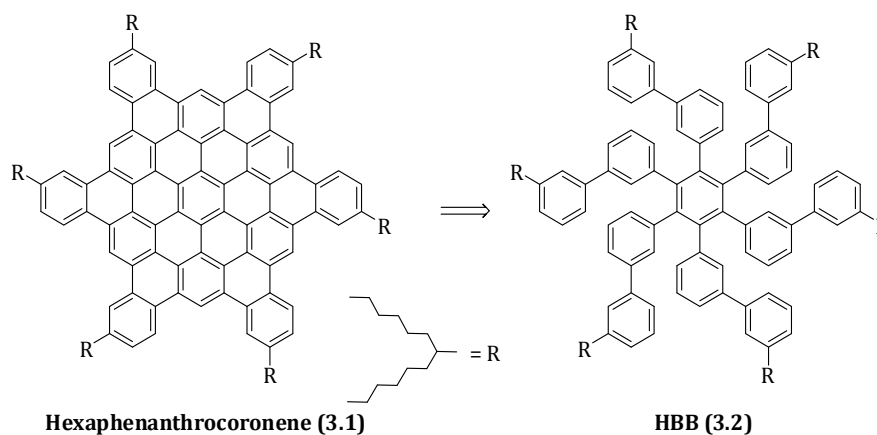
Hexaphenanthrocoronene (3.1)

Figure 3.5: Chemical structure of the **hexaphenanthrocoronene 3.1**.

3.4 Results and discussion

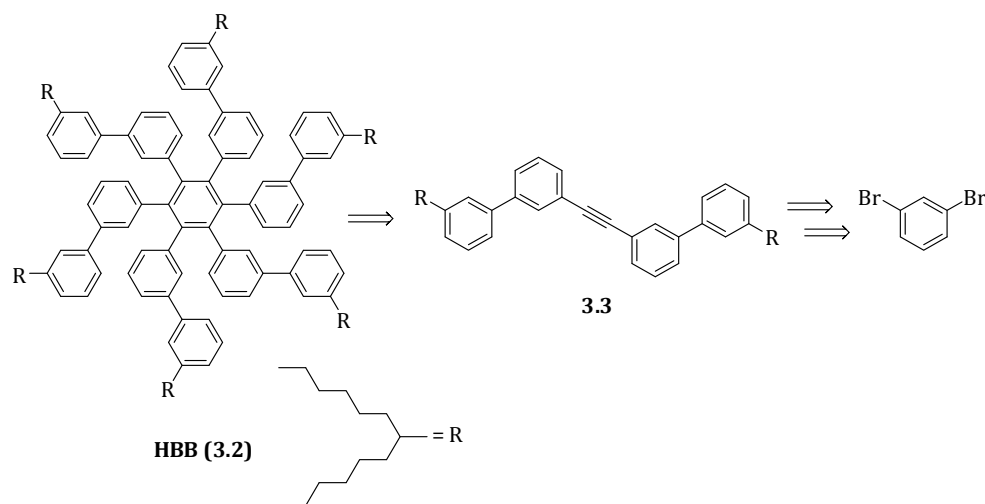
3.4.1 Retrosynthetic analysis

The **hexaphenanthrocoronene 3.1** can be disconnected in last analysis to the hexabiphenylbenzene precursor **HBB (3.2)**.



Scheme 3.4: Retrosynthetic analysis of the **hexaphenanthrocoronene 3.1**.

The symmetric hexabiphenylbenzene precursor **HBB (3.2)** can be disconnected to the alkyne-bearing precursor **3.3**^{16, 26}, deriving in last analysis from 1,3-dibromobenzene (**Scheme 3.5**).

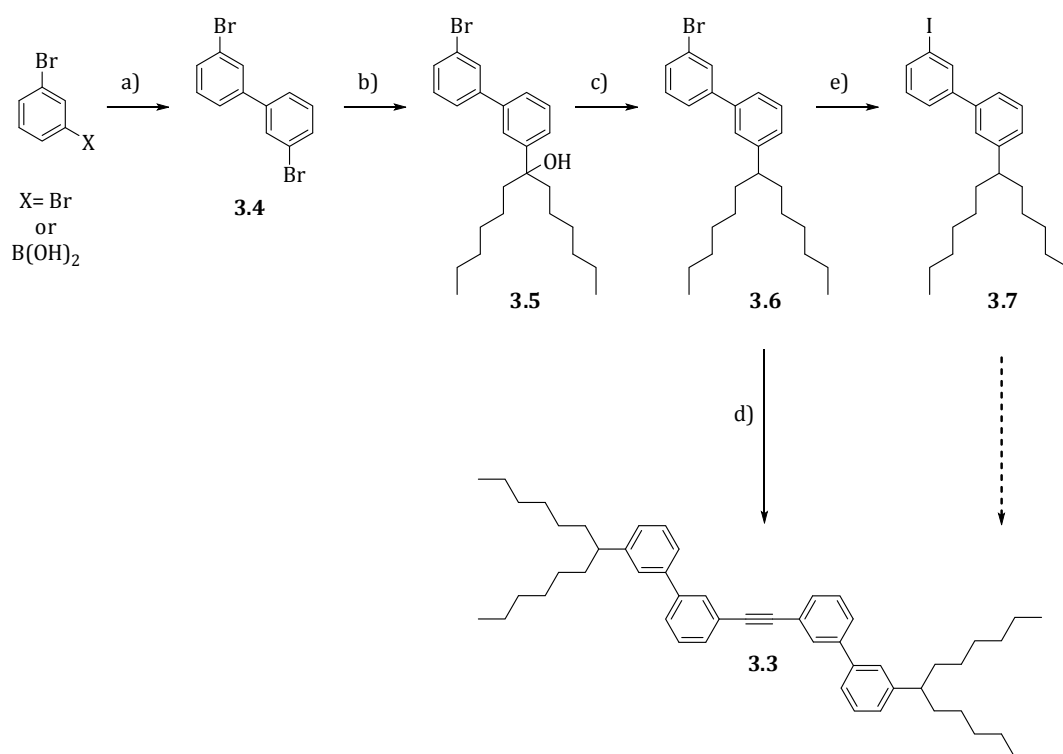


Scheme 3.5: Retrosynthetic analysis for the hexabiphenylbenzene precursor **HBB (3.2)**.

3.4.2 Synthesis

3.4.2.1 Synthesis of the alkyne precursor 3.3

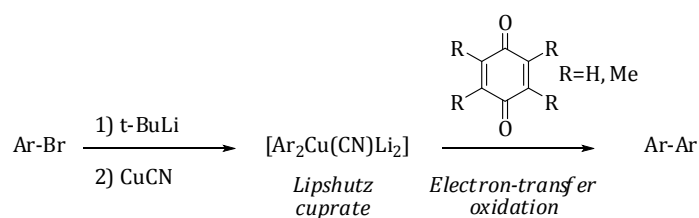
The synthesis of the alkyne precursor **3.3** was carried out following the approach summarized in **Scheme 3.6**.



Scheme 3.6: Synthesis of the alkyne precursor **3.3**. a) Homocoupling via a *Lipshutz cuprate* or Ullman reaction; b) Lithiation, then addition on dihexylketone; c) Reduction of the alcoholic function by triethylsilane; d) Bromine-iodine exchange, via lithiated intermediate or by copper/iodine catalysis, e) One-pot double Sonogashira

Step a)

In a first step, 1,3-dibromobenzene was homo-coupled to afford 3,3'-dibromobiphenyl **3.4**. The conditions for the synthesis were already reported in the literature²⁹. The formation of the new aryl-aryl bond was based on an *electron-transfer oxidation* reaction of a *Lipshutz cuprate*²⁷ by tetramethyl-p-benzoquinone (**Scheme 3.7**).

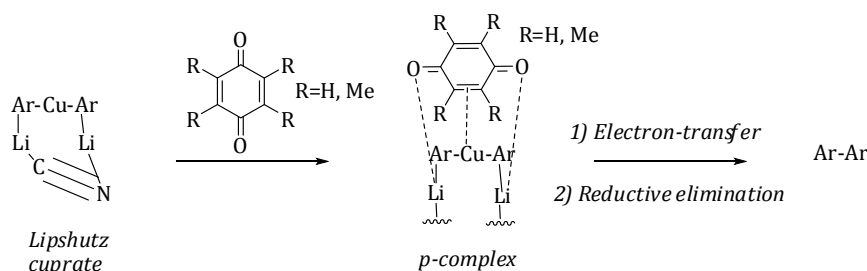


Scheme 3.7: Electron transfer reaction from Lipshutz cuprates to 1,4-benzoquinones to afford biaryls^{28,29}.

The mechanism of the coupling reaction can be rationalized in three steps (**Scheme 3.8**)²⁸: 1) the aryl lithium species derived from the aryl bromide (Ar-Br) reacts with copper cyanide, affording the *Lipshutz cuprate*; 2) the *Lipshutz cuprate* forms a π -complex with 1,4-benzoquinone (lithium...carbonyl and copper...olefin coordinations); 3) *electron transfer* occurs

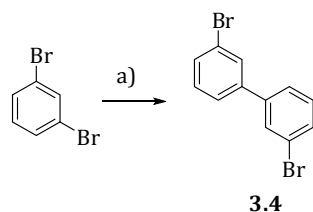
from the cuprate to 1,4-benzoquinone, to generate, after reductive elimination, the homocoupling product (Ar-Ar).

If it has been shown that *Lipshutz cuprate* reactants can be very efficiently oxidized thanks to the linear structure of the C-Cu(I)-C bond, allowing an efficient complexation to 1,4-benzoquinones²⁹, the exact mechanism of electron transfer is not clear. Experimental evidences point towards the hypothesis of the formation of a semiquinone radical anion that would re-oxidize to 1,4-benzoquinone under the employed work-up conditions, rather than leading to the formation of 1,4-hydroxyquinone²⁹.



Scheme 3.8: Electron transfer reaction from Lipshutz cuprates to 1,4-benzoquinones to afford biaryls^{28,29}.

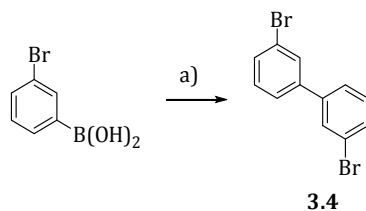
In our case (**Scheme 3.9**), the Lipshutz cuprate was generated by treatment of the 1,3-dibromobenzene with 1.1 equivalents of *tert*-butyllithium in dry diethyl ether at low temperature (T=-78°C), followed by the addition of 0.5 equivalents of copper cyanide (T=-60°C).



Scheme 3.9: Synthesis of the precursor **3.4**. Conditions: a) i: *t*-BuLi (1.1 eq.), dry Et₂O, -78°C, 1.5h; ii: CuCN (0.5 eq.), 22°C, 5 mins.; iii: tetramethyl-*p*-benzoquinone (1.4 eq.), 23°C, 3h, 89%.

The addition of 1.5 equivalents of tetramethyl-*p*-benzoquinone (T=22°C) allowed over 3 hours the oxidation of the cuprate, to give product **3.4** as a white solid, after silica gel column chromatography purification (hexane), in good yields (89%). It is interesting to note that the reaction could be conducted on a ten grams scale, provided to keep the aryl-bromide concentration lower than 0.08 Mⁱⁱ.

ⁱⁱ In the reference paper (reference 29) it is suggested to employ 0.02 M as concentration, but we needed to work with higher concentrations to adapt the procedure to our laboratory glassware.

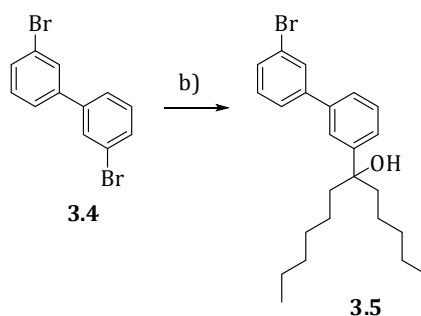


Scheme 3.10: Synthesis of the precursor **3.4**. Conditions: a) CuCl (2%), MeOH, 19h, 21°C, 63%.

A second, more convenient, procedure to afford **3.4** consisted in the Ullmann homo-coupling of 3-bromophenylboronic acid³⁰ (**Scheme 3.10**). The reaction was conducted in methanol, in the presence of 2% of copper chloride. The product could be recovered as a white solid with a column chromatography on silica gel, employing hexane as eluent, with a 63% yield. The reaction could be carried out in a multigram scale as well (10 gr or over).

Step b)

The second step (**Scheme 3.11**) allowed the insertion of a C6 “dove-tail” alkyl chain on 3,3'-dibromobiphenyl **3.4**. The experimental procedure consisted in activating one aryl carbon atom by lithium-bromine exchange and reacting it with dihexylketone, in a carbonyl addition reaction, to afford alcohol **3.5**, after aqueous work-up. The lithium source employed was *n*-butyllithium in solution 1.4 M in hexane (the concentration was determined by titrating a solution of diphenylacetic acid³¹) and the addition to **3.4** was conducted at -78°C in dry diethyl ether. One equivalent of *n*-butyllithium was employed in order to avoid the formation of the product of bi-substitution of the bromines. Dihexylketone (1.05 equivalents) was added to the reaction mixture at 45°C in solution of dry diethyl ether at room temperature (21°C), then the reaction mixture let to warm at 21°C and to stir for 17 hours.



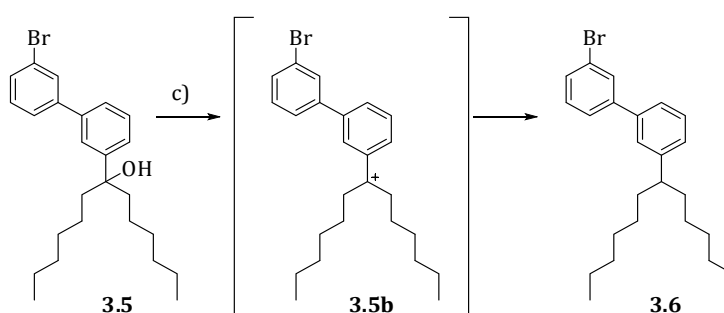
Scheme 3.11: Synthesis of the precursor **3.5**. Conditions: b) i: *n*-BuLi (1 eq.), dry Et₂O, -78°C, 45 mins.; ii: dihexylketone (1.05 eq.), dry Et₂O, -45°C -> 21°C, 17h, 69% wt/wt (impure at 5.4%).

The recovery of pure alcohol **3.5** was possible by column chromatography purification: hexane was employed as eluent, then hexane : dichloromethane 8:2 on silica gel. The purification procedure was not straightforward due to the presence of an impurity of the same polarity

(identified as unreacted dihexylketone, by mass spectrometry). Since the impurity (5.4 % from NMR analysis) was not representing a possible interferent in the following step^{iii,32}, the purification conditions were not further improved and the synthesis carried on on the impure compound **3.5**.

Step c)

The alcohol **3.5** was reduced to **3.6** by employing triethylsilane as hydride donor and trifluoroacetic acid as dehydrating reagent in dry dichloromethane at low temperature (**Scheme 3.12**).



Scheme 3.12: Synthesis of the precursor **3.6**. Conditions: c) Et₃SiH (3 eq.), TFA (3 eq.), CH₂Cl₂ dry, -35°C-0°C, 3h, 78% yield.

Experimentally, trifluoroacetic acid (3 equivalents) was added dropwise to a pre-cooled solution of **3.5** (1 equivalent) and triethylsilane (3 equivalents) in dry dichloromethane: this procedure allowed to generate the carbocation^{iv,33} **3.5b** directly in presence of the hydride donor, thus favouring the reduction (S_N1) versus the possible elimination (E₁) reaction (originating **3.6b**, **Scheme 3.13**). Two sets of temperature were tested: 1) addition of trifluoroacetic acid at -15°C, reaction conducted at -15°->0°C; 2) addition of trifluoroacetic acid at -35°C, reaction conducted at -35°->0°C. In the first case, a certain amount of elimination subproduct **3.6b** was obtained (**Scheme 3.13**): the ratio between the quantity of the products **3.6** and **3.6b** was estimated from the ¹H-NMR spectrum to be 4:1 and the yield of **3.6** was calculated to be 67% in weight^v. The desired product **3.6** could be isolated from the subproduct **3.6b** by preparative flash-chromatography purification on reversed phase (water/acetonitrile 8:2) or by supercritical fluid chromatography purification (with 15% of petroleum ether)^{vi}. In

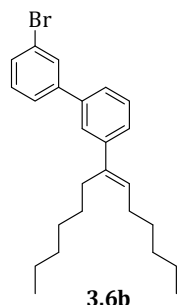
ⁱⁱⁱ In step c) triethylsilane was employed as reducing agent and silanes appear to be able to undergo hydride transfer only to relatively stable carbenium ions (i. e. benzylic), see reference iii.

^{iv} It has been established that the reduction mechanism is based on the formation of a carbocation and hydride transfer from silanes cannot occur to a simply protonated alcohols.

^v The yield was expressed in weight percentage since the starting material was not a pure compound.

^{vi} The HPLC-purification was carried out by Ms Chantal Zedde at the HPLC service of Paul Sabatier University (Toulouse).

the second case, **3.6b** was not formed in appreciable quantity and the yield of **3.6** was estimated to be of 78%, after a simple filtration on silica employing hexane as eluent.

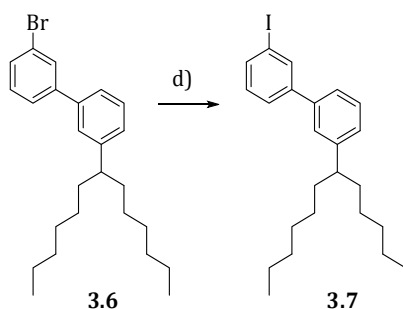


Scheme 3.13: Subproduct deriving from the elimination pathway, isolated during the synthesis of **3.6**.

Step d)

At the same time, we decided to exchange the halogen from bromine to iodine on **3.6** in order to evaluate if the outcome of the Sonogashira reaction on the iodurated substrate **3.7** could be facilitated, respect to that on the less reactive bromo-compound **3.6**.

In a first attempt (**Scheme 3.14**) we devised to perform the halogen exchange by passing through an aryl-lithium intermediate: **3.6** was reacted with 1.1 equivalents of *n*-butyllithium (1.6 M in hexane) in dry diethyl ether at -78°C and the activated species was then quenched with iodine (two equivalents, previously solubilized in dry diethyl ether). The reaction appeared not to be very efficient in these conditions: in some cases, only unreacted **3.6** could be recovered; in others, only a small amount of iodinated product could be isolated (11% yield), together with the dehalogenated subproduct **3.6b**. No other iodine electrophiles (for ex. 1,2-diiodoethane) were tested.

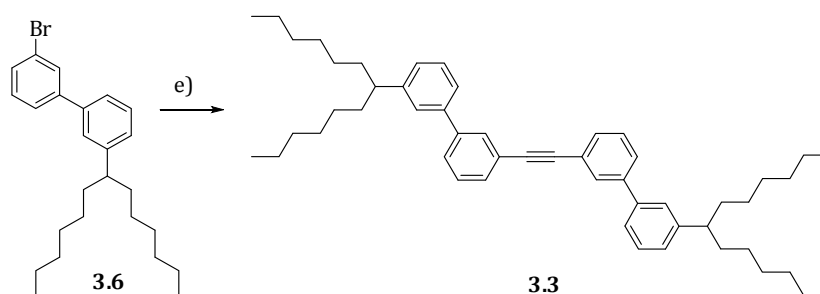


Scheme 3.14: d) i: *n*-BuLi (1.1 eq.), distilled THF, -78°C , 1.5h; ii: I_2 (2 eq.), distilled THF, 22°C , 1 h, 11%; or CuI (10%), NaI (2.5 eq.), (+/-)-trans-1,2-diaminocyclohexane (0.23 eq.), dry dioxane, 110°C , 70h, 89% wt/wt, 90% of **3.6**.

In a second attempt (**Scheme 3.14**), we devised to employ a copper catalyst in order to carry out the bromine-iodine exchange reaction (the so called “aromatic Finkelstein reaction”

³⁴³⁴). The activity of Cu(I) salts in activating aromatic nucleophilic substitution reactions on rather inert aromatic bromides by iodides was already object of study in the literature³⁵ and we applied the conditions optimized by Buchwald³⁴. The procedure implied the use of a catalytic amount of copper iodide (10%), sodium iodide (2.5 equivalents) and a diamine ligand to accelerate the halogen exchange reaction ((+/-)-trans-1,2-diaminocyclohexane, 22%) in dry dioxane, warming at 110°C for 70 hours. The quantity of desired product **3.7** that was recovered appeared interesting (89% wt/wt, 90% of **4** from NMR analysis), but since the Sonogashira coupling **e)** directly on the brominated derivative gave good yields with one step less, we did not pursue along this route.

Step e)



Scheme 3.15: Sonogashira reaction to afford **3.3** Conditions: e) TMSA (0.5 eq.), Pd(PPh₃)₂Cl₂ (6%), CuI (10%), DBU (6 eq.), H₂O (4 eq.), toluene dry, 80°C, 72h, 78%.

Compound **3.3** was synthesized by a double Sonogashira reaction starting from **3.6** (**Scheme 3.15**). The conditions adopted for the synthesis were adapted from those already described in the literature for similar compounds³⁶. This procedure appeared quite interesting allowing the possibility of performing the first Sonogashira coupling to **3.6** with trimethylsilylacetylene, deprotection of the alkyne and second Sonogashira coupling directly one-pot. Experimentally, bis(triphenylphosphine)palladium(II) dichloride (6%) and copper iodide (10%) were employed as catalytic system, in 1,8-diazabicycloundec-7-ene/ toluene (1 : 5.5), warming at 80°C for 72 hours. In order to promote the removal of the trimethylsilyl group, four equivalents of water were added. The product **3.3** could be obtained by an easy silica gel chromatographic purification (hexane) with a 78% yield.

3.4.2.2 Characterization of the alkyne **3.3**

The identity of the derivative **3.3** was confirmed by multinuclear (¹H and ¹³C) mono and bi-dimensional NMR spectroscopy and high-resolution mass spectrometry.

The assignment of the proton and carbon resonances was based on the crossed analysis of COSY, HSQC and HMBC spectra.

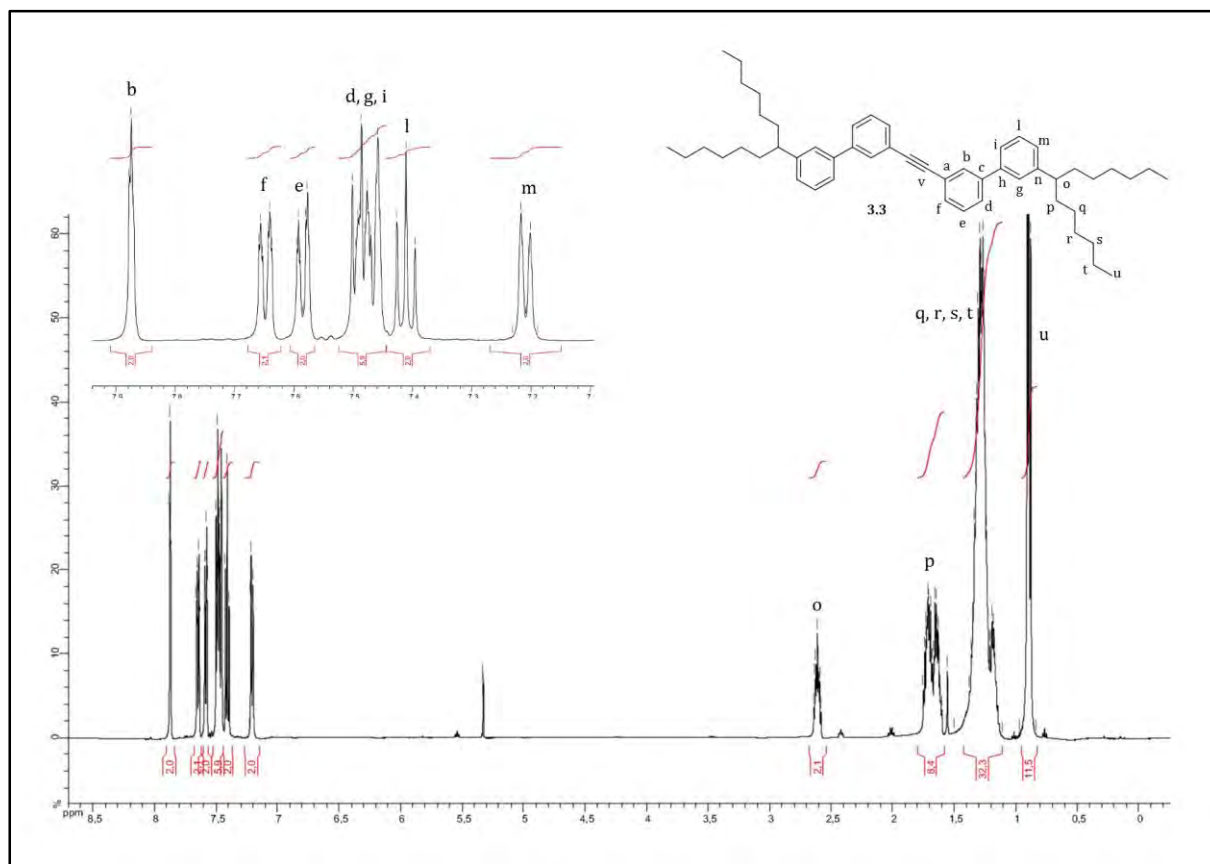


Figure 3.6: $^1\text{H-NMR}$ spectrum (500 MHz, CD_2Cl_2) of the precursor **3.3**.

The $^1\text{H-NMR}$ spectrum (500 MHz, CD_2Cl_2 , **Figure 3.6**) presented, as expected, signals characteristic of aromatic and alkyl protons. The multiplet integrating for two protons at 7.8-7.9 ppm was attributed to the protons H_b , experiencing more than the other aromatic protons the effect of deshield of the alkyne cone. The doublets integrating for two protons each at 7.65 and 7.59 ppm were attributed to the aromatic protons H_f and H_d , both coupling to H_e with an ortho coupling constant of 8 Hz; the resonance of H_e was instead localized in the multiplet at 7.4-7.6 ppm, together with the signals of the protons H_g and H_i . The protons H_l were resonating as a triplet at 7.41 ppm, characterized by an ortho coupling constant of 7.3 Hz, revealing its coupling to the doublet characteristic of H_m at 7.21 ppm. The multiplet at 2.5-2.6 ppm integrating for two protons was assigned to H_o . Other signals characteristic of the alkyl chains were the multiplet at 1.6-1.8 ppm, attributed to the eight methylenic protons H_p , the multiplet at 1.1-1.4 ppm, assigned to the thirty-two protons $\text{H}_{q,r,s,t}$ and finally the multiplet of the twelve terminal methyl protons at 0.8-1.0 ppm.

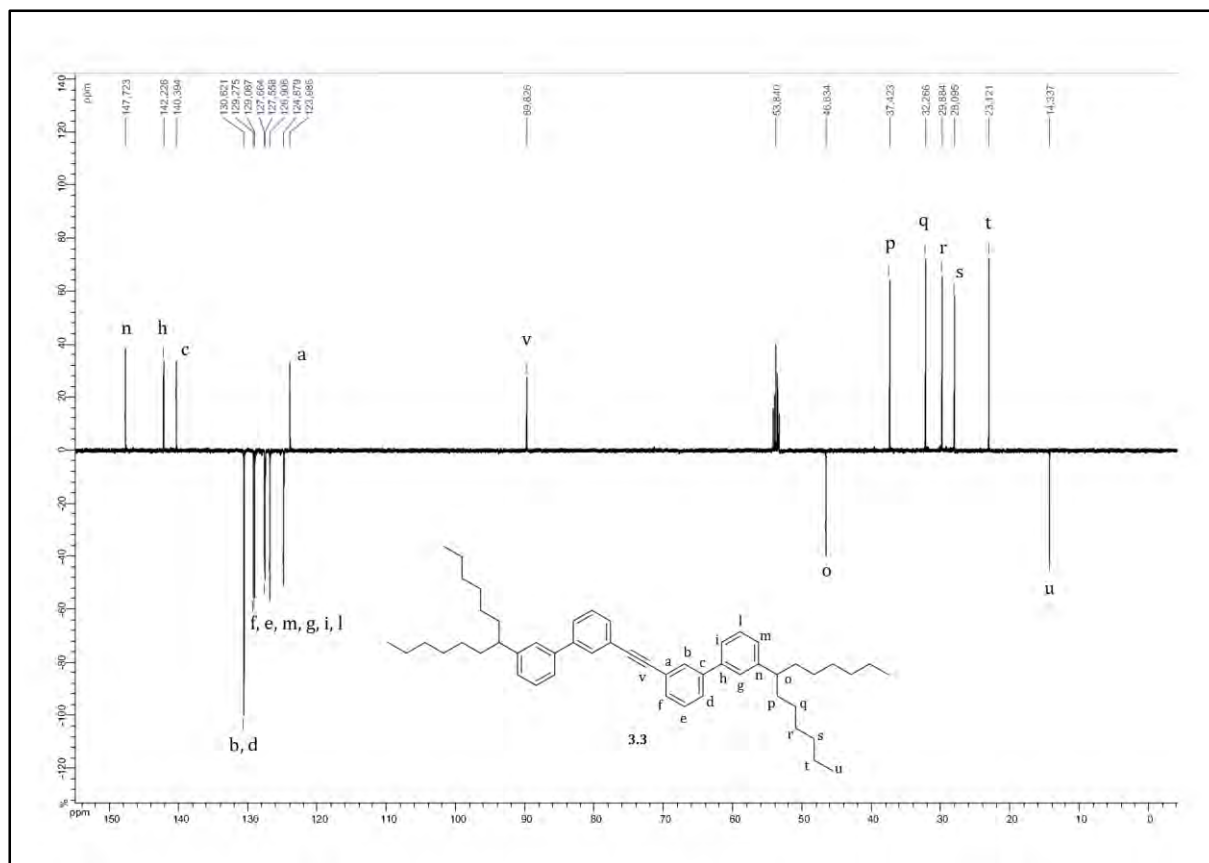


Figure 3.7: ^{13}C -NMR spectrum (125 MHz, CD_2Cl_2) of the alkyne precursor **3.3**.

The ^{13}C -NMR spectrum (125 MHz, CD_2Cl_2 , **Figure 3.7**) was recorded by a “J-modulation” experiment, which outcome is that ternary (CH) and primary carbons (CH_3) are characterized by an opposite phase respect to quaternary and secondary (CH_2) ones. This experiment appeared a useful help in the assignment procedure, quite complex considering the molecular structure. In our case, the solvent dichloromethane was characterized in the spectrum by a positive phase signal, implying that quaternary and secondary protons have a positive phase while primary and tertiary protons a negative one.

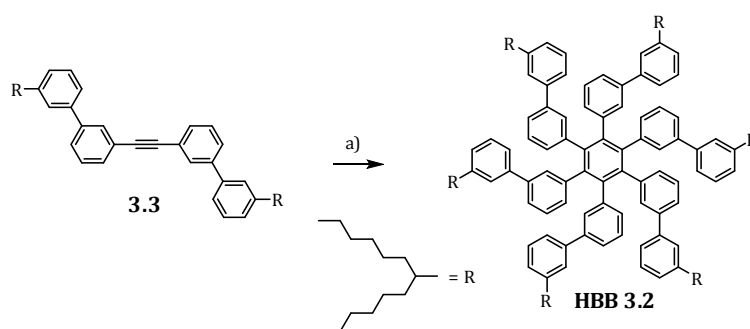
The signals with positive phase at δ 147.7, 142.2 and 140.4 ppm were attributed respectively to the C_n , C_h and C_c quaternary carbons and 123.9 ppm was assigned to C_a carbon (the most deshielded quaternary aromatic carbon, due to the alkyne shielding-cone). The other signals in the region 124.9-130.6 ppm, presenting a negative phase, were characteristic of the aryl tertiary carbons (CH) and could not be attributed unambiguously due to the low resolution of the HMBC spectrum: δ 130.6 ppm was assigned to C_b and C_d ; δ 129.1 and 129.3 to C_f and C_e ; δ 127.6 and 127.7 ppm to C_m and C_g ; δ 124.9 and 126.9 ppm to C_i and C_l . The positive phase signal at 89.8 ppm was assigned to the quaternary C_v alkyne carbons. As for the alkyl chains, the two negative phase signals at 46.6 and 14.3 ppm were respectively attributed to the ternary carbon C_o and the primary methylic carbon C_u , while the other positive phase signals in the region 23.1-

37.4 ppm were characteristic of the methylenic carbons: 37.4 ppm for C_p , 32.3 ppm for C_q , 29.9 for C_r , 28.09 for C_s , 23.1 for C_t .

The high resolution mass spectra (DCI- CH_4 ionization source and time of flight analyser) confirmed further the identity of the product, showing a molecular peak at m/z 694.5494, corresponding to the radicalic species $[M]^+$ (calculated value: 694.5478).

3.4.2.3 Cyclotrimerization affording HBB 3.2

With **3.3** in hands, the precursor **HBB 3.2** could be synthesized by the procedure summarized in **Scheme 3.16**.



Scheme 3.16: Cyclotrimerization to afford **HBB 3.2**. Conditions: a) $Co_2(CO)_8$ (5%), dioxane dry, 111°C, 40h, 72%.

3.3 was submitted to a catalytic cyclotrimerization reaction employing 5% of cobalt carbonyl as catalyst³⁷, in dry degassed dioxane for 40 hours at 111°C, in an argon atmosphere (**Scheme 3.16**). The long reaction time appeared to be a requisite to promote the conversion of the highly sterically hindered **3.3** to **HBB 3.2**: for lower reaction times (for example 21 hours), only the unreacted alkyne precursor **3.3** could be recovered (38%), together with some unidentified subproducts. After the reaction, the raw mixture was let to stir at air in order to oxidize the catalyst from Co(0) to Co(II), to facilitate its removal, then filtered on silica gel. In most of the cases, the raw product obtained contained still some impurities of catalyst, showing an aspect of purple oil. The impurities were identified by the characteristic carbonyl signals in ^{13}C -NMR (signal at ~200 ppm) and FT-IR spectra (bands at 1800-2100 cm^{-1})³⁸. The ability of cobalt to form stable aryl complexes is, in fact, known³⁸. In order to favour the decomplexation of cobalt, the raw product was stirred in diethylamine at room temperature^{vii}. **HBB 3.2** could finally be purified by two chromatographies on silica gel (hexane: dichloromethane 94:6 and flash chromatography in petroleum ether) and obtained as a colorless oil with 72% yield.

^{vii} The instability of arene-cobalt complexes towards nucleophiles is known.

3.4.2.4 Characterization of HBB 3.2

The derivative **HBB 3.2** was completely characterized by multinuclear (^1H and ^{13}C) mono and bi-dimensional NMR spectroscopy and high-resolution mass spectrometry.

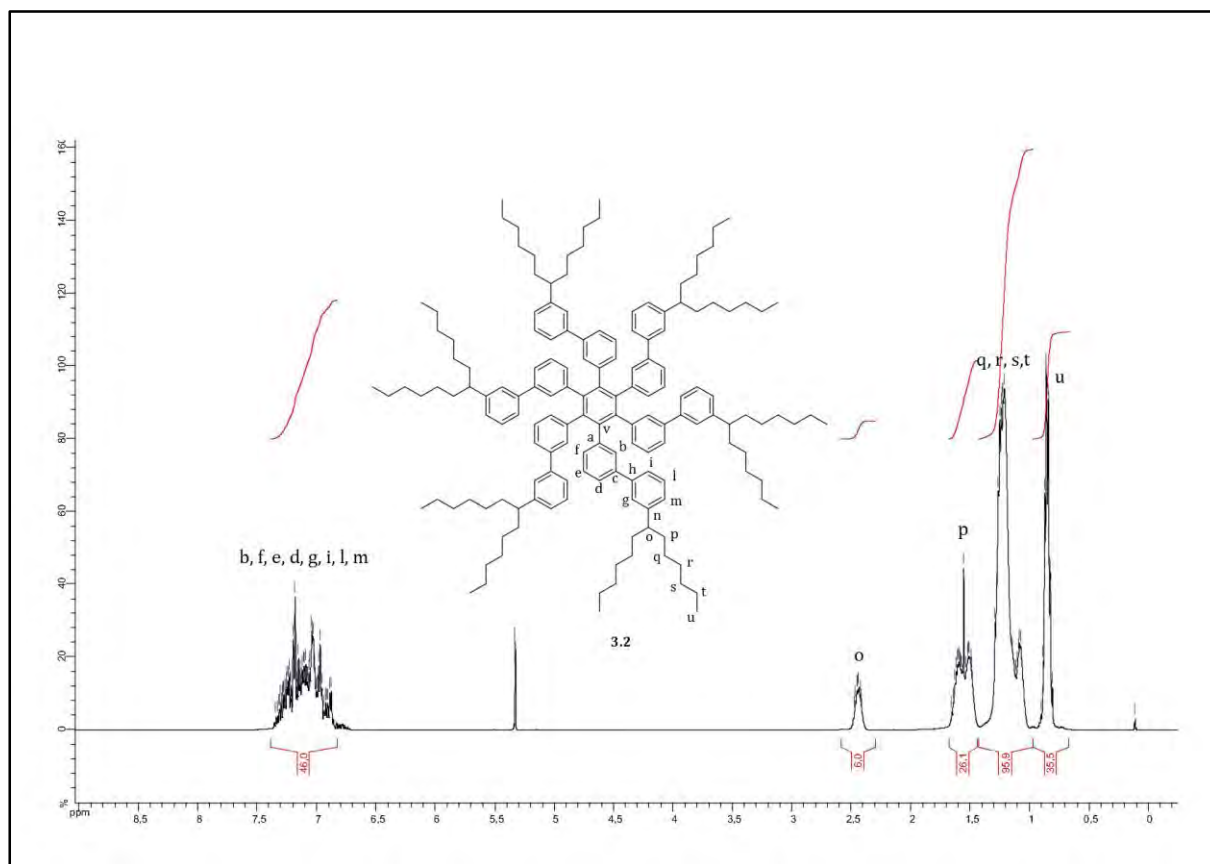


Figure 3.8: ^1H -NMR spectrum (500 MHz, CD_2Cl_2) of the precursor **HBB 3.2**.

The ^1H -NMR spectrum (500 MHz, CD_2Cl_2 , **Figure 3.8**) presented a series of multiplets, in the aromatic and alkyl chain regions. The complexity of the spectrum is due to the twisting of phenyls determining that each proton in the molecule is experiencing a different chemical environment (the rotations of the phenyls are hindered).

The signals present in the spectrum were: one multiplet integrating for all the forty-eight aromatic protons in the region 6.8-7.4 ppm; the signal of protons H_o at 2.3-2.5 ppm, integrating for six protons; a multiplet at 1.5-1.7 ppm, attributed to the twenty-four methylenic protons H_p ; the multiplet at 1.1-1.3 ppm, integrating for the ninety-six protons of the alkyl chains ($\text{H}_{q,r,s,t}$) and finally the multiplet at 0.8-0.9 ppm, attributed to the thirty-six terminal methyl protons H_u . The correct integration ratio allowed to assess the correct chemical structure of the compound obtained, which was further confirmed by ^{13}C -NMR spectroscopy.

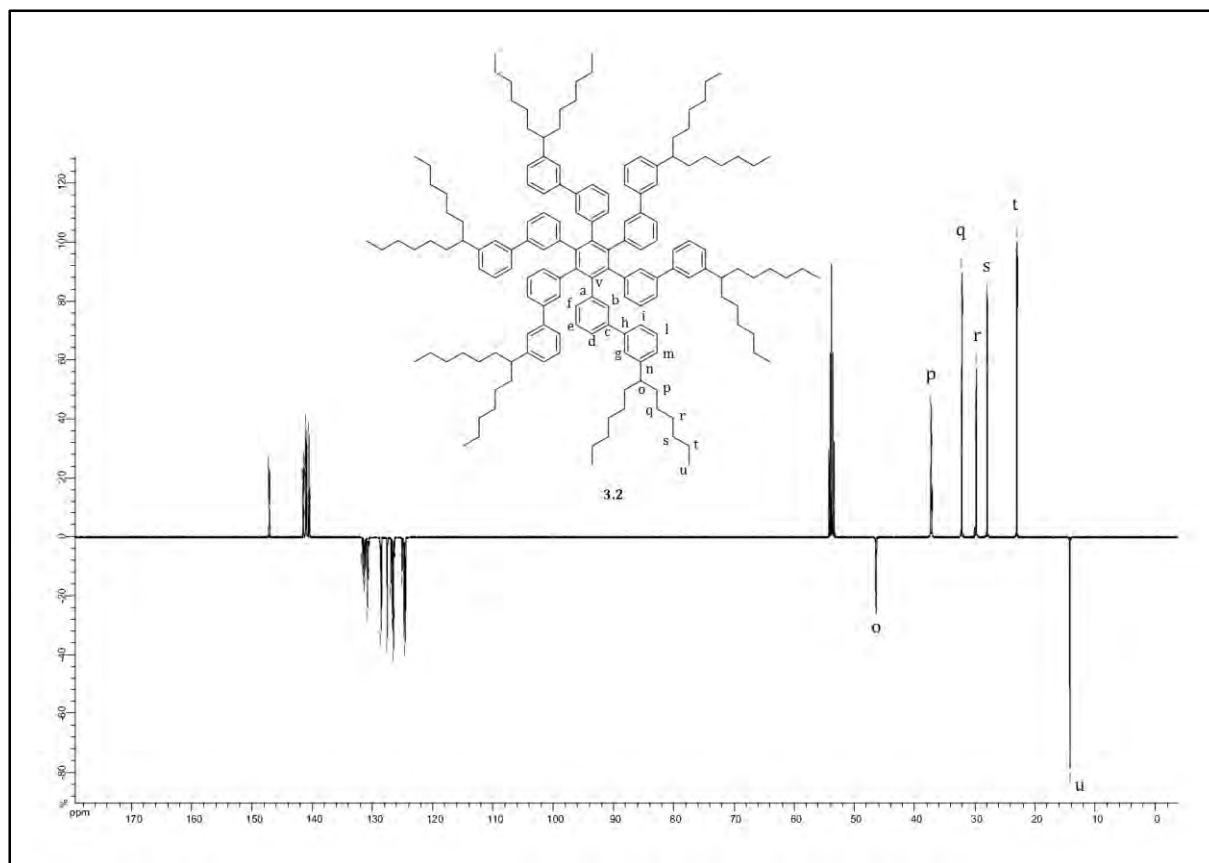
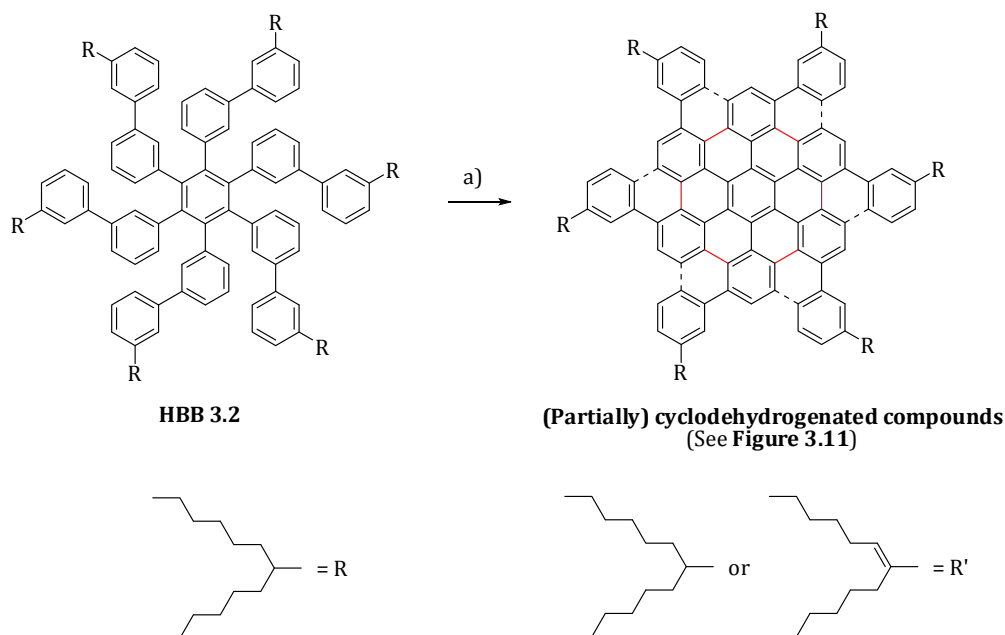


Figure 3.9: ^{13}C -NMR spectrum (125 MHz, CD_2Cl_2) of the precursor **HBB 3.2**.

The ^{13}C -NMR spectrum (125 MHz, CD_2Cl_2 , **Figure 3.9**) presented, as well, a complex series of peaks, due to the same reasons of lack of symmetry described before. The peaks in the aromatic region (124.6-147.3 ppm) could not be attributed to specific carbons, except the system of peaks at 147.3, assigned to C_n . The monitoring the disappearance of the signal at 89.8 ppm, characteristic of the alkyne moiety in **3.3** (carbons C_v), was a prove of the positive overcome of the cyclization reaction. The signals at higher fields could be attributed as follows: the systems of peaks at 46.4-46.5 ppm and 14.2-14.3 ppm were assigned respectively to the ternary carbons C_o and the primary carbons C_u ; the signals at 37.2-37.3, 32.1-32.3, 29.8-29.9, 27.8-28.0, 23.0-23.1 were characteristic of the alkyl chain methylene carbons $\text{C}_{p,q,r,s,t}$.

A further confirmation of the identity of the product was given by the high resolution mass spectra (MALDI ionization source, with DCTB matrix and time of flight analyser), showing a molecular peak at m/z 2083.6382, corresponding to the radical species $[\text{M}]^{\bullet+}$ (calculated 2083.6433).

3.4.2.5 Oxidative cyclodehydrogenation affording partially cyclodehydrogenated compounds:



Scheme 3.17: Cyclodehydrogenation affording (partially) cyclodehydrogenated compounds: Conditions: a) DDQ (12 eq.), Triflic acid / CH_2Cl_2 1:9, 0-5°C, 30 mins., 93%.

In order to synthesize the target molecule **hexaphenanthrocoronene 3.1**, we tested an oxidative cyclodehydrogenation reaction on the precursor **HBB 3.2**, employing the conditions suggested by R. Rathore^{19,20} and Kawasumi *et al.*³⁹. In particular, 2,3-dichloro-5,6-dicyano-1,4-benzoquinone (DDQ)/ H^+ was employed as oxidizing agent (**Scheme 3.17**). One equivalent of DDQ per each new C-C bond to be formed was employed. The solvent was 1% triflic acid in dichloromethane and the reaction was run at 0-5°C for 30 minutes. After basic work up and a filtration on silica gel, with toluene as eluent ($R_f=1$), a red laque, showing solubility in low polarity solvents (toluene, dichloromethane, hexane...) was isolated (in a 93% yield).

The red compound was characterized by MALDI-TOF mass spectrometry (**Figure 3.10**) and variable temperature $^1\text{H-NMR}$ spectroscopy (**Figure 3.12**).

In the high resolution MALDI-TOF mass spectrum (in DCTB matrix, **Figure 3.10 a**) the principal system of peaks was observed at 2061.4734 Da (indicated by a blue rectangle in the figure), which isotopic mass distribution was in accordance with a $\text{C}_{156}\text{H}_{188}$ molecular structure (by comparison with the calculated value 2061.4711 Da, **Figure 3.10 c**). The presence of two excess protons in the molecular formula (with respect to the formula of the target compound $\text{C}_{156}\text{H}_{186}$, a) in **Figure 3.11**) could indicate that the oxidative cyclodehydrogenation of **HBB 3.2** was not complete (**Scheme 3.17**), yielding globally to the formation of only eleven over the twelve possible new C-C bonds (for example, compound f) in **Figure 3.11**). In order to verify if it was possible to obtain the fully dehydrogenated product **hexaphenanthrocoronene 3.1**

(compound a) in **Figure 3.11**) by increasing the molar concentration of the oxidant, we repeated the reaction on the precursor **HBB 3.2** with an excess of DDQ (14 equivalents), but obtained the same result (**Figure 3.10 b**) as before.

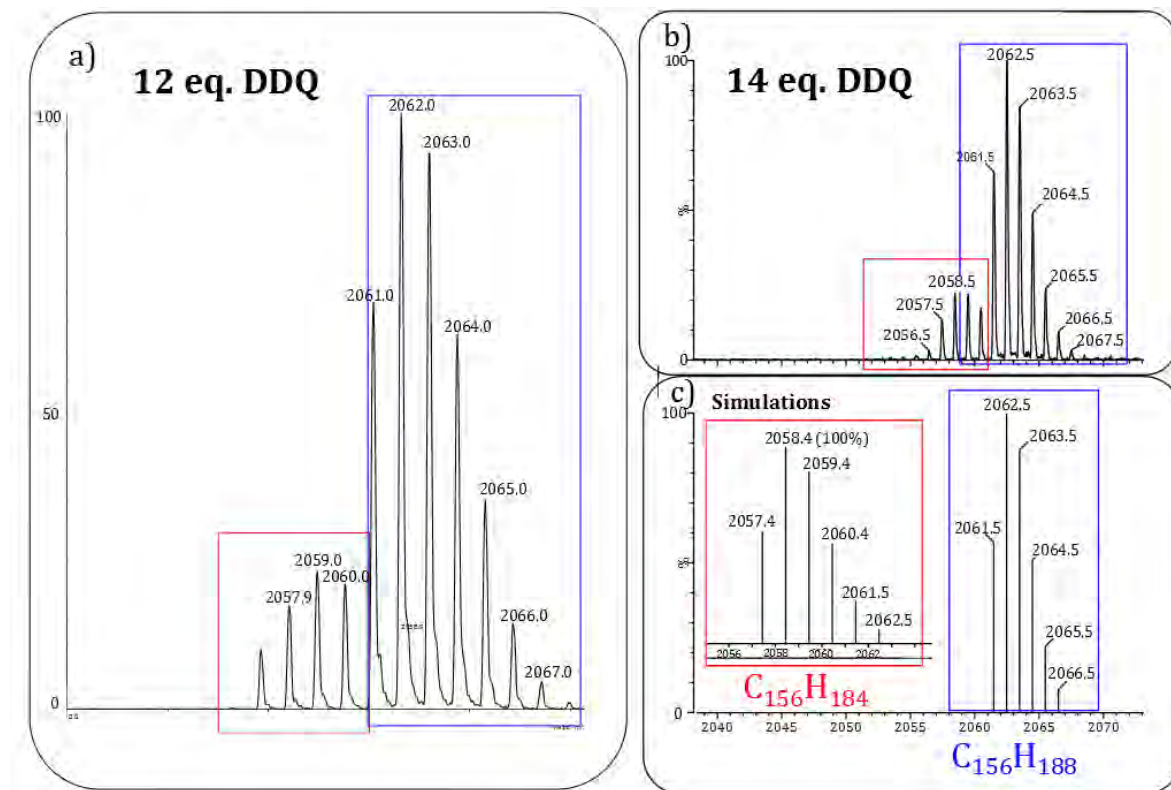


Figure 3.10: MALDI-TOF mass spectra of the product isolated from the reaction reported in **Scheme 3.17**.

In the mass spectra another distribution of signals at lower molecular weights was present (indicated by a red rectangle in **Figure 3.10 a** and **b**). The molecular weight 2058.4 Da was in accordance with a molecular formula $C_{156}H_{184}$, which could be attributed to compounds like d) or e) in **Figure 3.11**, deriving from either the oxidation of the benzylic carbon of the lateral dove-tail chains of the target molecule (compound d)) or by different other combinations of oxidized benzylic carbons/ unformed C-C bonds in the aromatic core (like in compound e) in **Figure 3.11**). Moreover, the isotopic pattern intensities observed experimentally was not in perfect agreement with the calculated one (**Figure 3.10 c**), so we could assume the presence of a distribution of additional benzylic-carbon oxidation products, like for example $C_{156}H_{182}$.

In addition to the less hindered isomers, we could also have obtained a series of sterically hindered isomers (for example, see compound c) in **Figure 3.11**), obtained by the oxidation one or more carbon atoms in *ortho* to the dove-alkyl chain. This hypothesis could not be ruled out by the analysis of the mass spectrum. However, the high steric hindrance would point against this possibility.

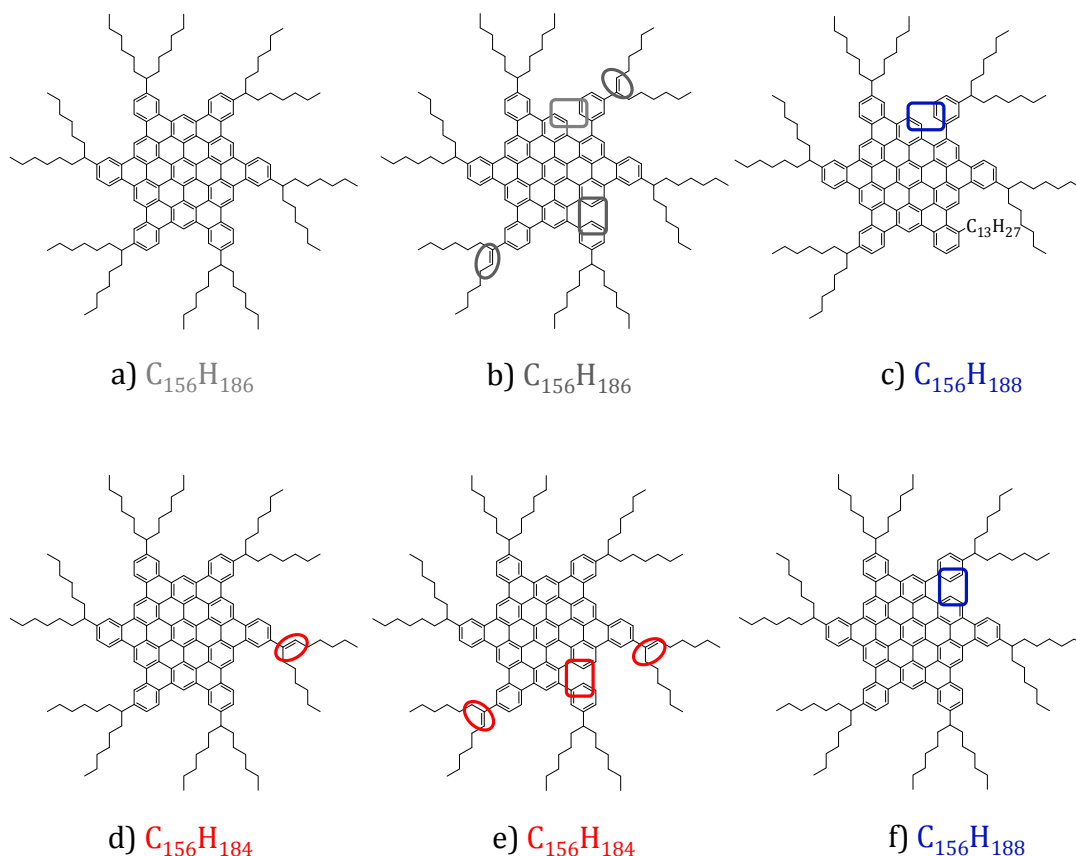


Figure 3.11: Possible isomers formed during the oxidative cyclodehydrogenation procedure: a) is the target isomer.

Unfortunately, NMR spectroscopy did not furnish any help in the identification of the molecular structure. In fact, the resolution of the spectrum was really poor (**Figure 3.12**). This observation could be explained both as due to the presence of numerous isomers and/or as a consequence of the tendency of the partially cyclodehydrogenated compounds to form pi-pi stacked aggregates, thus giving largely extended signals⁴⁰. Even at high temperatures ($T \geq 50^\circ\text{C}$) the resolution of the signals could not be improved, possibly due to the necessity of working at elevated concentration ($\sim 8 \times 10^{-3} \text{ M}$), imposed by the instrument sensitivity^{viii}.

Our hypothesis is that the DDQ oxidizing reagent is partially consumed in the oxidation of the benzylic position, preventing the complete aromatization of the core. Another possibility is that the intermediate radical-cation is somehow stabilized, preventing the last oxidation step⁴¹.

Other tests are in progress, in order to verify the possibility of obtaining the completely cyclodehydrogenated product **hexaphenanthrocoronene-12H** of molecular formula $C_{156}H_{174}$,

viii a) The sensitivity of the instrument at a frequency 400 MHz is not enough to allow the recording of the spectra of solutions more diluted than $\sim 8 \times 10^{-3} \text{ M}$ with a limited number of scans; b) it appeared not opportune for the spectrometer to warm at high temperature for longer times in order to increase the number of scans and thus analyse more diluted solutions. The high-frequency NMR spectra were recorded at the NMR-service of University Paul Sabatier (Toulouse).

characterized by the oxidation of the the six benzylic carbons (which calculated mass would be 2047.36156 Da, **Figure 3.13**). Once obtained this product and made sure (for example by X-Ray analysis) to have only the less-sterically hindered isomer, the following step would consist in hydrogenating the benzyl position to obtain the target **hexaphenanthrocoronene 3.1**.

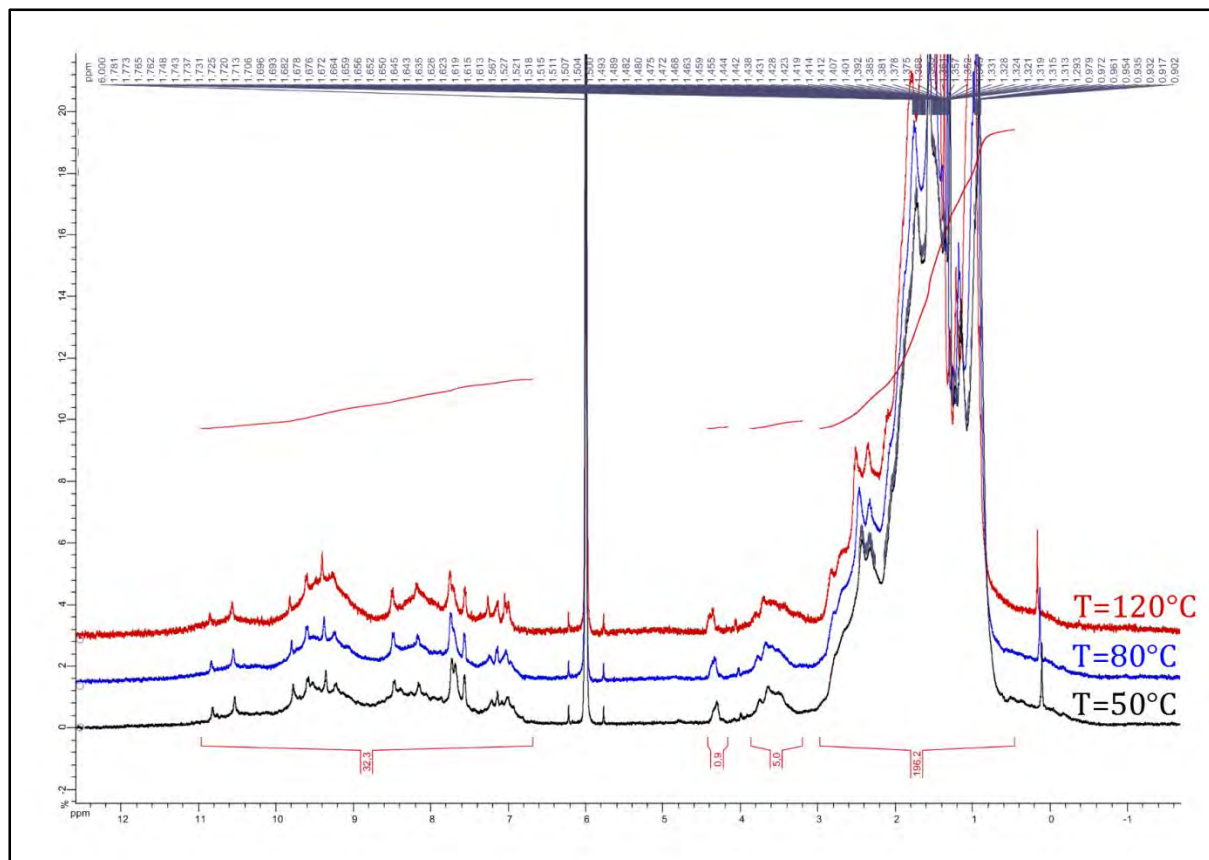


Figure 3.12: Variable temperature $^1\text{H-NMR}$ (400 MHz, $\text{C}_2\text{D}_2\text{Cl}_4$) spectrum of a solution $\sim 8 \times 10^{-3}$ M of the red laque (129 scans).

3.5 Conclusions

A new HBC derivative has been designed, **hexaphenanthrocoronene 3.1**, as a potential electron donor towards epitaxial graphene/SiC. The dove-tail alkyl chains have the role of driving the molecular organisation on the surface. At the same time, the presence of the chains renders the intermediates nicely soluble, facilitating the synthetic and purification procedures. The synthesis has been optimized until the generation of the hexabiphenylbenzene precursor **HBB 3.2**, obtained with a global yield over five steps of 19-26%. The last oxidative cyclodehydrogenation step have been carried out by employing DDQ/ H^+ as oxidizing system. Unfortunately, the product **hexaphenanthrocoronene 3.1** has not been obtained. A red product (fluorescent at $\lambda_{\text{exc}}=365$ nm) was isolated, soluble in different solvents (toluene, dichloromethane, hexane...), which could correspond to the partially cyclodehydrogenated

compound f) in **Figure 3.11** for its molecular weight. However we could not have a confirmation of the chemical structure by $^1\text{H-NMR}$ spectroscopy, due to the low resolution of the signals even at high temperatures (for a sample of concentration $\sim 8 \times 10^{-3}$ M). Moreover, the eventual presence of sterically hindered isomers (compound c) in **Figure 3.11**) could not be discarded. The studies are being pursued in order to afford the completely dehydrogenated target **hexaphenanthrocoronene 3.1** as the only isomer, by passing through the intermediate **hexaphenanthrocoronene-12H** and a following catalytic hydrogenation of the benzylic positions.

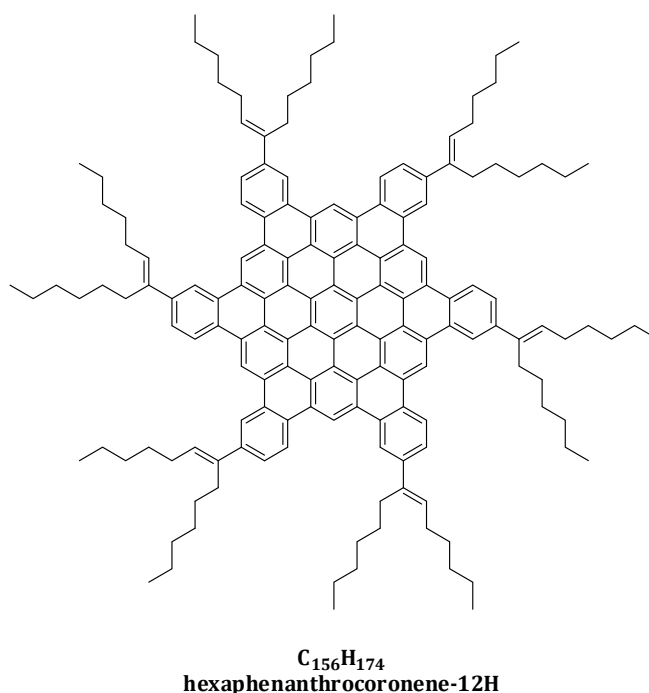


Figure 3.13: Hexaphenanthrocoronene characterized by six oxidized benzylic positions (**hexaphenanthrocoronene-12H**).

3.6 References

- ¹ Feng, X., Pisula, W., Müllen, K., *Pure Appl. Chem.*, **2009**, *81*, 12, 2203-2224.
- ² a) Schleyer, P. V. R., *Chem. Rev.*, **2001**, *101*, 1115-1119 and references therein; b) Gross, L., Mohn, F., Moll, N., Schuler, B., Criado, A., Guitián, E., Peña, D., Gourdon, A., Meyer, G., *Science*, **2012**, *337*, 6100, 1326-1329.
- ³ Wu, J., Pisula, W., Müllen, K., *Chem. Rev.*, **2007**, *107*, 718-747.
- ⁴ Ito, S., Wehmeier, M., Brand, J. D., Kübel, C., Epsch, R., Rabe, J. P., Müllen, K., *Chem. Eur. J.*, **2000**, *6*, 4327-4342.
- ⁵ Feng, X., Marcon, V., Pisula, W., Hansen, M. R., Kirkpatrick, J., Grozema, F., Andrienko, D., Kremer, K., Müllen, K., *Nat. Mat.*, **2009**, *8*, 421-426.
- ⁶ Soe, W.-H., Manzano, C., Renaud, N., de Mendoza, P., De Sarkar, A., Ample, F., Hliwa, M., Echavarren, A. M., Chandrasekhar, N., Joachim, C., *ACS Nano*, **2011**, *5*, 2, 1436-1440.
- ⁷ a) Grill, L., Dyer, M., Lafferentz, L., Persson, M., Peters, M. V., Hecht, S., *Nature Nanotechnol.* **2007**, *2*, 687-691; b) Lafferentz, L., Eberhardt, V., Dri, C., Africh, C., Comelli, C., Esch, F., Hecht, S., Grill, L., *Nature Chem.*, **2012**, *4*, 215-220.
- ⁸ a) Bieri, M., Nguyen, M.-T., Gröning, O., Cai, J., Treier, M., Ait-Mansour, K., Ruffieux, P., Pignedoli, C. A., Passerone, D., Kastler, M., Müllen, K., Fasel, R., *J. Am. Chem. Soc.*, **2010**, *132*, 46, 16669-16676; b) Treier, M., Pignedoli, C. A., Laino, T., Rieger, R., Müllen, K., Passerone, D., Fasel, R., *Nat. Chem.*, **2011**, *3*, 61-67; c) Cai, J., Ruffieux, P., Jaafar, R., Bieri, M., Braun, T., Blankenburg, S., Muoth, M., Seitsonen, A. P., Saleh, M., Feng, X., Müllen, K., Fasel, R., *Nature*, **2010**, *466*, 470-473.
- ⁹ a) Otero, G., Biddau, G., Sánchez-Sánchez, C., Caillard, R., López, M. F., Rogero, C., Palomares, F. J., Cabello, N., Basanta, M. A., Ortega, J., Méndez, J., Echavarren, A. M., Pérez, R., Gómez-Lor, B., Martín-Gago, José A., *Nature*, **2008**, *454*, 865-869; b) Amsharov, K., Abdurakhmanova, N., Stepanow, S., Rauschenbach, S., Jansen, M., Kern, K., *Angew. Chem. Int. Ed.*, **2010**, *49*, 9392-9396; c) Pinardi, A. L., Otero-Irurueta, G., Palacio, I., Martínez, J. I., Sanchez-Sanchez, C., Tello, M., Rogero, C., Cossaro, A., Preobrajenski, A., Gómez-Lor, B., Jancarik, A., Stara, I. G., Star, I., Lopez, M. F., Méndez, J., Martín-Gago, J. A., *ACS Nano*, **2013**, *7*, 4, 3676-3684.
- ¹⁰ Sun, Q., Zhang, C., Li, Z., Kong, H., Tan, Q., Hu, A., Xu, W., *J. Am. Chem. Soc.*, **2013**, *135*, 8448-8451.
- ¹¹ a) Kittelmann, M., Nimmrich, M., Lindner, R., Gourdon, A., Kühnle, A., *ACS Nano*, **2013**, *7*, 6, 5614-5620; b) Kittelmann, M., Rahe, P., Nimmrich, M., Hauke, C. M., Gourdon, A., Kühnle, A., *ACS Nano*, **2011**, *5*, 8420-8425.
- ¹² a) Clar, E., *Polycyclic Hydrocarbons*, Academic Press: New York, **1964**, Vol. I/II; b) Clar, E., *The Aromatic Sextet*, Wiley-VCH, London, **1972**; c) Scholl, R., Seer, C., Weitzenböck, R. *Chem. Ber.*, **1910**, *43*, 2202; d) Scholl, R., Seer, C. *Liebigs Ann. Chem.*, **1912**, *394*, 111; e) Scholl, R., Seer, C. *Chem. Ber.* **1922**, *55*, 330; f) Clar, E., Stewart, D. G., *J. Am. Chem. Soc.*, **1953**, *75*, 2667-2672.
- ¹³ a) Pérez, D., Peña, D., Guitián, E., *Eur. J. Org. Chem.* **2013**, 5981-6013; b) Alonso, J. M., Díaz-Álvarez, A. E., Criado, A., Pérez, D., Peña, D., Guitián, E., *Angew. Chem. Int. Ed.*, **2012**, *51*, 173-177.
- ¹⁴ Gómez-Lor, B., Echavarren, A. M., *Org. Lett.*, **2004**, *6*, 17, 2993-2996.
- ¹⁵ Watson, M. D., Fechtenkötter, A., Müllen, K., *Chem. Rev.* **2001**, *101*, 1267-1300.
- ¹⁶ Vollhardt, K. P., *Acc. Chem. Res.*, **1970**, *10*, 1-8.
- ¹⁷ Kovacic, P., Jones, M. B., *Chem. Rev.*, **1987**, *87*, 357-379 and references therein.

- ¹⁸ Dötz, F., Brand, J. D., Ito, S., Gherghel, L., Müllen, K., *J. Am. Chem. Soc.*, **2000**, *122*, 32, 7707-7717.
- ¹⁹ Zhai, L., Shukla, R., Rathore, R., *Org. Lett.*, **2009**, *11*, 15, 3474-3477.
- ²⁰ Zhai, L., Shukla, R., Wadumethrige, S. H., Rathore, R., *J. Org. Chem.*, **2010**, *75*, 4748-4760.
- ²¹ Rempala, P., Kroulík, J., King, B. T., *J. Am. Chem. Soc.*, **2004**, *126*, 15002-15003.
- ²² Simpson, C. D., Brand, J. D., Berresheim, A. J., Przybilla, L., Räder, H. J., Müllen, K., *Chem. Eur. J.*, **2002**, *8*, 6, 1424-1429.
- ²³ Simpson, C. D., Mattersteig, G., Martin, K., Gherghel, L., Bauer, R. E., Räder, H. J., Müllen, K., *J. Am. Chem. Soc.*, **2004**, *126*, 3139-3147.
- ²⁴ Keil, M., Samori, P., dos Santos, D. A., Kugler, T., Stafström, S., Brand, J. D., Müllen, K., Brédas, J. L., Rabe, J. P., Salaneck, W. R., *J. Phys. Chem. B*, **2000**, *104*, 3967-3975.
- ²⁵ a) Piot, L., Marchenko, A., Wu, J., Müllen, K., Fichou, D., *J. Am. Chem. Soc.*, **2005**, *127*, 16245-16250; b) Feng, X., Wu, J., Ai, M., Pisula, W., Zhi, L., Rabe, J. P., Müllen, K., *Angew. Chem. Int. Ed.*, **2007**, *46*, 3033-3036.
- ²⁶ Kaufman, R. J., Sidhu, R. S., *J. Org. Chem.*, **1982**, *47*, 4941-4947.
- ²⁷ Lipshutz, B. H., Wilhelm, R. S., Floyd, D. M., *J. Am. Chem. Soc.*, **1981**, *103*, 7672-7674.
- ²⁸ Miyake, Y., Wu, M., Rahman, M. J., Iyoda, M., *Chem. Commun.*, **2005**, 411-413.
- ²⁹ Miyake, Y., Wu, M., Rahman, M. J., Kuwatani, Y., Iyoda, M., *J. Org. Chem.*, **2006**, *71*, 16, 6110-6117.
- ³⁰ Wagner, D., Hoffmann, S. T., Heinemeyer, U., Münster, I., Köhler, A., Strohmriegl, P., *Chem. Mater.*, **2013**, *25*, 3758-3765.
- ³¹ Kofron, W. G., Baclawski, L. M., *J. Org. Chem.*, **1976**, *41*, 10, 1879-1880.
- ³² West, C. T., Donnelly, S. J., Kooistra, D. A., Doyle, M. P., *J. Org. Chem.*, **1973**, *38*, 15, 2675-2681.
- ³³ Carey, F. A., Tremper, H. S., *J. Am. Chem. Soc.*, **1968**, *90*, 10, 2578-2583.
- ³⁴ Klapars, A., Buchwald, S. L., *J. Am. Chem. Soc.*, **2002**, *124*, 14844-14845.
- ³⁵ For example see: a) Suzuki, H., Kondo, A., Ogawa, T., *Chem. Lett.*, **1985**, 411-412; b) Cannon, K. A., Geuther, M. E., Kelly, C. K., Lin, S., MacArthur, A. H. R., *Organometallics*, **2011**, *30*, 4067-4073.
- ³⁶ Mio, J., Kopel, L. C., Braun, J. B., Gadzikwa, T. J., Hull, K. L., Brisbois, R. G., *Org. Lett.*, **2002**, *4*, 19, 3199-3202.
- ³⁷ For the reaction mechanism, see for example: Baxter, R. J., Knox, G. R., Moir, J. H., Pauson, P. L., Spicer, M. D., *Organometallics*, **1999**, *18*, 2, 206-214.
- ³⁸ Kaganovich, V.S., Rybinskaya, M.I., *Journal of Organometallic Chemistry*, **1995**, *498*, 2, 155-163.
- ³⁹ Kawasumi, K., Zhang, Q., Segawa, Y., Scott, L. T., Itami, K., *Nature Chem.*, **2013**, *5*, 739-744.
- ⁴⁰ Kastler, M., Pisula, W., Wasserfallen, D., Pakula, T., Müllen, K., *J. Am. Chem. Soc.*, **2005**, *127*, 4286-4296.
- ⁴¹ Feng, X., Wu, J., Enkelmann, V., Müllen, K., *Org. Lett.*, **2006**, *8*, 6, 1145-1148.

Part II

Synthesis of molecules for covalent functionalization of graphene

In **Part I**, we have described the synthesis of molecules for the non-covalent functionalization of graphene/SiC, by formation of self-assembled monolayers in UHV conditions. We want now to employ the concepts of supramolecular chemistry in order to drive the organization on epitaxial graphene/SiC of functional groups interacting through the formation of a *covalent bond* with the surface. The study is motivated in particular by the possibility of exerting a stronger modification of the electronic properties of the material by this strategy. The covalent reaction, can, in fact, induce the transformation of the hybridization of the reacting carbon atom from sp^2 to sp^3 , removing its electrons from the conjugation and thus allowing the local opening of a band gap^{1,2}. This characteristic appears to be interesting, for example, in the perspective of employing graphene in electronic devices, such as transistors.

The possibility of employing STM not only as a characterization mean, but also as the tool for activating chemical reactivity (**Appendix A1**), allows to envisage the possibility of choosing which particular groups to react with graphene, once the molecules organized on the surface. This would allow in principle the generation of *alternating conductive* (sp^2 conjugated carbons) and *insulating* (sp^3 hybridized carbons) areas, with a geometry defined by the molecular design (**Figure II.1**).

The necessity of creating a stable monolayer extended all over the epitaxial graphene/SiC surface, as to stabilize the molecules from diffusion, has already been assessed in the previous chapters. In order to achieve the possibility of spatially and temporally control the chemical reactivity, the chosen functional group should be enough stable on graphene not to react spontaneously, but only upon a proper STM “pulse”. The requisite of stability is also imposed by the characteristics of the UHV-procedure for the deposition on the surface that is in general conducted by sublimation, i. e. at elevated temperatures. However, graphene is very chemically unreactive, in reason of its extended pi-conjugated nature, thus requires strongly *unstable* reagents (for example, radicals) to be covalently functionalized. This point renders the choice of the reactive group very challenging.

In this context, we proposed two different solutions: the first one consists in generating the reactive group directly on the surface, by decomposition of an adapted precursor. The reactive group considered is an *aryl radical*, generated by the decomposition of a brominated compound. The second

strategy is based on the employment of *Diels-Alder reactants*, such as anthracene as diene and maleimide derivatives as dienophiles.

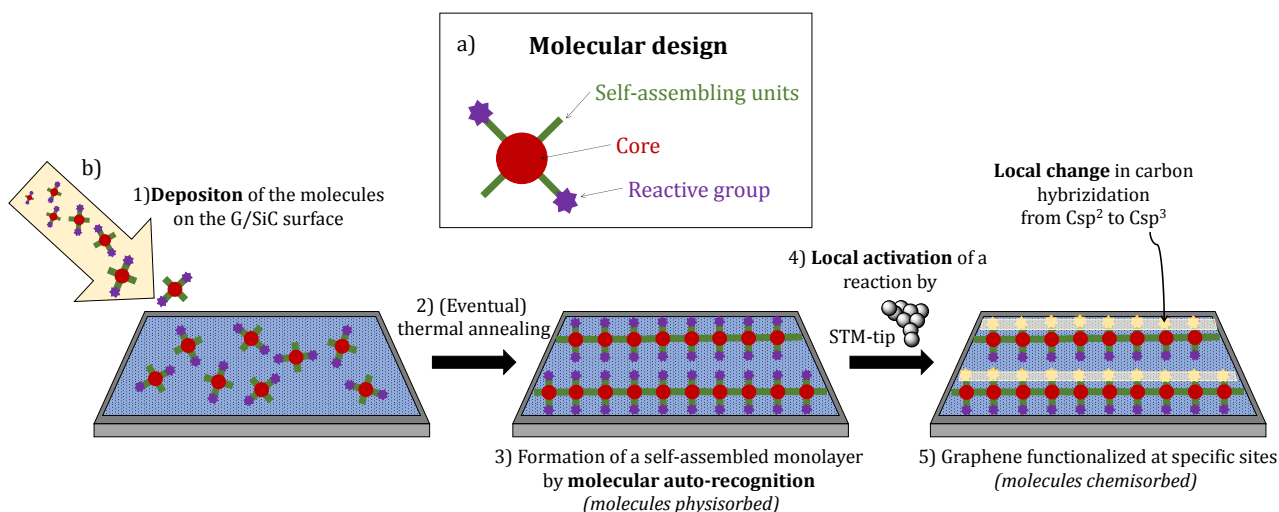


Figure II.1: a) Schematic molecular structure of the molecules for non-covalent functionalization of epitaxial graphene/SiC. b) Strategy envisaged in order to afford a spatially controlled functionalization of graphene/SiC: 1) deposition in UHV (by sublimation) and absorption on the surface; 2) (eventual) thermal annealing in order to favour the 3) organization of the molecules in periodic structures; 4) local activation of a reaction leading to the formation of a covalent bond between graphene and a reactive group; 5) graphene functionalized at specific sites.

The design and synthesis of the different derivatives to be tested on the surface is described respectively in **Chapter 4, 5 and 6**.

References

¹ Balog, R., Jørgensen, B., Nilsson, L., Andersen, M., Rienks, E., Bianchi, M., Fanetti, M., Lægsgaard, E., Baraldi, A., Lizzit, S., Slijivančanin, Z., Besenbacher, F., Hammer, B., Pedersen, T. G., Hofmann, P., Hornekær, L., *Nature Mat.*, **2010**, *9*, 315-319.

² Hossain, Z., Walsh, M. A., Hersam, M. C., *J. Am. Chem. Soc.*, **2010**, *132*, 43,15399–15403.

Chapter 4

Synthesis of molecules for covalent functionalization of graphene by radicalar addition

4.1 Introduction

As introduced in **Chapter 1**, radicalar additions constitute one of the most developed chemistries on graphene. In particular, aryl radicals derived from the decomposition of diazonium salts are commonly employed in the functionalization of graphene surfaces in solution, allowing the introduction of differently functionalized aryl groups on the surface¹. However, due to the UHV-sublimation constraint, requiring warming, the employment of a diazonium salt does not seem a viable solution for our tests of reactivity on surface. The diazonium group could, in fact, decompose already in the evaporator, generating radicals that would, in principle, auto-react before getting on the surface.

4.2 Objective

Our objective (**Figure 4.1**) is to design and synthesize molecules bearing a reactive functionality that, thanks to a controlled STM activation, can form a radical reactive with graphene. The radical can be generated after homolytic cleavage of a particular bond on the molecule, by an STM potential pulse (see **Appendix A1**). After generation of the radical, we expect that it reacts readily with the underlying graphene surface, driving to the formation of a covalent bond. Our target molecules need also to be able to form a self-assembled monolayer on a graphene/SiC (0001) surface in UHV, in order to drive a defined spatial organization of the reactive groups on the surface.

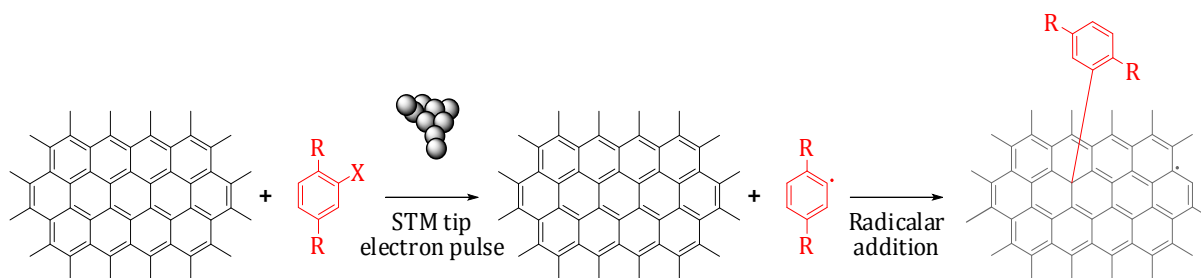


Figure 4.1: General objective.

4.3 Molecular design

In order to pursue our objective, three molecules were designed and synthesized: **Br1** (4.1), **Br2** (4.2) and **TBr** (4.3) (Figure 4.2):

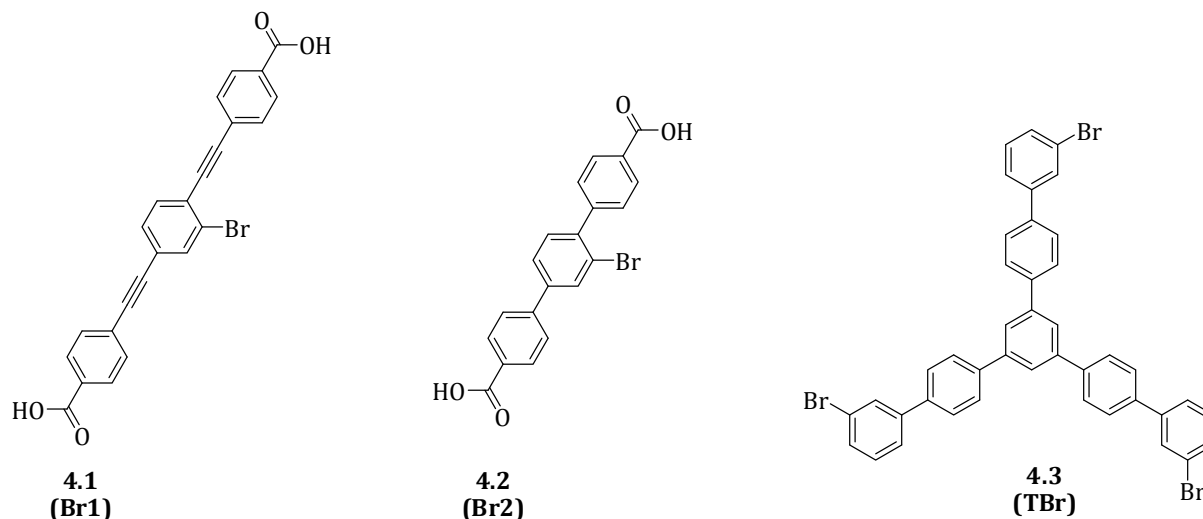


Figure 4.2: Structure of the brominated derivatives **Br1** (4.1), **Br2** (4.2), **TBr** (4.3).

4.3.1 Choice of the reactive group

The designed molecules are endowed with an *aryl-bromine substituent* as the reactive group: an STM activated homolytical cleavage of the C-Br bond is meant to be the key step in the generation of the reactive carbon centred radical (C•).

The preference of a bromine substituent over other possibilities (like hydrogen or other halogens) is dictated by energetic considerations. The C-Br bond energy is intermediate between the energies of the very strong C-F or C-H and the rather weak C-I (Table 4.1).

Substituent (X)	Bond energy (C-X) (KJ/mol)
I	268
Br	336
Cl	397
F	485
H	411

Table 4.1: Homolytic bond dissociation energies of different C-X bonds².

This choice in the molecular design takes into account the different problematics related to the various steps of the STM study in Ultra High Vacuum (UHV):

- 1) the *deposition* on the surface, by sublimation under UHV conditions;
- 2) the *activation of the C-X bond*, in order to generate the reactive radical.

On one side, it is preferable not to insert in the molecule a fragile bond that could be broken during the evaporation procedure, which presumably will necessitate high temperatures. In fact, considering the molecular structures, it is possible to foresee high molecular sublimation points, due to the strong intermolecular forces, related to the π - π interactions between the cores and hydrogen bonds between the carboxylic moieties.

On the other side, C-X bonds much stronger than C-Br (like C-F or C-H) would demand a higher energy for the radical generation. Following these considerations, the most suitable substituents appear to us to be bromine and chlorine and different examples of cleavage of C-Br or C-Cl by STM tip activation already exist in the literature³.

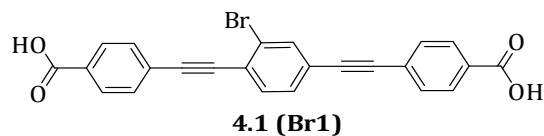
The bromine substituent is introduced directly on the phenyl ring, in order to allow the generation of a highly reactive *aryl-radical*. An *orto* or *meta* position are preferred over the *para* in the benzene ring for the placement of the substituent. This choice is dictated by steric considerations. In fact, in order to favour the radicalar addition reaction, it seems necessary to allow the sp^2 orbital of the newly formed radical to be perpendicular to the graphene surface. To this aim, we designed molecules where the free rotation around the σ bonds, should in principle allow the radicalar orbital to get perpendicular to the surface.

4.3.2 Self-assembling strategies

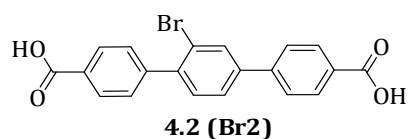
As for the *self-assembling moieties*, two different types of functionalities are employed: **Br1** (4.1) and **Br2** (4.2) are characterized by the presence of carboxylic acids moieties that should favour the establishment of hydrogen bond interactions. **TBr** (4.3), instead, is bearing only the brominated substituent. The bromine substituents should, in principle, promote the establishment of weak hydrogen bond interactions C-H \cdots Br⁴ with the aryl-CH bonds themselves, or Br-Br halogen bonds⁵ driving the self-assembly. Hydrogen bonds, such as C-H \cdots O, C-H \cdots N or C-H \cdots F⁶, and halogen bonds^{4, 7b} have already been employed in the literature to drive the formation of 2D self-assembled monolayers on a variety of surfaces.

4.3.3 Design

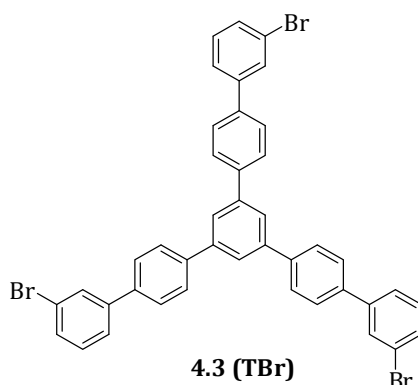
As already pointed out, the main challenge in the design of this class of targets is to individuate a proper geometry, such as not to hinder the reaction for steric reasons, letting the sp^2 generated radicalar orbital to be perpendicular to the surface. Hereafter, the devised solutions are described.



Br1 (4.1): The first molecule in the series is characterized by a linear geometry: the aryl ring bearing the bromine substituent is functionalized by two ethynyl-benzoic acid moieties in position 1, 4 that constitute the self-assembling units. The ethynyl connections are chosen in virtue of their known conformational flexibility. In principle they should be enough flexible to allow a rotation of the phenyl ring along the sigma bonds in order for the aryl radical orbital to get perpendicular to the graphene surface, thus allowing its addition. At the same time, **4.1** should absorb with a more planar conformation than **4.2**, due to the larger distance between the phenyl units.



Br2 (4.2): This molecule is characterized by a linear geometry analogous to **Br1**, but the benzoic acid moieties are directly connected to the middle aryl ring in position 1,4, by a simple C-C bond. Comparing the behaviour of **Br1** and **Br2** appeared interesting for two main reasons: 1) being the melting point of **Br1** quite elevated (above 270°C), the alkyne bridges could represent a point of fragility and could possibly be broken during the evaporation procedure: a simplified molecular structure could be helpful in easing the deposition phase; 2) the aryl radical is free to rotate along the C-C sigma bonds and the molecule, even if more rigid than **Br1**, is endowed with a certain degree of conformational flexibility: it would be interesting to verify if it is enough flexible to be able to adapt its geometry and allow for a reaction between the radical and graphene.



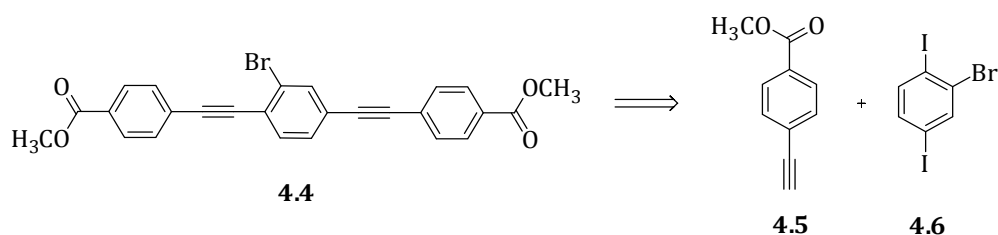
TBr (4.3): The third molecule of the series is an extended triphenylene derivative. The large number of benzene rings should enhance the absorption on the surface by establishing π - π interactions. The bromine substituent is placed in a *meta* position. It appeared, in fact,

interesting to test the steric hindrance effects on the radical addition for a radical originated in this position. Even after breaking one C-Br bond, the other two halogen-interactions among the molecules should allow for a stabilization of the self-assembled monolayer. The molecule **4.3** should be more easily sublimed than **4.1** and **4.2**, in virtue of the establishment of weaker intermolecular interactions in the solid state (due to the absence of the carboxylic acid moieties). The adsorption of polyphenyl derivatives like **4.3** has already been investigated on HOPG (Highly Oriented Pyrolytic Graphite) in UHV conditions⁴ and the liquid–solid interphase⁷, evidencing a planar adsorption geometry of the organic backbones driven by π - π interactions with the graphite substrate.

4.4 Molecules with linear geometry

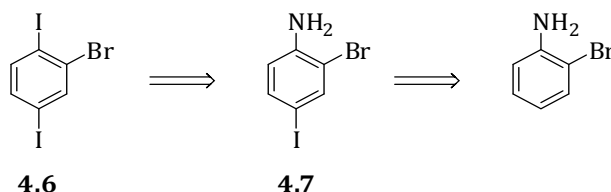
4.4.1 Retrosynthetic analysis of the linear derivative Br1 (4.1)

From a retrosynthetic point of view, **Br1** can be obtained from the precursor **4.4**, that, on his turn, can be disconnected to the ester **4.5** and 2-bromo-1,4-diiodobenzene **4.6** (**Scheme 4.1**).



Scheme 4.1: Retrosynthetic analysis for **4.4**.

The precursors **4.5** and **4.6** are not commercial, but they can be readily synthesized. In particular, **4.5** is a derivative of methyl p-iodo benzoate, while **4.6** can be disconnected in last analysis to 2-bromoaniline (**Scheme 4.2**).

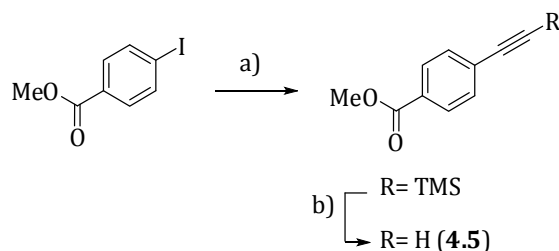


Scheme 4.2: Retrosynthetic analysis for **4.6**.

4.4.2 Synthesis of the linear derivative Br1

4.4.2.1 Synthesis of the ester **4.5**

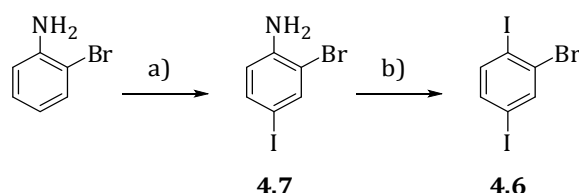
The synthesis was carried on following a procedure already reported in the literature⁸ (**Scheme 4.3**).



Scheme 4.3: Synthesis of **4.5**. Conditions: a) TMSA, Pd(PPh₃)₂Cl₂ (3%), CuI (5%), Et₃N, 25°C, 2h, 96%; b) K₂CO₃, CH₂Cl₂/CH₃OH, 25°C, 2h, 97%.

In a first step, the trimethylsilyl protected alkyne moiety was introduced by means of a Sonogashira⁹ cross coupling reaction on methyl p-iodo benzoate. The conditions employed were 3% of Pd(PPh₃)₂Cl₂ and 5% of CuI in triethylamine (0.25 M). The high reaction rate at room temperature and high yield were expected from the activated nature of the iodo-aryl substrate, bearing a methyl ester substituent. The reaction was found to be very clean: only the desired product was obtained and purified by a simple filtration on silica, in order to remove the catalysts. The alkyne moiety was then deprotected from the trimethylsilyl protecting function, by stirring it at room temperature in dichloromethane/methanol in the presence of an excess of potassium carbonate for two hours. The product was recovered as a yellow solid after a filtration on silica (with dichloromethane as eluent) with a global 92% yield over the two steps.

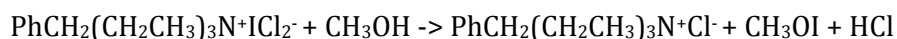
4.4.2.2 Synthesis of 2-bromo-1,4-diiodobenzene **4.6**:



Scheme 4.4: Synthesis of **4.6**. Conditions: a) Benzyltriethylammonium dichloroiodate 1 eq., NaHCO₃ (2 eq.), DCM / MeOH, 0-18°C, 1h, 34% ; b) **4.7**, BF₃O(Et)₂ (4 eq.), Et₂O dry, -30°C, 30 mins; tBuONO (3.5 eq.), -30°C -10°C, 1.5h; NaI, CH₃CN dry, 22°C, 4h, 63%.

Step a)

In the first step, 2-bromoaniline was iodinated in the 4 position, following the procedure reported by J. Tour¹⁰. Benzyltriethylammonium dichloroiodate (BTEA ICl₂) (1 eq.) was employed as iodinating agent, in the presence of sodium hydrogen carbonate (2 eq.), in methanol / dichloromethane 1:1 at room temperature (18°C) for one hour. Quaternary ammonium polyhalides are, in fact, commonly employed as iodinating reagents for anilines¹¹. The main active species generating the iodonium electrophile (I⁺) is considered to be methyl hypoiodite, produced in a reaction of BTEA ICl₂ with methanol:

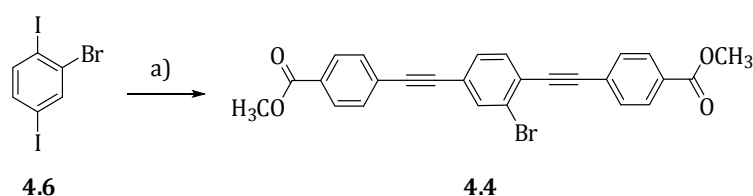


Sodium hydrogen carbonate is meant to neutralize the hydrogen chloride generated during the reaction. The strongly electron donating amino group (mesomeric effect) activates the *para* position and drives the aromatic electrophilic substitution. The monoiodination is controlled by the reagent molar ratio. The yield of product **4.7** is quite low (34%), but comparable to the one reported in literature¹⁰. It could, in principle, be improved by optimizing the reaction conditions in order to reduce the amount of polar subproducts originated during the reaction and the quantity of unreacted 2-bromoaniline (that cannot be separated completely from the product and constitutes a 10% impurity, as estimated from the NMR spectrum).

Step b)

In the following step (b) the amino functionality was substituted by a iodine substituent. The procedure was already described in the literature by J. Tour¹². The amino functionality of **4.7** was at first transformed in a diazonium salt by reacting it with tert-butyl nitrite in dry diethyl ether at -30°C - -10°C. The diazonium salt bearing a tetrafluoroborate anion was then isolated and finally reacted with sodium iodide in dry acetonitrile at room temperature (22°C) to afford the iodinated compound **4.6**. 2-bromo-1,4-diiodobenzene **4.6** was recovered after a simple filtration on silica, washing with ethyl acetate, as a slightly impure white solid, with a 63% yield.

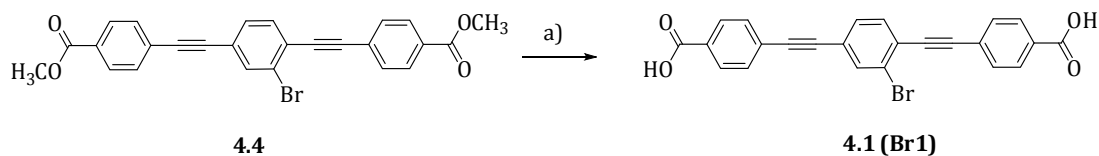
4.4.2.3 Synthesis of the methyl diester precursor 4.4



Scheme 4.5: Synthesis of **4.4**. Conditions: a) Pd(PPh₃)₂Cl₂ (6.7%), CuI (10%), DCM/Et₂NH, 18°C, 16h, 53%.

Compound **4.6** was coupled by Sonogashira reaction with the ester **4.5** to yield the precursor **4.4**. The conditions employed were bis(triphenylphosphine)palladium(II) dichloride (3.3% for each iodine functionality) and copper iodide (5% for each iodine functionality) as catalysts, in dichloromethane/diethylamine as solvent (0.04 M). The higher reactivity of the carbon-iodine with respect to the carbon-bromine bond in the step of oxidative addition to palladium allowed to carry on the coupling reaction at room temperature, affording only the desired bi-functionalized product **4.4**. The product was recovered by precipitation from dichloromethane as a white solid with a 53% yield.

4.4.2.4 Deprotection of the methyl ester functions: synthesis of Br1 (4.1):



Scheme 4.6: Deprotection of the methyl ester function. Conditions: a) LiOH (10eq.), THF/H₂O, 50°C, 22h, 33%.

The methyl ester functions were deprotected to the corresponding carboxylic acids by stirring **Br1 (4.1)** in a mixture water / tetrahydrofuran at 50°C for 22 hours. After acidic work up, a solid was recovered, that was successively triturated in a mixture acetone/ethanol/tetrahydrofuran 0.5/0.5/9 at 50°C. The product was obtained pure as a yellow solid with a 33% yield. The low yield might be due to an incomplete recovery of the product due to its partial solubility in ethanol at 50°C.

The global yield for the synthesis of **4.1 (Br1)** is calculated as 3.5% over the six steps.

4.4.3 Characterization of the linear derivative Br1

The product **Br1 (4.1)** was characterized by ¹H and ¹³C NMR spectroscopy (mono and bidimensional) and high-resolution mass spectrometry.

The ¹H-NMR spectrum (DMSO, 500 MHz, **Figure 4.3**) allowed to confirm the identity of the product. The signals in the ¹H-NMR spectrum could be attributed by the crossed analysis of the ¹H, ¹³C and bidimensional NMR spectra. The aspect was characteristic of an asymmetrically functionalized compound and the signals were generally badly resolved, as a consequence of the low solubility of the compound. In particular, the broad singlet at 7.94 ppm was attributed to the proton H_a; the multiplet integrating for four protons at 7.87 ppm was attributed to H_{e,e'}, deshielded respect to H_{d,d'} (giving a multiplet at 7.4-7.5 ppm) due to the vicinity of the bromine substituent. The other signals were two doublets at 7.68 and 7.59 ppm, characterized by a coupling constant of 8 Hz and characteristic of protons H_b and H_c.

The high resolution mass analysis (Electrospray Ionization Source in negative ions mode and Time of Flight mass Analyser) confirmed the identity of the product with one peak at m/z 442.9915 Da. attributed to the singly deprotonated molecule, of molecular formula C₂₄H₁₂O₄Br (the calculated value was 442.9919). The isotopic pattern was in accordance with the presence of one bromine substituent.

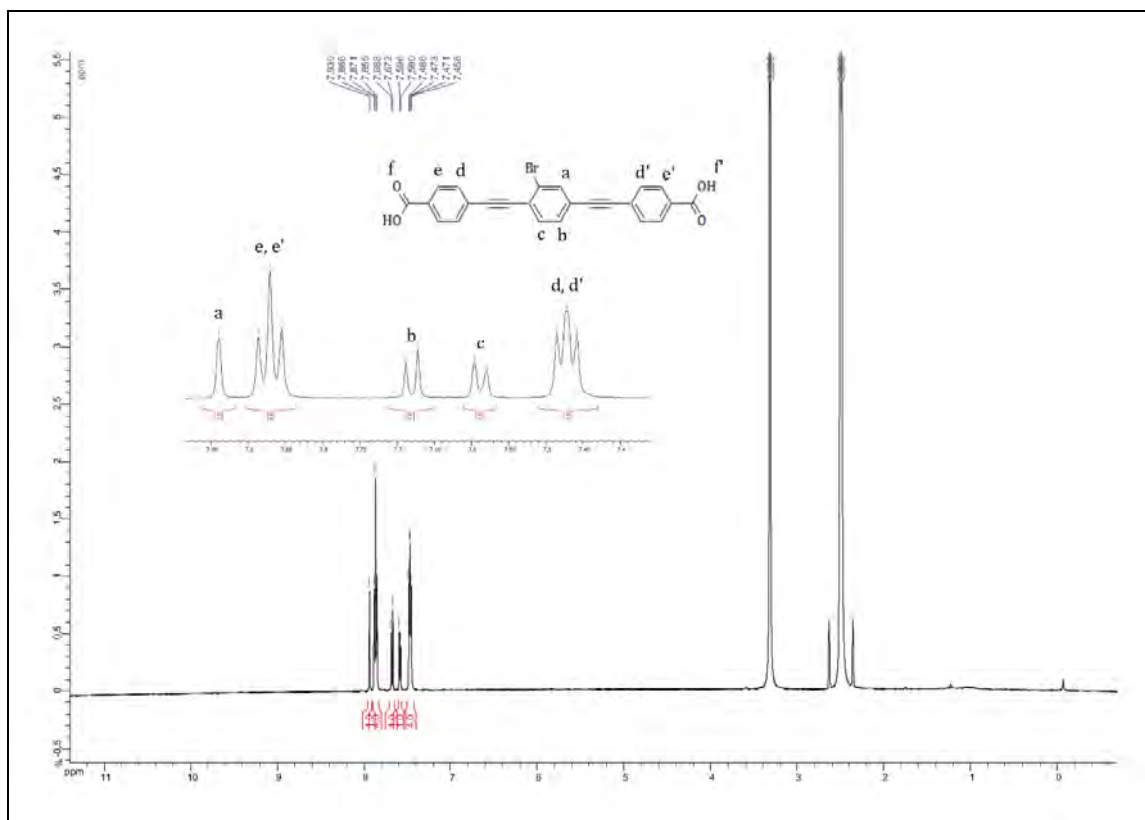
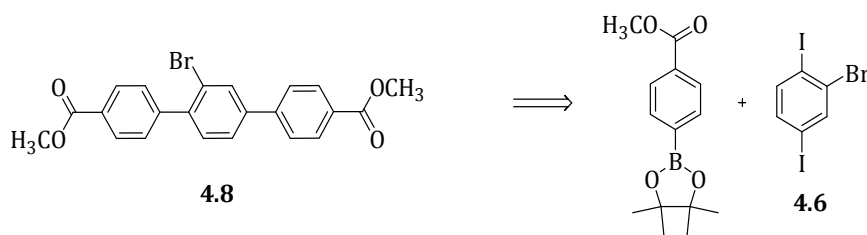


Figure 4.3: $^1\text{H-NMR}$ (500 MHz, DMSO) of Br1 (4.1).

4.4.4 Retrosynthetic analysis for the linear derivative Br2 (4.2)

From a retrosynthetic point of view, 4.2 can be obtained from the precursor 4.8, that, on his turn, can be disconnected to 4-methoxycarbonyl-phenylboronic acid pinacol ester and 2-bromo-1,4-diiodobenzene 4.6 (Scheme 4.7).

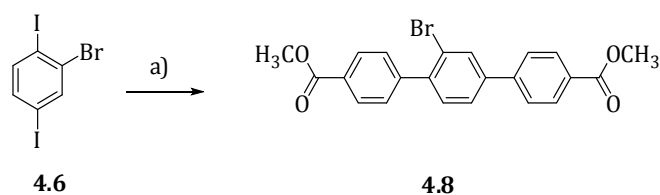


Scheme 4.7: Retrosynthetic analysis for 4.8.

The boronic ester is commercial, while the synthesis of 4.6 has been described in the previous section (4.4.2.2).

4.4.5 Synthesis of the linear derivative Br2

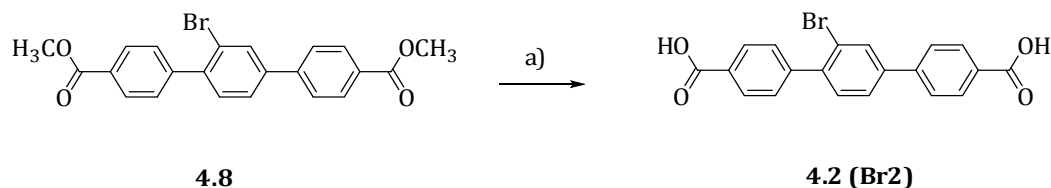
4.4.5.1 Synthesis of the methyl diester precursor 4.8



Scheme 4.8: Synthesis of **4.8**. Conditions: a) 4-methoxycarbonyl-phenylboronic acid pinacol ester (2.05 eq.), Pd(PPh₃)₄ (6.8%), K₂CO₃ (6 eq.), dioxane/H₂O, 90°C, 18h, 55%.

The precursor **4.8** was synthesized by Suzuki cross coupling reaction between **4.6** and 4-methoxycarbonyl-phenylboronic acid pinacol ester (**Scheme 4.8**). The reaction was conducted employing tetrakis(triphenylphosphine)palladium(0) as catalyst (3.4% mol for each iodine) and potassium carbonate as base, stirring in a mixture dioxane/water at 90°C for 18 hours. At this reaction temperature, the substitution was performed only on the iodines, while the bromine substituent was not involved. The product could be recovered as a yellow solid by silica gel column chromatography with hexane:ethyl acetate 9:1 as eluent and following recrystallization from cold ethanol (2-4°C), with a 55% yield.

4.4.5.2 Deprotection of the methyl ester functions: synthesis of **4.2 (Br2)**



Scheme 4.9: Deprotection of the methyl ester function. Conditions: a) LiOH (9 eq.), THF/H₂O, 50°C, 19h, 57%.

The final product **Br2 (4.2)** was generated from the precursor **4.8** by deprotecting the methyl ester groups by reaction with lithium hydroxide, conducted in tetrahydrofuran/water at 50°C for 19 hours. The product could be precipitated by acidic work up (until pH 2-3) as a pink/brown solid and was recovered with a 57% yield.

The global yield for the synthesis of **Br2 (4.2)** is calculated as 6% over the six steps.

4.4.6 Characterization of the linear derivative **Br2**

The product was characterized by ¹H and ¹³C NMR spectroscopy (mono and bidimensional) and high-resolution mass spectrometry.

The ¹H-NMR spectrum (DMSO, 500 MHz, **Figure 4.2**) allowed to confirm the identity of the product. The signals in the ¹H-NMR spectrum could be attributed by the crossed analysis of the ¹³C and bidimensional NMR spectra. The aspect was characteristic of an asymmetrically

functionalized compound. In particular, the doublet at 8.13 ppm was attributed to the proton H_a , coupled with a $J_{meta} = 2\text{Hz}$ to H_b . The signal of H_b could be found at 7.87 ppm, as a doublet of doublets, characterized by $J_{ortho} = 8.7\text{Hz}$ and $J_{meta} = 2\text{Hz}$. The proton H_c is giving a doublet signal at 7.55 ppm, characterized by a $J_{ortho} = 8.7\text{Hz}$. The others signals that can be observed in the spectrum are the doublet of doublets at 8.04 ppm ($J_{ortho} = 8.7\text{ Hz}$, $J_{meta} = 2\text{ Hz}$) characteristic of the protons H_e and $H_{e'}$ and the doublets at 7.90 and 7.59 ($J_{ortho} = 8.7\text{Hz}$) characteristic respectively of H_d and $H_{d'}$, H_d being deshielded respect to $H_{d'}$ due to the vicinity of the bromine substituent.

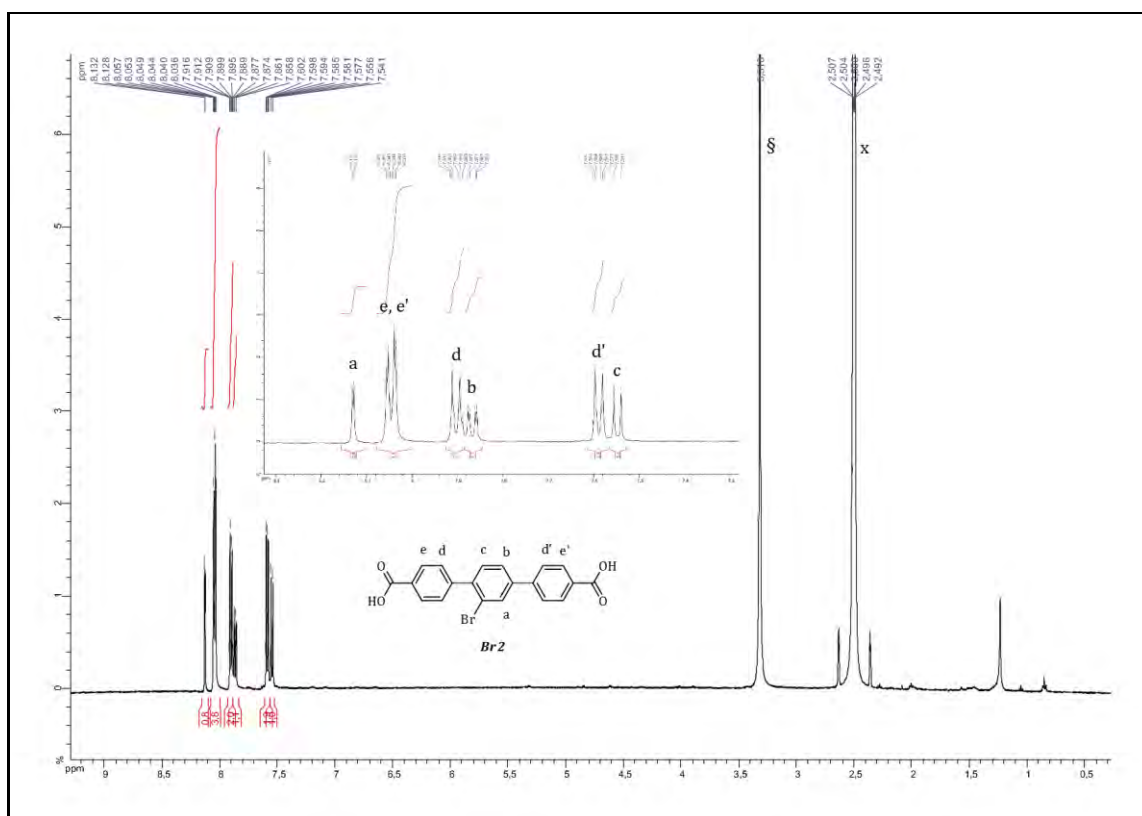
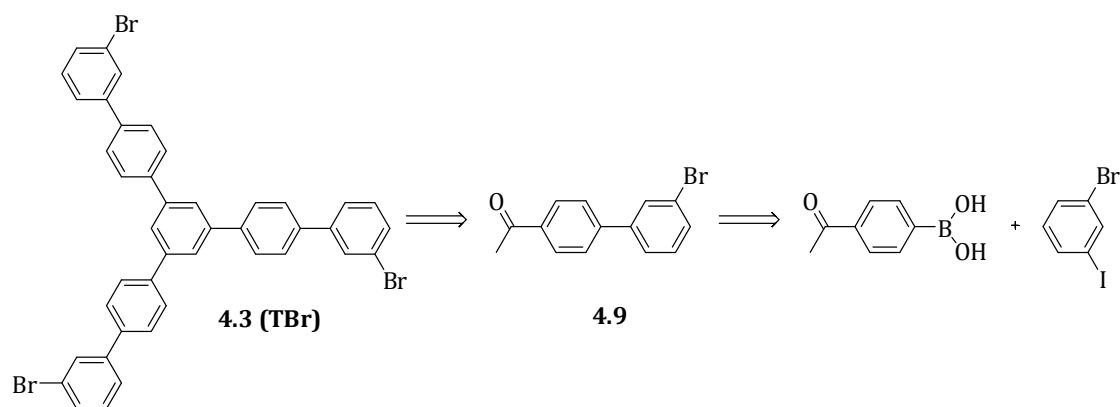


Figure 4.4: $^1\text{H-NMR}$ (500 MHz, DMSO) of **4.2 (Br₂)** (§ and x are, respectively, water and DMSO residuals).

The high resolution mass analysis (Electrospray Ionization Source in negative ions mode and Time of Flight Analyser) confirmed the identity of the product. In the spectrum it was present one peak at m/z 394.9914 Da. attributed to the singly deprotonated, of molecular formula $\text{C}_{20}\text{H}_{12}\text{BrO}_4$ (the calculated value was 394.9919). The isotopic pattern was in accordance with the presence of one bromine substituent.

4.5 Molecule with C₃ symmetry

4.5.1 Retrosynthetic analysis of the derivative TBr (4.3)

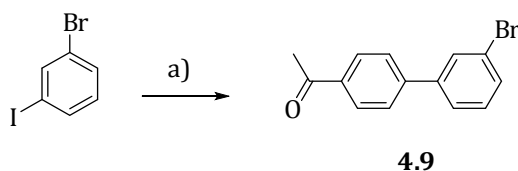


Scheme 4.10: Retrosynthetic analysis for **TBr (4.3)**.

The compound **TBr (4.3)** can be disconnected in first analysis to the methyl ketone precursor **4.9**, from which it can be obtained by an aldolic cyclotrimerization reaction. In its turn, **4.9** can be obtained by Suzuki coupling of the commercial reagents 4-acetylphenylboronic acid and 1-bromo-3-iodobenzene.

4.5.2 Synthesis of the derivative **TBr**

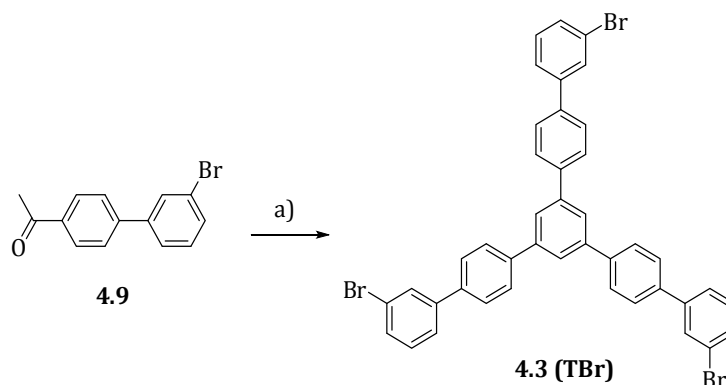
4.5.2.1 Synthesis of the methyl ketone precursor **4.9**



Scheme 4.11: Synthesis of **4.9**. Conditions: a) 4-acetylphenylboronic acid (1.05 eq.), Pd(PPh₃)₄ (1.1%), K₂CO₃ (3 eq.), dioxane/H₂O, 90°C, 19h, 72%.

The compound **4.9** could be synthesized by Suzuki cross coupling from 1-bromo-3-iodobenzene with 1.05 equivalents of 4-acetylphenylboronic. Tetrakis(triphenylphosphine)palladium(0) (1.1% mol.) was employed as catalyst, in the presence of potassium carbonate (3 equivalents) in a mixture dioxane / water at 90°C for 19 hours. Keeping the temperature at 90°C allowed to control the chemoselectivity of the functionalization, leaving the C-Br bond unaltered. The product could be recovered as a yellow oil after silica gel column chromatography (hexane 100%, then hexane : dichloromethane 5:5) with a 72% yield. Compound **4.9** was already described in the literature by Friedel-Crafts acylation¹³, but it seemed more convenient to adapt to our case the conditions described in a paper by Grigg¹⁴ for a similar product.

4.5.2.2 Aldolic cyclotrimerization affording TBr (4.3):



Scheme 4.12: Aldolic cyclotrimerization affording **4.3 (TBr)**. Conditions: a) SiCl_4 (10 eq.), ethanol / toluene dry, 18°C , 48h, 46%.

With **4.9** in hands, **TBr (4.3)** could be readily synthesized by an aldolic cyclotrimerization reaction, promoted by the Lewis acid SiCl_4 in dry toluene/ethanol (1:3) at room temperature (18°C) for 48 hours, under an atmosphere of argon¹⁵. The product **TBr (4.3)** could be recovered after aqueous work-up, by a recrystallization from dichloromethane, as a yellow solid, with a 46% yield.

The global yield for the synthesis of **TBr (4.3)** is calculated as 33% over the two steps.

4.5.3 Characterization of the derivative TBr

The product was characterized by ^1H and ^{13}C mono and bidimensional NMR spectroscopy and high resolution mass spectrometry.

The ^1H -NMR spectrum (500 MHz, DMSO/toluene 1:1, **Figure 4.5**) allowed to confirm the identity and purity of the product **TBr (4.3)**. The spectrum was characteristic of a symmetrically tri-functionalized compound and only a series of peaks in the aromatic region could be observed, conforming to the molecular structure. In particular, the singlet at 8.11 ppm, integrating for three protons was attributed to the protons H_g , while the doublets at 8.05 and 7.55 ppm integrating for six protons each and presenting an *ortho* coupling constant of 8.5 Hz were characteristic respectively of H_e and H_f . The signal of H_d could be seen as a triplet at 7.99 ppm, integrating for three protons and presenting a *meta* coupling constant of 1.6 Hz. The protons H_a and H_c were resonating at 7.77 and 7.60 ppm doublets integrating for three protons each, characterized by an *ortho* coupling constant of 7.9 Hz (the $J_{meta} = 1.6$ Hz related to the coupling to H_d could not be observed, instead). Finally the signal of the proton H_b could be individuated as a triplet integrating for three protons at 7.46 ppm, characterized by an *ortho* coupling constant of 7.9 Hz.

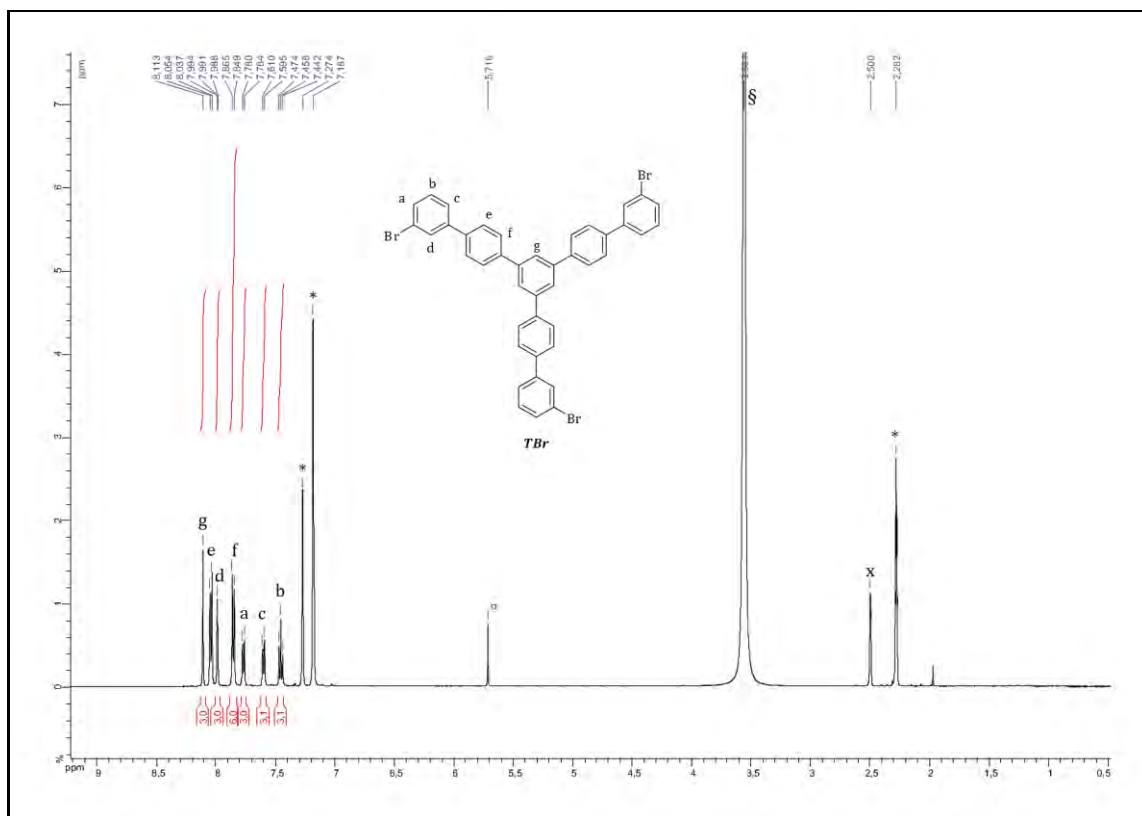


Figure 4.5: $^1\text{H-NMR}$ (500 MHz, Toluene/DMSO 1:1) of **TBr** (**4.3**)
(§, *, x and ° are, respectively, water, toluene, DMSO and DCM residuals).

The High Resolution mass spectrum (Methane Direct Chemical Ionization in positive ion mode, with Time of Flight analyser) confirmed further the identity of the product, by showing a molecular peak at 767.9639 Da, that corresponded to the molecular ion radical $[\text{C}_{42}\text{H}_{27}\text{Br}_3]^{\bullet}$ and was in good accordance with the calculated value of 767.9663 Da.

4.6 Conclusions

Three different brominated derivatives have been designed in order to self-assemble on graphene/SiC(0001) and generate a reactive aryl radical upon STM activation. The molecules **Br1** (**4.1**) and **Br2** (**4.2**) have been sent to the group of Prof. M. Yu at the Harbin Institute of Technology (China) and the **TBr** (**4.3**) has been sent to the group of L. Simon at the Institut des Science Moléculaires de Mulhouse (France) for the tests on surface (the works are in progress).

4.7 References

- ¹ a) Paulus, G. L. C., Wang, Q. H., Strano, M. S., *Acc. Chem. Res.*, **2013**, *46*, 1, 160-170; b) Koehler, F. M., Stark, W. J., *Acc. Chem. Res.*, **2013**, *46*, 10, 2297-2306.
- ² <http://www.wiredchemist.com/>
- ³ a) Thesis of Leif Lafferentz, Fachbereich Physik der Freien Universität Berlin, Berlin, Germany, page 74, Mai **2013**; b) Sakulsermsuk, S., Sloan, P. A., Palmer, R. E., *ACS Nano*, **2010**, *4*, 12, 7344-7348.
- ⁴ Walch, H., Gutzler, R., Sirtl, T., Eder, G., Lackinger, M., *J. Phys. Chem. C*, **2010**, *114*, 29, 12604-12609.
- ⁵ Gutzler, R., Walch, H., Eder, G., Kloft, S., Heckl, W. M., Lackinger, M., *Chem. Commun.*, 2009, 4456-4458.
- ⁶ Thesis of Jacob Cramer, iNANO and Department of Chemistry, Aarhus University, Aarhus, Denmark, March **2013**.
- ⁷ a) Jürgen F. Dienstmaier, J. F., Medina, D. D., Dogru, M., Knochel, P., Bein, T., Heckl, W. M., Lackinger, M., *ACS Nano*, **2012**, *6*, 8, 7234-7242; b) Silly, F., *J. Phys. Chem. C*, **2013**, *117*, 20244-20249.
- ⁸ Feng, Y. S., Xie, C. Q., Qiao, W. L., Xu, H. J., *Org. Lett.*, 2013, *15*, 4, 936-939, Zhao, Y.-L., Liu, L., Zhang, W., Sue, C.-H., Li, Q., Miljanić, O. Š., Yaghi, O. M., Stoddart, J. F., *Chem. Eur. J.*, **2009**, *15*, 13356-13380.
- ⁹ Chinchilla, R., Nájera, C., *Chem. Rev.*, **2007**, *107*, 874-922.
- ¹⁰ Shirai, Y., Osgood, A. J., Zhao, Y., Yao, Y., Saudan, L., Yang, H., Yu-Hung, C., Alemany, L. B., Sasaki, T., Morin, J.-F., Guerrero, J. M., Kelly, K. F., Tour, J. M., *J. Am. Chem. Soc.*, **2006**, *128*, 14, 4854-4864.
- ¹¹ Kajigaeshi, S., Kakinami, T., Yamasaki, H., Fujisaki, S., Okamoto, T., *Bull. Chem. Soc. Jpn.*, **1988**, *61*, 600-602.
- ¹² Morin, J. F., Shirai, Y., Tour, J., *Org. Lett.*, **2006**, *8*, 8, 1713-1716.
- ¹³ Berliner, E., Blommers, E. A., *J. Am. Chem. Soc.*, **1951**, *73*, 2479-2483.
- ¹⁴ Grigg, R. D., Van Hoveln, R., Schomaker, J. M., *J. Am. Chem. Soc.*, **2012**, *134*, 39, 16131-16134.
- ¹⁵ The procedure was adapted to our case from the paper: Yuan, M., Okamoto, K., Bronstein, H. A., Luscombe, C. K., *ACS Macro Letters*, **2012**, *1*, 3, 392-395.

Chapter 5

Synthesis of anthracene derivatives for covalent functionalization of graphene by Diels-Alder reaction

5.1 Reactivity of carbon nanomaterials as dienophiles

In the last years, the possibility of employing Diels-Alder chemistry as a mean of functionalization of different carbon surfaces has been investigated. In order to better understand the reactivity of graphene in Diels-Alder reactions, it is thus useful to compare it with that of fullerenes and carbon nanotubes. As already introduced in **Chapter 1 (section 1.3.2)**, fullerenes are expected to present an enhanced chemical reactivity than carbon nanotubes and graphene, due to the high strain characterizing some C-C bonds, expressed by the value of the C orbitals pyramidalization angle¹.

Fullerenes behave like electron deficient olefines. Due to the increased reactivity of the 6,6-ring junction common to two annulated six-membered rings, respect to the 5,6-ring junction, they can be functionalized selectively to this position. The reactivity has been demonstrated for different kind of dienes, such as cyclopentadienes², o-quinodimethanes³, isofurans⁴ and anthracenes⁵. In particular, for some reactive anthracene derivatives, the reaction is viable already at room temperature and the adduct can then be thermally decomposed at 50-90°C⁵. The characterization of fullerenes Diels-Alder adducts is quite straightforward by NMR, mass spectrometry or X-Ray analysis and allows assessing without doubts the covalent functionalization.

The reactivity of carbon nanotubes seems to be inversely dependent on the diameter of the nanotubes, together with the particular characteristics of the reactants. If with the most reactive dienes, such as o-quinodimethanes⁶, the Diels-Alder reaction is considered to be spontaneous, in other cases, a strong form of activation is necessary in order to enhance the nanotubes electrophilic character. Some examples are fluorination⁷ or complexation with organo-metallic species, such as Cr(CO)₆ and the employment of elevated pressures⁸. By these procedures, reactivity with a series of dienes has been observed, including activated butadienes⁸ and anthracenes⁷. Another report describes the selective reactivity of semi-metallic carbon nanotubes with 1-aminoanthracene at high temperatures (120-200°C)⁹. The debate around the possible functionalization of carbon nanotubes with dienes arises in large part from the difficulties in characterization and in assessing the covalent bond formation. The analytical tool mainly employed is Raman spectroscopy (see **section 6.7.7.1, Chapter 6**). An alternative

consists in NMR analysis in solution¹⁰ or at solid state⁷. Very often, the formation of a covalent bond is declared on the basis of a combination of logic considerations, based on Thermal Gravimetric and Elemental analysis and X-Ray Photoelectron Spectroscopy results¹¹

The reactivity of graphene in Diels-Alder reactions is introduced in **Chapter 1 (section 1.3.2.2)**. R. Haddon has reported for the first time on the formation of Diels-Alder adducts with 9-methylanthracene and different kinds of graphene surfaces, i.e. HOPG or exfoliated in solution, at 130°C in p-xylene for 12 hours. As expected, the reaction appears also to be thermally reversible at 160°C, allowing to remove the sp³ defects introduced on the material. The covalent bond formation between graphene and 9-methylanthracene is clearly evident by the Raman characterization. However, as already introduced in **Chapter 1** a debate has recently arisen based on the publication of two theoretical¹² and one experimental¹³ papers, suggesting that the graphene functionalization with dienes would be possible only at edges and defects, while would not be viable on the basal plane, giving origin to thermodynamically unstable products.

Due to the possibility of STM techniques to visualize molecules with an atomic scale resolution and even follow chemical reactions on a real time, it appeared thus interesting to test the possibility of reacting graphene in Diels-Alder reactions directly on surface. The direct activation by STM-tip (see **Appendix A1**) would furnish a high deal of energy in a localized region. Moreover, the presence of additional catalysers is unnecessary. Last but not least, the reversibility of the Diels-Alder reaction offers the interesting possibility of defunctionalizing locally some areas allowing a sort of “error correction”.

5.2 Objective

The objective tackled in this chapter (Figure 5.1) consists in investigating the possibility of reacting graphene with anthracene derivatives in a [4+2] Diels-Alder reaction, activated locally by an STM tip-driven process. Anthracene seems to be a viable functional group for the tests on surface in UHV, due to its possibility to absorb on graphene by π - π interactions and being endowed with thermal stability, necessary in the deposition by sublimation phase. In order to accomplish the study, it is first of all necessary to favour the formation of a stable self-assembled monolayer of anthracene derivatives on the epitaxial graphene/SiC (0001). In a second time, the possibility of locally inducing the formation of the Diels-Alder adduct, between the anthracene core and graphene, by STM-tip activation can be tested.

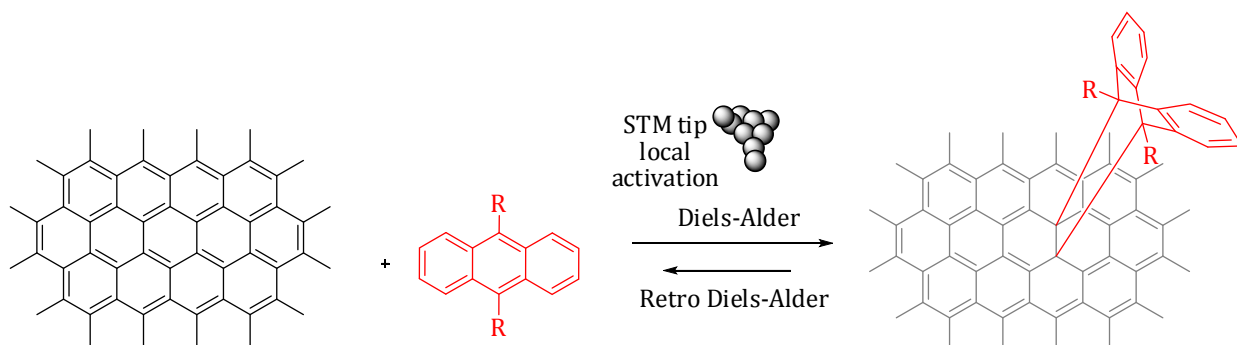
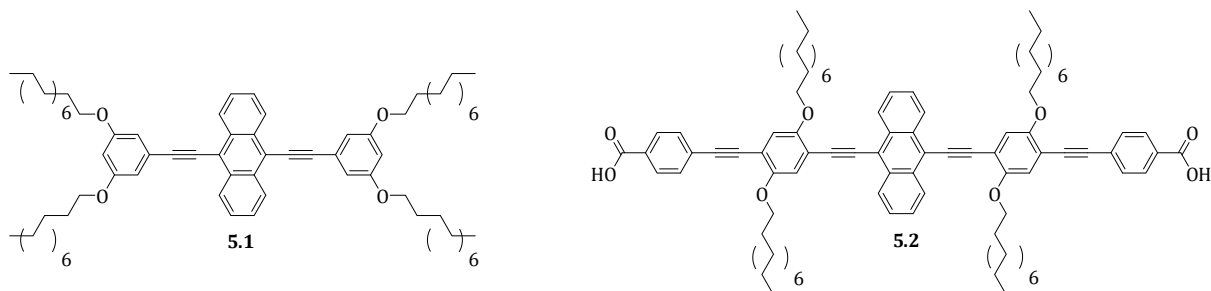


Figure 5.1: General objective.

5.3 Molecular design

In order to study the reactivity of graphene/SiC (0001) as a dienophile in Diels-Alder cycloaddition reactions with anthracene in UHV conditions, the molecules **5.1** and **5.2** were designed and synthesized.

Figure 5.2: Chemical structures of the anthracene derivatives **5.1** and **5.2**.

The two molecules were characterized by the presence of some common structural features:

- A *phenylene-ethynylene backbone* as polyaromatic rigid core, in order to favour the molecular physisorption on graphene/SiC(0001) by π - π interactions. The choice was dictated by these advantages: a) the modularity and the possibility of this kind of derivatives of being functionalized with a large number of different functional groups; b) the structural conformational flexibility related to the alkyne function (allowing possible conformational distortions after the eventual chemical reaction); c) the “shape” rigidity connected to the polyaromatic backbone and possibility of designing different molecular geometries. Moreover, the formation of self-assembled monolayers of poly-phenylene-ethynylene derivatives has already been observed at the solid/liquid interphase on HOPG (highly oriented pyrolytic graphite)¹⁴ and on carbon nanotubes¹⁵. On the contrary, only a few examples of physisorption are reported on graphene in solution¹⁶ and still no studies are reported on graphene/SiC (0001) in UHV, although ethynyl-derivatives have already been imaged on other surfaces¹⁷ (for ex. Au(111)).

- *Long alkyl-chains* with a double role: a) enhancing the molecular adsorption on the surface by establishing CH- π interactions¹⁸; b) favouring the organisation and self-assembly of the molecules by van der Waals interactions (see Chapter 1).

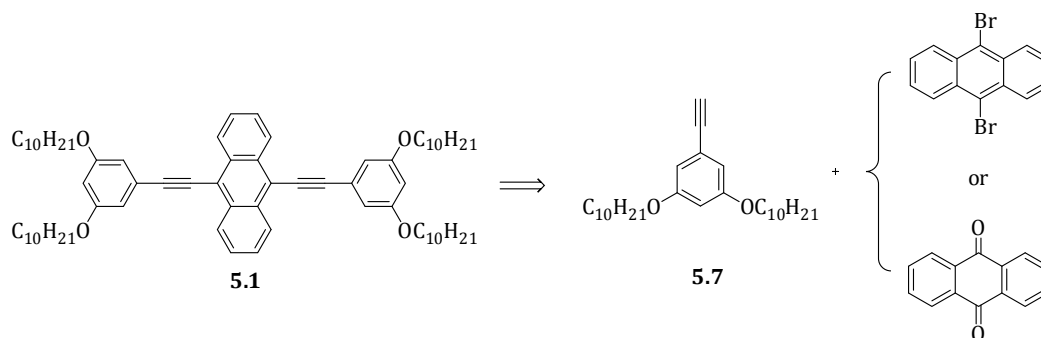
- An anthracene *core* was chosen as reactive group for two main reasons: a) there already exist reports on its reactivity with graphene¹⁹ in solution; b) the planar and conjugated structure should favour its physi-sorption on the surface. Moreover, after the eventual chemical reaction, the molecular conformation is expected to change (i.e. from planar to butterfly), affording a different contrast in the STM image and thus providing a mean to distinguish the reactants from the products.

The anthracene derivative **A2** (5.2) presented two additional *carboxylic acid moieties*, in order to favour the organization of a self-assembled layer by additional hydrogen bonding interactions.

5.4 Anthracene derivative A1 (5.1)

5.4.1 Retrosynthetic analysis for A1

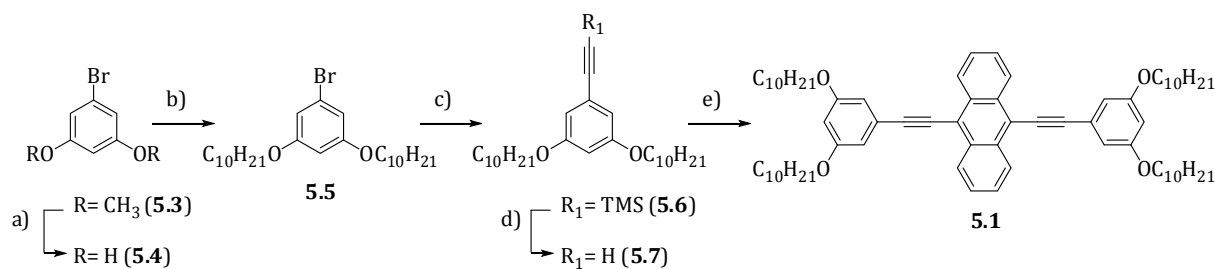
From a retrosynthetic point of view, the anthracene derivative **A1** (5.1) can be disconnected to the alkyne-bearing moiety **5.7**, deriving in last analysis from dimethyl 5-bromo isophthalate, and 1,9-dibromoanthracene or 1,9-antraquinone (**Scheme 5.1**)



Scheme 5.1: Retrosynthetic analysis for the anthracene derivative **A1** (5.1).

5.4.2 Synthesis of A1

The synthesis of the anthracene derivative **5.1** was carried out following the approach summarized in **Scheme 5.2**.



Scheme 5.2: Synthesis of the anthracene derivative **5.1**. Conditions: a) HBr/AcOH, 110°C, 10h, 81%; b) 2.9 eq. C₁₀H₂₁Br, K₂CO₃, DMF, 65°C, 18h, 90%; c) TMSA, Pd(PPh₃)₄ (10%), CuI (1%), (iPr)₂NH, 100°C, 6h, 91%; d) CsF, MeOH/THF, 25°C, 4h, 96%; e) 1,9-anthraquinone, nBuLi, -78°C → 20°C, 3h; SnCl₂, HCl, 25°C, 1h, 82% or 9,10-dibromoanthracene, Pd(PPh₃)₄ (4%), CuI (4%), (iPr)₂NH, Toluene/ACN or THF, 100°C, 6h, 20-30%

5.4.2.1 Synthesis of the self-assembling group 5.7

Step a)

In a first step, the oxygen atoms of the starting material dimethyl 5-bromo isophthalate were demethylated by treatment with an equivolumic mixture of hydrobromic acid (48%) in acetic acid (glacial) at 110°C for 10 hours. The product **5.4** was obtained with a 81% yield as a white solid, after column chromatography on silica. In the procedure classically reported in the literature, it is usually rather employed BBr₃ as demethylating reagent, but we found the HBr/AcOH more convenient and less time consuming, not necessitating to work in dry conditions.

Step b)

The phenolic oxygens of **5.4** were subsequently reacted with 1-bromodecane in a S_N₂ reaction promoted by potassium carbonate in dimethylformamide at 65°C for 18 hours, to give compound **5.5** with a 90% yield, after column chromatography on silica gel. The same reaction was conducted also in acetone at 60°C for 18 hours, giving only a 53% yield. The lower yield could be explained by the lower polarity of acetone, with a lower stabilizing effect (by hydrogen bonds) on the generated phenoxide anions.

Step c)

In the following step, the alkyne moiety was introduced on compound **5.5** by a palladium catalysed Sonogashira cross coupling reaction²⁰. The best yields for product **5.6** (91%) were found by employing 10% of Pd(PPh₃)₄ and 1% of CuI as catalysers and di-isopropylamine as solvent (0.34 M), warming at 100°C for 6 hours, then purifying by column chromatography on silica gel. The high loading of palladium catalyser was meant to enhance the reaction rate by favouring the step of oxidative addition to palladium of the aryl-bromide **5.5**, quite difficult due

to the presence of the two deactivating $-\text{OC}_{10}\text{H}_{21}$ groups in meta and the relatively low reactivity of the C-Br bond.

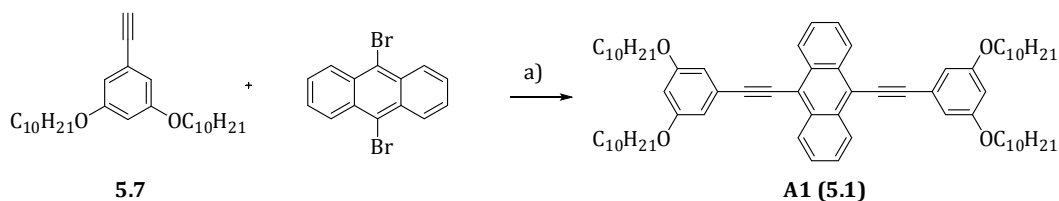
Step d)

The trimethylsilyl protective group was removed from the alkyne moiety of compound **5.6** by reacting it with cesium fluoride in tetrahydrofuran, with a small percentage of methanol as the proton donor. Although the deprotection procedure was repeated twice, at first for 4 hours, then for 18 hours at 25°C, it was not possible to bring the reaction to completion and a small quantity of starting material was still present in the reaction mixture (7%, from $^1\text{H-NMR}$ analysis), that was not possible to remove by chromatographic separation. The neat yield of the reaction was estimated to be 89% (obtained 0.29 g of product dirty at 7%). Neither different deprotection conditions (KOH in 1.03 excess, in THF/MeOH/ H_2O 1:1:0.1, for 3 hours) helped in enhancing the conversion yield of the reaction (in these conditions a 6% of protected compound was still present, on 0.74 g). Since the impurity did not represent a possible interference with the following step, the synthesis was carried on without further improving the reaction conditions.

5.4.2.2 Coupling of the self-assembling group to the anthracene core

1.4.2.2.1 Coupling strategy a)

The final product **A1 (5.1)** could be obtained by two different coupling procedures (**Scheme 5.3** and **5.4**).



Scheme 5.3: First strategy of coupling to yield the anthracene derivative **A1 (5.1)**. Conditions: a) $\text{Pd}(\text{PPh}_3)_4$ (4%), CuI (4%), $(i\text{Pr})_2\text{NH}$, Toluene/ CH_3CN or THF, 100°C, 6h, 20-30%

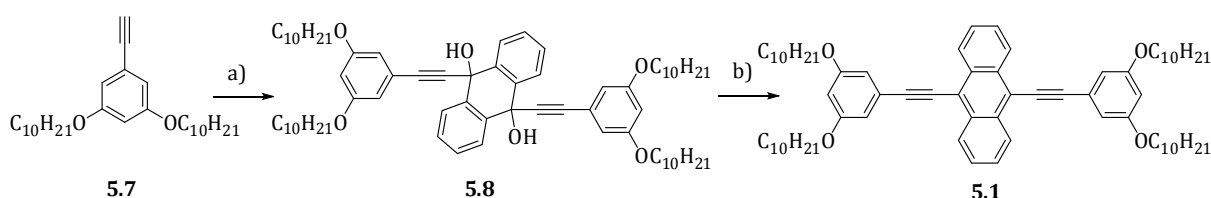
In a first attempt, the deprotected alkyne **5.7** was reacted with 1,9-dibromoanthracene in a Sonogashira cross coupling reaction, catalysed by $\text{Pd}(\text{PPh}_3)_4$ (4% for each bromine functionality) and CuI (4% for each bromine functionality). Two mixtures of solvents were tested: di-isopropylamine/toluene/acetonitrile and di-isopropylamine/tetrahydrofuran, both giving low yields (20% - 30%) and a mixture of products that was quite difficult to purify. In both cases, the complete removal of the impurities (respectively giving signals in the $^1\text{H-NMR}$ spectrum in the aromatic or in alkyl chains regions) was not possible to achieve, neither by

chromatography nor by recrystallization. The difficulty of the reaction could be ascribed to the inertness of the electron rich and sterically hindered 9,10-dibromoanthracene towards oxidative additions to palladium.

The global yield of the reaction, considering the *coupling strategy a)*, was estimated to be 13-19%.

The reaction conditions for the Sonogashira coupling could have been certainly improved to give better yields, but in our case we decided rather to explore a second coupling strategy, based on a carbonyl addition to anthraquinone (**Scheme 5.4**).

1.4.2.2.2 Coupling strategy b)



Scheme 5.4: Second strategy of coupling to yield the anthracene derivative **A1** (**5.1**). Conditions: a) n-BuLi, THF, -78°C->20°C, 9,10 anthraquinone, 3h; b) SnCl₂, HCl, THF, 25°C, 1h; yield over the two steps: 82%

In a first step, the alkyne **5.7** was deprotonated by n-butyllithium and the anion was reacted with 9,10-anthraquinone in dry THF, to give, after acidic work up, a double product of addition to the carbonyl, the di-alcohol **5.8**. The alcoholic product **5.8** was then submitted to a reductive aromatization reaction promoted by tin (II) dichloride in a 10% solution of hydrochloric acid for 10 minutes at 20°C. The column chromatography purification of the was found highly facilitated and the product **5.1** was obtained as an orange solid with an 82% yield.

The global yield of the reaction, considering the “Coupling strategy b)”, was 52%.

5.4.3 Characterization of A1

The anthracene derivative **A1** (**5.1**) was completely characterized by multinuclear (¹H and ¹³C) mono and bi-dimensional NMR spectroscopy, high-resolution mass spectrometry.

The ¹H-NMR spectrum (500 MHz, CD₂Cl₂; **Figure 5.2**) allowed to assess the symmetric functionalization of the anthracene core: only two multiplets, at 8.6-8.7 and 7.6-7.7 ppm, integrating for four protons each, were observed for the protons *a* and *b*. At higher fields, the presence of two other signals in the aromatic region was observed: a doublet at 6.92 ppm (J=2.5 Hz) integrating for four protons, attributed to the protons *c* and a triplet at 6.55 ppm (J=2.5 Hz)

integrating for two protons and attributed to *d*. The triplet at 4.03 ppm ($J=7$ Hz), was attributed to the protons *e* shifted at lower field due to the presence of the oxygen and benzene ring. Other signals characteristic of the alkyl chains were found at 1.82 (*f*), 1.50 (*g*), 1.3-1.4 (chain), and 0.90 ppm (*h*). The correct integral ratio let to confirm that the anthracene core was di-substituted by two C_{10} -alkyl-chains functionalized benzene rings.

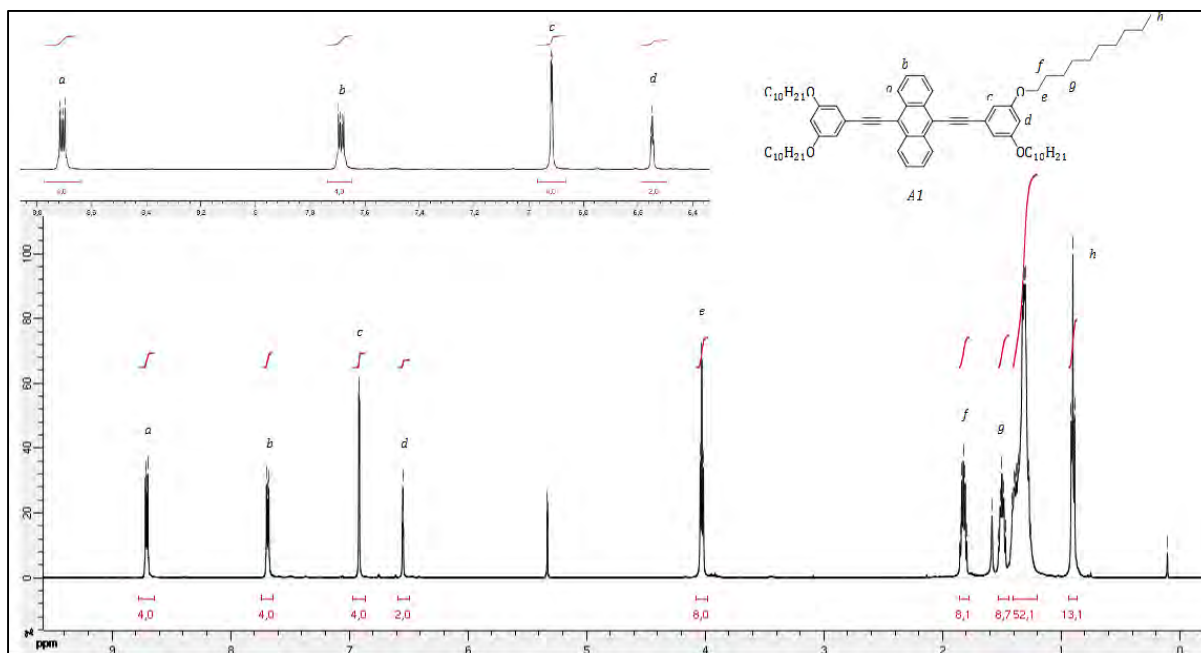


Figure 5.3: $^1\text{H-NMR}$ spectrum (500 MHz, CD_2Cl_2) of the anthracene derivative **A1** (5.1).

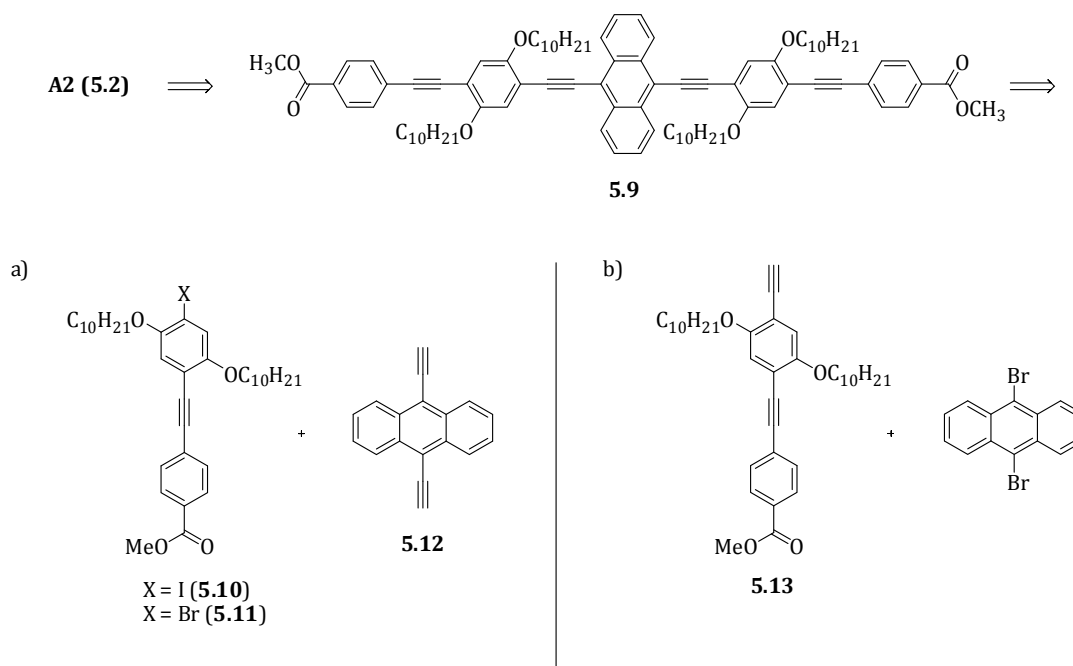
The high resolution mass spectra (DCI- CH_4 ionization source and time of flight analyser) confirmed further the identity of the product, showing a molecular peak at m/z 1003.7539, corresponding to the mono-protonated species $[\text{M}+\text{H}]^+$.

5.5 Anthracene derivative A2 (5.2)

5.5.1 Retrosynthetic analysis of A2

The anthracene derivative **A2** (5.2) can be obtained by deprotection of the methyl ester functionalities of **5.9**. For **5.9**, different disconnections could be envisioned. For our synthesis, we choose to adopt a strategy based on a convergent approach (**Scheme 5.5**), consisting in synthesizing the self-assembling units **5.10**, **5.11** or **5.13** and incorporating it on the anthracene core only in a final step. This approach allowed to work with soluble and “simple” compounds all through the synthesis, facilitating the purification and limiting the number of steps of purification of anthracene derivatives, that sometimes are found difficult. Moreover, the strategy offered the interesting perspective of varying the length of the self-assembling units

(thus the density of reactive groups on the surface), by just changing the number of phenyl moieties in the self-assembling group.



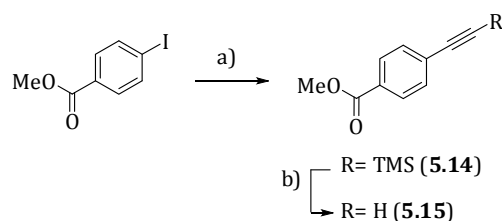
Scheme 5.5: Retrosynthetic analysis for the anthracene derivative **A2 (5.2)**.

Two synthetic strategies were compared: in the *coupling strategy a)* the self-assembling group **5.10** or **5.11** was synthesized and reacted with a previously alkyne-functionalized anthracene core; in the *coupling strategy b)* the alkyne functionalized self-assembling moiety **5.13** was reacted with 9,10-dibromoanthracene. Most of the steps of the synthesis of the self-assembling groups were common to the two strategies.

5.6 Synthesis of **A2 (5.2)**ⁱ

5.6.1 Synthesis of the self-assembling groups **5.10**, **5.11** and **5.13**

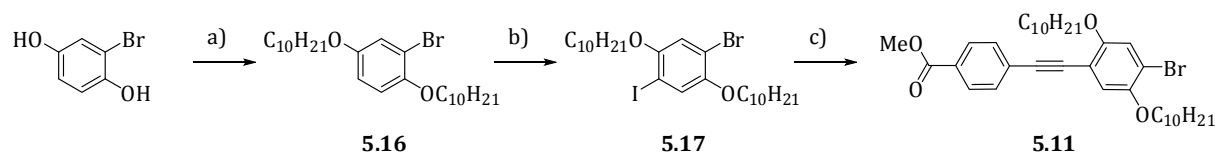
The synthesis of the carboxylic acid bearing moiety **5.15** was carried out following a procedure already reported in the literature²¹ (**Scheme 5.6**, see compound **4.5** in the previous chapter).



Scheme 5.6: Synthesis of **5.15**. Conditions: a) TMSA, Pd(PPh₃)₂Cl₂ (3%), CuI (5%), Et₃N, 25°C, 2h, 96%; b) K₂CO₃, CH₂Cl₂,/CH₃OH, 2h, 97%.

ⁱ The synthesis was carried out with the collaboration of a internship student, Hiromi Nagashima, from NAIST (Nara Institute of Technology), Japan.

5.6.1.1 Synthesis of the self-assembling group 5.11



Scheme 5.7: Synthesis of **5.11**. Conditions: a) KOH, C₁₀H₂₀Br (2.2 eq.), EtOH, 80°C, 18h, 94%; b) I₂ (0.55 eq.), KIO₃ (0.2 eq.), AcOH / H₂O / H₂SO₄, 113°C, 17h, 81%; c) **5.15** (1.05 eq.), Pd(PPh₃)₂Cl₂ (3%), CuI (5%), Et₃N / THF, 22°C, 16h, 91%

Step a)

In a first step, the diphenolate anion obtained by deprotonation of 2-bromohydroquinone with potassium hydroxide was alkylated with bromodecane (2.2 eq.), in a S_N2 reaction conducted in ethanol at reflux (80°C) for 18 hours. The desired product **5.16** was obtained as an incolour solid, after column chromatography on silica, with a 94% yield. The conditions applied were those reported in the literature²² for similar compounds.

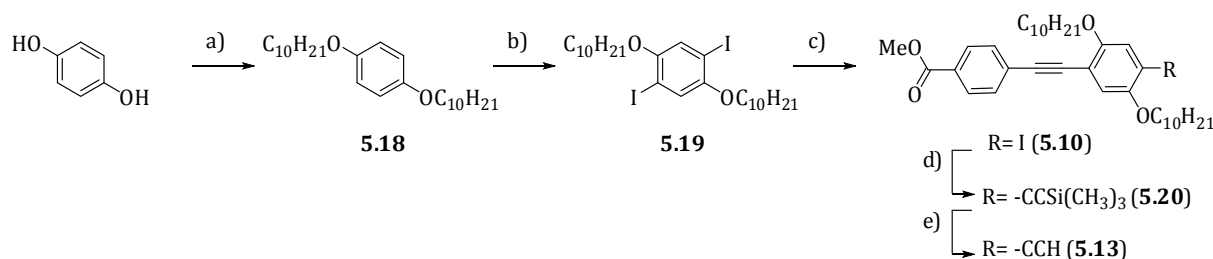
Step b)

5.16 was successively iodinated in position 5 by a electrophilic aromatic substitution reaction involving iodine and potassium iodate, in acidic medium (acetic acid 92%, sulphuric acid 1%, water 7%), at reflux (110°C) for 17 hours²³. Potassium iodate was employed as oxidant for iodine, in order to generate the iodonium electrophilic species (I⁺) in acidic medium. The iodation is directed in *ortho* to the oxygen in position 4 by combined electronic effects of the substituents -OC₁₀H₂₁ and Br. The product **5.17** was obtained pure as an incolour solid with a 81% yield. For the synthesis, we applied conditions already reported in the literature for similar compounds.

Step c)

The last step consisted in coupling the product **5.15** with **5.17** in a Sonogashira reaction. The conditions employed were quite standard, Pd(PPh₃)₂Cl₂ (3% respect to the iodine) and CuI (5% for each iodine), in triethylamine/tetrahydrofurane 1:1 (0.09 M for each iodine), at 22°C for 16 hours. In these conditions (T=22°C) the oxidative addition to palladium (0) is favoured only for the C-I bond, and not for the stronger C-Br bond, so only the mono-coupled product was obtained. After column chromatography purification, the title compound **5.11** was obtained with a 91% yield.

5.6.1.2 Synthesis of the self-assembling groups 5.10 and 5.13



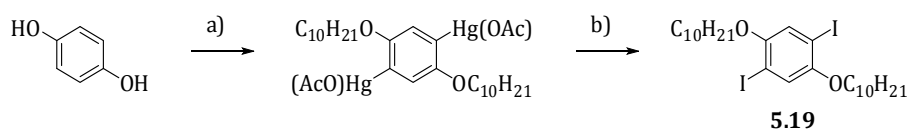
Scheme 5.8: Synthesis of **5.10** and **5.13**. Conditions: a) KOH, $\text{C}_{10}\text{H}_{20}\text{Br}$ (2.2 eq.), EtOH, 80°C , 18h, 76%; b) I_2 (2.5 eq.), $\text{Hg}(\text{OAc})_2$ (2.5 eq.), CH_2Cl_2 , 22°C , 48h, 73%; c) **5.15** (0.6 eq.), $\text{Pd}(\text{PPh}_3)_2\text{Cl}_2$ (0.66%), CuI (1%), Et_3N / THF, 22°C , 6h, 43%; d) TMSA, $\text{Pd}(\text{PPh}_3)_2\text{Cl}_2$ (3%), CuI (5%), Et_3N / THF, 23°C , 2h, 92%; e) K_2CO_3 , CH_2Cl_2 / CH_3OH , 23°C , 2h, 95%

Step a)

The first step consisted in a Williamson etherification: a diphenolate was generated from 1,4-hydroquinone in basic medium and reacted in a $\text{S}_{\text{N}}2$ reaction with 2.2 equivalents of bromodecane in ethanol, warming at reflux (80°C) for 18 hours. The choice of ethanol for a $\text{S}_{\text{N}}2$ reaction appears quite unusual, since polar aprotic solvents are generally preferred for this kind of reactions. The justification is that ethanol can stabilize the very electron rich diphenolate anions by hydrogen bonding. The desired product **5.18** was obtained as an incolour solid, after recrystallization from methanol, with a 76% yield. The product **5.18** is already well known in the literature²⁴.

Step b)

In the following step, 1,4-bis(decyloxy)benzene **5.18** was iodinated in the presence of mercury acetate, in dichloromethane at 22°C for 48 hours. The arene is di-mercured in *ortho* to the oxygens by an aromatic electrophilic aromatic substitution and mercury acetate can be successively substituted by an iodine electrophile²⁵, (**Scheme 5.9**). The reaction is efficient and the compound **5.19** is obtained after recrystallization from ethanol with a 73% yield as an incolour solid. The procedure reported in a paper of J. M. Tour²⁶ was followed.

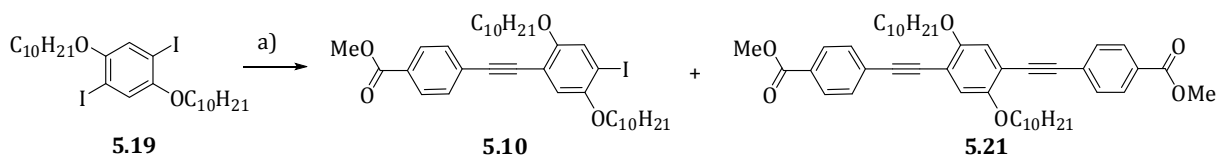


Scheme 5.9: Mechanism of iodination by mercury acetate.

Step c)

The di-iodinated compound **5.19** was then reacted in a Sonogashira reaction with precursor **5.15**. For the reaction, standard conditions were employed, $\text{Pd}(\text{PPh}_3)_2\text{Cl}_2$ (0.3% for each iodine, 1% for each alkyne) and CuI (0.7% for each iodine, 2% for each alkyne) as

catalysers in diethylamine/dichloromethane 1:1 (0.02M for the alkyne). The iodinated compound **5.15** was employed in 1.5 eq. with respect to the alkyne, to give a final iodine/alkyne excess of 3:1 and thus favour the monofunctionalization, with respect to difunctionalization, that is favoured being the monofunctionalized product **5.10** more activated than **5.19** due to the presence of the carboxylic acid moiety. In these conditions, the product could be recovered as a yellow solid after a column chromatography on silica, with yields ranging from 27 to 43%, being compound **5.21** the major byproduct formed.



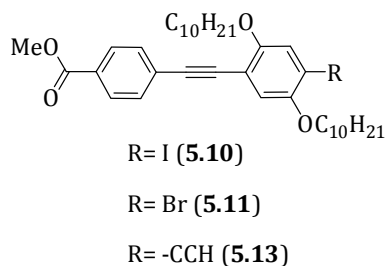
Scheme 5.10: Synthesis of **5.10**. Conditions: a) **5.16** (0.6 eq.), Pd(PPh₃)₂Cl₂ (0.66%), CuI (1%), Et₃N / THF, 22°C, 6h, 27-43%.

Steps d and e)

Compound **5.10** was functionalized with a trimethylsilyl-protected ethynyl function, by a Sonogashira reaction (**Scheme 5.8**). The conditions employed were adapted from the literature²⁷ for different compounds, varying the composition of the solvent and the conditions for the purification to our compound. The reaction was conducted employing as catalysers Pd(PPh₃)₂Cl₂ (3% respect to the iodine) and CuI (5% for each iodine), in triethylamine/tetrahydrofuran 1:1 (0.09 M for each iodine), at 22°C for 16 hours. The product **5.20** (**Scheme 5.8**) was obtained in a 92% yield after column chromatography on silica.

The alkyne functionality of **5.20** (**Scheme 5.8**) was finally deprotected in basic conditions, employing 5 eq. of potassium carbonate in dichloromethane/methanol 1:1. In a concentrated medium (0.16 M for **5.20**), the reaction was rapid and it could be completed in two hours at 23°C. The product **5.13** was purified from an impurity at lower R_f on TLC, by column chromatography on silica and obtained as a yellow solid with a 95% yield.

5.6.2 Coupling of the self-assembling groups to the anthracene core



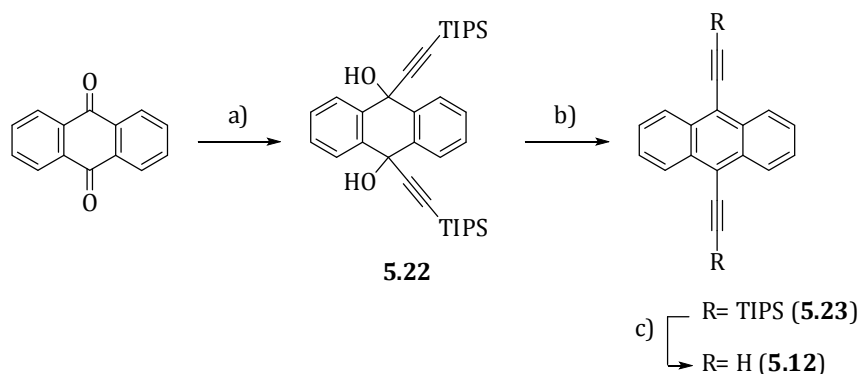
Scheme 5.11: Self-assembling groups **5.10**, **5.11** and **5.13**.

As already introduced in **section 5.4.1**, we compared two strategies in order to couple the self-assembling groups to the anthracene core:

- in “Coupling strategy a)” we reacted 9,10-diethynylantracene with the previously synthesized self-assembling groups **5.10** or **5.11**;
- in “Coupling strategy b)” we introduced the alkyne moiety directly on the self-assembling group (compound **5.13**), then inserted it on the 9, 10-dibromoanthracene core in a following step.

5.6.2.1 Synthesis of 9, 10 diethynylantracene **5.12**

The employed synthetic procedure was adapted from the literature²⁸ and is reported in **Scheme 5.12**.



Scheme 5.12: Synthesis of **5.12**. Conditions: a) TIPSA (2.5 eq.), nBuLi (2.5 eq.), THF/Et₂O, -78°C → 22°C, 20h, then NH₄Cl aq., HCl aq.; b) SnCl₂, AcOH/H₂O/Acetone, 22°C, 1h, global yield over the two steps a) and b) was 37%; c) TBAF, THF, 0-5°C → 22°C, 15 min., then NH₄Cl aq., 12%.

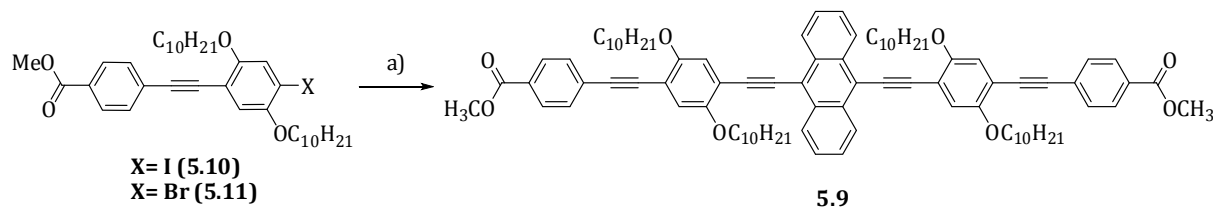
Steps a and b)

Tri-isopropylsilyl protected acetylene was deprotonated with n-butyl lithium at low temperature (-78°C) and the generated carbanion was then reacted with 9,10-anthraquinone in a carbonyl addition reaction, to give the dialcohol **5.22**, after acidic treatment. The dihalcohol **5.22** was isolated as a light yellow solid and purified by column chromatography, before being reduced with tin (II) chloride in the presence of acetic acid, to yield 9,10-bis[(triisopropylsilyl)ethynyl]anthracene **5.23**, as a yellow fluorescent solid. The global yield over the two steps was 37% after column chromatography on silica.

The last step consisted in the deprotection of the di-isopropylsilyl-ethynyl groups and was conducted with tetrabutylammonium fluoride in tetrahydrofuran at room temperature for 30 minutes, followed by acidic work-up. The obtained diethynyl-anthracene **5.12** was very sensitive to oxidation²⁹ and a consistent polymerization of the alkyne moieties was observed during the rotavapor evaporation procedure (at 40°C) and the silica column chromatography purification, which could explain the low reaction yield (12%).

The diethynyl-anthracene **5.12** was functionalized with the self-assembling group **5.10** or **5.11**, following the procedure described in the following section (**Scheme 5.13** and **5.14**).

5.6.2.2 Coupling strategy a)



Scheme 5.13: Coupling strategy a). Conditions: **5.12**, Pd(PPh₃)₂Cl₂ (3% for bromine), CuI (5% for bromine), Et₃N/THF, 90°C, 16h, <11%; or **5.12**, Pd(PPh₃)₂Cl₂ (5% for iodine), CuI (5% for iodine), Et₂NH/THF, 22°C, 6h, <48%.

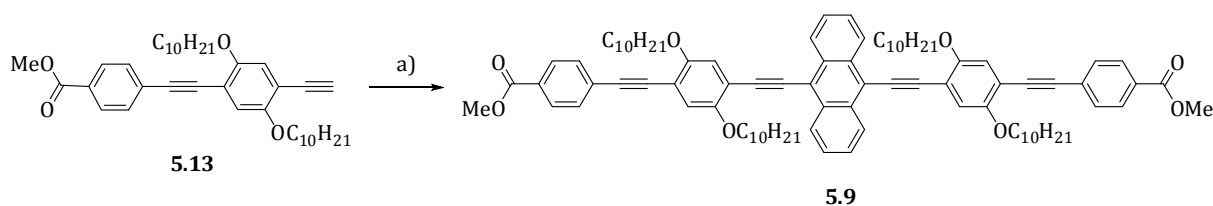
In a first attempt, we tested the possibility of coupling the precursors **5.10** or **5.11** and diethynylanthracene **5.12**, by Sonogashira reaction.

The coupling of **5.11** was carried out employing Pd(PPh₃)₂Cl₂ (3% with respect to the bromine) and CuI (5% for each bromine), in triethylamine/tetrahydrofuran 1:1 (0.03 M for each bromine), at 90°C for 16 hours. A very small quantity of product was obtained (yield was estimated to be inferior to 11%), that was not possible to purify completely by column chromatography or recrystallization. The unsuccess of the reaction could be attributed to the low reactivity of the highly sterically hindered ethynyl functions, together with the already observed propensity of the anthracene-ethynyl moieties to polymerize upon warming.

With the aim of increasing the reaction efficiency, we employed the iodine-substituted group **5.10**, that, showing enhanced reactivity respect to **5.11** due to the less strong nature of the carbon-iodine bond, would have allowed to avoid the warming during the reaction and reduce the reaction time. The conditions employed were Pd(PPh₃)₂Cl₂ (5% with respect to the iodine) and CuI (5% for each iodine), in diethylamine/tetrahydrofuran 1:1 (0.07 M for each iodine), at 22°C for 6 hours. In this case, the conversion to **5.9** appeared to be higher, but still the product was impure and a complete purification could not be achieved. A large amount of insoluble compound (presumably deriving from the diethynyl-anthracene polymerization) was still observed.

Since the problems of oxidation of the diethynyl-anthracene resulted to be important and difficult to overcome, we decided to explore a different coupling strategy, based on a Sonogashira reaction of **5.13** to 9,10-dibromoanthracene.

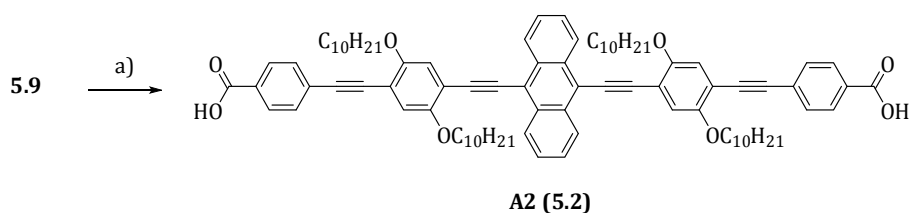
5.6.2.3 Coupling strategy b)



Scheme 5.14: Coupling strategy b). Conditions: a) 9,10-dibromoanthracene, Pd(PPh₃)₄ (3% for iodine), CuI (5% for iodine), (iPr)₂NH/THF, 80°C, 20h, 70%.

The coupling reaction between **5.13** and 9,10-dibromoanthracene was conducted employing Pd(PPh₃)₄ (3% with respect to each alkyne function) and CuI (5% for each alkyne function), in diisopropylamine/tetrahydrofuran 1:1 (0.03 M for each bromine and alkyne), at 80°C for 20 hours. In order to favour the oxidative addition step of anthracene to palladium (0), a solution of 9,10-dibromoanthracene and the catalysers, was warmed at 45°C for one hour, before adding the ethynyl derivative **5.13**. The reaction worked efficiently, giving a quite pure product, that could be purified by recrystallization from cold dichloromethane, to yield **5.31** as a red solid, with a 70% yield.

5.6.3 Deprotection of the methyl-esters



Scheme 5.15: Deprotection of the methyl-esters. Conditions: LiOH, H₂O/THF, 50°C, 22h, 99%.

The target compound **5.2** was obtained by deprotecting the ester derivative **5.9** in basic conditions. Lithium hydroxide was employed as base. In order to carry out the reaction, it was necessary to warm at 50°C for 22 hours: at room temperature the kinetic was in fact very slow, and even after 96 hours the quantity of product recovered was minimal. After acidic work up, the product was recovered as a red solid, with a 99% yield.

5.7 Characterization of A2

The anthracene derivative **A2** was completely characterized by multinuclear (¹H and ¹³C) mono and bi-dimensional NMR spectroscopy and high-resolution mass spectrometry.

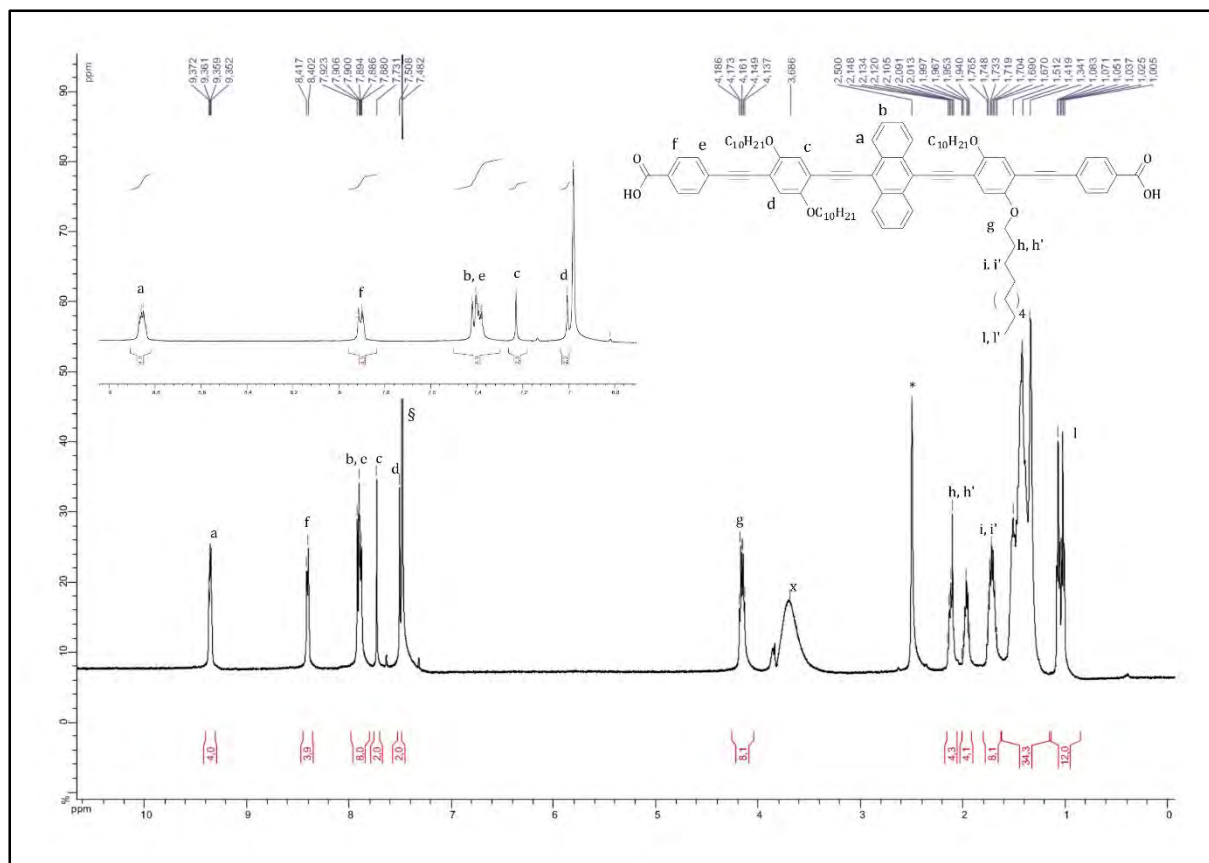


Figure 5.4: $^1\text{H-NMR}$ spectrum (500 MHz, C_6D_6 95%, DMSO 5%) of the anthracene derivative **5.2 (A2)**. (δ , x, * are respectively the signals of residual benzene, water and DMSO).

The $^1\text{H-NMR}$ spectrum (**Figure 5.4**, 500 MHz, C_6D_6 95%, DMSO 5%) allowed to assess the identity and purity of the product. Being the product **5.2 (A2)** only partially soluble in apolar solvents, the spectrum was recorded in a mixture of benzene- D_6 (95%) and DMSO- D_6 (5%). The signals were in general poorly resolved due to aggregation phenomena by π - π stacking and were attributed as following: the multiplet at 9.3-9.4 ppm was assigned to the anthracene protons Ar- H_a ; the multiplet at 8.3-8.4 ppm to the protons Ar- H_f , resonating at low fields due to the vicinity of the ester group; the multiplet at 7.8-7.9 ppm was characteristic of the protons Ar- H_b and Ar- H_e , the singlets at 7.73 and 7.51 ppm, integrating for two protons each, were attributed to the protons Ar- H_c and Ar- H_d . In the alkyl chains region, we could assign the signals as following: the multiplet at 4.1-4.2 ppm was characteristic of the eight methylenic protons close to the phenolic oxygens (CH_g); the multiplets at 2.0-2.1 ppm and 1.9-2.0 were assigned to the methylenic protons (CH_h and h') (it is not clear why the two groups of protons experience a different environment, determining the difference in the chemical shift); the multiplet at 1.6-1.8 ppm was assigned to the protons (CH_i and i'), the multiplet at 1.0-1.1 ppm was instead characteristic of the terminal CH_3 . The large multiplet at 1.3-1.6 ppm was attributed to the methylene groups of the alkyls chains.

The high resolution mass spectra (MALDI ionization source with DCTB matrix and time of flight analyser) confirmed further the identity of the product, showing a molecular peak at m/z 1290.7886, corresponding to the radicalic species $[M]^{\bullet+}$ (calculated value 1290.7888).

5.8 Conclusions

Two anthracene derivatives, **A1** (5.1) and **A2** (5.2), designed to self-assemble on graphene/SiC(0001) and react with it by a STM-tip activated Diels-Alder reaction, have been designed and synthesized. Up to the time that this manuscript is being finished, the molecules were not yet deposited and tested on the surface.

5.9 References

- ¹ Koehler, F. M., Stark, W. J., *Acc. Chem. Res.*, **2013**, *46*, 10, 2297-2306.
- ² Giovane, L. M., Barco, J. W., Yadav, T., Lafleur, A. L., Marr, J. A., Howard, J. B., Rotello, V. M., *J. Phys. Chem.*, **1993**, *97*, 8560-8561.
- ³ Belik, P., Gugel, J.; Spickermann, K.; Müllen, K., *Angew. Chem. Int. Ed. Engl.*, **1993**, *32*, 78.
- ⁴ Chuang, S.-C., Sander, M., Jarrosson, T., James, S., Rozumov, E., Khan, S. I., Rubin, Y., *J. Org. Chem.*, **2007**, *72*, 2716-2723.
- ⁵ a) Herranz, M. A., Echegoyen, L., *New. J. Chem*, **2004**, 513-518; b) Schlueter, J. A., Seaman, J. M., Taha, S., Cohen, H., Lykke, K. R., Wang H. H., Williams, J. M., *J. Chem. Soc., Chem. Commun*, **1993**, 972-974 and references therein.
- ⁶ Sakellariou, G., Ji, H., Mays, J. W., Hadjichristidis, N., Baskaran, D., *Chem. Mater.*, **2007**, *19*, 6370-6372.
- ⁷ Lei Zhang, Jianzhong Yang, Christopher L. Edwards, Lawrence B. Alemany, Valery N. Khabashesku, Andrew R. Barron, *Chem. Commun.*, **2005**, 3265-3267.
- ⁸ Ménard-Moyon, C., Dumas, F., Doris, E., Mioskowski, C., *J. Am. Chem. Soc.*, **2006**, *128*, 14764-14765.
- ⁹ Sun, J.-T, Zhao, L.-Y., Hong, C.-H., Pan, C.-Y., *Chem. Comm.*, **2011**, *47*, 10704-10706.
- ¹⁰ Delgado, J. L., de La Cruz, a, P., Langa, F., Urbina, A., Casadoc, J., López Navarrete, J. T., *Chem. Commun.*, **2004**, 1734 - 1735.
- ¹¹ Yameen, B., Nicolas Zydziak, N., Weidner S. M., Bruns, M., Barner-Kowollik, C., *Macromolecules*, **2013**, *46*, 2606-2615.
- ¹² a) Cao, Y., Osuna, S., Liang, Y., Haddon, R. C., Houk, K. N., *J. Am. Chem. Soc.*, **2013**, *135*, 17643-17649; b) Denis, P. A., *Chem. Eur. J.*, **2013**, *19*, 15719-15725.
- ¹³ Bian, S., Scott, A. M., Cao, Y., Liang, Y., Osuna, S., Houk, K. N., Braunschweig, A. B., *J. Am. Chem. Soc.*, **2013**, *135*, 9240-9243.
- ¹⁴ a) Jester, S.-S., Idelson, A., Schmitz, D., Eberhagen, F., Höger, S., *Langmuir*, **2011**, *27*, 8205-8215; b) Mu, Z. Shu, L., Fuchs, H., Mayor, M., Chi, L., *J. Am. Chem. Soc.*, **2008**, *130*, 10840-10841.
- ¹⁵ a) Llanes-Pallas, A., Yoosaf, K., Traboulsi, H., Mohanraj, J., Seldrum, T., Dumont, J., Minoia, A., Lazzaroni, R., Armaroli, N., Bonifazi, D., *J. Am. Chem. Soc.*, **2011**, *133*, 39, 15412-15424 ; b) Zhang, Z., Che, Y., Smaldone, R. A., Xu, M., Bunes, B. R., Moore, J. S., Zang, L., *J. Am. Chem. Soc.*, **2010**, *132*, 40, 14113-14117.
- ¹⁶ Qi, X., Pu, K.-Y., Li, H., Zhou, X., Wu, S., Fan, Q.-L., Liu, B., Boey, F., Huang, W., Zhang, H., *Angew. Chem. Int. Ed.*, **2010**, *49*, 49, 9426-9429.
- ¹⁷ For STM studies of phenylene-ethynylene derivatives in UHV on other surfaces, see for example: a) Vives, G., Tour, J. M., *Acc. Chem. Res.*, **2009**, *42*, 3, 473-487; b) Weigelt, S., Bombis, C., Busse, C., Knudsen, M. M., Gothelf, K. V., Lægsgaard, E., Besenbacher, F., Linderoth, T. R., *ACS Nano*, **2008**, *2*, 4, 651-660.
- ¹⁸ Groszek, A. J., *Proc. Roy. Soc. Lond. A.*, **1970**, *314*, 473-498.

- ¹⁹ R. Haddon reported for the first time on the reactivity of 9-methylanthracene with graphene in p-xylene at 130°C for 12 hours: Sarkar, S, Bekyarova, E., Niyogi, S., Haddon, R. C., *J. Am. Chem. Soc.*, **2011**, *133*, 3324–3327.
- ²⁰ Chinchilla, R., Nájera, C., *Chem. Rev.*, **2007**, *107*, 874-922.
- ²¹ Feng, Y. S., Xie, C. Q., Qiao, W. L., Xu, H. J., *Org. Lett.*, **2013**, *15*, 4, 936-939, Zhao, Y.-L., Liu, L., Zhang, W., Sue, C.-H., Li, Q., Miljanić, O. Š., Yaghi, O. M., Stoddart, J. F., *Chem. Eur. J.*, **2009**, *15*, 13356-13380.
- ²² Meier, H., Ickenroth, D., Stalmach, U., Koynov, K., Bahtiar, A., Bubeck, C., *Eur. J. Org. Chem.* **2001**, 4431-4443.
- ²³ Castruita, G., Arias, E., Moggio, I., Pérez, F., Medellín, D., Torres, R., Ziolo, R., Olivas, A., Giorgetti, E., Muniz-Miranda, M., *Journal of Molecular Structure*, **2009**, *936*, 1-3, 177-186.
- ²⁴ Moy, C. L., Kaliappan, R., McNeil, A. J., *J. Org. Chem.*, **2011**, *76*, 20, 8501–8507.
- ²⁵ Hepworth, J. D., Waring, M. J., Waring, D. R., Berry, M., Drayton, C., Abel, E. W., Davies, Phillips, D., Woollins, J. D., “Aromatic Chemistry”, Royal Society of Chemistry (October 25, 2002), ISBN-10: 0854046623.
- ²⁶ Shirai, Y., Zhao, Y., Cheng, L., Tour, J. M., *Org. Lett.*, **2004**, *6*, 13, 2129–2132.
- ²⁷ Feng, Y. S., Xie, C. Q., Qiao, W. L., Xu, H. J., *Org. Lett.*, **2013**, *15*, 4, 936-939.
- ²⁸ Fujihara, T., Tomike, Y., Ohtake, T., Terao, J., Tsuji, Y., *Chem. Comm.*, **2011**, *47*, 9699-9701.
- ²⁹ a) Khan, M. S., Al-Mandhary, M. R. A., Al-Suti, M. K., Al-Battashi, F. R., Al-Saadi, S., Ahrens, B., Bjernemose, J. K., Mahon, M. F., Raithby, P. R., Younus, M., Chawdhury, N., KKhler, A., Marseglia, E. A., Tedesco, E., Feeder, N., Teat S. J., *Dalton Trans.*, **2004**, 2377 – 2385; b) Taylor, M. S., Swager, T. M., *Angew. Chem. Int. Ed.*, **2007**, *46*, 8480-8483; c) Alvey, P. M., Ono, R. J., Bielawski, C. W., Iverson, B. L., *Macromolecules*, **2013**, *46*, 718–726.

Chapter 6

Synthesis and study of maleimide derivatives for covalent functionalization of graphene by Diels-Alder reaction

6.1 Reactivity of carbon nanomaterials as dienes

As a complement to the study of graphene's reactivity as a dienophile, presented in **Chapter 5**, we intend now to investigate its potentiality to react as a diene. As in the previous chapter, we start by introducing a state of the art on the reactivity of carbon nanomaterials as dienes.

Due to their electron deficient character, fullerenes normally do not react with dienophiles and important modifications to the carbon skeleton have to be brought about, in order to generate a functionalizable cyclopentadiene unit¹.

The behaviour of single and multi-wall carbon nanotubes as dienes has been, as well, less investigated. In one report², the functionalization has been shown to be possible with maleimides and maleic anhydride at relatively low temperatures (around 75°C), affording, in general, robust adducts.

In the case of graphene, the first report on the reactivity as a dienophile is also in this case a paper of R. Haddon³. The Diels-Alder functionalization is shown to be possible with tetracyanoethylene at room temperature on HOPG or exfoliated graphene (mechanically exfoliated or in solution). Another dienophile that has been proven to be reactive is maleic anhydride, at different temperatures depending on the different substrate: 70°C on epitaxial graphene (on silicon carbide), 120°C on HOPG and 130°C on exfoliated graphene in solution. The reversibility of the reaction at higher temperatures was also proven. The same debate (as expressed in **Chapter 5**) aimed at establishing if the functionalization is possible only at the edges and defects or also on the basal plane area, concerns also the reactivity of graphene as diene⁴.

6.2 Objective

We chose to employ, as dienophiles for our studies, maleimide derivatives, that can be readily functionalized with different groups, driving their adsorption and self-assembly on the surface (**Figure 6.1**). Similarly to the case of anthracene, we expect the molecules to be reactive with graphene by Diels-Alder reaction, locally activated by the STM tip (see **Appendix A1**).

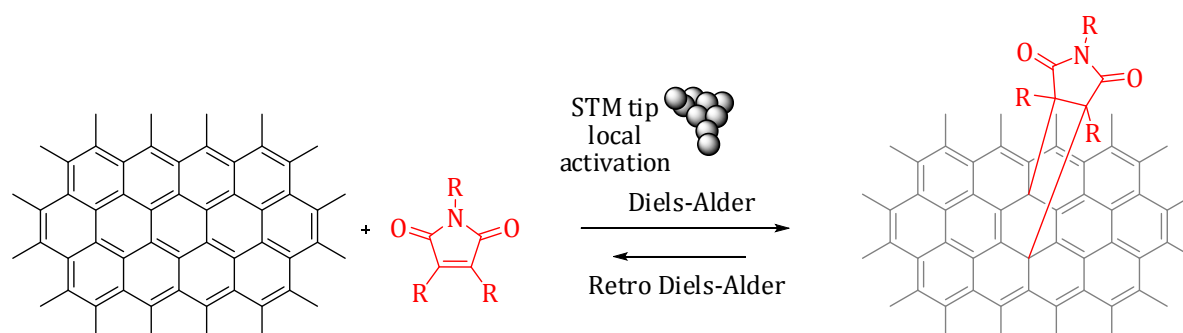


Figure 6.1: General objective.

6.3 Molecular design

In order to study the reactivity of epitaxial graphene/SiC as a diene in Diels-Alder cycloaddition reactions with maleimides in UHV conditions, three molecules were designed and synthesized: **M1 (6.1)**, **M2 (6.2)** and **M3(6.3)** (Figure 6.2).

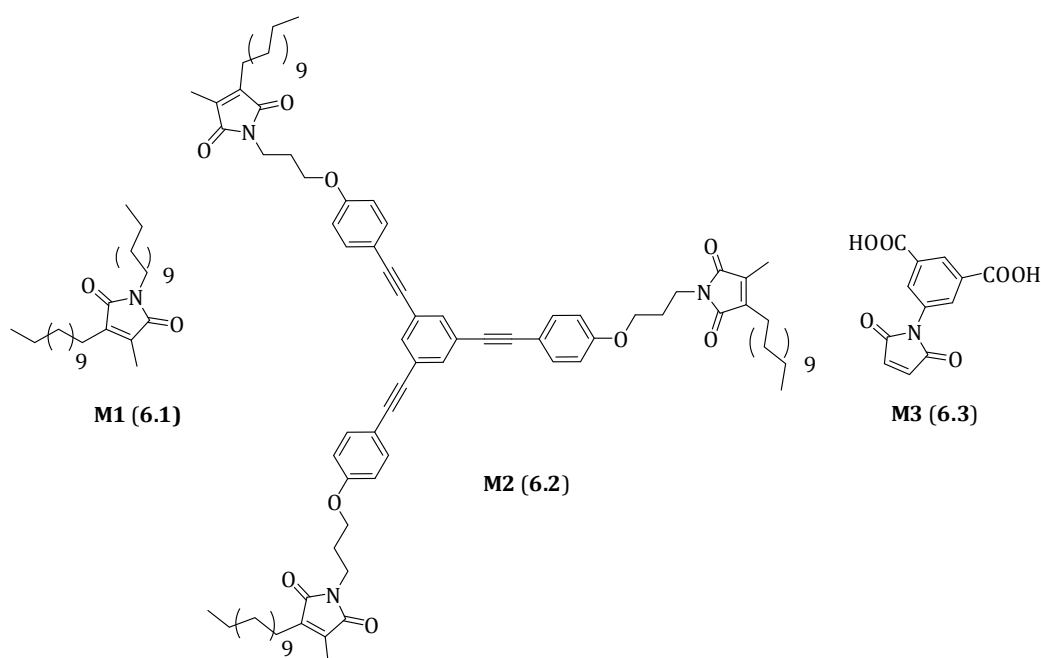


Figure 6.2: Structure of the maleimide derivatives **M1**, **M2** and **M3**.

M1 (6.1): the first maleimide derivative of the series is bearing two alkyl chains $-C_{12}H_{25}$ directly connected to the core at the positions 1 and 3. The position 4 is functionalized with a $-CH_3$ group, deriving from the particular synthetic strategy that was adopted (see section 6.4.2.1.2). The presence of the two long alkyl chains should favour the adsorption of the molecule on the surface, by establishment of $CH-\pi$ interactions (see Chapter 1, section 1.3.1.1). At the same time it should allow a self-organization of the molecules in linear features on the graphene surface.

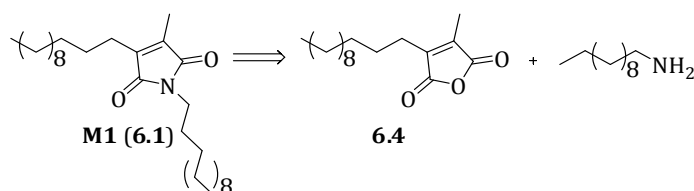
M2 (6.2): the second derivative that was synthesized presents a slightly more complex structure. The maleimide reactive groups are being born by a triethynylbenzene platform. This kind of polyaromatic core is chosen for two reasons: 1) it could favour the molecular adsorption on the surface thanks to π - π interactions; 2) could allow the tuning of reactive sites density on the surface by varying the length of the phenyl-ethynyl spacers. The maleimide groups are functionalized in position 4 by a $-\text{CH}_3$ group, in position 3 by a $-\text{C}_{12}\text{H}_{25}$ alkyl chain and in position 1 by a $-\text{C}_3\text{H}_6$ chain, connecting it to the aromatic platform by an ether bond. The $-\text{C}_3\text{H}_6$ chain is adopted in order to guarantee to the maleimide core enough flexibility such as to adapt the correct geometrical conformation upon Diels-Alder reaction. The role of the alkyl chain $-\text{C}_{12}\text{H}_{25}$ is to promote the adsorption on the surface by establishment of $\text{CH}-\pi$ interactions.

M3 (6.3): the third derivative is bearing as substituent an isophtalic moiety directly linked to the nitrogen of the maleimidic core. This substituent should favour the molecular adsorption on the surface by π - π interaction and drive an organization on the surface mediated by hydrogen bond interactions (see **Chapter 1, section 1.3.1.2**).

6.4 Alkyl-chains functionalized maleimide derivative M1 (6.1)

6.4.1 Retrosynthetic analysis for M1

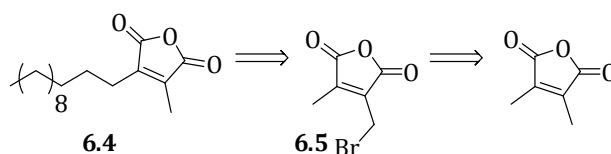
From a retrosynthetic point of view, **M1** can be disconnected to the alkyl-functionalized maleic anhydride **6.4** and 1-dodecylamine (**Scheme 6.1**):



Scheme 6.1: Retrosynthetic analysis for the maleimide derivative **M1**.

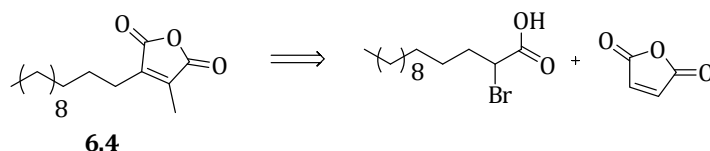
Different disconnections can be envisaged for the alkyl-functionalized maleic anhydride **6.4**. The synthesis of this kind of derivatives has largely been studied in the literature, due to their interesting biological activity⁵. Two kind of disconnections appeared the most interesting to us, for simplicity reasons (**Scheme 6.2** and **Scheme 6.3**).

A first strategy implies the introduction of a $-\text{C}_{11}\text{H}_{23}$ chain by an alkylation reaction of the 3-bromomethyl derivative **6.5**, obtained from 3,4-dimethylmaleic anhydride.



Scheme 6.2: Retrosynthetic analysis for the anhydride derivative **6.4**: first strategy.

A second strategy leads instead to disconnect the anhydride **6.4** directly to maleic anhydride and 2-bromo-tetradecanoic-acid.



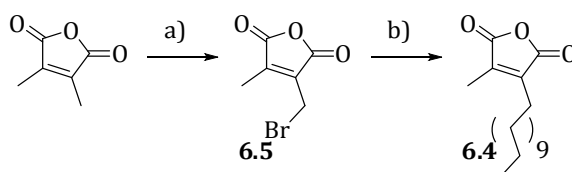
Scheme 6.3: Retrosynthetic analysis for the anhydride derivative **6.4**: second strategy.

6.4.2 Synthesis of M1

6.4.2.1 Synthesis of the alkyl-functionalized anhydride **6.4**:

6.4.2.1.1 First strategy

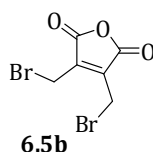
In a first attempt, we tried to achieve the anhydride derivative **6.4**, following the approach summarized in (**Scheme 6.4**):



Scheme 6.4: Synthesis of the functionalized maleic anhydride **6.4**. Conditions: a) NBS, Benzoyl peroxide, CCl_4 , 80°C , 20h, 35% wt/wt, 66% of 2.; b) $\text{C}_{11}\text{H}_{23}\text{MgBr}$, CuI, HMPA, diethyl ether, -5°C , then 20°C , 18 h, 0%.

Step a)

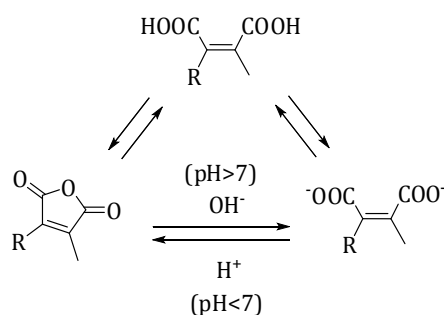
The starting material 3,4-dimethylmaleic anhydride was brominated in position 3 by reaction with N-bromosuccinimide, catalysed by benzoyl peroxide, in carbon tetrachloride at 80°C for 10 hours. The purification was carried on by silica gel column chromatography (petroleum ether : ethyl acetate 8:2), then vacuum distillation on a Kugelrohr apparatus (47 mbar at 120°C then 130°C). It was not possible to purify the product **6.5** from the unreacted 3,4-dimethylmaleic anhydride and the dibromated subproduct **6.5b**. The raw mixture was obtained with a 35% yield (in weight). From NMR analysis it was estimated that product **6.5** represented 66% of the mixture.



Step b)

For the introduction of the alkyl chain, we tested a Grignard reaction following the procedure reported by Deshpande⁶.

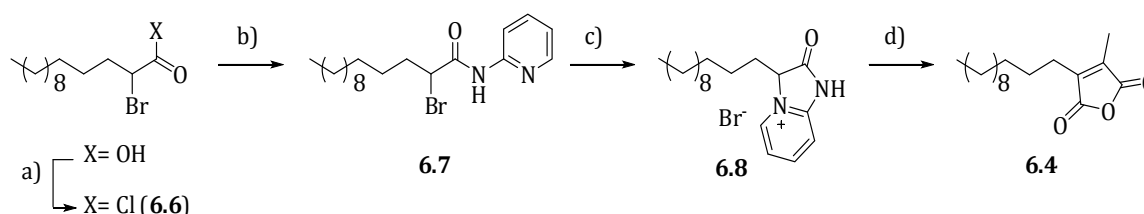
The Grignard reagent was generated by reacting 1-bromo undecane with isopropyl magnesium chloride in anhydrous tetrahydrofuran, at -10°C for one hour⁷. The freshly prepared solution of Grignard reagent was then added to a solution of 3-(bromomethyl) maleic anhydride, CuI and HMPA in diethyl ether at -5°-0°C, then the mixture was let to stir at room temperature for 8 hours. After acidic work up, the only product that was isolated was the 1-bromoundecane reactant. The acidic work up was meant to drive the equilibrium (**Scheme 6.5**) towards the closure of the anhydride cycle. A possible explanation of the failure of the product recovery could be that that, in the conditions employed, the dicarboxylic product did not cyclize and was lost in the work up phase. Other possibilities could be that the Grignard reagent was not completely formed, or that it reacted in an uncontrolled way with an anhydride carbonyl carbon.



Scheme 6.5: Equilibria between the cyclized and not cyclized forms of maleic anhydrides.

6.4.2.1.2 *Second strategy*

Due to the difficulties met in the first strategy, a second more convenient approach was adopted for the synthesis of **6.4** and is summarized in **Scheme 6.6**:



Scheme 6.6: Synthesis of the alkyl-functionalized maleic anhydride **6.4**. Conditions: a) oxalyl chloride (1.6 eq.), DMF cat., toluene, 20°C, 2h; b) 2-aminopyridine (1 eq.), triethylamine (1 eq.), diethyl ether, 20°C, 3h; c) *tert*-butanol, 82°C, 18h; d) maleic anhydride (1 eq.), sodium acetate (1 eq.), acetic acid, 120°C, 5h. Yield over the four steps: 27%.

The described strategy is characterized by a sequence of reactions that can all be performed in a one-pot fashion. The synthetic procedures were adapted by those proposed by Argade et al.⁸ for the synthesis of “Chaetomelic Anhydride A” (a biological-interest molecule).

Step a)

In a first step, 2-bromo-tetradecanoic-acid was activated transforming it into an acyl chloride, by employing an excess of oxalyl chloride, in dry toluene at room temperature for 2 hours, under an argon atmosphere. The addition of a catalytic amount of dimethyl-formamide allowed to accelerate the reaction, through generation of an iminium intermediate⁹. The product was obtained as a yellow oil after evaporation of the solvent and was employed without any purification in the following step.

Step b)

The second step consisted in a nucleophilic acyl substitution by 2-aminopyridine. The reaction was conducted in dry diethyl ether at room temperature for 3 hours, employing triethylamine as “sacrificial” base, in order to trap the chlorhydric acid released during the reaction. The selectivity of the attack is due to the higher nucleophilicity of the aniline nitrogen in these conditions. Product **6.7** was obtained as a yellow solid after solvent evaporation under reduced pressure and employed without any purification in the following step.

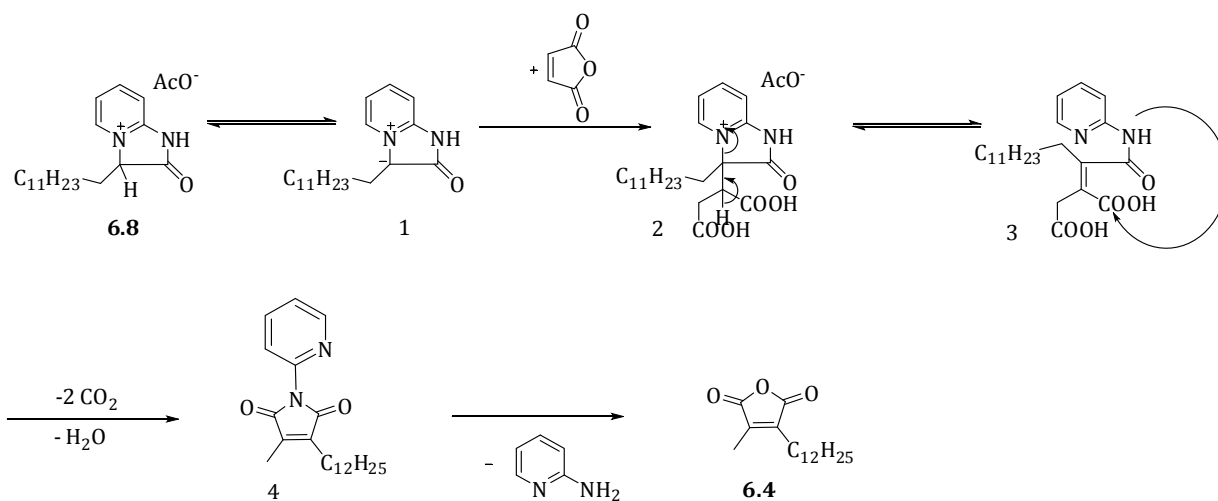
Step c)

In the third step (c) the derivative **6.7** was cyclized to product **6.8** by stirring it in refluxing *tert*-butanol for 18 hours. **6.8**, obtained as a dark thick oil after solvent evaporation, was employed for the following reaction without any purification.

Step d)

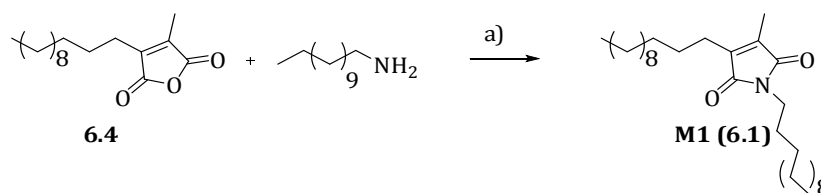
The last step consisted in reacting **6.8** with maleic anhydride, in the presence of one equivalent of sodium acetate, in refluxing acetic acid for 5 hours. The reaction mechanism has been described by Bauman et al.¹⁰ and can be rationalized as follows (**Scheme 6.7**). The proton in alfa to the carbonyl group of **6.8** is made particularly acidic by the presence of the quaternary nitrogen substituent ($pK_a \approx 4$)¹⁰. In the employed conditions, it is possible to assume the presence of an equilibrium between the protonated and deprotonated form: the so formed carboanion (1) can act as a Michael donor and attack maleic anhydride in position 3, to give an adduct that after a sequence of reactions (β -elimination, ring opening and decarboxylation) yields to the 1-pyridine-3-dodecyl-4-methyl functionalized maleimide (4) (**Scheme 6.7**). Hydrolysis in the acidic environment and a following cyclization leads to the desired 3-dodecyl-4-methyl maleic anhydride¹⁰ (**6.4**).

The product **6.4** could be isolated by silica gel column chromatography (eluent petroleum ether : diethyl ether 9:1) as a yellow oil, with a yield over four steps of 27%.



Scheme 6.7: Mechanism of formation of the maleic anhydride **6.4**.

6.4.2.2 Synthesis of the maleimide **M1**:



Scheme 6.8: Synthesis of the maleimide derivative **M1**: a) 1-dodecylamine, ZnBr₂, HMDS, toluene dry, 80°C, 19h, 89%.

The alkyl functionalized maleic anhydride **6.4** was reacted with 1-dodecylamine to yield the maleimide **M1**. The employed conditions were adapted to our case from those suggested by Reddy et al.¹¹ for similar compounds. The anhydride ring was opened by the carbonyl addition of 1-dodecylamine, in toluene at room temperature. After taking the mixture to 80°C, the Lewis acid zinc dibromide was added, followed by hexamethyldisilazane and the mixture was then refluxed for 19 hours, to afford the cyclized maleimide with an 89% yield. Although the mechanism of the amic acid cyclization is not yet clearly defined, it is assumed to consist in a Lewis acid / HMDS promoted silylation of an intermediate amic acid to a labile trimethylsilyl ester, followed by subsequent thermal deoxysilylation¹¹.

It is interesting to notice that the cyclization reaction by more “standard” conditions⁵ (i.e. refluxing in acetic anhydride in the presence of sodium acetate), in this particular case was unsuccessful and only the starting reagent was recovered.

6.4.3 Characterization of M1

The maleimide derivative **M1** was completely characterized by multinuclear (^1H and ^{13}C) mono and bi-dimensional NMR spectroscopy, mass spectrometry and elemental analysis.

The ^1H -NMR spectrum (500 MHz, CDCl_3 , **Figure 6.3**) allowed to assess the identity and purity of the product. In the spectrum, the two triplets at $\delta=3.44$ ppm ($J=7.5$ Hz) and 2.35 ppm ($J=7.5$ Hz) were attributed, respectively, of the methylenic protons H_a and H_e , H_e resonating at higher fields respect to H_a , due to the vicinity to the nitrogen atom. The two signals were integrating for two protons each and confirmed the presence of the two alkyl chain substituents. Another interesting signal was the singlet at 1.94 ppm, attributed to the methyl protons H_b , integrating for three protons. Two multiplets characteristic of the methylenic protons of the alkyl chains were observed at $\delta=1.2$ -1.3 ppm and 1.4-1.6 ppm. At $\delta=0.87$ ppm it was possible to observe the presence of a triplet attributed to the terminal methyl protons H_p and H_q .

The mass spectra (DCI- NH_3 ionization source and quadrupole analyser) confirmed the identity of the product, showing a peak at m/z 465, corresponding to the species $[\text{M}+\text{NH}_4]^+$.

A further confirmation could be obtained by elemental analysis: the experimentally found elemental ratio percentage was in accordance with the calculated one (%C 77.58 %H 11.32 %N 3.13 %O 7.97 (found for $\text{C}_{29}\text{H}_{53}\text{NO}_2$) vs %C 77.79 %H 11.93 %N 3.13 %O 7.15 (calculated for $\text{C}_{29}\text{H}_{53}\text{NO}_2$)).

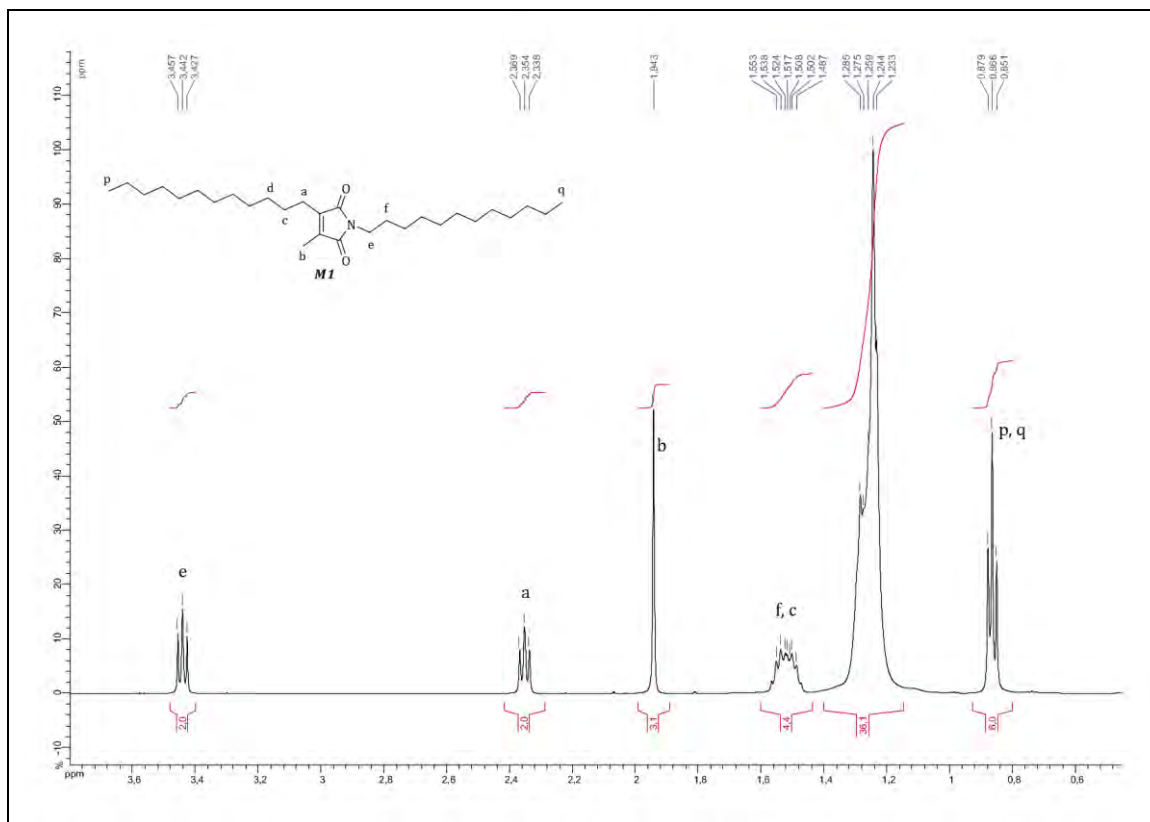
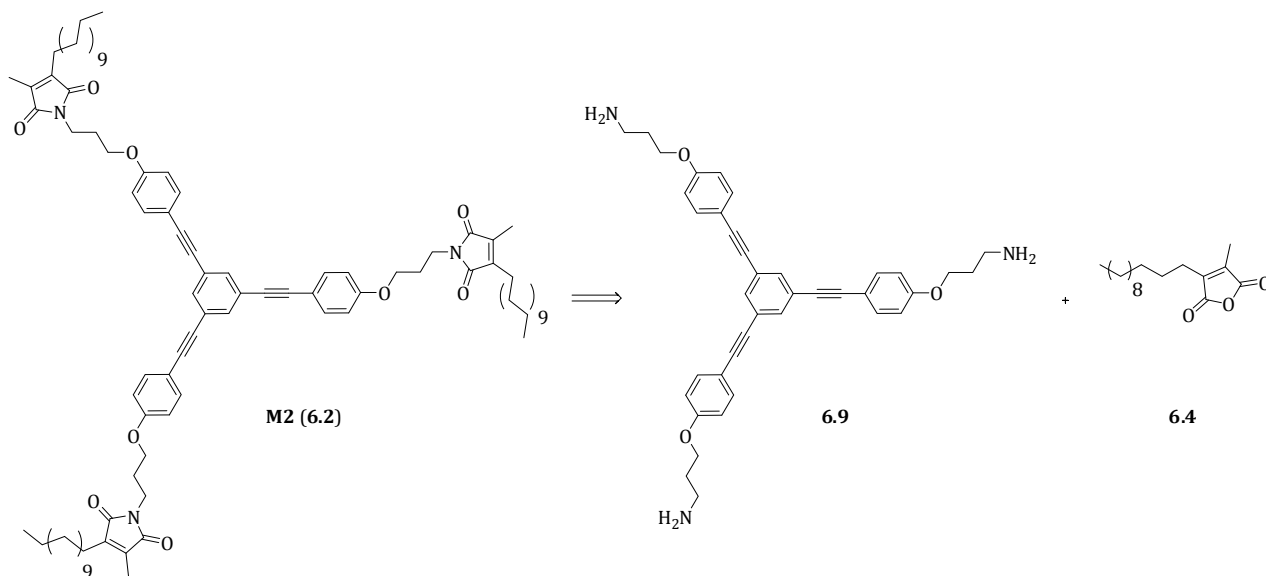


Figure 6.3: ^1H -NMR spectrum (500 MHz, CDCl_3) of the maleimide derivative **M1**.

6.5 C3-symmetry maleimide derivative M2 (6.2)

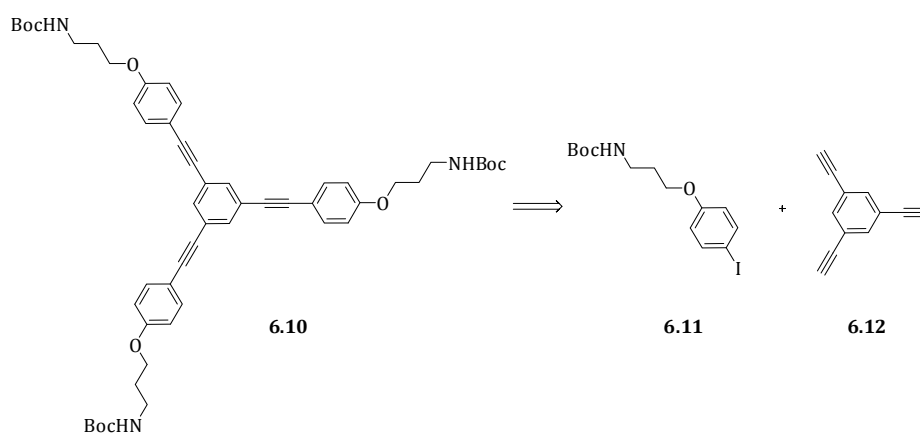
6.5.1 Retrosynthetic analysis for M2

Among the different retrosynthetic paths that can be envisaged, we choose to adopt the one described in **Scheme 6.9**:



Scheme 6.9: Retrosynthetic analysis for the maleimide derivative **M2** (4.2): first strategy.

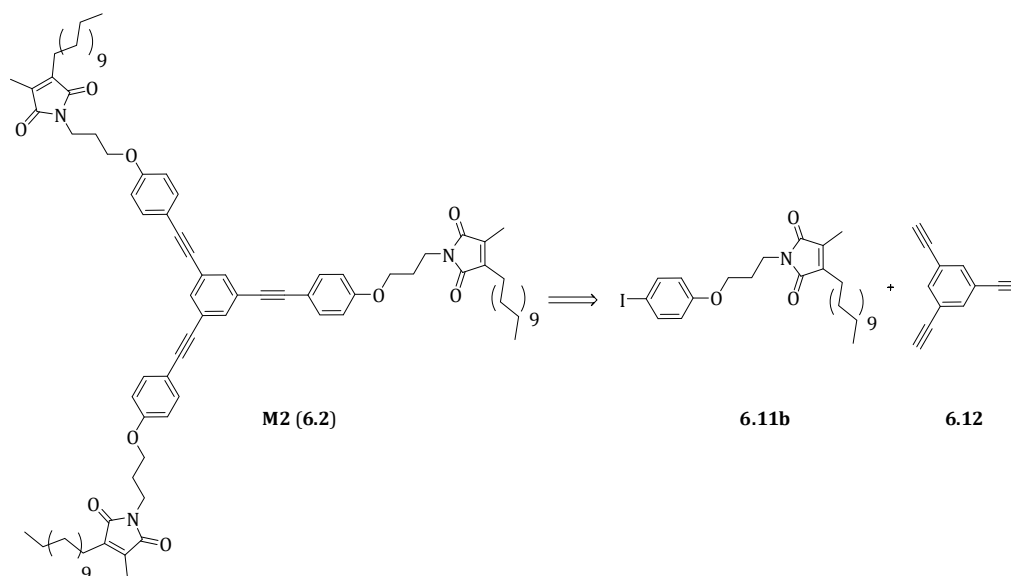
The concept on which the strategy is based is to generate the maleimide bond at the end of the synthesis, by reacting the amine-nitrogens of the precursor **6.9** with the formerly prepared functionalized maleic anhydride **6.4**. The precursor **6.9** can be obtained from **6.10** (**Scheme 6.10**) which, in his turn, can be disconnected to the compounds **6.11** and **6.12**, derived respectively from p-iodophenol and 1,3,5-tribromobenzene.



Scheme 6.10: Retrosynthetic analysis for the precursor **6.10**.

Another synthetic possibility would have been to perform the Sonogashira reaction between the preformed maleimide **6.11b** (**Scheme 6.11**). In a first time, this strategy was not taken into

account, due to the possible instability of maleimides towards bases (determining, in some reaction conditions, the opening of the ring). However, a paper by Souffrin et al.¹² appeared after that the synthesis was already completed, showing the possibility to perform Sonogashira reactions on maleimides, provided a careful choice of the base.

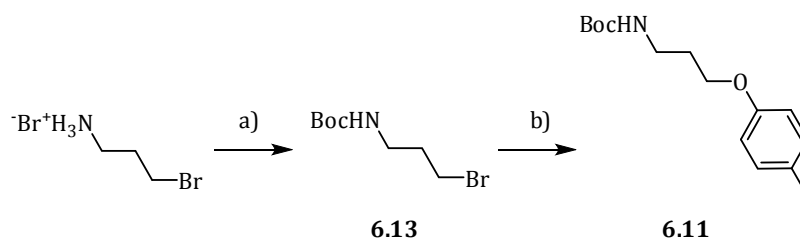


Scheme 6.11: Retrosynthetic analysis for the maleimide derivative **M2**: second possible strategy.

6.5.2 Synthesis of M2

6.5.2.1 Synthesis of the precursor 6.11

The synthesis was carried out by the two-steps procedure reported in **Scheme 6.12**:



Scheme 6.12: Synthesis of the precursor **6.11**: a) NaOH, Boc₂O, H₂O/THF, 0°C-22°C, 5h, 90%; b) p-iodophenol, Cs₂CO₃, NaI, CH₃CN dry, 65°C, 5h, 83%.

Step a)

In a first step, the amine group of 3-bromopropanamine hydrobromide was protected as a tert-butyloxycarbonyl (Boc). It was chosen to employ Boc as a protecting group, due to its known stability towards basic conditions¹³. The reaction was performed by employing already published conditions¹⁴. 3-bromopropanamine hydrobromide was stirred in a system water/tetrahydrofuran in the presence of di-*tert*-butyl dicarbonate, at room temperature for 5 hours. Sodium hydroxide was employed to promote the reaction in a 2.3 molar excess ratio. After acidic work up (it must be paid attention not to

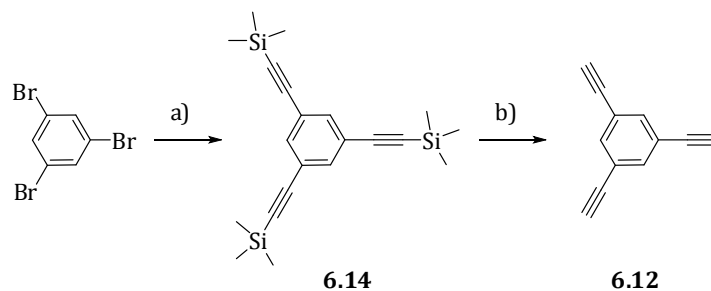
take the pH below 4, in order not to remove the Boc group), the product **6.13** was obtained without any purification with a 90% yield.

Step b)

The second step consisted in the O-alkylation of p-iodophenol with the chain **6.13**. In this purpose, we adapted to our case conditions already published for similar compounds¹⁵. p-Iodophenol was deprotonated by cesium carbonate in acetonitrile at 65°C; the as-generated nucleophile was then alkylated in a S_N2 reaction, promoted by sodium iodide¹⁶. The product **6.11** was obtained with a 83% yield as a yellow solid after column chromatography on silica gel.

6.5.2.2 Synthesis of the 1,3,5-Tris(ethynyl)benzene precursor **6.12**

The synthesis was carried on by the procedure reported in (Scheme 6.13), employing conditions already published in the literature¹⁷.



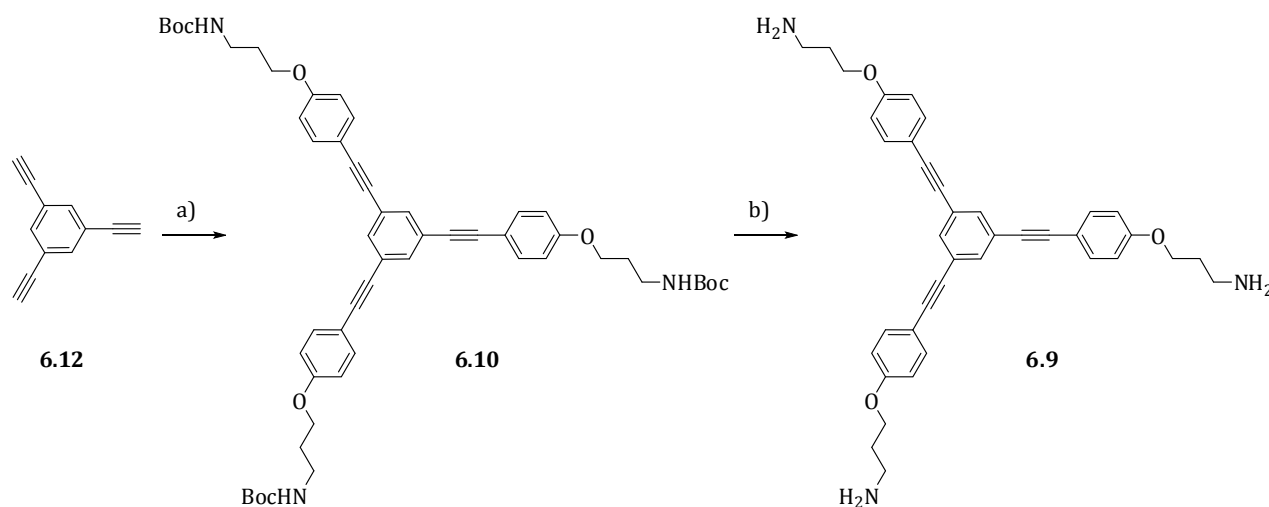
Scheme 6.13: Synthesis of the 1,3,5-Tris(ethynyl)benzene precursor **6.12**: a) TMSA, Pd(PPh₃)₂Cl₂ (1.8%), CuI (0.8%), Et₂NH dry, 70°C, 17h, 80%; b) KOH, THF/MeOH, 22°C, 5h, 92%.

Steps a and b)

In a first step the trimethylsilyl-protected ethynyl functions were introduced on 1,3,5-tribromobenzene by Sonogashira coupling reaction¹⁸. As catalysts, we employed dichlorobis(triphenylphosphino)palladium(II) and copper iodide, in the ratio 0.6% and 0.26% respectively per each bromine functionality. The reaction was run in dry and degassed diethylamine, at 70°C for 17 hours. The product **6.14** was recovered as a light yellow solid after column chromatography (eluent: hexane) with a 80% yield. These conditions^{17a} allowed to carry out the reaction at a large product scale (two grams).

The free alkyne **6.12** was generated by removing the trimethylsilyl protecting groups. **6.14** was stirred in the presence of an excess of potassium hydroxide, in tetrahydrofuran/methanol, for five hours at room temperature (22°C). The pure product was obtained after aqueous work up, as a yellow solid, with a 92% yield.

6.5.2.3 Synthesis of the tri-amine precursor 6.9



Scheme 6.14: Synthesis of the precursor **6.9**: a) **6.11**, Pd(PPh₃)₂Cl₂ (6%), CuI (2.3%), THF/Et₂NH, 45°C, 4h, 48%; b) μ W (230 W), DMF, 180°C, 10 mins., 100%.

Step a)

The compound **6.10** was obtained by Sonogashira cross coupling¹⁸ between 1,3,5-triethynylbenzene **6.12** and the precursor **6.11**. The reagents were stirred in tetrahydrofuran/diethylamine, in the presence of bis(triphenylphosphine)palladium(II) dichloride (2% per each alkyne) and copper iodide (0.8% per each alkyne) as catalysts. The reaction temperature was optimized at 45°C and the reaction time to four hours. The moderate warming allowed to speed up the reaction, in particular the palladium C-I insertion step, unfavoured by the presence of the electron donor substituent in para to the iodine, on **6.11**. By these conditions, the product **6.10** was obtained after a simple column chromatography (cyclohexane : ethyl acetate 6:4) with a 48% yield as a light yellow solid.

Alternative conditions, such as: tetrahydrofuran/triethylamine as solvents, copper iodide (2.7% per each alkyne) and tetrakis(triphenylphosphine)palladium(0) (1.3% per each alkyne) as catalysts, at room temperature (22°C) for 18 hours, allowed as well to obtain **6.10**, but the yields were slightly lower (ranging from 24 to 48%) and the purification more difficult.

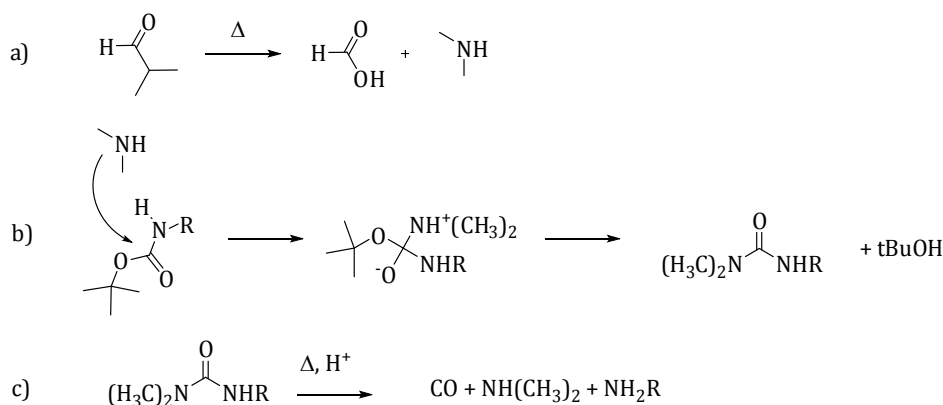
Step b)

In the following step, the tert-butyloxycarbonyl (Boc) protecting group was removed to generate the free-amines of **6.9**.

In order to perform the reaction, a solution of **6.10** in *N,N*-dimethylformamide (0.04 M) was irradiated with microwaves at a power of 230 Watts, adjusting the microwave reactor parameters such as to keep the reaction temperature at 180°C for 10 minutes. In these conditions, the Boc decomposition was quite rapid and **6.9** could be recovered quantitatively as a brown thick oil, showing

only a partial solubility in dimethylsulphoxide. Due to the high polar character of the molecule, related to the presence of the free amines, it was not possible to carry on a chromatographic purification, but the product was just treated with petroleum ether in order to remove some non-polar impurities.

Thermal Boc deprotection promoted or not by microwave irradiation¹⁹ is not considered among the “classical” methodologies, but it has raised more and more interest during the last years, as it is shown by the publication of a certain number of papers on the subject²⁰. Likely, the deprotection mechanism in the presence of *N,N*-dimethylformamide, could be related to the solvent decomposition in formic acid and dimethylamine, at high temperatures²¹ (**Scheme 6.15**). The as-generated dimethylamine would be the nucleophilic species attacking the Boc carbonyl, determining the formation of an urea group, that would then thermally decompose to finally yield the free amines.



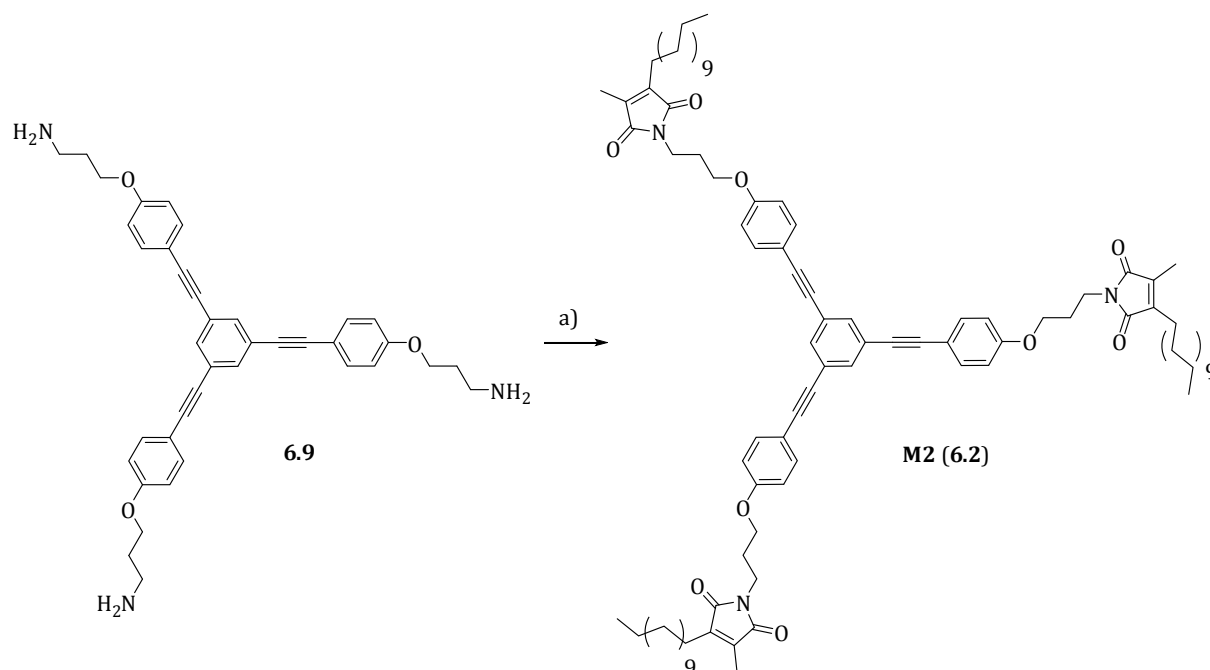
Scheme 6.15: Proposed mechanism for the Boc thermal decomposition.

We tested also a “classical” deprotection procedure in acidic medium¹⁵. **6.10** was dissolved in a solution 4M of hydrochloric acid in tetrahydrofuran and the reaction run at 0°C for ten minutes then at 22°C for 30 minutes. The product could be recovered after basic work up, by extraction with ethyl acetate with yields going up to 75%. However, the extraction procedure suffered from lack of reproducibility and many difficulties were encountered in the recovery of **6.9**, probably due to its insolubility in ethyl acetate (as in other organic solvents, except dimethylsulphoxide). Another problem that we had to deal with, was the cleavage of the phenolic-ether bond that can be promoted in these conditions¹³, leading to the recovery of the only alkyl chain moiety.

All these difficulties underline the superiority of the thermal microwave deprotection procedure in this case.

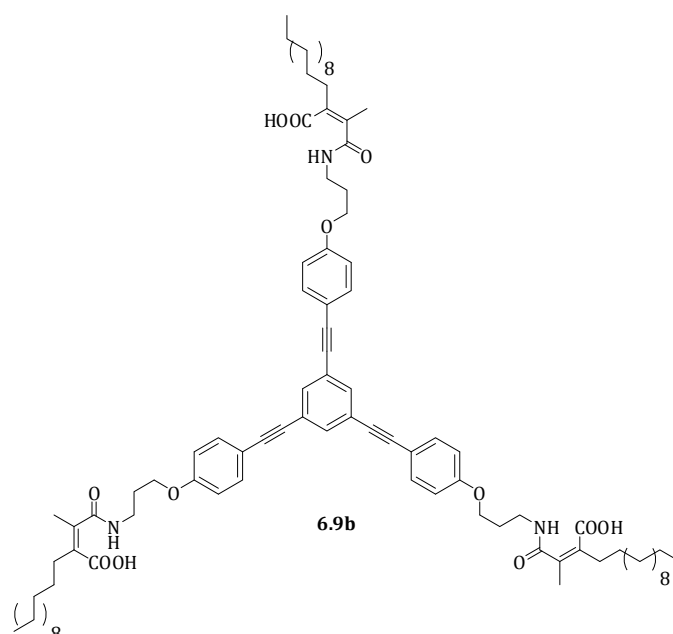
6.5.2.4 Synthesis of the tri-maleimide **M2** (**6.2**):

In this step, the tri-amine **1.2** was condensed with the maleic anhydride **6.4** to yield the tri-maleimide **M2** (**6.2**). The reaction was carried on analogously to the synthesis of the functionalized maleimide **M1** (**Scheme 6.16**).



Scheme 6.16: Synthesis of the tri-maleimide **M2**: a) i: **6.4**, toluene dry, 111°C, 16h; ii: ZnBr₂, HMDS, 80°C, 5h, then 22°C, 11h, 20%.

The anhydride **6.4** cycle was at first opened by reacting it in an acyl nucleophilic substitution with the amine nitrogens of **6.9**, in toluene. Due to the insolubility of **6.9** in toluene, a solution of the anhydride **6.4** in toluene was added to the flask containing the thick oil **6.9** and it was warmed at 111°C for 16 hours: by this procedure, **6.9** could be brought in solution as its derived carbamic acid **6.9b** (Scheme 6.17). Afterwards, **6.9b** was cyclized to **M2** by employing the system ZnBr₂/HMDS described before. **M2** could be recovered by two column chromatography purifications on silica gel: (eluent 1) hexane : ethyl acetate 6:4; 2) hexane : diethyl ether 95 : 5, then diethyl ether 100%) with a 20% yield. The global yield over the seven steps was 5%.



Scheme 6.17: Carbamic acid derived from the condensation of **6.4** and **6.9**.

6.5.3 Characterization of M2

The identity and purity of the product were confirmed through ^1H and ^{13}C -NMR mono and bi-dimensional spectroscopies and high resolution mass spectrometry.

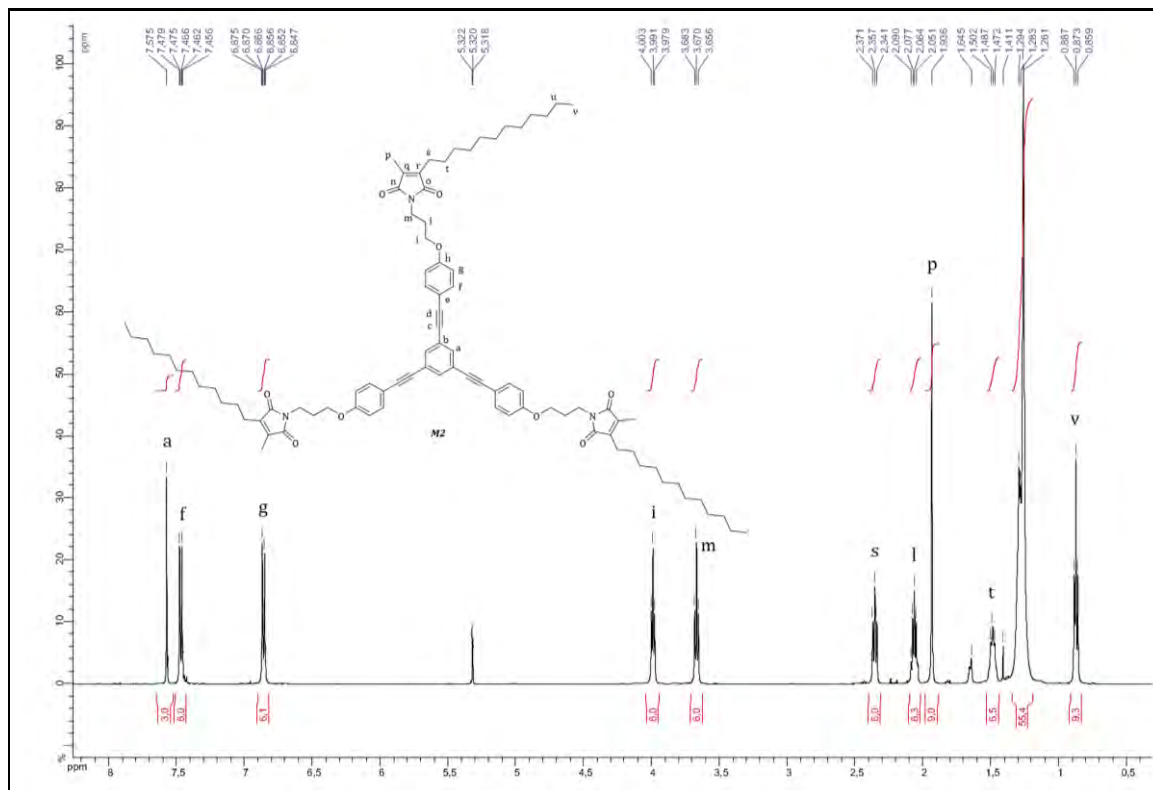


Figure 6.4: ^1H -NMR spectrum (500 MHz, CDCl_3) of the tri-maleimide derivative **M2**.

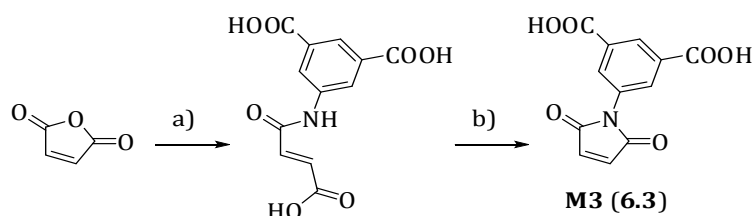
The ^1H -NMR spectrum (500 MHz, CDCl_3 , **Figure 6.4**) allowed to confirm the identity and purity of the product. In particular, the singlet at $\delta=7.59$ ppm could be attributed to the three aromatic protons H_a , while the doublets at 7.48 and 6.87 ppm, integrating for six protons each and showing an *ortho* coupling constant of $J=8.7$ Hz were attributed respectively to the aromatic protons H_f and H_g . The correct integration ratio confirmed the tri-functionalized structure. The triplets at 4.00 ppm and 3.68 ppm, integrating for six protons each and characterized by a coupling constant of 6 and 6.5 Hz respectively, were attributed to the three-carbon atoms chain protons H_i and H_m , resonating at lower fields due to the vicinity of the O and N atoms respectively. The proton H_l was instead resonating at 2.07 ppm as a multiplet, integrating for six protons. In the alkyl chains region it was possible to observe the presence of the signals characteristic of the maleimide substituents, the singlet characteristic of the three methyl protons H_p at 1.95 ppm, the triplet at 2.36 ppm characteristic of H_s , the triplet at 0.88 ppm characteristic of H_v and the multiplets at 1.4-1.5 ppm and 1.2-1.3 ppm characteristic respectively of H_t and the rest of the alkyl chain. The integration ratio between all the methylenic protons signals and the aromatic protons was exactly the one expected for the molecular structure and allowed to confirm the presence of the maleimide unit on the polyaromatic core.

The high resolution mass spectrum (MALDI ionization source, with DCTB matrix and Time Of Flight analyser) confirmed further the identity of the product, showing a peak at m/z 1383.8790 Da. corresponding to the molecular formula $C_{90}H_{117}N_3O_9$, characteristic of $[M]^+$, in agreement with the calculated value (m/z 1383.8790 Da. for $C_{90}H_{117}N_3O_9$).

6.6 Isophthalic-acid N-functionalized maleimide derivative **M3**

M3 (6.3) can be synthesized from maleic anhydride and 5-amino isophthalic acid (**Scheme 6.18**). The synthesis consists in two steps that can be carried out one-pot.

6.6.1 Synthesis of **M3**



Scheme 6.18: Synthesis of the maleimide **M3**: a) i: 5-amino isophthalic acid, THF, 22°C, 3h; ii) Ac_2O , NaOAc, 16h, 80°C, 3h, 50%.

Maleic anhydride cycle was at first opened by an acyl nucleophilic substitution by 5-amino isophthalic acid to a carbonyl carbon. Due to the high reactivity of the anhydride carbonyl carbon, the reaction could be performed at room temperature in tetrahydrofuran. Following, the maleimide cycle was closed by condensing the nitrogen with the second carbonyl, by refluxing a solution in acetic anhydride, in the presence of sodium acetate. The system sodium acetate/acetic anhydride works as a dehydrating reagent and the cycle closure reaction was fast. **M3(6.3)** could be obtained pure as a yellow solid by precipitation from water with a 50% yield.

The product **M3** was characterized by 1H and ^{13}C -NMR mono and bi-dimensional spectroscopy and high resolution mass spectrometry.

6.7 Conclusions

Three differently functionalized maleimide derivatives prone to self-assemble on graphene/SiC(0001) and react with it upon STM activation by Diels-Alder reaction, have been synthesized. As far as this manuscript is being completed, the molecule **M1** has been deposited on the graphene/SiC(0001) surface at room temperature (in UHV). However, it was not possible to image it yet (and thus to test its reactivity under the STM tip), due to the high diffusivity at this temperature. The following step would consist in lowering the surface temperature (for ex. 6K) in order to limit the

diffusion. The studies on **M2** and **M3** on surface are ongoing, in the groups of L. Simon in Mulhouse and M. Yu at the Harbin Institute of Technology (China), respectively.

6.8 Tests of reactivity at the solid/liquid interface

6.8.1 Objective

As a complement to the foreseen STM experiments, we devised to preliminarily test the reactivity of maleimides at the solid liquid/interface, by employing “classical” means of thermal activation (i.e. oil bath, microwave heating...). Since we wanted to carry out the reaction in mild conditions, we devised to employ a good dienophile for our tests (**MF**, **6.15**, **Figure 6.5**).

We employed for our study mechanically exfoliated graphene on silicon oxide (G/SiO₂) and epitaxial graphene on silicon carbide (G/SiC) (see **Appendix A2**).

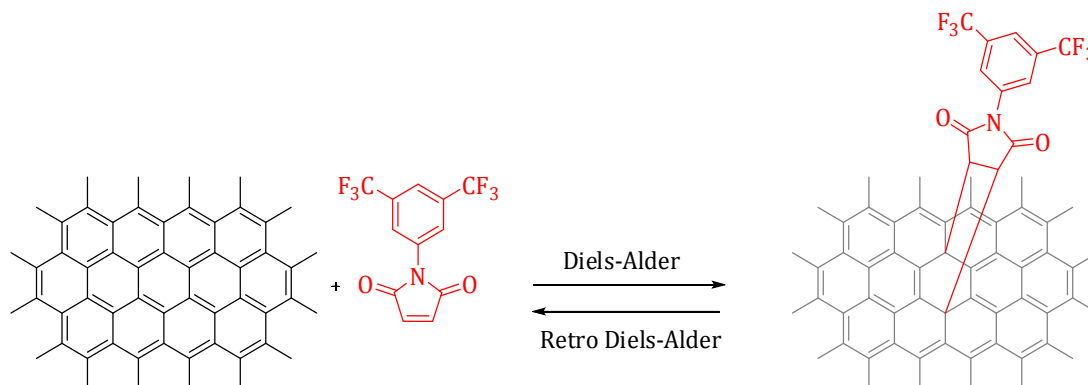


Figure 6.5: General objective: Diels-Alder reaction between the maleimide **MF** and graphene.

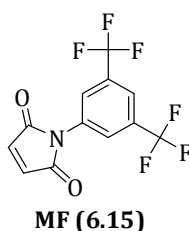
6.8.2 Different contributions to the work

The preparation of the samples of exfoliated graphene, the experiments of functionalization and the Raman characterization were carried out by M. Rubio-Roy in the team of E. Dujardin, in Group Nanosciences, CEMES (Toulouse, France).

The preparation of the samples of epitaxial graphene on silicon carbide and the XPS and STM characterizations were carried out by the team of L. Simon, at the IS2M of Mulhouse (France).

I participated in the experiments by synthesizing the reactive molecule, assisted in the functionalization procedure and helped in interpreting the Raman results.

6.8.3 Molecular design



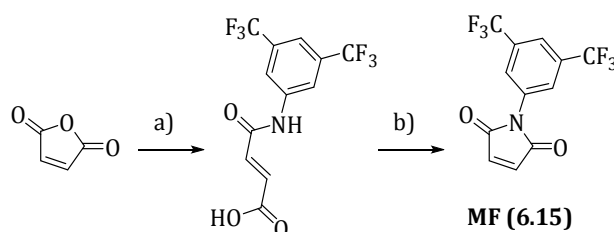
Scheme 6.19: Target molecule **MF (6.15)**.

The maleimide derivative **MF (6.15)** that we devised to employ is bearing a 3,5-bis(trifluoromethyl)phenyl substituent at the nitrogen position. The substituent was chosen according to the following considerations, based both on reactivity and characterization requisites:

- The highly electronegative fluorine atoms are meant to polarize strongly (by inductive effect) the molecule, reducing the electronic density on the maleimidic double bond. The strong fluorine-induced polarization has the effect of enhancing the double bond maleimidic-carbon atoms electrophilicity: the double bond carbons, in fact, have experimentally shown extremely high reactivity in Michael additions with weak nucleophiles, such as carboxylatesⁱ. In principle, the effects of the polarization of the double bond should also contribute to increase the dienophilic character of the molecule and render it reactive in Diels-Alder reactions in mild conditions (i.e. relatively low temperature and high reaction rate).
- Fluorine is, moreover, considered as a good tag in view of XPS (X-ray Photoelectron Spectroscopy) characterization. The element is, in fact, not naturally present in the natural atmosphere, avoiding risk of accidental contamination of the graphene sample.

The maleimide **MF** is already known in the literature²². It was employed as reagent in radical polymerization reactions^{22b,c} and, more rarely, in Diels-Alder reactions^{22a}.

6.8.4 Synthesis of MF



Scheme 6.20: Synthesis of the maleimide **MF (6.15)**: a) 3,5-bis(trifluoromethyl)aniline, DCM, 50°C, 19h; b) Ac₂O, 110°C, 1.5h, 77%.

ⁱ See the paragraph relative to the synthesis of the molecule for more detailed information.

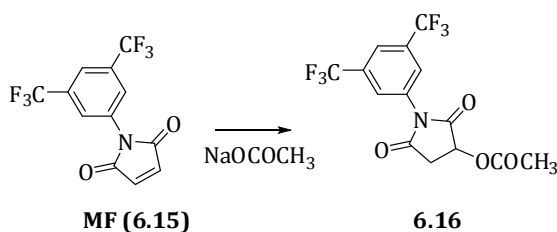
The maleimide derivative **MF (6.15)** was synthesized from the commercial precursors maleic anhydride and 3,5-bis(trifluoromethyl)aniline, by a slightly modified procedure, respect to that reported in literature^{22a}.

Step a)

In a first step (**Scheme 6.20**) the maleic anhydride cycle was opened by an acyl nucleophilic substitution by 3,5-bis(trifluoromethyl)aniline to a carbonyl carbon. In reason of the low reactivity of the aniline nitrogen, due to the deactivation by the trifluoromethyl groups, the reaction required a moderate heating in order to proceed, and was runned at 50°C for 19 hours. The maleamic acid product precipitated from the solution as a white solid, was recovered by filtration and employed in the following step without further purification.

Step b)

In the following step, the maleimide was cyclized by reacting the nitrogen atom on the second carbonyl carbon. The reaction was carried out by refluxing a solution of maleamic acid in acetic anhydride for 1.5 hours. In this case, sodium acetate was not employed, as dehydrating agent, as suggested in the literature procedure. It was, in fact, observed that the addition of sodium acetate to the reaction medium was determining an increase in the quantity of subproduct **6.16**, originated by the Michael addition to the maleimidic double bond, by the acetate nucleophile (**Scheme 6.21**).



Scheme 6.21: Michael addition to **MF** generating the sub-product **6.16**ⁱⁱ.

The compound **MF** was obtained pure by vacuum sublimation (66°C at 6 mmmHg), with a global yield over the two steps of 77%.

6.8.5 Characterization of MF

The product **MF (6.15)** was characterized by mono and bi-dimensional ¹H, ¹³C and ¹⁹F-NMR. The ¹H and ¹⁹F-NMR spectra were in accordance with those reported in literature²². Thanks to the

ⁱⁱ **6.16** can be synthesized by reacting an equimolar amount of **MF** and CH₃COONa in acetone at 40°C for 2 hours. It shows a red coloration in polar solvents, likely due to an intramolecular charge transfer process.

improvement of the reaction and purification conditions, the signals characteristic of the subproduct **6.16** was not observed in our case.

The mass spectroscopy characterization was complicated to perform, due to the molecular structure. Two ionization techniques were employed: Electrospray and Direct Chemical Ionization with methane (positive ions mode and Time Of Flight mass analyser in both cases). In the first case, molecular ionization was not observed; in the second case, high fragmentation was observed, but no molecular peak. In particular, only the two peaks at 173.0138 Da. And 230.0411 Da could be attributed, respectively to the decomposition products phenylmaleimide and 3,5-bis(trifluoromethyl)phenyl ammonium.

6.8.6 Experimental procedure for graphene functionalization

The experiments were conducted on graphene supported on two kinds of substrates: 1) mechanically exfoliated graphene on silicon oxide (G/SiO₂) and 2) epitaxial graphene on silicon carbide (G/SiC). For a description of the preparation and characteristics of the graphene samples, see **Appendix A2**).

6.8.6.1 Functionalization of mechanically exfoliated graphene

The exfoliated graphene samples employed in the functionalization experiment are named in the text **G/SiO₂**. In particular, **G/SiO₂ (bf)** is the sample before functionalization and **G/SiO₂ (af)** is the sample after the functionalization and washing procedures.

The SiO₂/Si wafer size is 1x1 cm². The surface is covered by a different amount of flakes of different thicknesses. The density of coverage, as well as the number of monolayer flakes that can be found, is variable from sample to sample (estimated to be around 10-15%). In our study, we analysed the changes brought about by the chemical functionalization procedures to a selected monolayer graphene (individuated on the substrate by optical microscopy and Raman spectroscopy).

The functionalization was carried out by immersing the sample wafer in 1 ml of a 0.06 M solution of fluorinated maleimide **MF** in dry toluene. The sample was left in the solution for 5 minutes at room temperature. After removal of the wafer from the solution, it was rinsed by immersing it for 2 minutes in a) dichloromethane, b) acetone (twice) and c) isopropanol (twice) at room temperature. The sample was dried by nitrogen flow and characterized. We estimated that this washing procedure was enough to remove all the species eventually weakly physisorbed on the surface. On the SiO₂/Si substrate, in fact, no molecular signal was observed after rinsing, indicating that all the eventually crystallized molecules on the substrate were removed. Moreover, defunctionalisation experiments (that will be described afterwards, see **section 6.8.8.3** in this chapter) showed that the molecular layer on graphene was stable at high temperatures (T~100°C).

6.8.6.2 Functionalization of epitaxial graphene/SiC(0001)

The epitaxial graphene samples employed in the functionalization experiment are named in the text **SiC02**. In particular, **SiC02 (bf)** is the sample before functionalization and **SiC02 (02)** is the sample after the different functionalization and washing procedures.

The graphene is grown all over the silicon carbide surface, on an area of 14x3 mm², as mono and bi-layer. In our study, we followed the modifications to the monolayer graphene surface.

The functionalization was carried out by immersing the sample wafer in 1 ml of a 0.06 M solution of fluorinated maleimide **MF** in dry toluene. The wafer was let in the solution for 21 hours at room temperature. After removal of the sample from the solution, it was rinsed by immersing it for 2 minutes in a) dichloromethane, b) acetone (twice) and c) isopropanol (twice) at room temperature. A further washing was accomplished by immersing the wafer in dichloromethane for 17 hours at room temperature. The sample was dried by nitrogen flow and characterized.

A second functionalization test was carried out at higher temperature. The same functionalization procedure described before was applied, but the temperature of the solution was set at 80°C (instead of at room temperature). After the same series of rinsing, it was observed an increase in the molecular bands intensityⁱⁱⁱ of about 1.5 times with respect to that for the sample functionalized at room temperature, but no significative variation of the intensity of the D graphene band intensity. This could have meant either that the temperature was not enough high to activate Diels-Alder, but also that the reaction was already happening at room temperature, and the low D peak intensity was due to another origin (for example a low density of functionalization, see **section 6.8.7.1.1**).

6.8.7 Characterization techniques

6.8.7.1 Raman Spectroscopy²³

Raman Spectroscopy is a technique employed to observe vibrational and rotational modes in a system. It relies on the measurement of the shift of the energy of the photons of a monochromatic laser upon their interaction with a vibrational level of the system (Visible, near-Infrared or near Ultra-Violet sources are commonly employed). The technique is considered to be complementary to Infrared (IR) spectroscopy: if a Raman signal can be observed for those systems characterized by a *polarizable* electron cloud, IR bands originate instead from a variation of a permanent *dipolar moment* upon excitation.

When radiation interacts with a molecule/system, many types of scattering can occur. In particular, the mechanism of scattering can be described as follows: the adsorption of a photon of energy $h\nu$ leads to the excitation of the system to a “virtual excited level”. After excitation, the systems can then relax, re-emitting a photon either with the same energy (Rayleigh Scattering) or with a

ⁱⁱⁱ Evaluated from a comparison of the 2180 cm⁻¹ band intensities, see section 6.8.8.2.2

different energy (Inelastic or Superelastic Scattering). Two situations leading to a Raman process can be found: 1) “Stokes Raman Scattering”, the molecule in the ground state is excited to a virtual vibrational state and relaxes back to a higher vibrational state than it had originally (re-emitting a photon of lower energy, $E=h\nu-\Delta E$); 2) “Anti-Stokes Raman Scattering”, the molecule is excited from a vibrational excited state to a virtual state and then relaxes back to the ground vibrational state (the photon is re-emitted with an higher energy, $E=h\nu+\Delta E$). Rayleigh scattering is the most common, but does not give any information about the molecular structure, while Anti-Stokes is not common. So, generally, only Stokes Scattering is employed in the Raman measurement (**Figure 6.6**).

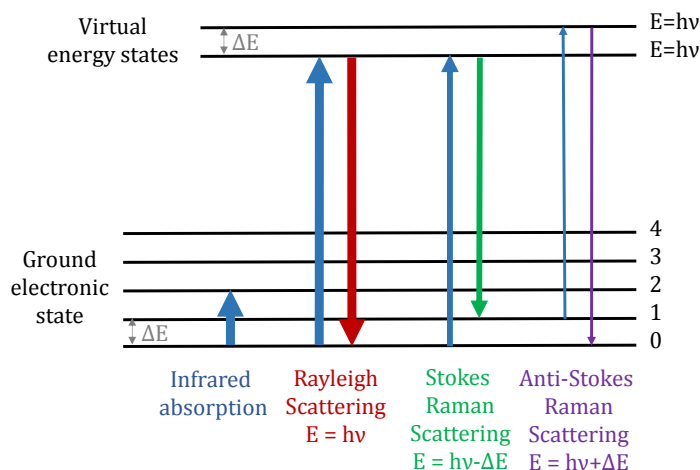


Figure 6.6: Three types of scattering by a molecule excited by a photon with energy $E = h\nu$ and comparison with Infrared adsorption.

In the Raman spectrum the frequency of the bands is determined by the shift of the energy of the photons of a monochromatic laser after Anti-Stokes scattering and in general reported in cm^{-1} on the X-axis; the intensity is, instead, determined by the system’s polarizability and generally reported in arbitrary units (a.u.), on the Y-axis.

6.8.7.1.1 Raman Spectroscopy for graphene characterization²⁴

The Raman spectrum of graphene presents a series of bands, which frequency, intensity and amplitude vary upon surface characteristics (n° of layers, functionalization...). In particular, the analysis of three intense bands in the spectrum (called as G, 2D and D) generally allows to retrieve many information relative to the geometrical and electronic modifications brought about to the graphene plane upon chemical functionalization or after physical modifications.

The G and 2D bands are always authorized bands:

- G-band is due to the in-plane vibrations of sp^2 carbon atoms. Its frequency is not a probe of the number of layers. On the contrary, a blue shift (accompanied by a sharpening of the band) is indicative of hole or electron doping.
- 2D-band is dependent on stacking order and number of graphene layers. For this reason, it is employed to distinguish monolayer graphene, from bilayer, few-layer graphene ($n=3, 4, 5$) or HOPG.

Other information that can be obtained by the analysis of the 2D band shift, intensity and amplitude (measured as “FWHM”, Full width at Half Maximum) are the hole/electron doping and/or strain induced by the substrate or by chemical functionalization. The 2D band frequency shows as well a dependence on the laser energy, accordingly to the relation $\left(\frac{\Delta\omega_{2D}}{\Delta E_L}\right) \sim 100 \text{ cm}^{-1}$ (where ω_{2D} is the frequency and E_L is the laser energy).

- D-band requires a defect in the sp^2 -conjugated lattice in order to be activated. Its frequency varies depending on the energy of the laser that is employed, according to the relation $\left(\frac{\Delta\omega_D}{\Delta E_L}\right) \sim 50 \text{ cm}^{-1}$ (where ω_D is the frequency and E_L is the laser energy). For ex. for a 2.33 eV laser energy ($\lambda=532 \text{ nm}$), the D band is expected at $\sim 1350 \text{ cm}^{-1}$, for a 1.94 eV laser energy ($\lambda=638 \text{ nm}$), the D band is expected at $\sim 1330 \text{ cm}^{-1}$. The ratio between the intensity of the D and G bands (I_D/I_G) is employed in the literature to evaluate the presence of defects (for example sp^3 carbon atoms) in graphene. The growth of the D band is accompanied by the growth of a second band, D', at 1620 cm^{-1} , as a shoulder of the band G. The intensity of the D peak depends not only on the number of defects introduced, but also on their density²⁵.

Due to the different nature of the substrate on which graphene is deposited and the sensitivity of the Raman bands of graphene to the environment, the positions of the G and 2D bands will be shifted depending on the substrate. Some bands typical of the substrate will also be visible in the spectrum (**Table 6.1**).

Graphene type	Substrate	G-band position (cm^{-1})	G-band FWHM (cm^{-1})	2D-band position (cm^{-1})	2D-band FWHM (cm^{-1})	Substrate characteristic bands (cm^{-1})
Mechanically exfoliated	SiO ₂ / Si	~ 1580 - 1588	~ 6 - 16	~ 2685	~ 25 - 32^*	~ 520.7 ~ 900 - 1000
Epitaxial	6H-SiC (0001)	~ 1591	~ 31	~ 2710	$\sim 59^{**}$	~ 795 ~ 970 ~ 1430 - 1750
Graphite	SiO ₂ / Si	~ 1580	~ 16	~ 2675 (2D1) ~ 2720 (2D2)	~ 41 (2D1) ~ 36 (2D2)	~ 520.7 ~ 900 - 1000

Table 6.1: Comparison between the G and 2D-bands positions and FWHM (Full Width at Half Maximum) for monolayer graphene on silicon oxide or silicon carbide substrates and comparison with graphite ($\lambda= 532 \text{ nm}$, from reference 26). * sharp and symmetric band; ** large asymmetric band.

6.8.7.2 X-Ray Photoelectron Spectroscopy (XPS)²⁷

X-Ray Photoelectron Spectroscopy (XPS) experiments are based on the photoelectric effect, i.e. the ejection of electrons from a material's surface upon its exposure to an electromagnetic radiation of sufficient energy.

In the experiment, the sample is irradiated with high-energy radiation in Ultra-High Vacuum: the electrons that are ejected are collected and their Kinetic Energies measured. In general, monochromatic aluminium ($h\nu = 1486.6$ eV) or magnesium ($h\nu = 1253.6$ eV) K_{α} X-Rays are employed as electromagnetic radiation. The surface spot width that can be analysed depends on the spectrometer and is generally about 10 μm ; several atomic layers are analysed over depths of 1 to 10 nm.

Thanks to the relation between the emitted electrons Kinetic Energy (KE) to the energy of the incident radiation ($h\nu$), it is possible to get information about the elemental composition of the sample. In particular, $KE = h\nu - E_b - \phi$, where E_b is the binding or ionization energy and ϕ is a work function, characteristic of the particular spectrometer. E_b is correlated to the electronic configuration in the atoms and orbitalic energies (i.e. 1s, 2s, 2p, 3s....). The information that can be retrieved are, thus, not only the presence and relative quantities of elements in one sample, but also their chemical states (i.e. oxidation state, atom hybridization) and environment (i.e. chemical bonds in the functional groups) in the sample.

The spectrum consists in the plot of the number of electrons detected (intensity, reported in general in counts per second, c/s, on the Y-axis) versus Binding Energies (B.E., in electron Volts, reported on the X-axis). A general survey scan allows identifying the type of different elements present in the material; high-resolution scans are then performed in order to gather more information about the chemical state of the elements: the originated large peaks can be deconvoluted by softwares in the constituting peaks, at the binding energies characteristic of a particular element in a particular state.

6.8.8 Results and discussion

6.8.8.1 Raman spectrum of the molecule MF

The Raman spectrum of the molecule MF deposited on a silicon oxide substrate as a solid is presented in **Figure 6.7**. In the spectrum, two bands characteristic of the SiO_2 substrate are visible, at 520.7 cm^{-1} and $\sim 900\text{-}1000\text{ cm}^{-1}$. Most of the molecular bands have been attributed accordingly to literature data for similar compounds and the interpretation is reported in **Table 6.2**.

The most intense signature is the C=O asymmetric stretching band at 1766 cm^{-1} ; another interesting band is found at 1075 cm^{-1} and attributed to the phenyl mode usually described as C-H in plane bending, which involves significant contributions from the maleimide part of the molecule (**Figure 6.8**)²⁸

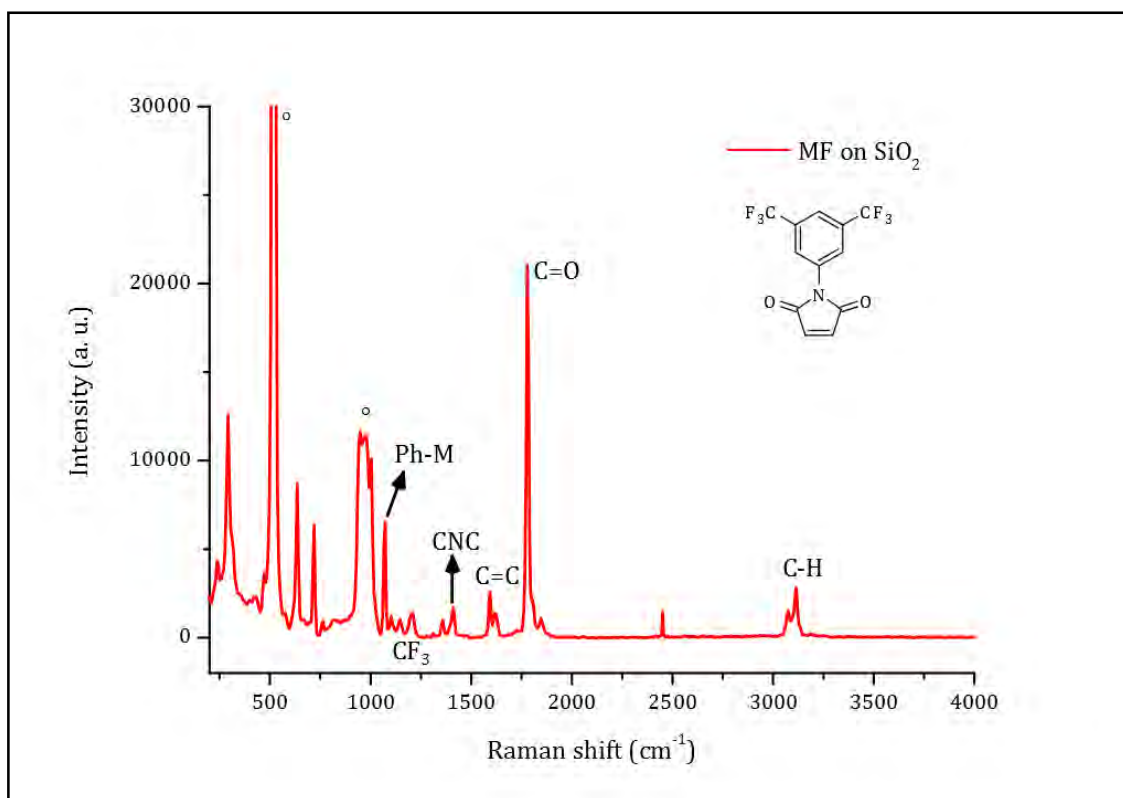


Figure 6.7: Raman spectrum of **MF** deposited as a solid on a SiO_2 substrate ($\lambda=532$ nm): \circ , SiO_2 1st and 2nd order bands; Ph-M, combination of maleimide and phenyl symmetric in plane bending; CF_3 , CF_3 vibrations, C=C, maleimide and phenyl ring signals; CNC, imide symmetric stretching; C-H, phenyl and maleimide CH stretching.

Raman shift (cm^{-1})	Attribution	Reference
~ 1075 (m)	Ph-M (phenyl symmetric in plane bending)	28
~ 1280 (w)	CF_3 , ν_s	29
~ 1170 (w)	CF_3 , ν_{as}	
~ 1130 (w)	CF_3 , ν_{as}	
~ 1390 (m)	CNC maleimide symmetric stretching	28
~ 1585 (w)	C=C phenyl symmetric and asymmetric stretching, maleimide stretching	28
~ 1720 (vw)	C=O symmetric stretching	28
~ 1766 (vs)	C=O asymmetric stretching	
~ 3070 - 3100 (w)	C-H maleimide symmetric and asymmetric stretching, phenyl stretching	28

Table 6.2: Raman bands assignment for MF deposited as a solid on a SiO_2 substrate ((w): weak, (vw): very weak, (m): medium, (s): strong, (vs): very strong band intensity).

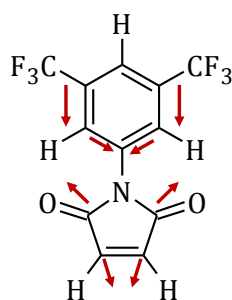


Figure 6.8: Phenyl symmetric in plane bending mode (originating the band at 1075cm^{-1} , indicated as Ph-M in the spectrum).

6.8.8.2 Raman spectrum of the adduct between MF and G/SiO₂

The Raman spectrum of the functionalized sample appears to be quite complex. The most striking feature is that the signal of the molecule is very intense, overlapping the silicon oxide and most of graphene bands (**Figure 6.9**). The numerous rinsing procedures and the fact that the layer is stable at high temperature ($\sim 100^\circ\text{C}$), see **section 6.8.8.3** can suggest us that the signal that we observe in the Raman spectrum is due to molecules strongly interacting with graphene.

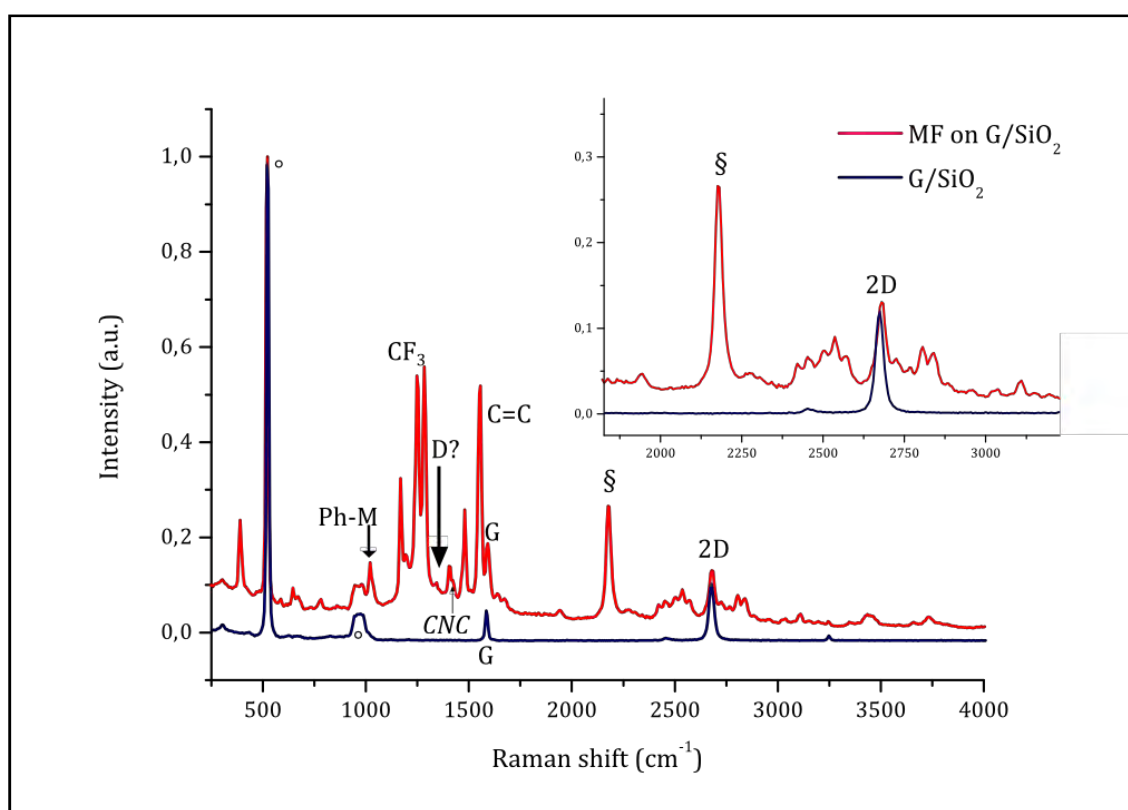


Figure 6.9: Raman characterization of the adduct between **MF** and G/SiO₂: blue= ML-G/SiO₂ (SiO₂ (bf)), red= ML-G/SiO₂ sample functionalized for 5 mins./R.T. with MF (solution 0.06 M in toluene) (SiO₂ (O2)) ($\lambda = 532\text{ nm}$). °, SiO₂ 1st and 2nd order bands; Ph-M, combination of maleimide and phenyl symmetric in plane bending, CF₃, CF₃ vibrations; D, possible D graphene band, C=C, phenyl ring signals; CNC, imide symmetric stretching; G, G graphene band; §, unknown band; 2D, 2D graphene band. The graphene was supported on a 90 nm SiO₂ substrate.

We observed that the molecular signal was reaching a saturation by dipping the sample in a solution at concentration 10^{-2} M in toluene at room temperature already after 5 minutes. Some tests carried out either by applying warming by microwave irradiation at an estimated temperature of 45°C or by keeping the sample dipped in the solution for a longer time (6 hours) at room temperature, followed by the same careful washing procedure described above (**section 6.8.6.1**) did not afford any increase in the molecular signal.

In order to get insight into the nature of interaction between graphene and the molecule MF, we analysed the graphene's and molecular bands in the Raman spectrum.

6.8.8.2.1 Analysis of graphene's bands

As already discussed in the **section 6.8.7.1.1** three bands are relevant in order to get information on the results of functionalization of graphene: G, 2D and D. We will now proceed to analyse the characteristics of these bands in the adduct spectrum in **Figure 6.9**:

- The G band can be found at 1592 cm^{-1} in the post-functionalization spectrum **SiO₂ (af)**, while in the pre-functionalization spectrum at 1582 cm^{-1} **SiO₂ (bf)**. The blue shift can be attributed to a doping effect induced on graphene by the molecule, either covalently bonded or physisorbed.

- The 2D band can be found at 2680.7 cm^{-1} in the post-functionalization spectrum **SiO₂ (af)**. The intensity of the bands before and after functionalization cannot be compared due to the presence of additional signals after functionalization, varying the apparent intensity of 2D. However, it is possible to measure a band shift from 2673 cm^{-1} to 2680 cm^{-1} ($\sim 7\text{ cm}^{-1}$) and to observe that the width of band does not vary ($\sim 27\text{ cm}^{-1}$). The shift of the 2D band can be ascribed either to a doping due to physisorption of the molecule (with a charge transfer contribution) or to a combination of change in the strain of the flake and doping effect upon the expected Diels-Alder reaction, followed by the introduction of sp^3 defects. Since the different contributions cannot be distinguished, it is not possible to assert the positive formation of the covalent bond between graphene and the molecule by the simple analysis of the 2D band.

- A band that could be identified as D is present in the reported spectrum at 1343 cm^{-1} (recorded at $\lambda=532\text{ nm}$). It is possible to check whether it is the D band (and not a molecular band) by comparing its Raman shift in a spectrum recorded at a different laser wavelength: at $\lambda=638\text{ nm}$ the D shift is 1338 cm^{-1} . Since the difference between the two frequencies is expected to be of the order of 20 cm^{-1} , we can attribute the band to a molecular mode (and not to D). In this case, if an increase in the D peak intensity upon functionalization is registered, as a consequence of the introduction of sp^3 centers, we cannot observe it due to the overlapping of the molecular signals.

6.8.8.2.2 Analysis of molecular bands

The Raman spectrum of the adduct between **MF** and graphene (**SiO₂ (af)**, **Figure 6.9**) presents significant differences with the spectrum of the molecule deposited as a solid on SiO₂/Si (**Figure 6.7**).

The origin of the differences can be attributed to the activation/ suppression of modes in the adduct, which can be originated both as a 1) consequence of the formation of a covalent bond between graphene and the molecule **MF**, or 2) by the adsorption of the molecule on graphene, by a non-covalent charge-transfer interaction. We can assume the establishment of a strong interaction between molecules and graphene from the shift of the 2D band and the stability of the molecular layer at high temperatures.

In particular, concerning the molecular bands, two variations observed in the spectra appeared to us to be the most relevant:

- Disappearance of the C=O signals at ~1720 and 1766 cm⁻¹ in the adduct spectrum (**SiO₂ (af)**, **Figure 6.9**).
- Appearance of new band at 2180 cm⁻¹ in the adduct spectrum (**SiO₂ (af)**, **Figure 6.9**), which attribution is not straightforward. This band is, in fact, in general characteristic of sp hybridized carbons, in functional groups like C≡O³⁰, C≡C³¹ or C≡N³² that are not present in **MF**.

Different hypothesis have been made in order to justify the origin of the band at 2180 cm⁻¹:

- Band characteristic of a decomposition product of the molecule.
- We hypothesized that the very electron poor molecule could be reduced by graphene, in a one-electron transfer mechanism analogue to the reduction of aryl diazonium salts³³. By cyclic voltammetry we were, in fact, able to determine **MF** reduction potential (-1V vs SCE in CH₂Cl₂) and to observe that the reduction process is not reversible^{iv}, the radical anion **MF**^{•-} being instable in solution. The presence in the spectra of the bands expected for the intact compound (CNC, CF₃, and, in particular, the band at ~1075 cm⁻¹, characteristic of a combination of molecular modes (**Figure 6.8**)) allowed us to discard this hypothesis.

- Shift of the carbonyl C=O band upon formation of the Diels-Alder adduct or physisorption of the molecule on graphene.
- Activation of an usually unauthorized mode of molecular vibration upon Diels-Alder reaction/ physisorption of the molecule on graphene. In particular, O=C=N asymmetric stretching vibrations can occur at this frequency (accompanied by a symmetric stretching at 1400-1450 cm⁻¹).
- Low intensity graphene bands are also found at this frequency (iTA-iTO combination mode for graphene phonons).

Raman spectra simulations would be useful in order to clarify the origin of the band.

^{iv} The voltammetry measurements have been performed by A. Saquet, at the LCC laboratory in Toulouse. The radical anion **MF**^{•-} is not any more detectable after ~30s by cyclic voltammetry experiment.

Due to the complexity of the Raman spectrum, and in particular the fact that the D graphene band region is covered, it is not possible to establish if the molecule has reacted by Diels-Alder mechanism, leading to the introduction of sp^3 carbon centres on the surface and thus to an increase of the I_D/I_G ratio, or it is just strongly physisorbed. The high shift of the 2D graphene band ($\sim 7\text{ cm}^{-1}$) can suggest either the formation of a covalent adduct or, in any case, a strong charge-transfer non-covalent interaction between graphene and MF, leading to a certain degree of graphene p-doping.

A confirmation of the strong character of the interaction between graphene and **MF** was obtained by the analysis of the results of a series of de-functionalization experiments.

6.8.8.3 De-functionalization experiments

In order to investigate the thermal stability of the adduct between graphene and **MF**, we warmed the sample **SiO₂ (af)** in clean toluene for different time intervals. In the text, the different samples are named as follows (**Figure 6.10**):

1. **SiO₂ (df1)** is the sample **SiO₂ (af)** warmed in toluene at 100°C for 40 minutes;
2. **SiO₂ (df2)** is the sample **SiO₂ (df1)** warmed in toluene at 130°C for 120 minutes.

In order to keep the solution highly diluted, thus avoid the eventual reformation of the adduct between graphene and **MF**, we employed high volumes of clean toluene (50-100 ml). In these conditions, considering a graphene surface of $1 \times 1\text{ cm}^2$, we calculated the *superior limit* of the molecular concentration in solution after de-functionalization, to be of the order of $3\text{-}6 \times 10^{-6}\text{ M}$. In the real conditions, the molecular concentration in solution will be certainly lower, since the area of the silicon wafer is only partially covered ($\sim 10\text{-}15\%$) by micrometric flakes of graphene (of different thicknesses) and the molecular signal has not been observed on the bare silicon. For this reason, we were able to consider the adduct's kinetic of reformation to be much slower than its decomposition's.

After performing the de-functionalization process, we registered a Raman spectrum and compared the variation of integrated area of some characteristic bands. We choose to analyse the area under the system at $\sim 1130\text{-}1280\text{ cm}^{-1}$ and the band at 2180 cm^{-1} . The results are reported in **Table 6.3**.

Raman band	Area [SiO ₂ (df1) / SiO ₂ (af)] %	Area [SiO ₂ (df2) / SiO ₂ (df1)] %
2180 cm^{-1}	$\sim 39\%$	$\sim 12\%$
$\sim 1130\text{-}1280\text{ cm}^{-1}$ (CF ₃)	$\sim 33\%$	$\sim 7\%$

Table 6.3: Percentage variation of the integrated areas after the de-functionalization procedures.

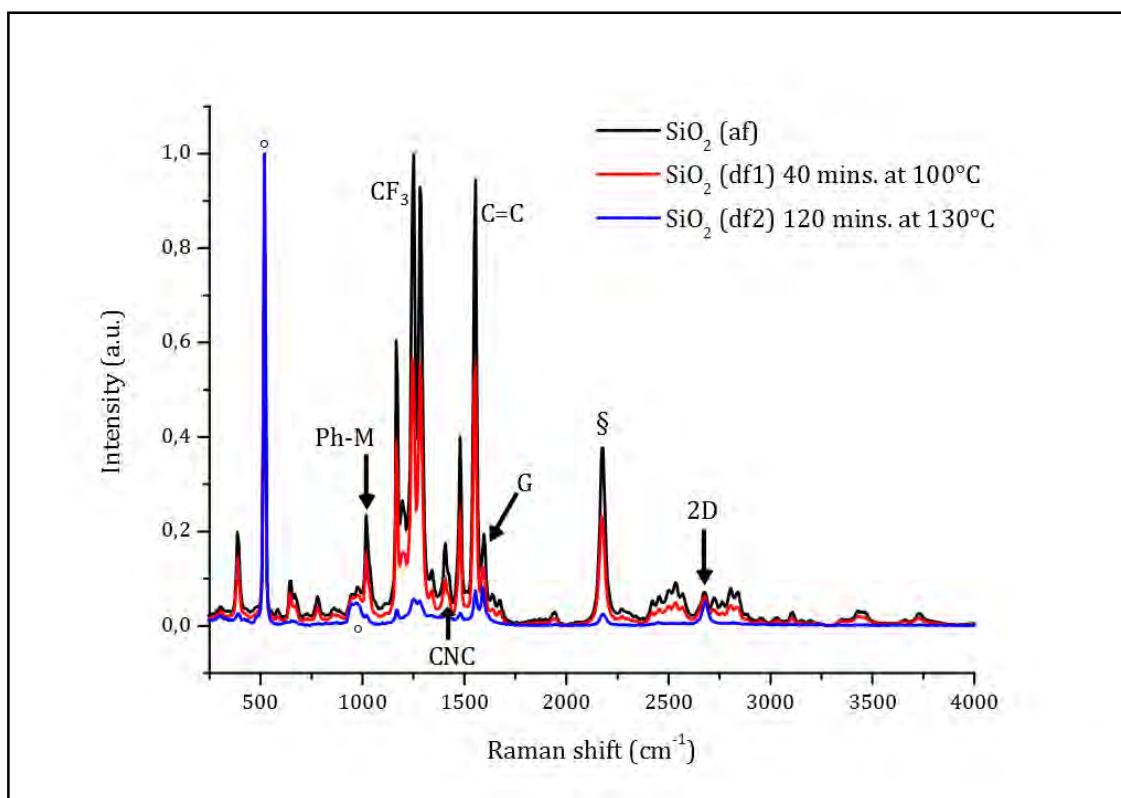


Figure 6.10: Raman characterization of the adduct between **MF** and G/SiO₂ before (black) and after (red and blue) two de-functionalisation procedures: red= sample de-functionalized for 40 mins. at 100°C; blue= sample de-functionalized for 120 mins. at 130°C ($\lambda = 532$ nm). °, SiO₂ 1st and 2nd order bands; Ph-M, combination of maleimide and phenyl symmetric in plane bending, CF₃, CF₃ vibrations; C=C, phenyl ring signals; CNC, imide symmetric stretching; G, G graphene band; §, unknown band; 2D, 2D graphene band. The graphene was supported on a 290 nm SiO₂ substrate.

We observed a considerable stability of the adduct **SiO₂ (af)**. Warming at 100°C for 40 minutes led to the desorption of only 30-40% of the molecules. By warming at higher temperature for a longer time (130°C, 120 minutes), the molecular signal intensity was significantly reduced, to ~10% of its original value.

The high thermal stability allowed us to infer once more the strong character of interaction between the molecules **MF** and graphene, attributed either to the formation of a Diels-Alder adduct or strong charge transfer complex. However, it was still not possible to discriminate between the two possibilities, since the increase in temperature could determine both a retro-Diels-Alder or the breaking of the charge-transfer interaction.

Often, in the literature, an analysis of the variation of reactivity with the layer thicknesses is presented, by comparing the variation of I_D/I_G upon functionalization, for different few-layers graphene thicknesses. In our case this analysis cannot be performed, D being not visible (or not present) in the spectrum. The Raman intensity of the molecular signals diminishes for increasing thicknesses, but this effect can be due also to a different screening effect of the substrate reflexions, that is higher for higher graphene thicknesses.

In order to get a better understanding, we devised to perform XPS and STM characterization. In this purpose, we had to switch to a different substrate, silicon carbide. This was due to two reasons: 1) since the XPS spot is extended over a $\sim 10 \mu\text{m}$ diameter, we needed a graphene flake larger than the micrometric flakes obtained by mechanical exfoliation. By epitaxial growth on silicon carbide, it is possible to obtain larger millimetric flakes. 2) G/SiC(0001) is more suitable for STM characterization (since it is endowed with flat-extended terraces).

This allows us also to discuss about the influence of the substrate on graphene reactivity.

6.8.8.4 Raman spectrum of the adduct between MF and G/SiC(0001)

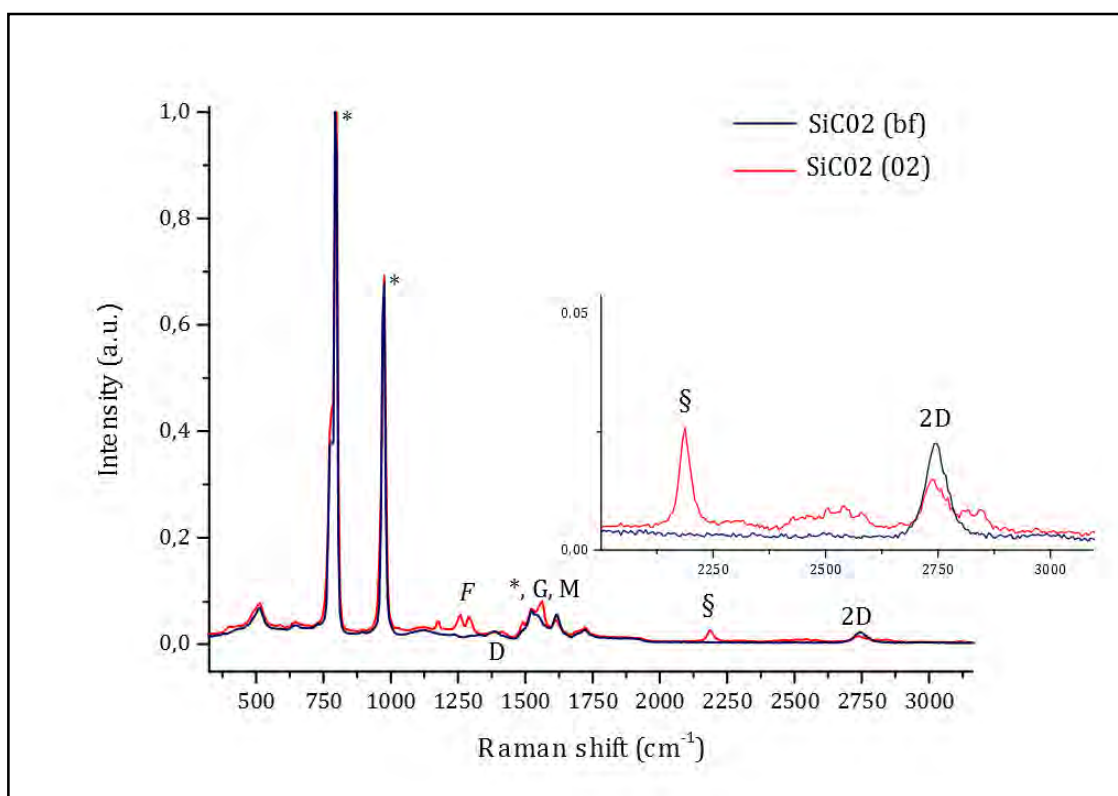


Figure 6.11: Raman characterization: blue= ML-G/SiC(0001) (SiC02 (bf)), red= ML-G/SiC(0001) sample functionalized for 21h/R.T. with MF (solution 0.06 M in toluene) (SiC02 (02)) ($\lambda = 532 \text{ nm}$). *, SiC signals; F, CF₃; D, D graphene band, M, phenyl ring signals; G, G graphene band; §, unknown band; 2D, 2D graphene band.

During the functionalization procedure, we observed that the time necessary to observe some molecular signal was longer than in the case of functionalization of graphene on SiO₂/Si. Precisely after 5 minutes in the same conditions (solution 0.06 M in toluene at room temperature), no molecular signal was observed on G/SiC(0001), while it was necessary to leave the substrate in the solution for 21 hours in order to observe a very small signal. This observation could be interpreted either as due to 1) a lower reaction kinetics, or 2) to a different optical enhancement of the molecular signal by the different substrates, or to a combination of the two effects.

In the spectrum (**Figure 6.11**) the most intense molecular signals were those characteristic of the trifluoromethyl groups (CF_3) and the “unknown band” at 2180 cm^{-1} . Some other signals were found in the range of frequencies $1430\text{--}1750\text{ cm}^{-1}$, in the same region as some SiC peaks.

As for graphene bands, the 2D band was present at 2745 cm^{-1} before functionalization and no significant shift or variation in FWHM was observed after functionalization. However, a diminution in intensity was registered. A D peak is naturally present on epitaxial graphene and an increase in intensity after chemical functionalization was not observed.

The analysis of the Raman spectrum showed evidences of the presence of the molecule (presumably in a small amount) but did not give information about the nature of the chemical interaction with graphene. In fact, a small ratio I_D/I_G could also be explained by a low density of defects²⁵.

6.8.8.5 XPS characterization of the adduct between MF and G/SiC(0001)

XPS analysis of the sample SiC02 (02) confirmed further the presence of the molecule. In the low resolution spectrum it was possible to observe a series of three signals: C1s in the binding energy region $280\text{--}290\text{ eV}$, O1s in the region $530\text{--}540\text{ eV}$ and F1s in the region $680\text{--}690\text{ eV}$.

The C1s and O1s bands can be deconvoluted in different components (**Figure 6.12**), related to the presence on the surface of the functional groups C=O, C-OR and COOH. The appearance of these chemical functionalities can be ascribed not only to the presence of the molecule MF, but also to the oxidation of reactive bonds at the graphene edges³⁴. For this reason, it did not allow to conclude on the presence of **MF** on the surface.

A clear confirmation of the presence of **MF** was, instead, retrieved by the appearance of the F1s signal at 688.55 eV . This band could be attributed to the F atoms in the trifluoromethyl- groups. The presence of ionic F^- (eventually originated due a charge transfer mechanism) was not revealed at lower binding energy ($\sim 685\text{ eV}$)^{35, 36}.

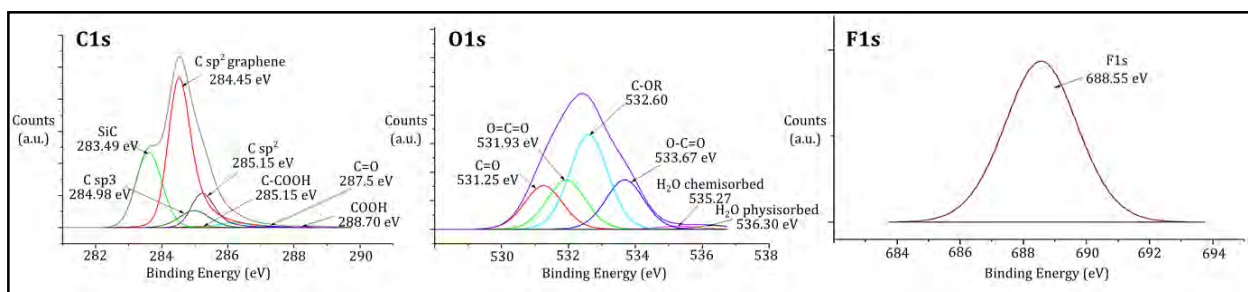


Figure 6.12: High resolution XPS spectra of the C1s, O1s and F1s regions (conditions: pass energy = 100 eV ; angular mode ($\pm 10^\circ$ range for collection of photo emitted electrons); X-Ray source = monochromatized $\text{AlK}\alpha$; Angle= grazing angle).

^v The sensitivity of the present measurements was not enough to allow the revelation of N1s signal.

6.8.8.6 STM characterization of the adduct between MF and G/SiC(0001)

In order to gain more insight on the aspects of the functionalization, the epitaxial graphene on SiC(0001) functionalized samples were imaged by STM in UHV. In particular, we expected to better understand these points: 1) nature of the chemical bond between molecule and graphene, 2) degree of coverage of the surface, 3) electronic properties of graphene after functionalization.

By STM microscopy, it was possible to identify a series of isolated defects randomly distributed on the surface (**Figure 6.13**). The atomic resolution image, allowed to distinguish inside the spot two brighter spots (lobes), which distance was 0.7 nm, possibly in accordance to the CF₃-CF₃ distances in **MF**. In the vicinity of the defects, standing waves appeared, comparable to those observed on graphene *only* in the presence of punctual defects³⁷, such as carbon vacancies, nitrogen substitution or sp³ carbon centres, as we would expect in the case of positive overcome of the Diels-Alder reaction. This could represent another indication of the formation of a strong interaction- possibly covalent bond- between graphene and the molecule. The density of the defects was estimated from the images to be lower than 1/(13x13) nm⁻² which could justify an increase in I_D/I_G lower than 0.1 in the Raman spectrum²⁵.

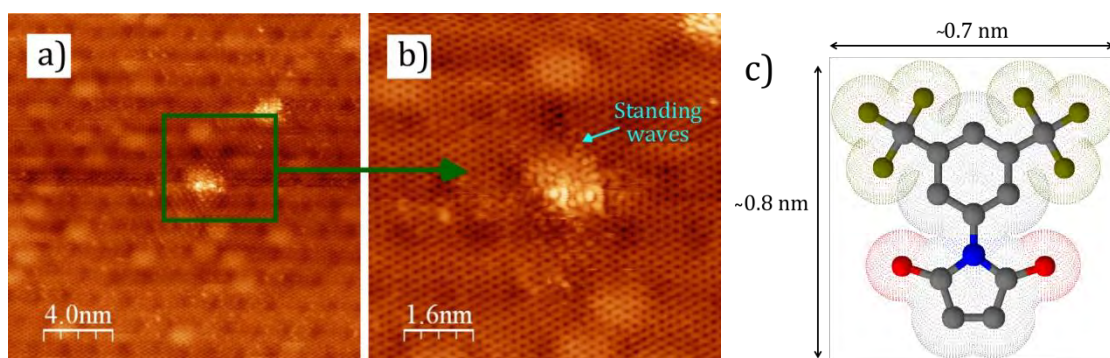


Figure 6.13: STM images of the sample **SiC02(02)**. a) small scale image ($U_t = -20$ up to -3 mV); b) high resolution image ($U_t = -20$ up to -3 mV). The molecules appear as a bright “round” features and an occupied molecular orbital is visible. Green = F; grey = C; Blue = N; Red = O.

6.8.9 Conclusions

The difficulties of characterization of these samples, related to the very small dimensions (i.e. quantity of matter that is analysable) and nature of the substrate, render very complex the assessment of positive outcome of the Diels-Alder reaction on graphene, with consequent formation of two covalent bonds with **MF**.

Some indications pointing to a strong interaction molecules-surface are: 1) the appearance of a strong molecular Raman signal, for the adduct molecule+graphene, with shift of the 2D band of $+7$ cm⁻¹; 2) the high thermal stability of the adducts; 3) the appearance of standing waves in the STM images.

The reactivity of **MF** is expected to be high, due to the enhanced electrophilic character of the maleimide double bond, and, as well, a higher reactivity is expected for graphene in Diels-Alder reactions, compared to other polyaromatic molecules, due to the high energy of the participating orbitals³⁸. The presence of only one signal for the fluorine, attributable to covalently bonded (and non ionic) fluorine (i.e. in CF₃), can be indication that the adduct is kept by a covalent bond, but still we do not have a striking direct prove.

Another hypothesis, that cannot be discarded, is that we have obtained a strong charge-transfer complex between the molecule and both types of graphene. It is in fact know that the first stage in the Diels-Alder reaction between maleimides and polyaromatic compounds consists in the formation of a charge-transfer adduct³⁹. Further experiments are ongoing in order to clarify the interaction between **MF** and graphene in the adducts.

6.9 References

- ¹ a) Yao, J., Xiao, Z., Zhang, J., Yang, X., Gan, L., Xiong Zhang, W., *Chem. Commun.*, **2009**, 401–403; b) *Angew. Chem. Int. Ed.*, **1999**, *38*, 16, 2360-2363.
- ² Munirasu, S., Albuerne, J., Boschetti-de-Fierro, A., Abetz, V., *Macromol. Rapid Comm.*, **2010**, *31*, 574-579.
- ³ Sarkar, S., Bekyarova, E., Niyogi, S., Haddon, R. C., *J. Am. Chem. Soc.*, **2011**, *133*, 3324–3327
- ⁴ Seo, J.-M., Jeon, I.-Y., Baek, J.-B., *Chem. Sci.*, **2013**, *4*, 4273-4277.
- ⁵ Chen, X., Zheng, Y., Shen, Y., *Chem. Rev.*, **2007**, *107*, 5, 1777-1830.
- ⁶ Deshpande, A. M., Natu, A. A., Argade, N. P., *J. Org. Chem.*, **1998**, *63*, 9557-9558.
- ⁷ Leazer, J. L. Jr., Cvetovich, R., Tsay, F-R, Dolling, U., Vickery, T., Bachert, D., *J. Org. Chem.*, **2003**, *68*, 3695-3698.
- ⁸ Argade, N. P., Naik, R. H., *Bioorg. Med. Chem.*, **1996**, *4*, 6, 881-883.
- ⁹ Clayden, Jonathan (**2001**). *Organic chemistry*. Oxford: Oxford University Press. pp. 276–296. ISBN 0-19-850346-6.
- ¹⁰ Baumann, M. E., Bosshard, H., Breitenstein, W., Rihs, G., Winkler, T., *Helvetica Chimica Acta*, **1984**, *67*, 1897-1905.
- ¹¹ Reddy, P. Y., Kondo, S., Toru, T., Ueno, Y., *J. Org. Chem.*, **1997**, *62*, 2652-2654.
- ¹² Souffrin, A., Croix, C., Viaud-Massuard, M. C., *Eur. J. Org. Chem.*, **2012**, 2499-2502.
- ¹³ Wuts, P. G. M., & Greene, T. W. (2007). *Greene's protective group in organic synthesis* (4th Ed.). New York: John Wiley & Sons.
- ¹⁴ van Scherpenzeel, M. van den Bergb, R. J.B.H.N. , Donker-Koopman, W. E., Liskampa, R. M. J., Aertsc, J. M.F.G., Overkleefb, H. S., Pieters, R. J., *Bioorg. Med. Chem.*, **2010**, *18*, 267-273.
- ¹⁵ Georgiades, S. N., Clardy, J., *Org. Lett.*, **2006**, *8*, 19, 4252-4254.
- ¹⁶ Finkelstein, H., *Ber. Dtsch. Chem. Ges.*, **1910**, *43*, 2, 1528-1532.
- ¹⁷ a) Uhl, W., Bock, H. R., Breher, F., Claesener, M., Haddadpour, S., Jasper, B., Hepp, A., *Organometallics*, **2007**, *26*, 9, 23673-2369; b) Yoosaf, K., Llanes-Pallas, A., Marangoni, T., Belbakra, A., Marega, R., Botek, E., Champagne, B., Bonifazi, D., Armaroli, N., *Chem. Eur. J.*, **2011**, *17*, 11, 3262-3273.
- ¹⁸ Chinchilla, R., Nájera, C., *Chem. Rev.*, **2007**, *107*, 874-922.
- ¹⁹ For a survey on microwave activated organic synthesis, see: Kappe, C. O., *Angew. Chem. Int. Ed.*, **2004**, *43*, 6250-6284.
- ²⁰ For literature examples of microwave activated Boc deprotection see: a) Lun, D. J., Waterhouse, G. I. N., Telfer, S. G., *J. Am. Chem. Soc.*, **2011**, *133*, 15, 5806–5809; b) Thaqi, A., McCluskey, A., Scott, J. L., *Tetrahedron Lett.*, **2008**, *49*, 49, 6962-6964; c) for an example of thermal Boc deprotection see: *J. Org. Chem.*, **2009**, *74*, 23, 9199-9201.
- ²¹ Wan, Y., Alterman, M., Larhed, M., Hallberg, A., *J. Org. Chem.*, **2002**, *67*, 6232-6235.
- ²² a) Callahan, R, Ramirez, O., Rosmarion, K., Rothchild, R., Bynum, K. C., *J. Heterocyclic Chem.*, **2005**, *42*, 889-898; b) Pfeifer, S., Lutz, J.-F., *Chem. Eur. J.*, **2008**, *14*, 10949-10957; c) El-Guweri, M., Hendlinger, P., Laschewsky, A., *Macromol. Chem. Phys.*, **1997**, *198*, 401-418.

- ²³ C. Paine, A. R. Barron, "Raman and Surface-Enhanced Raman Spectroscopy", <http://creativecommons.org/licenses/by/3.0>, **2010**.
- ²⁴ C. N. R., Rao, Sood, A.K., "Graphene. Synthesis, Properties and Phenomena", Wiley-VCH, 2013.
- ²⁵ Cançado, L. G., Jorio, A., Martins Ferreira, E. H., Stavale, F., Achete, C. A., Capaz, R. B., Moutinho, M. V. O., Lombardo, A., Kulmala, T. S., Ferrari, A. C., *Nano Lett.*, **2011**, *11*, 3190-3196.
- ²⁶ Wang, Y. Y., Ni, Z. H., Yu, T. Shen, Z. X., Wang, H. M., Wu, Y. H., Chen, W., Wee, A. T. S., *J. Phys. Chem. C*, **2008**, *112*, 10637-10640.
- ²⁷ Bratt, A., Barron, A. R., "XPS of carbon nanomaterials", <http://cnx.org/content/m34549/1.2/>, **2011**.
- ²⁸ Parker, S. F., *Spectrochimica Acta Part A*, **2006**, *63*, 544-549.
- ²⁹ Kobayashi, Y., Chinen, E., *Chem. Pharm. Bull.*, **1967**, *15*, 12, 1896-1900.
- ³⁰ Martínez-Salvador, S., Falvello, L. R., Martín, A., Menjón, B., *Chem. Eur. J.*, **2013**, *19*, 14540-14552.
- ³¹ Ruiz Delgado, M. C., Casado, J., Hernandez, V., Lopez Navarrete, J. T., Fuhrmann, G., Bäuerle, P., *J. Phys. Chem. B*, **2004**, *108*, 10, 3158-3167.
- ³² Meneghetti, M., Pecile, C., *J. Chem. Phys.*, **1986**, *84*, 4149-4162.
- ³³ Paulus, G. L. C., Wang, Q. H., Strano, M. S., *Acc. Chem. Res.*, **2013**, *46*, 1, 160-170.
- ³⁴ a) Reckinger, N., Felten, A., Santos, C. N., Hackens, B., Colomer, J.-F., *Carbon*, **2013**, *63*, 84-91; b) Bagri, A., Mattevi, C., Acik, M., Chabal, Y. J., Chhowalla, M., Shenoy, V. B., *Nature Chem.*, **2010**, *2*, 581-587.
- ³⁵ <http://cnx.org/content/m34549/1.2/#id1163798736743>.
- ³⁶ Riedl, C., Coletti, C., Starke, U., *J. Phys. D: Appl. Phys.*, **2010**, *43*, 374009.
- ³⁷ Simon, L., Bena, C., Vonau, F., Aibel, D., Nasrallah, H., Habar, M., Peruchetti, J. C., *Eur. Phys. J. B*, **2009**, *69*, 351-355.
- ³⁸ Sarkar, S., Bekyarova, E., Haddon, R. C., *Acc. Chem. Res.*, **2012**, *45*, 4, 673-682.
- ³⁹ Nishioka, Y., Yamaguchi, T., Yoshizawa, M., Fujita, M., *J. Am. Chem. Soc.*, **2007**, *129*, 7000-7001.

General conclusions

In this thesis, we designed and synthesised a series of molecules to be deposited and studied by STM on epitaxial graphene surfaces (on silicon carbide, SiC(0001)), in Ultra High Vacuum (UHV) conditions. The general objective was to induce a modification of the electronic properties of graphene, through the control of the chemical functionalization. In particular, two approaches were envisaged: *non-covalent* and *covalent*.

As general characteristics, the synthesized molecules presented three distinct structural components:

1. a *polyaromatic core*, favouring the absorption on graphene by π - π interactions;
2. an “*active*” *group* able to interact with graphene by either charge-transfer interaction or by a chemical reaction driving to the formation of a covalent bond. In the second case, the reactivity had to be triggered by means of the STM tip, such as to afford the possibility to select the spatial location of functionalization with an atomic scale precision;
3. different *self-assembling groups* allowing the molecular organization on the surface, in order both to prevent the molecular diffusion (generally important on epitaxial graphene/SiC surfaces) and to define a spatial organization of the “*active*” functional groups.

The molecular design had to take into account the different experimental constraints imposed by the UHV environment. One of the most important parameters was the thermal stability of the chemical functionalities, necessary in order to allow the UHV-sublimation and deposition on the surface. Based on these considerations and on the existing literature, different original solutions were proposed.

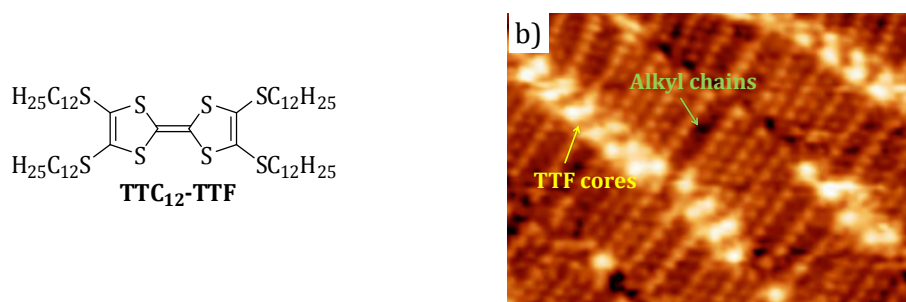
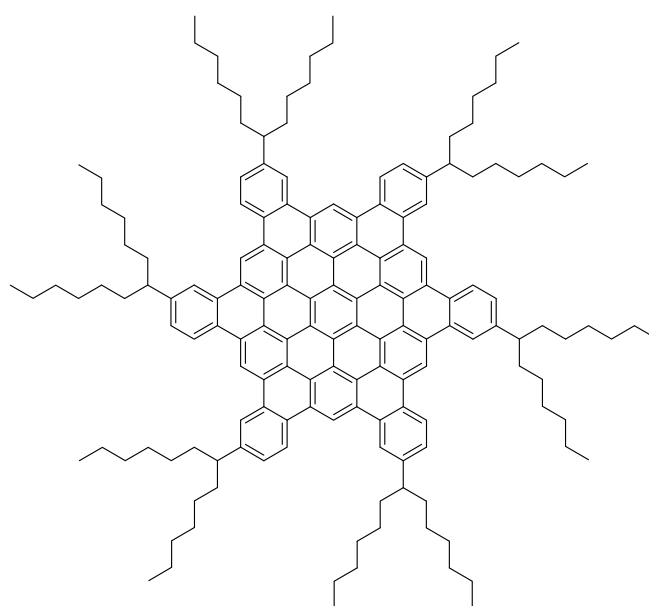


Figure 1: a) TTC₁₂-TTF- (**2.1**) molecule for the non-covalent functionalization of graphene/SiC; b) STM picture showing the self-assembled structure formed in UHV on graphene/SiC ($U_t = -1.6$ V, 6.4×6.4 nm²): note the edge-on molecular conformation.

For the *non-covalent* functionalization of graphene/SiC, we synthesized a tetrathiafulvalene (**TTC₁₂-TTF**, **2.1**) (**Figure 1**) and undertook the synthesis of a hexabenzocoronene derivative,

hexaphenanthrocoronene 3.1 (Figure 2). As *self-assembling elements* we choose to employ alkyl chains. The *active groups*, chosen for their potential electron donor properties towards graphene, had also the role of driving the molecular absorption on the surface.

The **TTC₁₂-TTF (Figure 1)** is functionalized with four twelve-carbon atoms alkyl chains. Although this molecule was already known in the literature and its self-assembling behaviour have been previously studied by STM at the HOPG/liquid interface, it was never been assessed before in the context of UHV experiments, on graphene/SiC. During the course of the thesis, this kind of STM study was performed and revealed an original *edge-on* absorption of **TTC₁₂-TTF** on graphene/SiC, dominated by the van der Waals interactions between the alkyl chains (“molecular fastener effect”). This conformation is very different from the *face-on* absorption observed on HOPG at the solid/liquid interface. While this organisation prevents the establishment of a charge-transfer interaction with the surface, it underlines the properties of graphene as a template for the building of molecular wires, interesting for future molecular electronic applications.



hexaphenanthrocoronene (3.1)

Figure 2: Chemical structure of the **hexaphenanthrocoronene 3.1**.

The **hexaphenanthrocoronene 3.1** is a new extended PAH. The structure is characterized by two components: firstly, a large aromatic *core*, that will allow for a strong interaction with graphene, possibly leading to a n-doping. Secondly, six C₆ dove-tail *alkyl chains*, that will provide the possibility of self-organization in a porous structure. The general synthetic scheme involved the synthesis of an hexabiphenyl precursor (**HBB 3.2**), to be planarized by oxidative cyclodehydrogenation in a last step. We optimized the synthesis up to the generation of the hexabiphenyl precursor (**HBB 3.2**) by aryne cyclotrimerization, with a global yield over five steps of 19-26%. Nevertheless, we could not isolate the

target **hexaphenanthrocoronene 3.1** yet, by employing DDQ/H⁺ as oxidizing system. We attributed this observation to the consuming of oxidizing reagent in a concurrent path, leading to the oxidation of part of the benzylic positions. The studies are being pursued in order to afford the target **hexaphenanthrocoronene 3.1**.

During the design phase of the molecules for graphene *covalent-functionalization*, one of the major challenges was to find functional groups being at the same time *reactive* with the extremely inert graphene basal plane, but enough *stable* in order to allow UHV sublimation, without any decomposition. The design also considered the mechanism envisaged for the local activation of reactivity, i.e. by STM tip manipulation and, least but not last, the necessity to endow the molecular structure with enough conformational flexibility to allow for the formation of a covalent bond with graphene.

In this context, we proposed two different approaches: firstly, we synthesized a series of *brominated precursors (Br1, Br2 or TBr, Figure 3)*, prone to generate an aryl radical species upon STM tip activation. The bromine substituent was chosen among other halogens for energetic considerations. As polyaromatic core, we devised to employ poly-phenyl or poly-phenyl-ethynyl derivatives, known for their possibility of absorbing on Highly Oriented Pyrolytic Graphite (HOPG) in liquid or UHV environments. Moreover, this cores offered the required conformational flexibility in order to allow the happening of the chemical reaction. As *self-assembling* moieties we choose carboxylic acids as hydrogen-bond donor-acceptor systems. The synthesis was carried out by employing Sonogashira, Suzuki and aldolic cyclotrimerization procedures. The molecules were not yet deposited and studied on the surface, at the moment of the writing of the manuscript.

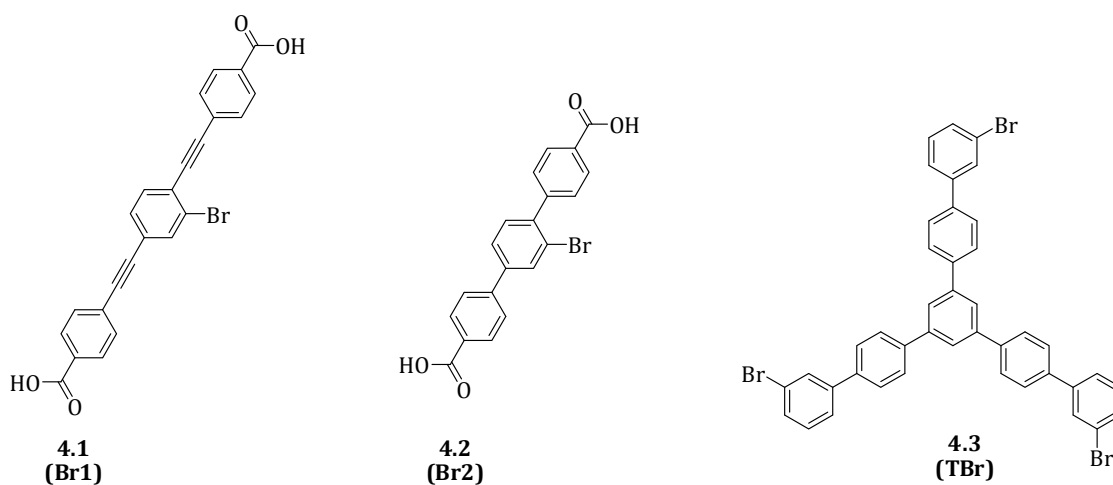


Figure 3: Molecules devised for a radicalar reactivity with graphene.

As a second approach, we suggested the employment of Diels-Alder reactive groups for the functionalization of graphene. Diels-Alder reactions present, in fact, undoubted advantages with respect to our objective of studying the reactivity on surface, such as a) the thermal stability of many reagents; b) the fact that catalysers are not necessary in order for the reaction to be activated. In this section, we proposed to employ *anthracene* as diene (**Figure 4**) and *maleimide* as dienophile (**Figure 5**) functional groups. The choice was dictated by the thermal stability of the two moieties, together with the possibility of inserting different types of functionalization.

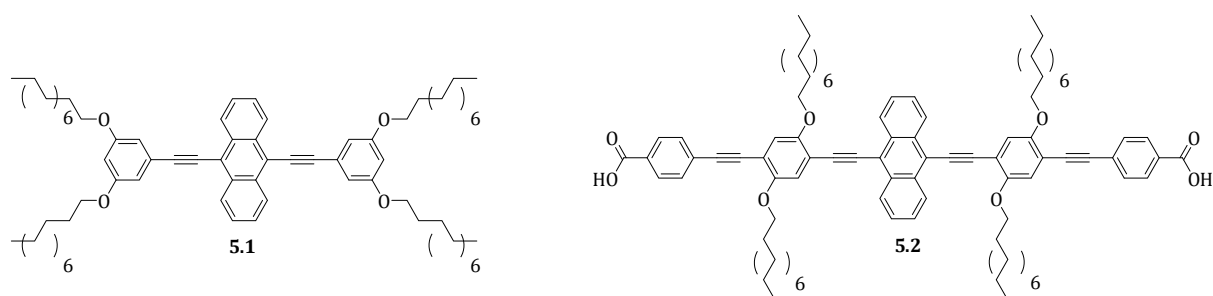


Figure 4: Anthracene derivatives devised for a Diels-Alder reactivity with graphene.

Two anthracene derivatives were synthesized, **A1 (5.1)** and **A2 (5.2)**. The anthracene aromatic core allows the absorption on the graphene surface, interaction that is enhanced by the insertion of additional aryl-ethynyl moieties. As *self-assembling moieties*, we choose to employ alkyl-chains (C10 for both **A1** and **A2**) and, in the case of **A2**, additional carboxylic acid moieties. The self-assembling groups have been introduced on the anthracene core by two different strategies, i. e. Sonogashira cross-coupling or carbonyl addition reactions. The two molecules are currently being deposited and tested on the surface.

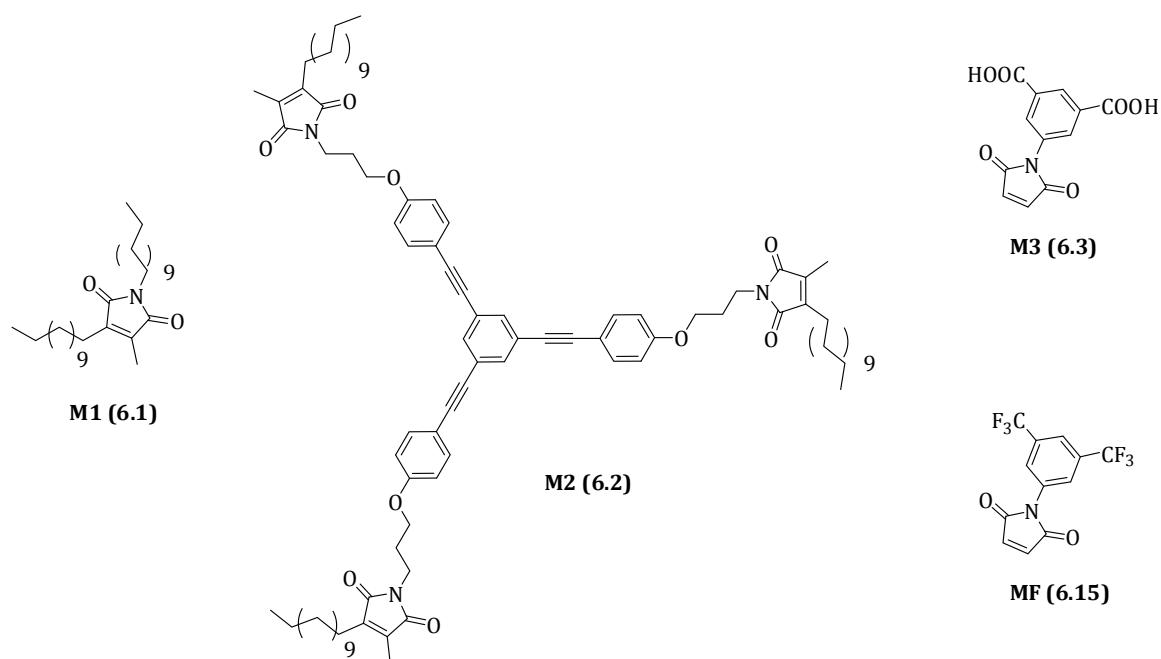


Figure 5: Maleimide derivatives devised for a Diels-Alder reactivity with graphene.

The maleimides dienophiles that we have synthesized are reported in **Figure 5**. Maleimide **M1 (6.1)** is functionalized with two alkyl chains, introduced in two steps, involving respectively a Michael addition to the maleic anhydride double bond and a carbonyl addition/dehydration reaction. The self-assembly can be governed by van der Waals interactions between the chains and involve also hydrogen-bonds with the oxygenated functions. **M1** has been deposited on graphene/SiC, but the molecules were showing a high diffusivity and it was not possible to image them at room temperature. The next step consists in repeating the STM experiment at low temperature (for example 6K).

M2 (6.2) and **M3 (6.3)** were designed in order to provide different geometrical organizations and eventually limit the molecular diffusivity at room temperature. In particular, **M2(6.2)** is characterized by the presence of three maleimide units connected by a tri-ethynyl benzene core, while **M3 (6.3)** is a simple maleimide core functionalized at the N-position with an isophthalic-acid group. Their studies on surface are ongoing.

The reactivity of a fourth derivative (**MF, 6.15**) has been tested, employing “classical” methods for the activation of the Diels-Alder reaction. Raman spectroscopy was employed as the main tool for characterization, showing the formation of an adduct, characterized by considerable thermal stability. Further characterizations need however to be performed in order to assess without doubts the formation of a covalent bond.

Perspectives of the work

In the course of the thesis, a large library of molecules for the *non-covalent* and *covalent* functionalization of graphene has been synthesized. We think that the study of these molecules could bring new interesting information concerning not only the phenomena of self-assembly on epitaxial graphene/SiC in UHV, but also on its basal plane reactivity.

On a long term, we expect that the results collected by the fundamental studies on the self-assembly and reactivity of the molecules synthesized in this work, will help providing the scientific community with the elements necessary to get a better control over the molecular organization and reactivity with graphene, by performing an optimal molecular design.

Once gained a full control on the spatial functionalization of graphene surfaces, it could be envisaged to employ the material as a support for atomically precise integrated circuits.

Experimental procedures

Generalities

Chemicals

Solvents

The solvents were bought from Sigma Aldrich or Acros Organics. If not otherwise specified, the solvents were dried on molecular sieves 3 Å¹. THF was either *distilled* on sodium/benzophenone or *dried* on molecular sieves 3Å. Anhydrous DMF and 1,4-dioxane were bought from Acros Organics and Sigma Aldrich respectively.

Reagents

All the reagents were bought from Sigma Aldrich or Acros Organics and employed without any purification, unless specified.

Chromatographic supports

Chromatographic purifications were carried out by employing silica gel (Fluka, pore size 6Å, 230-400 Å mesh) or neutral alumina (Acros Organics) stationary phases. The progress of the reaction was followed by thin layer chromatography on direct (Merck, silica gel 60, F254) and reverse phase silica gel (Silica gel 60 RP 18, F254) or neutral alumina (Merck, aluminium oxide 60, F254). The revelation was carried out by Uv lamp (254 or 365 nm) or by the employment of the opportune indicators (for ex. potassium permanganate).

Analytical tools and devices

NMR spectroscopy

The NMR spectra were recorded at the NMR-service of University Paul Sabatier (Toulouse), on Bruker Avance 300, 400 or 500 MHz spectrometers. The spectra were treated with the software NMR Notebook. As internal reference, the signal of the non-deuterated solvent was employed²: CDCl₃ at $\delta_{\text{H}} = 7.26$ ppm, $\delta_{\text{C}} = 77.16$ ppm, CD₂Cl₂ at $\delta_{\text{H}} = 5.33$ ppm, $\delta_{\text{C}} = 53.84$ ppm, CD₃OD at $\delta_{\text{H}} = 3.31$ ppm, $\delta_{\text{C}} = 49.00$ ppm, C₂D₂Cl₄ at $\delta_{\text{H}} = 6.0$ ppm, $\delta_{\text{C}} = 73.8$ ppm, [D₆]DMSO at $\delta_{\text{H}} = 2.50$ ppm and $\delta_{\text{C}} = 39.52$ ppm. The following abbreviations have been employed in order to describe the signals: s= singlet, d= doublet, t= triplet, dd= doublet of doublets, q= quintuplet, m= multiplet.

Mass spectrometry

The mass spectra were recorded at the Mass-spectrometry service of University Paul Sabatier (Toulouse), in MALDI-TOF, ESI-TOF, DCI (CH₄)-TOF, DCI (CH₄ or NH₃)-quadrupole modes.

IR spectroscopy

The IR spectra were recorded on a Perkin Elmer Spectrum 100 spectrometr.

¹ Williams, D. B. G., Lawton, M., *J. Org. Chem.*, **2010**, 75, 24, 8351–8354.

² Fulmer, G. R., Miller, A. J. M., Sherden, N. H., Gottlieb, H. E., Nudelman, A., Stoltz, B. M., Bercaw, J. E., Goldberg, K. I., *Organometallics*, **2010**, 29,9, 2176–2179.

Elemental analysis

Elemental analyses were carried out by the Service d'Analyse de l'ICSN (Paris).

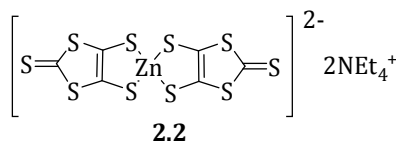
HPLC

The HPLC purifications have been carried out at the HPLC-service of University Paul Sabatier (Toulouse). The columns employed are: Princeton SFC 2-Ethylpyridine 60Å, 5μ (4.6x250) mm (for supercritic carbon anhydride mobile phases) or C18 functionalized flash chromatographic columns of the brands Agela or Macherey Nagel.

Microwaves reactor

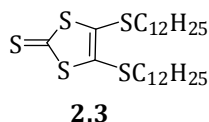
Microwave heating was carried out in closed vials with a CEM-Discover monomode microwave apparatus under the specified conditions (power, temperature, time).

Chapter 2: TTC₁₂ -TTF



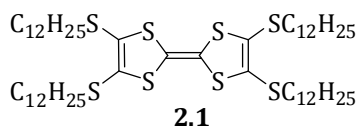
Synthesis of 2.2

In a 1L three necks oven dried round bottom flask (equipped with a mechanic stirrer) were introduced 160 ml of degassed DMF and 78.5 ml of dry and degassed carbon disulfide (99.0 gr, 1.3 mol) at 0°C and under argon, followed by 4.78 gr (0.208 mol) of sodium (cut in small pieces). The mixture was stirred until dissolution of sodium (19 hours) at 25°C. The undissolved residual of sodium was destroyed by adding to the mixture at 0-5°C, 20 ml of 2-propanol and 30 ml of methanol. To the obtained mixture, a solution of 7.09 gr (0.052 mol) of zinc dichloride in 170 ml of NH₃ (28%) was added drop by drop over 30 minutes. The product was precipitated from the heterogeneous mixture by adding a solution of tetraethylammonium bromide (21.86 gr, 0.104 mol) in 104 ml of water. After stirring for 18 hours at room temperature, the product (a red powder) was isolated by filtration and washed with 250 ml of water, 200 ml of isopropanol and 200 ml of diethyl ether. The yield was 27%. Melting point: 195-200°C.



Synthesis of 4,5-bis(dodecylthio)-1,3-dithiole-2-thione (2.3)

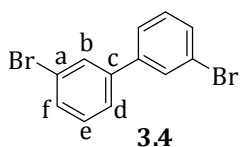
In a 250 ml three necks round bottom flask, an excess of 1-bromododecane (4.4 ml, 4.6 gr, 18.4 mmol) was added to 3 gr of compound 2.3 (4.2 mmol) in solution in 150 ml of acetone. The reaction mixture (dark pink suspension) was heated at reflux (T=560°C) for 18 hours. The following morning (the colour of the heterogeneous mixture was changed to orange) the solvent was evaporated under reduced pressure. 50 ml of cyclohexane were added to the residual and the suspension was filtered to remove the zinc and tetraethylammonium salts. The product 2 (a yellow solid, MP 56-58°C) was recovered pure by chromatographic purification on silica (eluent hexane, R_f on silica gel 0.22), with a quantitative yield. Melting Point: 56-58°. ¹H-NMR (500 MHz, CDCl₃): δ (ppm) 2.86 (t, J=7 Hz, 4H, -SCH₂), 1.66 (q, J=7 Hz, 4H, -SCH₂CH₂), 1.40 (q, J=7 Hz, 4H, -SCH₂CH₂CH₂), 1.2-1.4 (m, 32H, CH₂ (chain)), 0.88 (t, J=6.5 Hz, 6H, -CH₃). ¹³C-NMR (125 MHz, CDCl₃): δ (ppm) 136.7, 37.1, 32.3, 30.0, 29.9, 29.8, 29.7, 29.4, 28.8, 23.0, 14.5. MS (DCI/NH₃⁺): m/z = 535 [M+H]⁺. Elemental Analysis: %C 59.94 %H 10.62 %S 29.44 (found for C₂₇H₅₀S₅) vs %C 60.61 %H 9.42 %S 29.97 (calculated for C₂₇H₅₀S₅).



Synthesis of bis(dodecylthio)-1,3-dithiol-2-ylidene]-4,5-bis(dodecylthio)-tetrathiafulvalene (2.1)

A solution of the thione 2.2 (1 gr, 1.9 mmol) in 40 ml of dry triethylphosphite was warmed at 130°C for 6 hours (the colour of the solution was orange-red). After this time, the reaction mixture was cooled at room temperature, then 50 ml of methanol were added. It was observed the precipitation of an orange solid, that was collected by filtration and washed with methanol. The orange solid was further purified by silica gel column chromatography (R_f= 0.69) with a gradient petroleum ether, then petroleum ether 9: dichloromethane 1, then dichloromethane 10. 2.1 was obtained as an orange solid with a 32% yield. Melting Point: 70-72°C. ¹H-NMR (500 MHz, CDCl₃): δ (ppm) 2.7-2.9 (m, 8H, -SCH₂), 1.63 (q, J=7.5 Hz, 8H, -SCH₂CH₂), 1.3-1.4 (m, 8H, SCH₂CH₂CH₂), 1.2-1.3 (m, 64H, CH₂ (chain)), 0.88 (t, J=7 Hz, 12H, CH₃). MS (DCI/NH₃⁺): m/z = 1005.6 [M+H]⁺. Elemental Analysis: %C 63.95 %H 11.68 %S 24.27 (found for C₅₄H₁₀₀S₈) vs %C 64.48 %H 10.02 %S 25.50 (calculated for C₅₄H₁₀₀S₈).

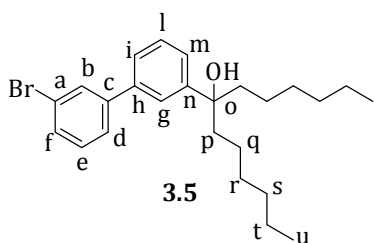
Chapter 3: Hexaphenanthrocoronene



Synthesis of 3,3'-Dibromobiphenyl (3.4)

Procedure a) (Miyake, Y., Wu, M., Rahman, M. J., Kuwatani, Y., Iyoda, M., *J. Org. Chem.*, **2006**, *71*, 16, 6110–6117): To a solution of 1,3-dibromobenzene (10.00 g, 42.4 mmol, 5.1 ml) in dry diethyl ether (500 ml) at -78°C was added drop by drop *tert*-butyllithium (27.4 ml of a solution 1.7 M in pentane, 46.6 mmol). The mixture was stirred at the same temperature for 1.5 hours, and CuCN (1.90 g, 21.2 mmol) was then added. The cooling bath was removed and the mixture was vigorously stirred ($T = -60^{\circ}\text{C}$) until CuCN dissolved. To the clear yellow solution (containing a Lipshutz cuprate) was added tetramethyl-*p*-benzoquinone (10.4 g, 63.5 mmol) to form a deep-blue-green solution of durosemiquinone. The mixture was stirred at room temperature ($T = 22^{\circ}\text{C}$) for 3 hours. After this time, 350 ml of water were added (the first additions were made drop by drop): the deep-blue-green colour disappeared quickly to give a yellow solution. The organic layer was separated and washed with two portions of 100 ml of distilled water, then dried over MgSO_4 and concentrated under reduced pressure. The product was obtained pure as a white solid ($49\text{--}51^{\circ}\text{C}$), by two silica gel column chromatographies, using 1) hexane : dichloromethane 8:2 ($R_f = 0.8$), 2) hexane as eluent, with a 89% yield.

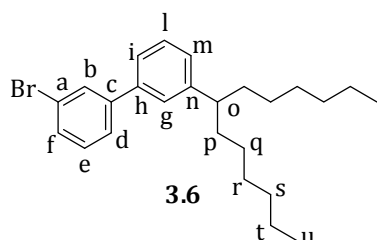
Procedure b) (Wagner, D., Hoffmann, S. T., Heinemeyer, U., Münster, I., Köhler, A., Strohrriegl, P., *Chem. Mater.*, **2013**, *25*, 3758–3765): To a solution of 3-bromophenylboronic acid (4.96 gr, 24.6 mmol) in 65 ml of methanol, copper(I)chloride (0.05 gr, 0.51 mmol) was added. The mixture was stirred for 19 hours at air, at room temperature (21°C). The solvent was evaporated under reduced pressure, the residue taken up in ethyl acetate and passed through a silica pad in order to remove the inorganic salts. The product was obtained pure as a white solid by silica gel column chromatography in hexane ($R_f = 0.6$) with a 63% yield. $^1\text{H-NMR}$ (300 MHz, CD_2Cl_2): δ (ppm) = 7.74 (t, $J = 1.8\text{ Hz}$, 2H, Ar- H_b), 7.53 (dd, $J_1 = 7.8\text{ Hz}$, $J_2 = 1.8\text{ Hz}$, 4H, Ar- H_f and Ar- H_d), 7.35 (t, $J = 7.8\text{ Hz}$, 2H, Ar- H_e). $^{13}\text{C-NMR}$ (75 MHz, CD_2Cl_2): δ (ppm) = 142.1, 131.2, 131.3, 130.9, 130.5, 126.2, 123.3. MS (DCI/ NH_3^+): m/z 311.8 [M^+]. Melting point: $49\text{--}51^{\circ}\text{C}$ (white solid), literature 52°C .



Synthesis of 7-(3'-bromophenyl-3-yl)tridecan-7-ol (3.5)

To a solution of **3.4** (2.37 gr, 7.6 mmol) in 30 ml of dry diethyl ether at -78°C , were added drop by drop under an argon atmosphere 5.5 ml (7.6 mmol) of a solution 1.4 M in hexane of *n*-butyllithium. The mixture was let to react at -78°C until -45°C for 40 minutes, then a solution of dihexylketone (1.61 gr, 8.1 mmol) in 10 ml of dry diethyl ether was added by cannula. The temperature was let to raise at 21°C and the mixture was let to stir for 17 hours. The reaction was quenched by adding 75 ml of a saturated solution of ammonium chloride. The organic phase was extracted and washed with two portions of 50 ml of distilled water, dried on MgSO_4 , then concentrated under reduced pressure ($R_f = 0.5$ in hexane : dichloromethane 8:2, on SiO_2). The product was recovered by silica gel column chromatography, using 1) hexane, then 2) hexane : dichloromethane 8:2 as eluent. The product was recovered as a yellow oil (2.3 gr, 69% wt/wt, 5.4% impurity) and was enough pure to be employed in the following step without further purification. $^1\text{H-NMR}$ (300 MHz, CD_2Cl_2): δ (ppm) = 7.80 (t, $J = 1.8\text{ Hz}$, 1H, Ar- H_b), 7.6–7.7 (m, 1H, Ar- H_g), 7.58 (dq, $J_1 = 7.8\text{ Hz}$, $J_2 = 0.9\text{ Hz}$, 1H, Ar- H_f), 7.50 (dq, $J_1 = 7.8\text{ Hz}$, $J_2 = 0.9\text{ Hz}$, 1H, Ar- H_d), 7.3–7.4 (m, 3H, Ar- $\text{H}_{i,l,m}$), 7.34 (t, $J_1 = 7.8\text{ Hz}$, 1H, Ar- H_e), 1.7–1.9 (m, 4H, CH_{2p} + impurity), 1.2–1.5 (m, 8H, $\text{CH}_{2q,r,st}$ + impurity), 0.8–1 (m, 6H, CH_{3u} + impurity). $^{13}\text{C-NMR}$ (75 MHz, CD_2Cl_2): δ (ppm) = 148.2, 144.3, 139.7, 130.8, 130.6, 130.5, 126.4, 125.6, 125.3, 124.7, 123.3, 77.4, 43.7, 39.8, 32.5, 30.6, 23.9, 23.2, 14.4. HR-MS (DCI/ CH_4^+ /TOF): m/z 431.1934 for $\text{C}_{25}\text{H}_{36}\text{OBr}$ (calculated 431.1950) (50%); some peaks

deriving from the fragmentation of the title compound were also observed: m/z 345.0885 for $C_{19}H_{22}BrO$ (calculated 345.0854) (100%), m/z 413.1818 for $C_{25}H_{34}Br$ (calculated 413.1844) (41%); additional signals were deriving from the unreacted ketone reagent: m/z 199.2066 for $C_{13}H_{27}O$ (calculated 199.2062).



Synthesis of 3-bromo-3'-(tridecan-7-yl)biphenyl (3.6)

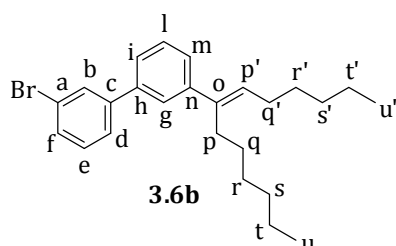
Procedure a): A solution of **3.5** (2.80 g) and triethylsilane (2.26 g, 3.1 ml, 19.5 mmol) in 35 ml of dichloromethane dry was cooled to $-15^{\circ}C$, under an atmosphere of argon. Trifluoroacetic acid was added dropwise (2.22 g, 1.5 ml, 19.5 mmol) and the mixture was let to react at $-15^{\circ}C$ - $0^{\circ}C$ for 5 hours. The reaction was quenched by adding a saturated

solution of $NaHCO_3$, until the formation of gas stopped (pH 6-7). The organic phase was extracted and washed with water (2x50 ml). The combined organic phases were dried on $MgSO_4$ and evaporated under reduced pressure. The product was purified by 1) column chromatography on silica, hexane 100%, $R_f=0.7$; 2) preparative HPLC (column C18, water/acetonitrile 8:2- \rightarrow 0:10) and obtained as an colourless oil (1.89 gr, 67% wt/wt).

NB: the yield was expressed in weight percentage since the starting material was not clean.

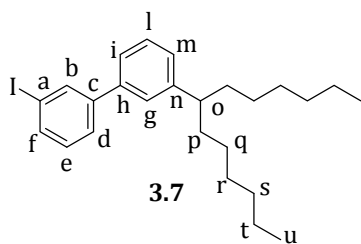
Procedure b): A solution of **3.5** (2.19 g, impure at xxx) and triethylsilane (1.78 g, 2.5 ml, 15.3 mmol) in 27 ml of dichloromethane dry was cooled to $-35^{\circ}C$, under an atmosphere of argon. Trifluoroacetic acid was added dropwise (1.74 g, 1.17 ml, 15.3 mmol) and the mixture was let to react at $-35^{\circ}C$ - $0^{\circ}C$ for 3 hours. The reaction was quenched by adding a saturated solution of $NaHCO_3$, until the formation of gas stopped (pH 6-7). The organic phase was extracted and washed with water (2x50 ml). The combined organic phases were dried on $MgSO_4$ and evaporated under reduced pressure. The product was purified by filtration on a short silica pad (eluent: hexane). The yield was 78%.

Characterization of 3.6: 1H -NMR (500 MHz, CD_2Cl_2): δ (ppm) = 7.6-7.7 (m, 1H, Ar- H_b), 7.56 (d, $J_1 = 8$ Hz, 1H, Ar- H_f), 7.49 (d, $J = 8$ Hz, 1H, Ar- H_d), 7.3-7.4 (m, 4H, Ar- $H_{g,l,i,e}$), 7.18 (d, $J=7$ Hz, 1H, Ar- H_m), 2.5-2.6 (m, 1H, Ar-CHO), 1.5-1.7 (m, 4H, CH_2 p,q), 1.2-1.3 (m, 12H, CH_2 r,s,t), 0.86 (t, 6H, $J=6.5$ Hz, CH_3 u). ^{13}C -NMR (125 MHz, CD_2Cl_2): δ (ppm) = 147.7, 144.0, 139.7, 130.6, 130.4, 130.3, 129.0, 127.7, 126.9, 126.2, 124.8, 123.0, 46.5, 37.3, 32.2, 29.8, 28.0, 23.0, 14.3. HR-MS (DCI/ CH_4^+ /TOF): m/z 443.2303 found for $C_{27}H_{40}Br$ [$M+C_2H_5$] $^+$, calculated 443.2313; 417.1975 found for $C_{25}H_{36}Br$ [$M+H$] $^+$, calculated 417.1980.



Characterization of 3.6b: 1H -NMR (500 MHz, CD_2Cl_2): δ (ppm) = 7.7-7.8 (m, 1H, Ar- H_b), 7.5-7.6 (m, 2H, Ar-H), 7.4-7.5 (m, 1H, Ar-H), 7.3-7.5 (m, 4H, Ar-H), 5.74 (t, 1H, $J=7$ Hz, $CH_{p'}$), 2.55 (t, 2H, $J=7$ Hz, CH_p), 2.24 (q, 2H, $J=7$ Hz, $CH_{2q'}$), 1.9-2.0 (m, 2H, CH_q), 1.4-1.5 (m, 2H, $CH_{2r'}$), 1.2-1.4 (m, 14H, $CH_{2r,s,t,s'}$), 0.8-0.9 (m, 6H, CH_3 u). ^{13}C -NMR (125 MHz, CD_2Cl_2): δ (ppm) = 144.7, 144.0, 140.2, 139.8, 130.7, 130.5, 130.4, 130.2, 129.0, 126.4, 126.3, 125.5, 125.54, 123.1, 32.1, 30.0, 29.9,

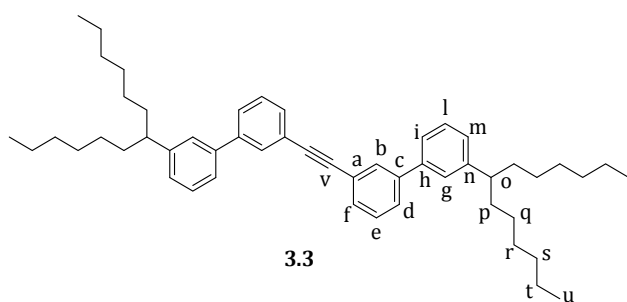
29.6, 29.1, 28.9, 23.0, 14.3, 14.2. HR-MS (DCI/ CH_4^+ /TOF): m/z 412.1773 for $C_{25}H_{33}Br$.



Synthesis of 3-iodo-3'-(tridecan-7-yl)biphenyl (3.7)

Procedure a): **3.6** (0.80 gr, 1.93 mmol) was dissolved in 70 ml of distilled tetrahydrofuran and the temperature cooled at -78°C by means of an acetone/liquid nitrogen bath, under an atmosphere of argon. Once this temperature was reached a solution of *n*-butyllithium (1.6 M in hexane) (2.14 mmol) was added drop by drop and it was let to react at -78°C for 1.5 hours. Iodine (0.98 gr, 3.86 mmol) was added, in solution of 7 ml of distilled tetrahydrofuran. The acetone/liquid nitrogen bath was removed and the mixture was let to react at 22°C for 1 hour. The reaction was quenched by adding 70 ml of a saturated solution of sodium sulphite and the organic phase was extracted with ethyl acetate (3x50 ml), then dried on sodium sulphate and evaporated under reduced pressure. The obtained oil was dissolved in hexane, filtered on silica (eluent hexane) then purified by HPLC (column SFC 2-Ethylpyridine, with 5% methanol). Yield 11%. $^1\text{H-NMR}$ (300 MHz, CD_2Cl_2): δ (ppm) = 7.95 (t, $J = 1.8$ Hz, 1H, Ar- H_b), 7.68 (d, $J_0 = 7.8$ Hz, 1H, Ar- H_f), 7.56 (d, $J_0 = 7.8$ Hz, 1H, Ar- H_d), 7.1-7.4 (m, 5H, Ar- $\text{H}_{e,g,i,l,m}$), 2.5-2.6 (m, 1H, Ar- CH_o), 1.5-1.7 (m, 4H, CH_p), 1.1-1.4 (m, 16H, CH_2), 0.8-0.9 (m, 6H, CH_{3p}). $^{13}\text{C-NMR}$ (75 MHz, CD_2Cl_2): δ (ppm) = 147.3, 144.0, 139.6, 136.3, 130.4, 128.8, 127.3, 126.6, 124.7, 94.9, 46.3, 37.1, 31.9, 29.6, 27.8, 22.8, 14.3. HR-MS (DCI/ CH_4^+ /TOF): m/z 462.1793 for $\text{C}_{25}\text{H}_{36}\text{I}^+$ (calculated 462.1784) (90%) (tolerance 5 ppm); other signals deriving from fragmentations: m/z 336.2841 for $\text{C}_{25}\text{H}_{36}^+$ (100%), m/z 377.0860 for $\text{C}_{19}\text{H}_{22}\text{I}^+$ (35%), m/z 251.1855 for $\text{C}_{19}\text{H}_{23}^+$ (10%), m/z 292.9892 (40%), m/z 183.2149 (25%), not attributed.

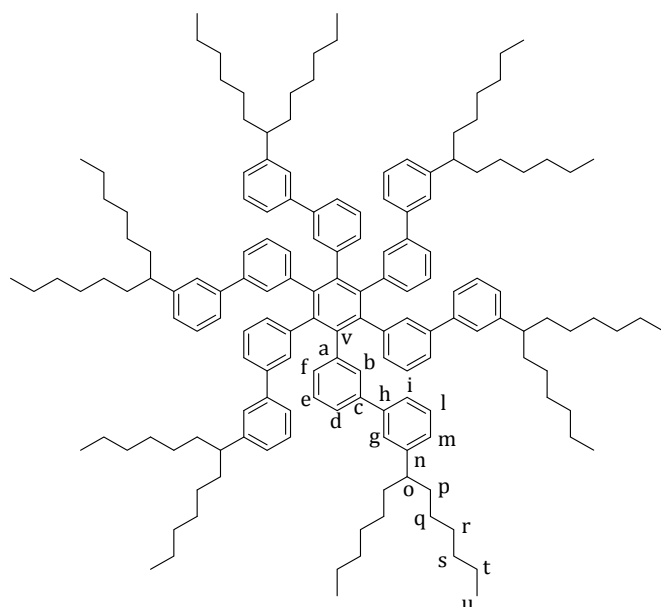
Procedure b): A dry Schlenk tube was charged with **3.6** (0.18 gr, 0.4 mmol) and dry dioxane (1 ml). The solvent was degassed by argon bubbling for 10 minutes then, copper iodide (0.007 gr, 0.04 mmol), sodium iodide (0.13 gr, 0.9 mmol) and (+/-)-trans-1,2-diaminocyclohexane (0.01 gr, 0.011 ml, 0.09 mmol) were added, the tube was sealed with a Teflon valve and the reaction mixture stirred at reflux (110°C) for 70 hours. The resulting suspension was allowed to reach room temperature, diluted with 10 ml of a 28% solution of ammonia, poured into water (20 ml) and extracted with dichloromethane (3x25ml). 0.16 g of mixture of products (colourless oil) was recovered: from NMR analysis it could be estimated a 90% conversion into the iodinated product (recovered 10% of reagent **3.6**). $^1\text{H-NMR}$ (300 MHz, CD_2Cl_2): δ (ppm) = 7.98 (t, $J = 1.8$ Hz, 1H, Ar- H_b), 7.69 (d, $J_0 = 7.8$ Hz, 1H, Ar- H_f), 7.59 (d, $J_0 = 7.5$ Hz, 1H, Ar- H_d), 7.1-7.4 (m, 5H, Ar- $\text{H}_{g,l,i,m}$), 2.5-2.6 (m, 1H, Ar- CH_o), 1.5-1.8 (m, 4H, CH_{2p}), 1.1-1.4 (m, 16H, CH_{2q-t}), 0.8-0.9 (m, 6H, CH_{3u}).



Synthesis of 1,2-bis(3'-(tridecan-7-yl)biphenyl-3-yl)ethyne (3.3)

Reagent **3.6** was charged (1.51 gr, 3.6 mmol) in a flame dried Schlenk tube and dissolved in 18 ml of dry toluene and 1,8-diazabicycloundec-7-ene (3.29 gr, 3.23 ml, 21.6 mmol). The solvent was degassed by argon bubbling for 20 minutes. Copper iodide (0.07 gr, 0.36 mmol), trimethylsilylacetylene (0.18 gr, 0.26 ml, 1.8 mmol) and water (0.026 gr, $26\ \mu\text{l}$, 1.44 mmol) were added and argon bubbled for 5 minutes more. Bis(triphenylphosphine)palladium(II) dichloride (0.14 gr, 0.2 mmol) was then added. The reaction was runned warming at 80°C for 72 hours then quenched by adding 40 ml of distilled water. The solution was acidified by adding HCl 37% down to pH 6-7. The organic phase was separated then washed with 3 x 50 ml of distilled water, dried on anhydrous magnesium sulphate and evaporated under reduced pressure. The product was recovered by column chromatography purification on silica gel (eluent hexane, $R_f = 0.35$) with a 78% yield as an colourless oil. $^1\text{H-NMR}$ (500 MHz, CD_2Cl_2): δ (ppm) = 7.8-7.9 (m, 2H, Ar-

H_b), 7.65 (d, J₀ = 8 Hz, 2H, Ar-H_f), 7.59 (d, J₀ = 8 Hz, 2H, Ar-H_d), 7.4-7.6 (m, 6H, Ar-H_{g,i,e}), 7.41 (t, J₀ = 7.3 Hz, 2H, Ar-H_l), 7.21 (d, J₀ = 7.3 Hz, Ar-H_m), 2.5-2.6 (m, 2H, Ar-CH_o), 1.6-1.8 (m, 8H, CH_{2p}), 1.1-1.4 (m, 32H, CH_{2q,r,s,t}), 0.8-1.0 (m, 12H, CH_{3u}). ¹³C-NMR (500 MHz, CD₂Cl₂): 147.7, 142.2, 140.4, 130.6, 129.3, 129.1, 127.7, 127.6, 126.9, 124.9, 123.9, 89.8, 46.6, 37.4, 32.3, 29.9, 28.09, 23.1, 14.3. HR-MS (DCI/CH₄⁺/TOF): m/z 694.5494 for C₅₂H₇₀⁺ (calculated 694.5478) (100%).



3.2

Synthesis of HBB (3.2)

In a flame dried Schlenk flask, **3.3** (0.38 gr, 0.55 mmol) was dissolved in 1.7 ml of dry dioxane and 0.009 gr (0.028 mmol) of cobalt octacarbonyl were added. The mixture was then let to react at 111°C for 46 hours, then for 1 hour at 22°C. The obtained brown solution was filtered on a silica pad and recovered by eluting with hexane:dichloromethane 9:1. The obtained dark oil was stirred for 26 hours in 3 ml of diethylamine and 0.3 ml of petroleum ether at 30°C and filtered on a short silica column, eluting with hexane. The title product **3.2** was obtained after chromatographic purification: silica gel, with 1) petroleum ether, 2) petroleum ether : dichloromethane 94:6 as eluent (R_f =

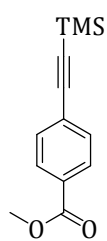
0.3). The yield was 72%. ¹H-NMR (500 MHz, CD₂Cl₂): δ (ppm) 6.8-7.4 (m, 48H, Ar-H_{f,e,d,b,i,l,m,g}), 2.3-2.5 (m, 6H, Ar-CH_o), 1.5-1.7 (m, 24H, CH_{2p}), 1.1-1.3 (CH_{2q,r,s,t}), 0.8-0.9 (m, 36H, CH_{3u}). ¹³C-NMR (500 MHz, CD₂Cl₂): δ (ppm) 147.1-147.3, 141.5-141.6, 141.1-141.2, 140.9-141.0, 140.5-140.7, 130.7-131.8, 128.6-128.8, 127.6, 126.9, 126.7, 126.6, 126.5, 125.1, 124.9, 124.6-124.7, 46.4-46.5, 37.2-37.3, 32.1-32.3, 29.8-29.9, 27.8-28.0, 23.0-23.1, 14.2-14.3. HR-MS (MALDI DCTB/TOF⁺): m/z 2083.6382 for C₁₅₆H₂₁₀⁺ (calculated 2083.6433) (100%), C₁₅₆H₂₁₀Na⁺ at m/z 2106.7.

Oxidative cyclodehydrogenation:

In a three necks flame-dried round bottom flask, reagent **3.2** (0.034 gr, 0.016 mmol) was dissolved in 1.4 ml of dry dichloromethane. The solvent was quickly degased by argon bubbling then the temperature cooled to 0-5°C by means of an ice bath. 2,3-Dichloro-5,6-Dicyanobenzoquinone (DDQ, 0.044 gr, 0.196 mmol) was added in one portion and the yellow heterogeneous mixture was stirred at 0-5°C for 5 minutes. Trifluoromethanesulfonic acid (0.16 ml) was added drop by drop and the obtained dark mixture was stirred at 0-5°C for 30 minutes. The reaction was quenched with 50 ml of a saturated solution of NaHCO₃ and 25 ml of dichloromethane were added. The organic phase was extracted and washed with three portions of 40 ml of a saturated solution of NaHCO₃ (until the aqueous phase was not turning yellow). The organic phase was then dried on MgSO₄ anhydrous and the product purified by a filtration on silica gel, with toluene as eluent (R_f=1, the product shows an orange fluorescence at 365 nm). The product was obtained as a red laque with a 93% yield. HR-MS (MALDI DCTB/TOF⁺): m/z 2061.4734 for C₁₅₆H₁₈₈⁺ (calculated 2061.4711).

Chapter 4: Radicalar precursors

Precursor Br1:

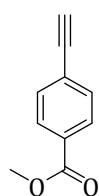


5.14

Synthesis of methyl 4-((trimethylsilyl)ethynyl)benzoate (5.14)

An oven dried 100 ml schlenk flask was charged with 2 gr (7.63 mmol) of methyl-4-iodobenzoate. 30 ml of dry triethylamine were added and argon was bubbled for 20 minutes. After this time copper iodide (0.07 gr, 0.38 mmol) and bis(triphenylphosphine)palladium(II) dichloride (0.16 gr, 0.23 mmol) were added in one portion as solids, followed by 1.2 ml (8.4 mmol) of trimethylsilylacetylene drop by drop. The mixture was stirred at room temperature for 2 hours then the solvent was removed under reduced pressure. The resulting solid was taken up in dichloromethane and filtered on a silica pad. A TLC control (Silica-C₁₈, hexane : ethyl acetate 9:1, R_f reag. = 0.9; R_f prod.= 0.8) revealed the presence of only one spot and the complete disappearance of the starting material. ¹H-NMR (300 MHz, CDCl₃): δ (ppm) 7.97 (d, 2H, J=8.7 Hz, Ar-H), 7.51 (d, 2H, J=8.7 Hz, Ar-H), 3.91 (s, 3H, -COOCH₃), 0.26 (s, 9H, -Si(CH₃)₃). ¹³C-NMR (300 MHz, CDCl₃): δ (ppm) 166.9, 132.2, 129.7, 128.1, 104.4, 98.0, 52.6, 0.2. DCI/NH₃⁺ : m/z 233.1 [M+H]⁺, 250.1 [M+NH₄]⁺.

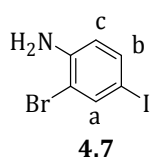
Rif. Bibl. Feng, Y. S., Xie, C. Q., Qiao, W. L., Xu, H. J., *Org. Lett.*, **2013**, 15, 4, 936-939.



4.5 or 5.15

Synthesis of methyl 4-ethynylbenzoate (4.5 or 5.15)

4-((trimethylsilyl)ethynyl)benzoate (5.14) (0.85 gr, 3.5 mmol) was dissolved in 25 ml of dichloromethane and 25 ml of methanol and the argon was bubbled in the solution for 10 minutes. Potassium carbonate (2.49 gr, 18 mmol) was added as a solid in one portion and it was let to stir for two hours. The solvents were evaporated under reduced pressure and the solid taken up in 50 ml of dichloromethane. The organic phase was washed with a saturated solution of ammonium chloride down to pH 7 (3 portions of 30 ml), dried on anhydrous magnesium sulphate and evaporated. The solid was then run through a short silica pad, with dichloromethane as eluent. The product was obtained as a yellow solid with a 97% yield. R_f on silica-C₁₈ = 0.63 (hexane : ethyl acetate 9:1). ¹H-NMR (MHz, CDCl₃): δ (ppm)= 7.99 (d, 2H, J=8.7Hz, Ar-H), 7.55 (d, 2H, J= 8.7 Hz, Ar-H), 3.92 (s, 3H, -COOCH₃), 3.23 (s, 1H, -CCH). ¹³C-NMR (MHz, CDCl₃): δ (ppm)= 166.8, 132.4, 130.5, 129.8, 127.1, 81.1, 80.4, 52.6. DCI/NH₃⁺ : m/z [M]⁺. Rif. Bibl. Zhao, Y.-L., Liu, L., Zhang, W., Sue, C.-H., Li, Q., Miljanić, O. Š., Yaghi, O. M., Stoddart, J. F., *Chem. Eur. J.*, **2009**, 15, 13356-13380.

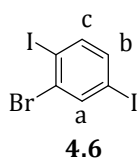


4.7

Synthesis of 2-bromo-4-iodoaniline (4.7)

2-bromoaniline (1 gr, 0.66 ml, 5.8 mmol) and sodium hydrogen carbonate (0.97 gr, 11.6 mmol) were dissolved in 6 ml of a 50% solution of dry dichloromethane in dry methanol. The solvent was degased for 5 minutes and the temperature was cooled at 0-5°C by means of an ice-bath. Benzyltriethylammonium dichloroiodate (2.26 gr, 5.8 mmol) was dissolved in 5 ml of dry and degased dichloromethane and was added drop by drop to the aniline solution at 0-5°C. The ice bath was removed and the temperature was let to raise up to 18°C and it was let to react for one hour. The reaction was quenched by adding 50 ml of water. The organic phase was recovered and washed with 2x50 ml of a saturated solution of sodium thiosulphate, then dried and evaporated under reduced pressure. The product was purified by column chromatography on silica gel (eluent: 40% dichloromethane in hexane) and obtained as a brown solid (0.64 g, 37% wt/wt, impure at 10% of 2-bromoaniline). The molar yield of the product is 34%. Melting point 70-73°C. ¹H-NMR (300 MHz, CD₂Cl₂): δ= 5.75 (d, 1H, J=1.8 Hz, ArH_a), 5.4 (dd, 1H, J₁= 8.4 Hz, J₂= 1.8 Hz, ArH_c), 4.6 (d, 1H, J= 6 Hz, ArH_b, J= 8.4 Hz), 2.2 (bs, 2H, -NH₂). ¹³C-NMR (75 MHz, CD₂Cl₂): δ= 120.7, 116.8, 113.8, 94.1, 86.8, 55.1. HR-MS DCI-CH₄⁺/TOF on [M][•] m/z 296.8654 for C₆H₅BrIN[•] (calculated 296.8650).

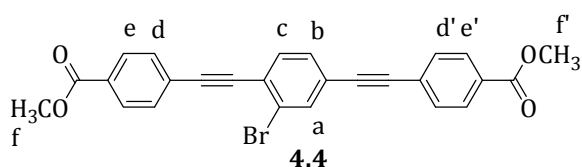
Rif. Bibl. : Shirai, Y., Osgood, A. J., Zhao, Y., Yao, Y., Saudan, L., Yang, H., Yu-Hung, C., Alemany, L. B., Sasaki, T., Morin, J.-F., Guerrero, J. M., Kelly, K. F., Tour, J. M., *J. Am. Chem. Soc.*, **2006**, *128*, 14, 4854-4864.



Synthesis of 2-bromo-1,4-diiodobenzene (4.6)

4.7 (0.60 gr, 2 mmol) was dissolved in 8.5 ml of dry diethyl ether. The solvent was degassed for 10 minutes and the temperature was cooled at -30°C by means of an acetone/liquid nitrogen bath. Boron trifluoride diethyletherate (1.2 gr, 0.9 ml, 8 mmol) was added and the solution was stirred at -30°C for 30 minutes. Tert-butyl nitrite (0.79 gr, 0.9 ml, 7 mmol) was added drop by drop and it was let to react at -30°C - -10°C for 1.5 hours. The white precipitate that was formed was filtered under argon and washed with dry diethyl ether. The solid was then dissolved in 20 ml of dry acetonitrile and the solution was added to a solution of sodium iodide in 16.5 ml of dry acetonitrile (upon the addition, the formation of bubbles was observed). It was let to react at 22° for 4 hours. The reaction was quenched by pouring it into 70 ml of a saturated solution of sodium thiosulphate. The organic phase was extracted with ethyl acetate (50 ml, then 25 ml), then dried on anhydrous magnesium sulphate and evaporated under reduced pressure. The product, a white solid was obtained pure after filtration on a silica pad, washing with ethyl acetate. Yield: 0.5 gr (63%). Rf on silica TLC in hexane is 0.9. $^1\text{H-NMR}$ (300 MHz, CDCl_3): δ = 7.94 (d, 1H, $J=2.1$ Hz, ArH_a), 7.54 (d, 1H, $J=8.3$ Hz, ArH_c), 7.29 (dd, 1H, $J=8.3$ Hz, ArH_b). $^{13}\text{C-NMR}$ (75 MHz, CDCl_3): δ = 144.8, 141.0, 137.8, 131.2, 100.9, 93.9. HR-MS DCI- CH_4^+ /TOF on $[\text{M}]^{+\bullet}$ m/z 407.7524 for $\text{C}_6\text{H}_3\text{BrI}_2$ (calculated 407.7508) (100%), 283.8538 $[\text{M-I}]^{+\bullet}$ (97%),

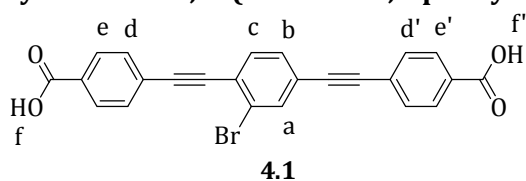
Rif. Bibl.: Morin, J.-F., Shirai, Y., Tour, J. M., *Org. Lett.*, **2006**, *8*, 8, 1713-1716.



Synthesis of dimethyl 4,4'-(2-bromo-1,4-phenylene)bis(ethyne-2,1-diyl)dibenzoate (4.4)

4.6 (0.25 gr, 0.6 mmol) and **4.5** or **5.15** (4-alkyne-methylbenzoic acid) were dissolved in 7 ml of dry dichloromethane and 7 ml of dry diethylamine. The solvent mixture was degassed by argon bubbling for 15 minutes then copper iodide (0.01 gr, 0.06 mmol) and bis(triphenylphosphine)palladium(II) dichloride (0.03 gr, 0.04 mmol) were added and it was let to react at room temperature (18°C) for 16 hours (already after some minutes of reaction, it was observed the precipitation of a solid). The solvent was evaporated under reduced pressure, the obtained solid dissolved in tetrahydrofuran and the mixture filtered on a silica pad, washing with tetrahydrofuran. The product was obtained by precipitation from dichloromethane as a white solid. Yield= 53%. Melting Point: at $209-211^{\circ}\text{C}$ it changes colour without melting. $^1\text{H-NMR}$ (500 MHz, $(\text{CD}_3)_2\text{SO}/\text{THF-}d_8$ 1:99): δ = 8.0-8.1 (m, 4H, $\text{Ar-H}_{e,e'}$), 7.92 (d, 1H, $J=1.7$ Hz, Ar-H_a), 7.6-7.7 (m, 5H, $\text{Ar-H}_{d,d',c}$), 7.60 (dd, 1H, $J_1=7.5$ Hz, $J_2=1.7$ Hz, Ar-H_b), 3.7-3.9 (m, 2H, $\text{OCH}_{3f,f'}$). $^{13}\text{C-NMR}$ (125 MHz, $(\text{CD}_3)_2\text{SO}/\text{THF-}d_8$ 1:99): δ = 166.4, 136.1, 134.4, 132.6, 132.5, 131.6, 131.3, 131.2, 131.5, 131.3, 131.2, 130.4, 127.9, 127.8, 126.0, 125.9, 125.4, 95.7, 92.5, 91.1, 90.9, 52.6. HR-MS DCI- CH_4^+ /TOF on $[\text{M}+\text{H}]^+$ m/z 473.0389 for $\text{C}_{26}\text{H}_{18}\text{O}_4\text{Br}$ (calculated 473.0402).

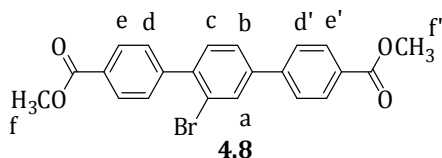
Synthesis of 4,4'-(2-bromo-1,4-phenylene) bis(ethyne-2,1-diyl)dibenzoic acid (4.1)



In a Schlenk flask, **4.4** (0.03 gr, 0.06 mmol) was dissolved in 7.5 ml of tetrahydrofuran. A solution of lithium hydroxide (0.014 gr, 0.6 mmol) in 1.9 ml of water was added and the obtained mixture was warmed at 50°C for 22 hours. The temperature was let to cool at R. T., then tetrahydrofuran was

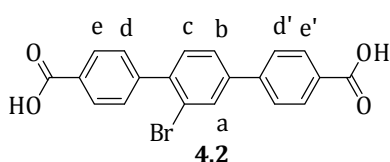
evaporated under reduced pressure, leaving only the water phase. The pH was acidified at 2-3 by adding a 3.7% solution of hydrochloric acid. The precipitated white solid was filtered and washed with 10 ml of distilled water and 4 ml of diethyl ether. The product was obtained pure as yellow solid by trituration from a mixture of acetone : ethanol : tetrahydrofuran 0.5:0.5:9 at 50°C. The yield was 0.009 g (33%). Melting point: decomposes for temperatures higher than 270°C (in air). ¹H-NMR (500 MHz, (CD₃)₂SO): δ (ppm) = 7.94 (bs, 1H, Ar-H_a), 7.87 (m, 4H, Ar-H_{e,e'}), 7.68 (d, 1H, J=8Hz, Ar-H_b), 7.59 (d, 1H, J= 8 Hz, Ar-H_c), 7.4-7.5 (m, 4H, Ar-H_{d,d'}). ¹³C-NMR (125 MHz, (CD₃)₂SO): δ (ppm)= 167.1, 134.6, 133.2, 130.5, 130.4, 130.3, 129.2, 129.1, 124.7, 124.4, 124.1, 96.2, 93.2, 87.9, 87.7. HR-MS ESI/TOF⁻ on [M-H]⁻ m/z 442.9915 for C₂₄H₁₂O₄Br (calculated 442.9919).

Precursor Br2:



Synthesis of 4.8

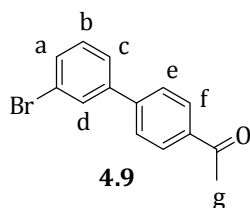
In a dry Schlenk flask, in an atmosphere of argon, **4.6** (0.18 gr, 0.44 mmol) and 4-methoxycarbonylphenylboronic acid pinacol ester (0.24 gr, 0.9 mmol) were dissolved in 2 ml of dry dioxane. 0.22 ml of water were added, followed by potassium carbonate (0.36 gr, 2.64 mmol). The solvent was degassed for 5 minutes by argon bubbling, then tetrakis(triphenylphosphine)palladium(0) (0.03 gr, 0.03 mmol) was added and the mixture was stirred under argon atmosphere at 90°C for 18 hours. Then, the mixture was let to cool at room temperature, then filtered on a silica pad, washing with ethyl acetate. The product was obtained pure by silica gel column chromatography with hexane:ethyl acetate 9:1 as eluent (R_f= 0.37) and recrystallization from cold ethanol (2-4°C). **5**, a yellow solid, was obtained with a 55% yield. ¹H-NMR (500 MHz, CDCl₃): δ= 8.13(m, 4H, Ar-H_{e,e'}), 7.95 (d, 1H, J=2 Hz, Ar-H_a), 7.68 (d, 2H, Ar-H_d), 7.63 (dd, 1H, J₁= 5.5 Hz, J₂= 1.5 Hz, Ar-H_c), 7.53 (d, 2H, J=8 Hz, Ar-H_{d'}), 7.42 (d, 1H, J₁= 8 Hz, Ar-H_b). ¹³C-NMR (500 MHz, CDCl₃): δ= 167.0, 166.9, 145.1, 143.5, 141.4, 141.2, 132.1, 131.6, 130.4, 129.8, 129.6, 129.5, 127.2, 126.4, 122.9, 52.4, 52.3. HR-MS DCI-CH₄⁺/TOF on [M+H]⁺ m/z for C₂₂H₁₈BrO₄ 425.0380 (calculated 425.0388).



Synthesis of Br2 (4.2)

4.8 (22 mg, 0.05 mmol) was dissolved in 2 ml of tetrahydrofuran. Lithium hydroxide (0.01 gr, 0.5 mmol) was added, dissolved in 0.5 ml of water. The mixture was stirred at 50°C for 19 hours. Tetrahydrofuran was evaporated and the pH of the water phase was brought to 2-3 by adding a 3.7% solution of hydrochloric acid. The product precipitated as a pink/brown solid and it was filtered. The yield was 57%. ¹H-NMR (500 MHz, DMSO): δ (ppm) = 8.13 (d, 1H, J=2 Hz, Ar-H_a), 8.04 (dd, 4H, J₁= 8.7 Hz, J₂= 2 Hz, Ar-H_e and Ar-H_{e'}), 7.90 (d, 2H, Ar-H_d), 7.87 (dd, 2H, J₁= 8.7 Hz, J₂= 2 Hz, Ar-H_b), 7.59 (d, 2H, J=8.7 Hz, Ar-H_{d'}), 7.55 (d, 1H, J= 8.7 Hz, Ar-H_c). ¹³C-NMR (125 MHz, DMSO): δ (ppm)= 144.2, 142.0, 140.6, 140.5, 131.8, 131.2, 130.0, 129.5, 129.2, 127.1, 126.6, 122.2. HR-MS ESI(-)/TOF on [M-H]⁻ m/z 394.9914 found for C₂₀H₁₂BrO₄ (calculated 394.9919).

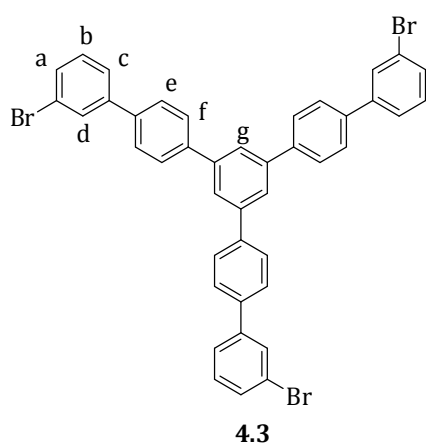
Precursor TBr:



Synthesis of 1-(3'-bromobiphenyl-4-yl)ethanone (4.9)

4-acetylphenylboronic acid (0.31 gr, 1.9 mmol), 1-bromo-3-iodobenzene (0.5 gr, 1.8 mmol, 0.22 ml) and potassium carbonate (0.75 gr, 5.4 mmol) were suspended in 4.5 ml of a mixture of dioxane and water (9:1). The solvent was degassed for 10 minutes by bubbling argon, then tetrakis(triphenylphosphine)palladium(0) (0.023 gr, 0.02 mmol) was added. It was let to stir at 90°C for 19 hours then the reaction mixture was filtered on a silica pad, washing with ethyl acetate. The solvent was evaporated under

reduced pressure. The product, a yellow oil, was obtained pure after silica gel column chromatography, with 1) hexane, 2) hexane : dichloromethane 5:5, with a 72% yield. $^1\text{H-NMR}$ (300 MHz, CDCl_3): δ = 8.04 (d, 2H, J = 8.4 Hz, Ar-H_f), 7.76 (t, 1H, J = 2.1 Hz, Ar-H_d), 7.65 (d, 2H, J = 8.4 Hz, He), 7.5-7.6 (m, 2H, Ha,c), 7.34 (t, 1H, J = 7.8 Hz, H_b), 2.64 (s, 3H, CH₃g). $^{13}\text{C-NMR}$ (75 MHz, CDCl_3): δ = 197.8, 144.4, 142.2, 136.6, 131.4, 130.7, 130.5, 129.3, 127.5, 126.2, 123.3, 27.2. HR-MS DCI- CH_4^+ /TOF on $[\text{M}]^+$ m/z 273.9994 found for $\text{C}_{14}\text{H}_{11}\text{BrO}^+$ (calculated 273.9993) (100%), m/z 258.9769 $[\text{M-CH}_3]^+$.



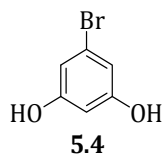
Synthesis of TBr (4.3)

In an oven dried Schlenk flask, **4.9** (0.22 gr, 0.8 mmol) was dissolved in 4 ml of a 3 : 1 mixture of dry ethanol and dry toluene. The solvent was degassed for 5 minutes by argon bubbling, then silicon tetrachloride (1.36 gr, 0.9 ml, 8 mmol) was added slowly drop by drop: upon addition it was noticed a change in the colour of the mixture from yellow to red. The mixture was let to stir for 48 hours at room temperature (18°C), under an atmosphere of argon. The reaction was quenched by adding 50 ml of distilled water. The organic phase was extracted with 25 ml of dichloromethane and successively washed with two portions of 50 ml of water, then dried on anhydrous magnesium sulphate and evaporated under reduced

pressure. The product **2** was obtained pure as a yellow solid (M. P. 228-231°C) by recrystallization from dichloromethane, with a 46% yield. $^1\text{H-NMR}$ (500 MHz, DMSO/Toluene 1:1): δ (ppm) = 8.11 (s, 3H, Ar-H_g), 8.05 (d, 6H, J = 8.5 Hz, Ar-H_e), 7.99 (t, 3H, J = 1.6 Hz, Ar-H_d), 7.85 (d, 6H, J = 8.5 Hz, Ar-H_f), 7.77 (d, 3H, J = 7.9 Hz, Ar-H_a), 7.60 (d, 3H, J = 7.9 Hz, Ar-H_c), 7.46 (t, 3H, J = 7.9 Hz, Ar-H_b). $^{13}\text{C-NMR}$ (500 MHz, DMSO/Toluene 1:1): δ (ppm) = 142.2, 141.3, 139.9, 138.0, 130.9, 130.2, 129.3, 128.7, 127.8, 127.7, 125.7, 122.5. HR-MS DCI- CH_4^+ /TOF on $[\text{M}]^+$ m/z 767.9639 found for $\text{C}_{42}\text{H}_{27}\text{Br}_3$ (calculated 767.9663) (100%).

Chapter 5: Anthracene derivatives

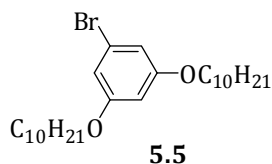
Anthracene A1:



Synthesis of 5-bromobenzene-1,3-diol (5.4)

Procedure a): Dimethyl 5-bromoisophthalate (4 gr, 18.4 mmol) was dissolved in 70 ml of a 50% solution of hydrobromic acid (48 %) in acetic acid (glacial) and it was let to react at 110°C for 10 hours. The temperature was let lower at R.T. and it was let to stir for 10 hours more. The acids were removed by evaporation under vacuum (until 30 ml were left), then 250 ml of water were added and the aqueous phase was extracted with 100 ml of ethyl acetate. The organic phase was dried on MgSO_4 and evaporated under vacuum. The product, a white solid (M. P. = 89°C) was obtained pure after column chromatography on silica gel (eluent : 20% ethyl acetate in petroleum ether), with a yield of 81%. Melting point: 89-91°C.

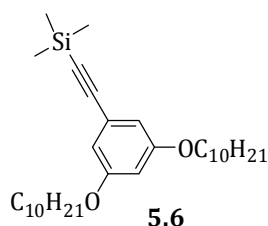
$^1\text{H-NMR}$ (300 MHz, MeOD): δ = 6.46 (d, J = 2.1 Hz, 2H, Ar-H), 6.22 (t, J = 2.1 Hz, 1H, Ar-H). $^{13}\text{C-NMR}$ (75 MHz, MeOD): δ = 161.4, 124.3, 111.9, 103.5. DCI/ NH_3^- : m/z 186.9 $[\text{M-H}]^-$ (calculated 186.9)



Synthesis of 1-bromo-3,5-bis(decyloxy)benzene (5.5):

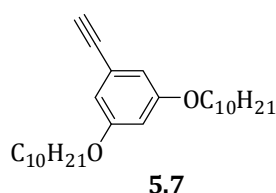
5.4 (0.81 gr, 4.3 mmol) was dissolved in 10 ml of dry DMF and the solvent was degassed by bubbling argon for 15 minutes, then K_2CO_3 sesquihydrate (1.94 gr, 12.4 mmol) was added and the mixture was let to react at room temperature for 10 minutes. 1-bromo-decane was

added and it was let to react at 65°C for 18 hours. DMF was then evaporated under reduced pressure and the product dissolved in 20 ml of ethyl acetate. The organic phase was washed three times with water, dried on MgSO₄ and evaporated under reduced pressure. The product, an colourless oil, was obtained pure after column chromatography on silica with hexane as eluent (R.F. = 0.5 on TLC SiO₂, hexane). ¹H-NMR (300 MHz, CD₂Cl₂): δ= 6.64 (d, J=2.4 Hz, 2H, Ar-H), 6.38 (t, J=2.1 Hz, 1H, Ar-H), 3.91 (t, J=6.6 Hz, 4H, O-CH₂), 1.75 (q, J=7.5 Hz, 4H, O-CH₂-CH₂), 1.3-1.5 (m, 28H, CH₂ chain), 0.8- 0.9 (m, 6H, CH₃). ¹³C-NMR (75 MHz, CD₂Cl₂): δ= 161.7, 123.5, 110.9, 101.3, 69.2, 32.7, 30.4, 30.1, 29.9, 27.7, 26.7, 23.5, 14.7. HR-MS DCI-CH₄⁺/TOF on [M+H]⁺ m/z 469.2642 for C₂₆H₄₆BrO₂ (calculated 469.2603); on [M+C₂H₅]⁺ m/z 497.3008 for C₂₈H₅₀BrO₂ (calculated 497.2994).



Synthesis of ((3,5-bis(decyloxy)phenyl)ethynyl)trimethylsilane (5.6)

5.5 (0.79gr, 1.7 mmol) was dissolved in 5 ml of di-isopropylamine (dried on molecular sieves 3 Å). The solvent was degased by argon bubbling for 15 minutes, then Pd(PPh₃)₄ (0.23 gr, 0.2 mmol), CuI (0.004 gr, 0.02 mmol) and TMSA (0.25gr, 0.36 ml, 2.5 mmol) were added and the reaction mixture was let to react at 100°C for 6 hours. After a filtration on a silica pad, 30 ml of a saturated solution of NH₄Cl were added and the aqueous phase was extracted with two portions of diethyl ether. The combined organic phases were dried on MgSO₄ and evaporated under reduced pressure. The product, a white solid, was obtained pure after a column chromatography purification on silica, with petroleum ether as eluent, with a yield of 91%. (R.F. = 0.5-0.6 on TLC SiO₂, petroleum ether). Melting point: 31-33°C. ¹H-NMR (300 MHz, CD₂Cl₂): δ= 6.58 (d, J=2.4Hz, 2H, Ar-H), 6.44 (t, J=2.4 Hz, 1H, Ar-H), 3.92 (t, J=6 Hz, 4H, O-CH₂), 1.76 (q, J=7.8 Hz, 4H, O-CH₂-CH₂), 1.2-1.5 (m, 28H, CH₂), 0.9-1.0 (m, 6H, CH₃), 0.25 (s, 9H, Si(CH₃)₃). ¹³C-NMR (75 MHz, CD₂Cl₂): δ= 160.9, 125.0, 110.8, 105.9, 103.8, 94.2, 69.1, 32.8, 30.4, 30.2, 30.0, 26.8, 23.6, 15.9, 14.7, 0.5. HR-MS DCI-CH₄⁺/TOF on [M]⁺ m/z 486.3904 for C₃₁H₅₄O₂Si (calculated m/z 486.3893).

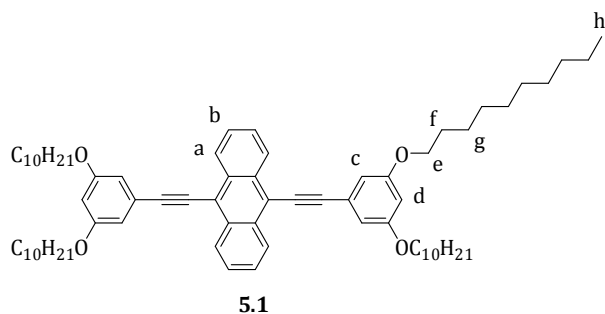


Synthesis of 1,3-bis(decyloxy)-5-ethynylbenzene (5.7)

Procedure a): **5.6** (0.36 gr, 0.74 mmol) was dissolved in 10 ml of THF. CsF (0.18 gr, 1.19 mmol) and one drop of MeOH were added and it was let to react under magnetic stirring for 4 hours at room temperature. The solvent was removed under reduced pressure and the obtained solid dissolved in 30 ml of CH₂Cl₂ and the organic phase extracted with two portions of 30 ml of water. The NMR analysis showed that the deprotection was not completed, so the reaction was restarted, dissolving the product in 10 ml of THF and adding 0.250 gr (1.64 mmol) of CsF and one drop of MeOH. After 18 hours, the solvent was evaporated under vacuum and the oil dissolved in 20 ml of ethyl acetate. The organic phase was washed with two portions of 30 ml each of water, dried on MgSO₄ and evaporated under vacuum, to give a white solid, that was used for the following step without any purification. The neat yield was estimated to be 89% (it was obtained 0.29 g of compound impure at 7%). (R.F. = 0.5-0.6 on TLC SiO₂, petroleum ether).

Procedure b): **5.6** (1 gr, 2 mmol) was dissolved in 20 ml of tetrahydrofuran and 20 ml of methanol, then KOH (0,12 gr, 2.06 mmol) in solution 1M of water (2.04 ml) was added then it was let to react at room temperature for 3 hours. The organic solvent was evaporated under reduced pressure. The obtained solid was taken up in 30 ml of ethyl acetate and the organic phase was extracted for two times with water (2 x 20 ml). The combined organic layers were washed with 30 ml of a saturated solution of NaCl, then dried over MgSO₄ and evaporated under

reduced pressure, to yield the product as a white solid. The neat yield was estimated to be 85% (it was obtained 0.74 g of compound impure at 6%).



Synthesis of 9,10-bis((3,5-bis(decyloxy)phenyl)ethynyl)anthracene (A1, 5.1)

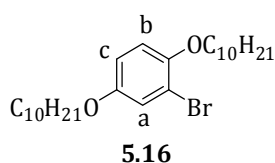
Procedure a): Sonogashira, Solvent mixture 1: 1,9-dibromoanthracene (0.10 gr, 0.3 mmol) was dissolved in a mixture of 30 ml of dry di-isopropylamine, 5 ml of dry toluene and 5 ml of dry acetonitrile. Argon was bubbled for 15 minutes, then Pd(PPh₃)₄ (0.06 gr, 0.05 mmol), CuI (0.009 gr, 0.05 mmol) and **5.7** (0.28 gr, 0.67 mmol) were

added and it was let to react under magnetic stirring for 18 hours. The mixture was filtered on a silica pad (the silica was washed with petroleum ether and ethyl acetate). The product was purified by a series of column chromatographies and recrystallizations: 1) Column on SiO₂, petroleum ether : dichloromethane 8 : 2; 2) Column on SiO₂, a. petroleum ether, b. petroleum ether : dichloromethane 9 : 1; 3) Column on Al₂O₃ neutral, a. petroleum ether : diethyl ether 98 : 2, b. petroleum ether : diethyl ether 6 : 4; 4) Repeated recrystallizations at R. T. from diethyl ether and acetone. Yield= 20%. (Rf on silica, with hexane : dichloromethane 8 : 2 as eluent, Rf=0.4).

Sonogashira, Solvent mixture 2: 1,9-dibromoanthracene (0.20 gr, 0.6 mmol) was dissolved in 10 ml of distilled tetrahydrofuran. **5.7** (0.48 gr, 1.15 mmol) was added in solution of 2 ml of tetrahydrofuran, followed by 27 ml of dry di-isopropylamine. Argon was bubbled for 15 minutes then Pd(PPh₃)₄ (0.056 gr, 0.048 mmol) and CuI (0.018 gr, 0.096 mmol) were added and it was let to react at 80°C for 18 hours. The temperature was let to lower at room temperature then the solution was passed on a short silica pad, washing with ethyl acetate. The product was purified by two column chromatographies: 1) Column on SiO₂, a. petroleum ether 100%, b. petroleum ether : dichloromethane 9:1; 2) Column on Al₂O₃ neutral, petroleum ether 100%. Yield = 30% (presence of an impurity in the alkyl chain region).

Procedure b): Carbonyl addition to 9,10-anthraquinone: To a solution of **5.7** in 10 ml of distilled tetrahydrofuran at -78°C, was added drop by drop 1.1 ml of a solution 1.6 M in hexane of n-butyllithium. The temperature was let to raise at 18°C and it was let to react for 30 minutes under magnetic stirring. To the yellow solution was added 9,10-anthraquinone as a solid in one portion. It was let to react at 18-22°C for 3 hours. To the orange solution were added 2.5 ml of a saturated solution of SnCl₂ in HCl (10%) and the colour turned immediately fluorescent yellow. After 10 minutes, to the reaction mixture they were added 30 ml of water, the organic phase was extracted, washed with water (2 x 30 ml), dried on MgSO₄ then evaporated under reduced pressure. The product was obtained pure after column chromatography on silica, with hexane : dichloromethane 8 : 2 (Rf=0.4) as eluent with a 82% yield. Melting point: 90-92°C (orange solid). ¹H-NMR (CD₂Cl₂, 500 MHz): δ (ppm) 8.6-8.7 (m, 4H, Ar-H(a)), 7.6-7.7 (m, 4H, Ar-H(b)), 6.92 (d, 4H, Jm=2.5 Hz, Ar-H(c)), 6.55 (t, 2H, Jm=2.5 Hz, Ar-H(d)), 4.03 (t, 8H, J=7 Hz, CH₂(e)), 1.82 (q, 8H, J=7 Hz, CH₂(f)), 1.50 (q, 8H, J=7 Hz, CH₂(g)), 1.3-1.4 (m, 48 H, CH₂ (chain)), 0.90 (t, 12H, J=7 Hz, CH₃(h)). ¹³C-NMR (CD₂Cl₂, 125 MHz): δ (ppm) 160.1, 131.8, 126.9, 126.7, 124.1, 118.1, 109.6, 102.6, 85.4, 68.1, 31.7, 29.5, 29.4, 29.3, 29.2, 29.1, 29.0, 25.8, 22.5, 13.7. HR-MS (DCI CH₄⁺ / TOF): m/z 1003.7539 found for C₇₀H₉₉O₄ (calculated 1003.7543); m/z 1002.7435 found for C₇₀H₉₈O₄ (100%) (calculated 1002.7465).

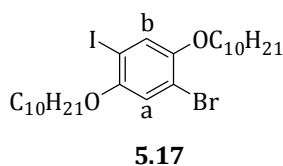
Anthracene A2:



Synthesis of 2-bromo-1,4-bis(decyloxy)benzene (5.16)

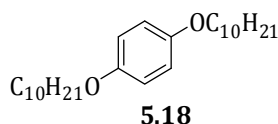
Bromohydroquinone (5 gr, 26.6 mmol) was dissolved in 50 ml of degassed ethanol. KOH was added (3.73 gr, 66.5 mmol) and the solution

was stirred under reflux for 30 minutes. 1-Bromodecane was added dropwise to the solution and the mixture stirred under reflux for 18 hours. Ethanol was then evaporated under reduced pressure. The solid residue was dissolved in 50 ml of dichloromethane and extracted with two portions of 100 ml of water. The organic phase was dried on dry MgSO_4 and concentrated under reduced pressure. The product was obtained pure as a colourless solid (M.P. 37-39° C) by column chromatography on silica with hexane : ethyl acetate 95:5 as eluent (Rf. on SiO_2 , hexane : ethyl acetate 9:1 = 0.75) with a 94% yield. Melting point : 37-39 °C. $^1\text{H-NMR}$ (300 MHz, CDCl_3): δ (ppm) 7.11 (d, 1H, $J=2.4$ Hz, Ar-H(a)), 6.7-6.8 (m, 2H, Ar-H(b,c)), 3.8-3.9 (m, 4H, $-\text{OCH}_2-$), 1.7-1.8 (m, 4H, $-\text{OCH}_2\text{CH}_2-$), 1.2-1.5 (m, 28H, CH_2 chains), 0.8-0.9 (m, 6H, CH_3). $^{13}\text{C-NMR}$ (75 MHz, CDCl_3): δ (ppm) 153.9, 150.1, 119.8, 115.1, 114.7, 113.1, 70.6, 69.1, 32.3, 29.9, 29.7, 29.68, 29.63, 26.4, 23.0, 14.5. HR-MS $\text{DCI}/\text{CH}_4^+/\text{TOF}$: m/z 468.2604 found for $\text{C}_{26}\text{H}_{45}\text{BrO}_2$ (calculated 468.2603).



Synthesis of 1-bromo-2,5-bis(decyloxy)-4-iodobenzene (5.17)

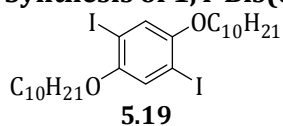
5.16 (11.46 gr, 24.4 mmol) was dissolved in 92 ml of acetic acid, 7 ml of water and 1 ml of sulphuric acid. Potassium iodate (1.04 gr, 4.88 mmol) and iodine (1.70 gr, 13.42 mmol) were added and the mixture was warmed at reflux (110°C) for 17 hours. To the orange solution, it was added a saturated solution of sodium thiosulfate, until decoloration, followed by 200 ml of ice-cold water. A yellow solid precipitated and was collected by vacuum filtration. The aqueous phase was extracted with three portions of 50 ml of hexane. The yellow solid was dissolved in diethyl ether (30 ml) and added to the hexane phase and the solution dried on anhydrous magnesium sulphate and evaporated under reduced pressure. The product, a white solid (MP 51-53°C), was obtained pure after silica gel column chromatography with hexane, then hexane : ethyl acetate 95:5 as eluent, with a 81% yield. The Rf of the product on silica TLC is 0.4 in hexane. $^1\text{H-NMR}$ (300 MHz, CDCl_3): δ (ppm) 7.28 (s, 1H, Ar-H(a)), 6.98 (s, 1H, Ar-H(b)), 3.9-4.0 (m, 4H, OCH₂), 1.7-1.8 (m, 4H, OCH₂CH₂), 1.2-1.5 (m, 28H, CH₂ chains), 0.8-0.9 (m, 6H, CH₃). $^{13}\text{C-NMR}$ (75 MHz, CDCl_3): δ (ppm) 152.9, 150.8, 124.6, 117.4, 112.9, 85.1, 70.7, 70.6, 32.3, 29.9, 29.7, 29.5, 29.4, 26.4, 26.3, 23.0, 14.5. HR MS $\text{DCI}-\text{CH}_4^+/\text{TOF}$: m/z 594.1584 found for $\text{C}_{26}\text{H}_{44}\text{O}_2\text{BrI}$ (calculated 594.1569).



Synthesis of 1,4-bis(decyloxy)benzene (5.18)

Hydroquinone (5 gr, 45.4 mmol) was dissolved in 45 ml of degassed ethanol. Potassium hydroxide was added (6.36 gr, 113.5 mmol) and the solution was stirred under reflux for 30 minutes. 1-Bromodecane was added dropwise to the solution and the mixture stirred under reflux for 18 hours. Ethanol was then evaporated under reduced pressure. The solid residue was dissolved in 50 ml of dichloromethane and extracted with two portions of 100 ml of water. The organic phase was dried on dry magnesium sulphate and concentrated under reduced pressure. The product was obtained pure as an colourless solid (M.P. 65-67° C) by recrystallization from methanol (Rf. on SiO_2 , hexane : ethyl acetate 9:1 = 0.64) with a 76% yield. Melting point : 65-67°C from methanol. $^1\text{H-NMR}$ (300 MHz, CDCl_3): δ (ppm) 6.82 (s, 4H), 3.89 (t, $J=6.6$ Hz, 4H), 1.75 (q, $J=6.6$ Hz, 4H), 1.2-1.5 (m, 28H), 0.88 (t, $J=6.3$ Hz, 6H). $^{13}\text{C-NMR}$ (75 MHz, CDCl_3): δ (ppm) 153.5 (2C), 115.7 (4C), 69.0 (2C), 32.3, 29.9, 29.8, 29.7, 26.4, 23.0, 14.5). HR-MS $\text{DCI}/\text{CH}_4^+/\text{TOF}$: m/z 390.3499 found for $\text{C}_{26}\text{H}_{46}\text{O}_2$ (calculated 390.3498). Moy, C. L., Kaliappan, R., McNeil, *J. Org. Chem.*, **2011**, 76, 20, 8501-8507.

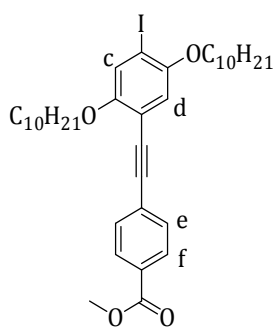
Synthesis of 1,4-Bis(decyloxy)-2,5-diiodobenzene (5.19)



To a two necks round bottom flask equipped with a magnetic stirrer was added 1,4-bis(decyloxy)benzene **5.18** (5 gr, 12.8 mmol), $\text{Hg}(\text{OAc})_2$ (10.20 gr, 32 mmol), I_2 (8.12 gr, 32 mmol) and 130 ml of dichloromethane. The reaction mixture was stirred for 48h at room temperature (22°C). The formed suspension was filtered through celite, rinsing with dichloromethane. The filtrate was washed with a saturated solution of $\text{Na}_2\text{S}_2\text{O}_3$ a saturated

solution of NaHCO_3 , water and brine and dried over dry MgSO_4 . The solvent was removed under reduced pressure and the crude product recrystallized from ethanol. The product (colourless flakes, MP 59-61°C) was obtained with a 73% yield. Melting point : 59-61°C. $^1\text{H-NMR}$ (300 MHz, CDCl_3): δ (ppm) 7.17 (s, 2H, Ar-H), 3.92 (t, 4H, $J=6.6$ Hz, $-\text{O}-\text{CH}_2-$), 1.80 (q, 4H, $J=6.6$ Hz, $-\text{O}-\text{CH}_2-\text{CH}_2-$), 1.4-1.5 (m, 4H, $-\text{O}-\text{CH}_2-\text{CH}_2-\text{CH}_2-$), 1.2-1.3 (m, 24H, $-\text{CH}_2-$), 0.8-0.9 (m, 6H, $-\text{CH}_3$). $^{13}\text{C-NMR}$ (75 MHz, CDCl_3): δ (ppm) 153.2, 123.1, 86.7, 70.7, 32.3, 29.9, 29.7, 29.6, 29.5, 26.4, 23.0, 14.5. HR-MS DCI/ CH_4^+ /TOF: m/z 642.1431 found for $\text{C}_{26}\text{H}_{44}\text{O}_2\text{I}_2$ (calculated 642.1431).

Rif. Bibl.: Shirai, Y., Zhao, Y., Cheng, L., Tour, J. M., *Org. Lett.*, **2004**, 6, 13, 2129-2132.

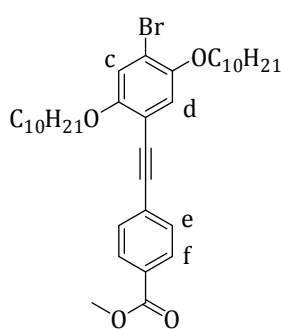


5.10

Synthesis of methyl 4-((2,5-bis(decyloxy)-4-iodophenyl) ethynyl) benzoate (5.10)

An oven dried schlenk flask was charged, under an atmosphere of argon, with **5.15** (0.10 gr, 0.6 mmol) and **5.19** (0.6 gr, 0.9 mmol). 15 ml of dry diethyl-amine and 15 ml of dry dichloromethane were added and argon was bubbled for 20 minutes. Copper iodide (0.002 gr, 0.012 mmol) and bis(triphenylphosphine)palladium(II) dichloride (0.004 gr, 0.006 mmol) were added as solids in one portion and the mixture was stirred for 6 hours at room temperature (20°-22°C). The solvent was evaporated under reduced pressure and the resulting solid taken up in 20 ml of dichloromethane and filtered on a silica pad. The product, a yellow solid was recovered after column chromatography on silica gel,

with hexane : ethyl acetate 96:4 as eluent (R_f on silica, in hexane : ethyl acetate 92:8 = 0.7; hexane : ethyl acetate 96:4 = 0.4) with a 43% yield. Melting point : 61-63°C. $^1\text{H-NMR}$ (500 MHz, CDCl_3): δ (ppm) 8.01 (dt, 2H, $J_o=8.2$ Hz, $J_p=1.5$ Hz, Ar-H(f)), 7.57 (dt, 2H, $J_o=8.2$ Hz, $J_p=1.5$ Hz, Ar-H(g)), 7.31 (s, 2H, Ar-H(d)), 6.90 (s, 2H, Ar-H(c)), 3.9-4.0 (m, 4H, $-\text{OCH}_2-$), 3.93 (s, 3H, $-\text{COOCH}_3$), 1.7-1.8 (m, 4H, $-\text{OCH}_2\text{CH}_2-$), 1.4-1.5 (m, 4H, $-\text{OCH}_2\text{CH}_2\text{CH}_2-$), 1.1-1.4 (m, 24H, CH_2 chains), 0.8-0.9 (m, 6H, $-\text{CH}_2\text{CH}_3$). $^{13}\text{C-NMR}$ (75 MHz, CDCl_3): δ (ppm) 166.9, 154.8, 152.1, 154.8, 152.1, 131.7, 129.8, 129.7, 128.5, 124.1, 116.2, 113.2, 93.7, 89.0, 88.7, 70.4, 70.1, 52.6, 32.3, 32.2, 30.0, 29.9, 29.8, 29.7, 29.69, 29.66, 29.62, 29.5, 26.4, 26.3, 23.0, 14.5, 14.4. HR-MS DCI/ CH_4^+ /TOF: m/z 674.2848 found for $\text{C}_{36}\text{H}_{51}\text{O}_4\text{I}$, 100% (calculated 674.2832), m/z 675.2914 found for $\text{C}_{36}\text{H}_{52}\text{O}_4\text{I}$, 93.13% (calculated 675.2910).

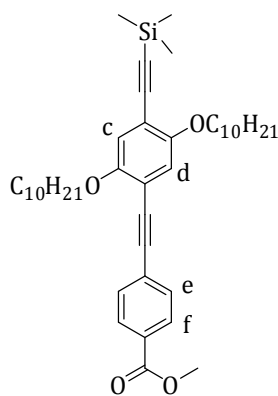


5.11

Synthesis of methyl 4-((4-bromo-2,5-bis(decyloxy)phenyl) ethynyl)benzoate (5.11)

5.15 (0.46 gr, 2.9 mmol) and **5.17** (1.6 gr, 2.7 mmol) were charged in an oven dried schlenk and dissolved in 30 ml of dry triethylamine and 30 ml of dry tetrahydrofuran. The solvent was degassed by argon bubbling for 10 minutes then bis(triphenylphosphine)palladium(II) dichloride (0.061 gr, 0.087 mmol) and copper iodide (0.028 gr, 0.15 mmol) were added as solids, then it was let to react at room temperature (22°C) for 16 hours. The solvent was evaporated under reduced pressure then the solid taken up in dichloromethane and filtered on a silica pad. The product, a light yellow solid, was purified by column chromatography on silica, with hexane : ethyl acetate 96 : 4

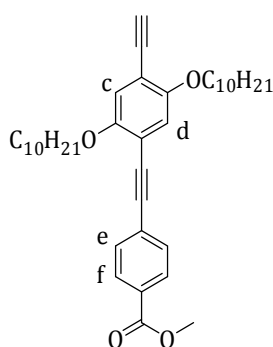
as eluent. The R_f on silica with hexane : ethyl acetate 96 : 4 as eluent is 0.45. Yield 91%. Melting point : 58-60°C. $^1\text{H-NMR}$ (300 MHz, CDCl_3): δ (ppm) 8.01 (d, 2H, $J_o=8.5$ Hz, Ar-H(f)), 7.57(d, 2H, $J_o=8.5$ Hz, Ar-H(e)), 7.11 (s, 1H, Ar-H(c)), 7.01 (s, 1H, Ar-H(d)), 3.9-4.0 (m, 4H, OCH_2), 3.9 (s, 3H, COOCH_3), 1.7-1.8 (m, 4H, OCH_2CH_2), 1.2-1.6 (m, 28H, CH_2 chain), 0.8-0.9 (m, 6H, CH_3). $^{13}\text{C-NMR}$ (75 MHz, CDCl_3): δ (ppm) 166.9, 154.7, 149.8, 131.7, 129.8, 129.7, 128.5, 118.3, 117.8, 114.3, 112.3, 93.5, 88.8, 70.5, 70.1, 52.5, 32.2, 30.0, 29.9, 29.7, 29.67, 29.60, 29.5, 26.4, 26.3, 23.0, 14.5. HR MS DCI- CH_4^+ /TOF : m/z 627.3069 found for $\text{C}_{36}\text{H}_{52}\text{BrO}_4$ (calculated 627.3049).



5.20

Synthesis of methyl 4-((2,5-bis(decyloxy)-4-((trimethylsilyl)ethynyl)phenyl)ethynyl)benzoate (5.20)

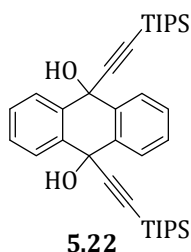
In an oven dried schlenk flask, **5.10** (0.88 gr, 1.3 mmol) was dissolved in 15 ml of dry triethylamine and 15 ml of dry tetrahydrofuran and the solvent was degassed by argon bubbling for 30 minutes. Bis(triphenylphosphine)palladium(II) dichloride (0.027 gr, 0.039 mmol) and copper iodide (0.012 gr, 0.065 mmol) were added, followed by trimethylsilylacetylene (0.14 gr, 0.2 ml, 1.4 mmol) drop by drop. The mixture was let to react at room temperature (23°C) for 48 hours then the solvent was evaporated under reduced pressure. The yellow solid obtained was taken up in dichloromethane and the solution passed through a short silica pad. The product, a yellow solid (53-55°C), was obtained pure by column chromatography purification on silica, with eluent hexane : acetone 92:8, with a 92% yield. (Rf of **5.20** on silica, hexane : acetone 92:8 is 0.7, blue fluorescent spot at 365 nm). Melting point : 53-55°C. ¹H-NMR (300 MHz, CDCl₃): δ (ppm) 8.01 (d, 2H, J=8.5Hz, Ar-H (f)), 7.57 (d, 2H, J=8.5, Ar-H(e)), 6.96 (s, 1H, Ar-H(c or d)), 6.95 (s, 1H, Ar-H(c or d)), 3.9-4.0 (m, 4H, OCH₂), 3.92 (s, 3H, COOCH₃), 1.7-1.8 (m, 4H, OCH₂CH₂-), 1.4-1.5 (m, 4H, OCH₂CH₂CH₂-), 1.1-1.4 (m, 24H, CH₂ chains), 0.8-0.9 (m, 6H, -CH₃), 0.3 (s, 9H, -Si(CH₃)₃). ¹³C-NMR (75 MHz, CDCl₃): δ (ppm) 166.9, 154.5, 154.0, 131.7, 129.8, 129.7, 128.5, 117.5, 117.2, 114.7, 113.8, 100.3, 100.8, 94.3, 88.3, 69.86, 69.84, 52.5, 32.2, 30.0, 29.9, 29.7, 29.6, 26.4, 23.0, 14.4, 0.3. HR-MS DCI/CH₄⁺/TOF: m/z 645.4330 found for C₄₁H₆₀O₄Si, 100% (calculated 645.4339).



5.13

Synthesis of methyl 4-((2,5-bis(decyloxy)-4-ethynylphenyl)ethynyl)benzoate (5.13)

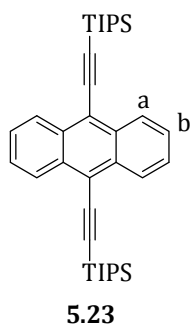
5.20 (0.25 gr, 0.39 mmol) was dissolved in 2.5 ml of dichloromethane and 2.5 ml of methanol and the solvent was degassed by argon bubbling for 5 minutes. The mixture was let to react under magnetic stirring for 2 hours at room temperature (23°C). The solvent was evaporated under reduced pressure, the solid taken up in dichloromethane and the solution passed through a short silica pad. The product, a yellow solid (MP = 41-43°C), was obtained pure by column chromatography purification, with eluent hexane : dichloromethane 6:4, with a 95% yield. (Rf of **5.13** on silica, hexane : dichloromethane 6:4 is 0.4, blue fluorescent spot at 365 nm). Melting point : 41-43°C. ¹H-NMR (300 MHz, CDCl₃): δ (ppm) 8.01 (d, 2H, J=8.4Hz, Ar-H (f)), 7.58 (d, 2H, J=8.4, Ar-H(e)), 6.99 (s, 1H, Ar-H(c or d)), 6.98 (s, 1H, Ar-H(c or d)), 3.9-4.0 (m, 4H, OCH₂), 3.93 (s, 3H, COOCH₃), 3.35 (s, 1H, CCH), 1.7-1.8 (m, 4H, OCH₂CH₂-), 1.2-1.5 (m, 28H, CH₂ chain), 0.8-0.9 (m, 6H, -CH₃). ¹³C-NMR (75 MHz, CDCl₃): δ (ppm) 166.9, 154.4, 154.0, 131.8, 129.8, 128.4, 118.1, 117.2, 114.3, 114.2, 94.4, 89.1, 82.9, 80.2, 70.0, 69.9, 52.6, 32.3, 31.9, 30.0, 29.9, 29.8, 29.7, 29.5, 26.4, 26.3, 23.0, 14.5. HR-MS DCI/CH₄⁺/TOF: m/z 573.3954 (found for C₃₈H₅₃O₄) (calculated 573.3944).



5.22

Synthesis of 9,10-bis((triisopropylsilyl)ethynyl)anthracene (5.23)

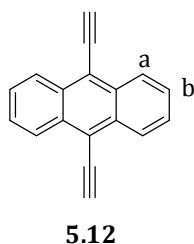
To a solution of tri-isopropylacetylene (5.4 ml, 24 mmol) in 40 ml of dry tetrahydrofuran and 20 ml of dry diethyl ether at -78°C, it was added drop by drop a solution of n-butyl-lithium 1.6 M in hexane (15 ml, 24 mmol). The temperature was let to raise at 20°C and it was let to stir for 1 hour. After this time, anthraquinone (2 gr, 9.6 mmol) was added in one portion as a solid and it was let to react at 22°C for 20 hours. The reaction was quenched by adding 120 ml of a saturated solution of NH₄Cl, then 15 ml of a 10% solution of HCl. The organic phase was extracted, washed with two portions of 100 ml of distilled water, then dried on anhydrous MgSO₄. The diol product **3a** was recovered pure by column chromatography on silica gel, using as eluent hexane : ethyl acetate 9:1, then 8:2 (yield = 50%). DCI/NH₃⁺ : m/z 660.1.



5.22 (2.79 gr, 4.87 mmol) was transferred in a three neck round bottom flask and dissolved in 20 ml of acetone and the argon was bubbled for 20 minutes. Then 20 ml of a solution of SnCl₂ (1.85 gr, 9.74 mmol) in 50% acetic acid in water, previously sparged with argon, were added drop by drop at room temperature: upon the addition, it was observed the precipitation of a yellow solid. It was let to react at 22°C for one hour, then the yellow precipitate was recovered by filtration. The filtrate was extracted with dichloromethane (2 x 50ml). The combined organic phases were neutralized with a saturated solution of NaHCO₃, then washed with water (2 x 40 ml) (formation of an emulsion). The emulsion was extracted with dichloromethane and the

combined organic phases were dried on dry MgSO₄ and evaporated under vacuum. They were obtained 2 gr of clean product (yellow solid, MP= 211-213°C, Rf 0.72 on silica in petroleum ether). The global yield for the two steps was 37%. Rf in hexane on SiO₂= 0.54. Melting point : 211-213°C. ¹H-NMR (300 MHz, CDCl₃): δ (ppm) 8.64 (m, 4H, Ar-H(a)), 7.60 (m, 4H, Ar-H(b)), 1.28 (m, 42H, CH(CH₃)₂). ¹³C-NMR (75 MHz, CDCl₃): δ (ppm) 132.8, 127.6, 127.1, 119.0, 105.2, 103.7, 19.3, 11.9. HR-MS DCI/CH₄⁺/TOF: m/z 539.3525 (calculated for C₃₆H₅₁Si₂ 539.3529, 100%), m/z 538.3469 (calculated for C₃₆H₅₀Si₂ 538.3451, 87.21%).

Rif. Bibl.: adapted from Schmidt, R., Götting, S., Leusser, D., Stalke, D., Krause, A.-M., Würthner, F., *J. Mat. Chem.*, **2006**, *16*, 3708-3714 .



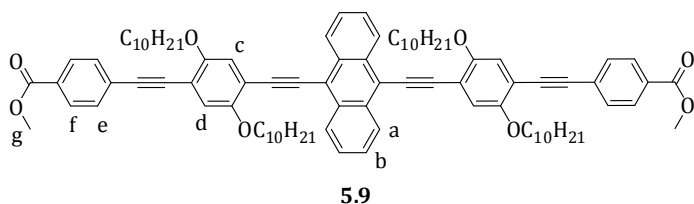
Synthesis of 9,10-diethynylanthracene (5.12)

5.23 (0.69 gr, 1.28 mmol) was charged in a 100 ml three necks flask and was dissolved in 15 ml of dry tetrahydrofuran. Argon was bubbled for 10 minutes then the temperature was taken at 0°-5° C by means of an ice bath. A solution of tetrabutylammonium-fluoride 1 M in THF (3 ml, 3 mmol) was added drop by drop (the colour became dark green/black). The ice bath was removed and the mixture was let to stir at room temperature (22°C) for 30 minutes, until the complete disappearance of the spot relative to the reagent (Rf of reagent

5.23, 0.7 on silica in petroleum ether, Rf of product **5.12**, 0.3). The reaction was quenched by adding 15 ml of a saturated solution of NH₄Cl. The mixture was additionated of 15 ml of ethyl acetate, then the organic phase was extracted and washed with two portions of 40 ml of distilled water, then dried on MgSO₄ and evaporated under reduced pressure. The product (an orange solid) was obtained pure by column chromatography on silica gel, with a gradient petroleum ether 100 % then petroleum ether: dichloromethane 8:2 with a yield of 12%. The low yield is probably due to the instability of **5.12** at ambient conditions, leading the ethynil groups to polymerize. Rf in hexane on SiO₂= 0.3. ¹H-NMR (300 MHz, CDCl₃): δ (ppm) 8.61 (m, 4H, Ar-H(a)), 7.62 (m, 4H, Ar-H(b)), 4.07 (s, 2H, CC-H).

Rif. Bibl.: Alvey, P. M., Ono, R. J., Bielawski, C. W., Iverson, B. L., *Macromolecules*, **2013**, *46*, 718-726.

Synthesis of dimethyl 4,4'-(4,4'-(anthracene-9,10-diylbis(ethyne-2,1-diyl))bis(2,5-bis(decyloxy)-4,1-phenylene))bis(ethyne-2,1-diyl)dibenzoate (5.9)



Procedure a) (Iodine): An oven dried schlenk flask was charged, under an atmosphere of argon, with **5.10** (0.10 gr, 0.148 mmol), 1 ml of dry diethyl-amine and 1 ml of dry tetrahydrofuran. The solvent was

degassed for 10 minutes then bis(triphenylphosphine)palladium(II) dichloride (0.005 gr, 0.007 mmol) and copper iodide (0.001 gr, 0.007 mmol) were added as solids in one portion, followed after 10 minutes by **4** (0.015 gr, 0.067 mmol). The mixture was stirred under argon for 6 hours at room temperature (22°C), then it was filtered on a silica pad, washing with dichloromethane.

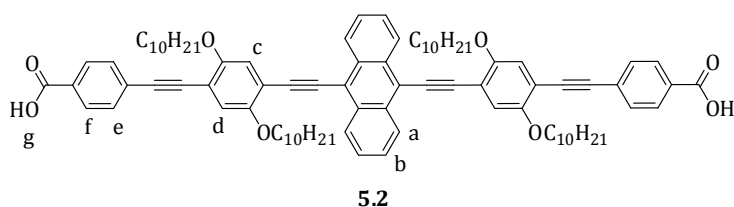
After evaporation of the solvent under reduced pressure, it was obtained a dark violet oil, from which the product was recovered by column chromatography on silica gel, using a gradient of petroleum ether : ethyl acetate from 95:5 to 8:2 (in petroleum ether : ethyl acetate 8:2 Rf=0,2, fluorescent at 365 nm). Yield < 48% (red solid).

Procedure a) (bromine): An oven dried schlenk flask was charged, under an atmosphere of argon, with **5.11** (1 gr, 1.6 mmol) and **4** (0.17 gr, 0.76 mmol), 30 ml of dry triethylamine and 30 ml of dry tetrahydrofuran. The solvent was degased for 30 minutes then bis(triphenylphosphine)palladium(II) dichloride (0.03 gr, 0.046 mmol) and copper iodide (0.014 gr, 0.076 mmol) were added as solids in one portion. The mixture was stirred under argon for 16 hours at 90°C. The solvent was evaporated under reduced pressure and the dark violet solid obtained taken up in dichloromethane and passed through a silica pad, washing with dichloromethane. The product was purified by multiple column chromatography (1) SiO₂ gel, hexane : ethyl acetate 95:5, then 9:1; 2) SiO₂ gel, hexane : THF 9:1; 3) Al₂O₃, hexane : THF 95:5; 4) SiO₂ gel, toluene (Rf=0.6, yellow fluorescent spot at 365 nm running together with a red trace) and precipitation from ice cold dichloromethane. Yield < 11% , orange fluorescent solid.

Procedure b): In an oven dried schlenk, 9,10-dibromoanthracene (0.05 gr, 0.14 mmol) was suspended in 2 ml of dry tetrahydrofuran and 1 ml of dry di-isopropylamine, under argon. Argon was bubbled in the solvent for 15 minutes then tetrakis(triphenylphosphine)palladium(0) (0.01 gr, 0.009 mmol) and copper iodide(0.002 gr, 0.009 mmol) were added. The mixture was warmed at 45°C for 1 hour, giving a yellow homogeneous solution. The alkyne **5.13** was dissolved in 3 ml of dry tetrahydrofuran, the solvent was degased and the solution was introduced drop by drop in the reaction flask by a cannula system. The mixture was warmed at 80°C for 20 hours under an argon atmosphere. The dark red solution was filtered on a silica pad, washing with 100 ml of tetrahydrofuran and the solvent was evaporated under reduced pressure. The product, an orange fluorescent solid, was recrystallized with ice-cold dichloromethane, with a 70% yield.

¹H-NMR (500 MHz, CDCl₃): δ (ppm) 8.8-8.9 (m, 4H, Ar-H), 8.04 (d, 4H, J=8.5 Hz, Ar-H_f), 7.6-7.7 (m, 4H, Ar-H), 7.63 (d, 4H, J=8.5 Hz, Ar-H_e), 7.29 (s, 2H, Ar-H_c), 7.15 (s, 2H, Ar-H_d), 4.1-4.2 (m, 8H, OCH₂), 3.92 (s, 6H, COOCH₃), 2.08 (q, 4H, J=7 Hz, OCH₂CH₂), 1.92 (q, 4H, J=7 Hz, OCH₂CH₂), 1.5-1.6 (m, 8H, OCH₂CH₂CH₂), 1.4-1.5 (m, 8H, OCH₂CH₂CH₂), 1.2-1.3 (m, 52H, alkyl chains), 0.8-0.9 (m, 12H, CH₂CH₃). ¹³C-NMR (125 MHz, CDCl₃): δ (ppm) 166.6, 154.3, 154.2, 132.4, 131.2, 130.0, 129.8, 128.3, 127.7, 127.2, 119.0, 116.7, 116.2, 114.5, 114.0, 99.9, 94.6, 92.9, 89.5, 77.9, 77.7, 77.4, 70.1, 69.8, 52.3, 32.3, 32.2, 29-30, 26.5, 26.4, 23.1, 23.0, 14.2. HR-MS MALDI-DCTB⁺/TOF: m/z 1318.8252 found for C₉₀H₁₁₀O₈ (calculated 1318.8201).

Synthesis of 4,4'-(4,4'-(anthracene-9,10-diylbis(ethyne-2,1-diyl))bis(2,5-bis(decyloxy)-4,1-phenylene))bis(ethyne-2,1-diyl)dibenzoic acid (**A2**, **5.2**)



5.9 (0.010 gr, 0.008 mmol) was dissolved in 1 ml of tetrahydrofuran and lithium hydroxide (0.002 gr, 0.07 mmol) was added, dissolved in 0.25 ml of distilled water. It was let to react

at 50°C for 22 hours: it was observed the precipitation of an orange solid that was filtered off on a fritted funnel and washed with 10 ml of dichloromethane. The solid was dissolved in a mixture composed of 90% of tetrahydrofuran and 10% of a 10% solution of hydrochloric acid (30 ml). The pH was further acidified down to pH=2 by adding 2 ml of a 10% solution of hydrochloric acid, then the organic phase evaporated. From the aqueous phase it precipitated the product as a red/ pink fluorescent solid that was filtered, washed with 10 ml of diethyl ether and dried under vacuum. Yield 99%. Melting point 154-156°C. ¹H-NMR (500 MHz, C₆D₆ 95%, DMSO 5%): δ (ppm)= 9.3-9.4 (m, 4H, Ar-H_a), 8.3-8.4 (m, 4H, Ar-H_f), 7.8-7.9 (m, 8H, Ar-H_b and Ar-H_e), 7.73 (s,

2H, Ar-H_c), 7.51 (s, 2H, Ar-H_d), 4.1-4.2 (m, 8H, -OCH₂-), 2.0-2.1 (m, 4H, -OCH₂CH₂-), 1.9-2.0 (m, 4H, -OCH₂CH₂-), 1.6-1.8 (m, 8H, , -OCH₂CH₂CH₂-), 1.3-1.6 (m, alkyl chains), 1.0-1.1 (m, 12H, -CH₃).¹³C-NMR (125 MHz, C₆D₆ 95%, DMSO 5%): δ (ppm)= 167.03, 153.8, 153.7, 118.6, 116.4, 115.9, 113.9, 113.6, 99.9, 94.5, 92.6, 89.3, 69.0, 68.8, 31.6, 31.5, 29.4, 29.3, 29.2, 29.1, 29.0, 28.9, 28.8, 25.8, 25.7, 22.4, 22.3, 13.8, 13.7. HR-MS MALDI-DCTB⁺/TOF: m/z 1290.7886 found for C₈₈H₁₀₆O₈ (calculated 1290.7888).

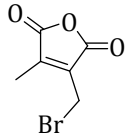
Alternative purification: THF was evaporated under reduced pressure, then water was added (about 6 ml) and the suspension was centrifuged at 14500 rpm for 15 minutes. The solid was decanted and dispersed in tetrahydrofuran (about 2 ml in each vial) and centrifuged at 14.500 rpm for 15 minutes. The solid was again decanted and dispersed by sonication in dichloromethane (about 2 ml in each vial) and centrifuged at 14.500 rpm for 15 minutes. The solid was recovered, suspended in 9 ml of tetrahydrofuran, then HCl (3.7 %) was added drop by drop (about 0.3 ml) down to pH= 2: upon acidification, the solid dissolved and the colour of the solution turned fluorescent orange. Tetrahydrofuran was evaporated and the precipitate red/pink fluorescent solid was dispersed in water and filtered, washing with 10 ml of dichloromethane. The solid was recovered from the fritted funnel by dissolving it in tetrahydrofuran and evaporation under reduced pressure.

Chapter 6: Maleimide derivatives

Maleimide M1:

First strategy:

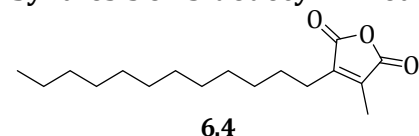
Synthesis 3-bromomethylfuran-2,5-dione (6.5)


6.5

A mixture of dimethylmaleic anhydride (2 g, 15.8 mmol), NBS (4.5 g, 25.3 mmol) and a catalytic amount of benzoyl peroxide (0.065 g, 0.27 mmol) in carbon tetrachloride (100 ml) was gently refluxed for 5h in a round bottom flask. The temperature was let to cool at R.T then another portion of benzoyl peroxide (0.065 g, 0.27 mmol) and NBS (4.5 g, 25.3 mmol) were added. The mixture was refluxed for 5 hours then let to stir overnight at room temperature. The mixture was filtered on a fritted funnel then the organic phase was washed with water (3 x 50 ml), dried on Na₂SO₄ and evaporated under reduced pressure. After column chromatography on silica (petroleum ether : ethyl acetate 8:2) and vacuum distillation (50 mbar at 120°, then 135°C), a mixture of monobrominated product **6.5** (66%), dibrominated product (29%) and reagent (5%) was obtained (1.1 gr (35% wt/wt)). The product was not further purified and employed in the following step. ¹H-NMR (300 MHz, CDCl₃) δ (ppm) = 2.18 (s, 3H), 4.18 (s, 2H).

Rif. Bibl.: Deshpande, A. M., Natu, A. A., Argade, N. P., *J. Org. Chem.*, **1998**, *63*, 9557-9558.

Synthesis of 3-dodecyl-4-methylfuran-2,5-dione (6.4)

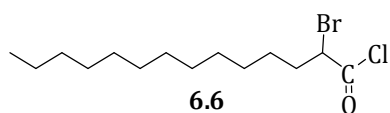


A 2 M room-temperature solution of *i*-PrMgCl (1.24 gr, 6.05 ml, 12.1 mmol) was added over a 10 min. period to a -10°C solution of 1-bromo-undecane (2.59, 2.45 ml, 11 mmol) in 50 ml of anhydrous THF, such that the reaction temperature never exceeded -5°C. The mixture was stirred at -10°C for 1h. The freshly prepared solution of Grignard reagent (11 mmol) in THF (50 ml) was added dropwise to the solution of 3-(bromomethyl)maleic anhydride (**6.5**, 1.12 g, 5.5 mmol) and CuI (0.10 g, 0.55 mmol) in diethyl ether (50 ml) and HMPA (3.94 gr, 3.83 ml, 22 mmol) under argon, at -5°C to 0°C over 15 min., by a cannule system, under magnetic stirring. The reaction mixture was allowed to reach R. T. and further stirred for 18h, then diluted with diethyl ether and acidified with 2 M H₂SO₄, down to pH 2. The aqueous layer was extracted with ether (50 ml x 3). The combined organic layers were washed with water (50 ml x 2), brine (50ml), dried over

Mg₂SO₄ and concentrated under reduced pressure. An NMR analysis of the raw product revealed only the presence of unreacted alkyl bromide.

Rif. Bibl.: Deshpande, A. M., Natu, A. A., Argade, N. P., *J. Org. Chem.*, **1998**, *63*, 9557-9558. For the preparation of the Grignard reagent was followed the procedure reported in: Leazer, J. L. Jr., Cvetovich, R., Tsay, F-R, Dolling, U., Vickery, T., Bachert, D., *J. Org. Chem.*, **2003**, *68*, 3695-3698.

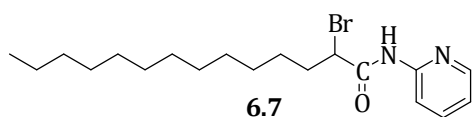
Second strategy: Rif. Bibl.: adapted from Argade, N. P., Naik, R. H., *Bioorg. Med. Chem.*, **1996**, *4*, 6, 881-883.



Synthesis of 2-Bromo-tetradecanoic-chloride (6.6)

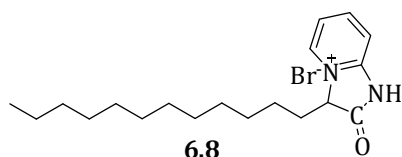
In an oven dried three necks flask, under an atmosphere of argon, to a solution of 5 gr (16.3 mmol) of 2-bromotetradecanoic acid in 80 ml of dry toluene, were added 13 ml (3.31 gr, 26.08 mmol) of a 2M solution of oxalyl chloride in dichloromethane, followed by a drop of dimethylformamide. The mixture was stirred for 2h at room temperature, then the solvent was removed under reduced pressure to give **6.6** as a yellow oil. The product was used for the following reaction without any further purification.

Rif. Bibl.: adapted from Padwa, A., Beall, L. S., Heidelbaugh, T. M., Liu, B., Sheehan, S. M., *J. Org. Chem.*, 2000, *65*, 9.



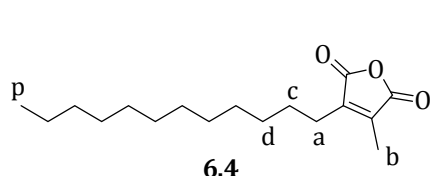
Synthesis of 2-bromo-N-(pyridin-2-yl) tetradecanamide (6.7)

To a solution of 2-aminopyridine (1.53 gr, 16.3 mmol) and dry triethylamine (2.27 gr, 16.3 mmol) in dry ether (100 ml) at room temperature under argon, was added the chloride **6.6** (5.3 gr, 16.3 mmol) in dry ether (30 ml) in a dropwise fashion over a period of 20 minutes under vigorous stirring (formation of a yellow suspension). The reaction mixture was further stirred for 3 h at R.T. (20°C) and the solvent removed under vacuum. The product (a yellow solid) was used for the following reaction without any further purification.



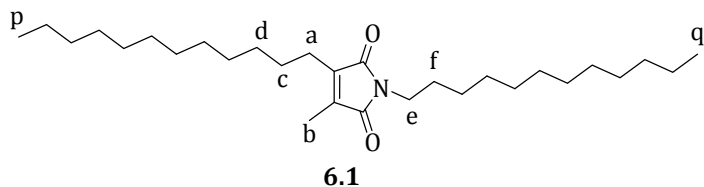
Synthesis of 3-dodecyl-2-oxo-2,3-dihydro-1H-imidazo [1,2-a] pyridin-4-ium bromide (6.8)

The total residue (**6.7**) was dissolved in 100 ml of tert-butanol and warmed at reflux (82°C) for 18 hours. The solvent was removed under reduced pressure, giving an orange oil that was used for the following step without any purification.



Synthesis of 3-dodecyl-4-methylfuran-2,5-dione (6.4)

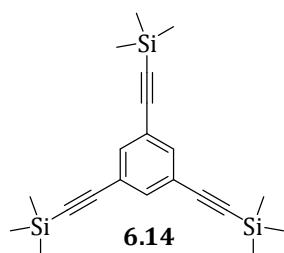
The residue **6.8** was reacted with maleic anhydride (1.60 gr, 16.3 mmol) in the presence of sodium acetate (1.34 gr, 16.3 mmol) in 98 % acetic acid (100 ml), under reflux (120°C) for 5 h under constant stirring. Acetic acid was then removed under vacuum and the residue dissolved in ether. The ether layer was washed with water (2x100 ml), brine (100 ml) and dried over magnesium sulphate. The product **4** was obtained as a yellow oil after column chromatography on silica gel (eluent petroleum ether : diethyl ether 9:1, R_f=0.53), with a 27 % yield (over 4 steps). ¹H-NMR (500 MHz, CDCl₃): δ (ppm) 2.45 (t, J=7.5 Hz, 2H, CH₂ (a)), 2.07 (s, 3H, CH₃ (b)), 1.5-1.6 (m, 2H, CH₂ (c)), 1.2-1.3 (m, 18H, CH₂ (chain)), 0.87 (t, J=7 Hz, 3H, CH₃ (p)). ¹³C-NMR (125 MHz, CDCl₃): δ (ppm) 166.6, 166.2, 145.1, 140.8, 32.2, 30.0, 29.9, 29.8, 29.7, 29.5, 24.8, 23.0, 14.5, 9.9. MS (DCI/NH₃⁺): m/z = 298 [M+NH₄]⁺. Elemental Analysis: %C 72.70 %H 9.70 %O 17.60 (found for C₁₇H₂₈O₃) vs %C 72.82 %H 10.06 %O 17.12 (calculated for C₁₇H₂₈O₃).

Synthesis of 1,3-didodecyl-4-methyl-1H-pyrrole-2,5-dione (M1, 6.1)

To a stirred solution of anhydride **6.4** (0.770 gr, 2.7 mmol) in dry toluene (20 ml) at RT (22°C), a solution of 1-dodecylamine (0.5 gr, 2.7 mmol) in dry toluene (10 ml) was added dropwise. The resulting suspension

was stirred for one hour, then zinc bromide (0.61 gr, 2.7 mmol) was added in one portion. While the resulting reaction mixture was heated at 80°C, a solution of hexamethyldisilazane (0.66 gr, 0.86 ml, 4.1 mmol) in 10 ml of dry toluene was added drop by drop, then the mixture was refluxed for 19 hours. The reaction mixture was cooled to RT and poured into 0.5N HCl (20 ml). The aqueous phase was extracted with ethyl acetate (3 x 30 ml). The combined organic extracts were dried over anhydrous magnesium sulphate. The solution was concentrated under reduced pressure and the residue purified by silica gel chromatography (Petroleum ether : diethyl ether 95:5), to afford the product as a yellow oil with a 89% yield.

¹H-NMR (500 MHz, CDCl₃): δ (ppm) 3.44 (t, J=7.5 Hz, 2H, CH₂ (a)), 2.35 (t, J=7.5 Hz, 2H, CH₂ (e)), 1.94 (s, 3H, CH₃ (b)), 1.4-1.5 (m, 4H, CH₂ (c,f)), 1.2-1.3 (m, 36H, CH₂ (chain)), 0.87 (t, J=6.5 Hz, 3H, CH₃ (p,q)). ¹³C-NMR (125 MHz, CDCl₃): δ (ppm) 177.8, 172.4, 141.3, 137.0, 36.3, 32.3, 30.0, 29.9, 29.8, 29.7, 29.6, 29.5, 29.0, 28.6, 27.1, 24.0, 23.0, 14.5, 9.0. MS (DCI/NH₃⁺): m/z = 465 [M+NH₄]⁺. Elemental Analysis : %C 77.58 %H 11.32 %N 3.13 %O 7.97 (found for C₂₉H₅₃NO₂) vs %C 77.79 %H 11.93 %N 3.13 %O 7.15 (calculated for C₂₉H₅₃NO₂).

Maleimide M2:**Synthesis of 1,3,5-Tris[(trimethylsilyl)ethynyl]benzene (6.14)**

Procedure a): 1,3,5-tribromobenzene (1 gr, 3.17 mmol) was dissolved in 7 ml of dry toluene and 7 ml of triethylamine (dried by molecular sieves of diameter 3 Å) and argon was bubbled in the mixture for 30 minutes. Tetrakis(triphenylphosphine)palladium(0) (0.15 gr, 0.13 mmol) and copper iodide (0.048 gr, 0.26 mmol) were added, followed by trimethylsilylacetylene (1.21 gr, 1.76 ml, 12.8 mmol). The mixture was warmed at 90°C for 20h under an atmosphere of argon. The

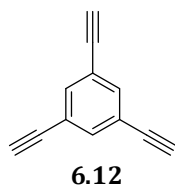
mixture was let to cool at room temperature and was filtered on a silica pad, washed with ethyl acetate. The solvent was removed under reduced pressure and the crude reaction product chromatographed on a silica gel column, employing petroleum ether as eluent (R_f on TLC, silica gel, petroleum ether = 0.4). The product, a yellow thick oil, was recovered with a yield of 86%. ¹H-NMR (300 MHz, CD₂Cl₂): δ (ppm) 7.47(s, 3H, Ar-H), 0.24 (s, 27H, -Si(CH₃)₃). ¹³C-NMR (75 MHz, CD₂Cl₂): δ (ppm) 135.5, 124.6, 103.6, 96.6, 0.3. MS (DCI/NH₃⁺): 384.1 [M+NH₄]⁺, 384.1 [M+H]⁺. (*works well only on one gram at maximum*).

Rif. Bibl.: Yoosaf, K., Llanes-Pallas, A., Marangoni, T., Belbakra, A., Marega, R., Botek, E., Champagne, B., Bonifazi, D., Armaroli, N., Chem. Eur. J., **2011**, 17, 11, 3262-3273. (already published product).

Procedure b): 1,3,5-tribromobenzene (2 gr, 6.4 mmol) was dissolved in 50 ml of dry diethylamine (dried on molecular sieves of diameter 3 Å) and argon was bubbled in the mixture for 30 minutes. Dichlorobis(triphenylphosphino)palladium(II) (0.084 gr, 0.12 mmol) and copper iodide (0.009 gr, 0.05 mmol) were added, followed by trimethylsilylacetylene (2.26 gr, 3.3 ml, 23.04 mmol). The mixture was warmed at 70°C for 17h under an atmosphere of argon and magnetic stirring. After this time, the mixture was let to cool at room temperature and was filtered on a silica pad, washed with ethyl acetate. The solvent was removed under reduced pressure and the crude reaction product chromatographed on a silica gel column, employing hexane as eluent (R_f on TLC, silica gel, hexane = 0.3). The product, a light yellow solid, was recovered with a yield of 80.5%. MP: 79-81°C. ¹H-NMR (300 MHz, CD₂Cl₂): δ (ppm) 7.47(s, 3H,

Ar-H), 0.24 (s, 27H, -Si(CH₃)₃).¹³C-NMR (75 MHz, CD₂Cl₂): δ (ppm) 135.5, 124.6, 103.6, 96.6, 0.3. MS (DCI/NH₃⁺): 384.1 [M+NH₄⁺], 367.1 [M+H⁺].

Rif. Bibl. : Uhl, W., Bock, H. R., Breher, F., Claesener, M., Haddadpour, S., Jasper, B., Hepp, A., *Organometallics*, **2007**, 26, 9, 23673-2369.

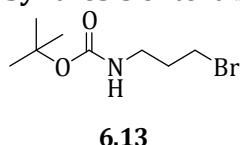


Synthesis of 1,3,5-Tris(ethynyl)benzene (6.12)

1,3,5-Tris[(trimethylsilyl)ethynyl]benzene (**6.14**) (1 gr, 2.7 mmol) was dissolved in 20 ml of tetrahydrofuran and 20 ml of methanol. To the solution were added 8.4 ml (0.47 gr, 8.4 mmol) of a 1M solution of KOH and the mixture was let to react under magnetic stirring for five hours at 22°C. The organic solvents were evaporated under reduced pressure. The residue was taken with 20 ml of ethyl acetate and the organic phase was extracted (x 2 times). The combined organic layers were washed with brine (2x20 ml), then dried over MgSO₄ and evaporated under reduced pressure. The obtained product (a light yellow solid, R_f on silica in hexane 0.5) was used for the following reaction without any further purification (yield 92%). MP: 101.4°C. ¹H-NMR (300 MHz, CD₂Cl₂): δ (ppm) 7.59 (s, 3H, Ar-H), 3.20 (s, 3H, Ar-CCH).¹³C-NMR (75 MHz, CD₂Cl₂): δ (ppm) 136.4, 123.8, 82.2, 79.4. HR-MS (DCI/CH₄⁺-TOF): m/z 150.0477 [M⁺]. DCI/CH₄⁺-TOF: found m/z 150.0477 for C₁₂H₆, m/z 150.0470 calculated for C₁₂H₆.

Rif. Bibl. : Yoosaf, K., Llanes-Pallas, A., Marangoni, T., Belbakra, A., Marega, R., Botek, E., Champagne, B., Bonifazi, D., Armaroli, N., *Chem. Eur. J.*, **2011**, 17, 11, 3262-3273.

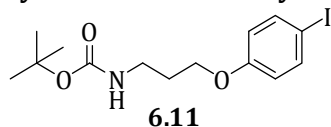
Synthesis of tert-butyl 3-bromopropylcarbamate (6.13)



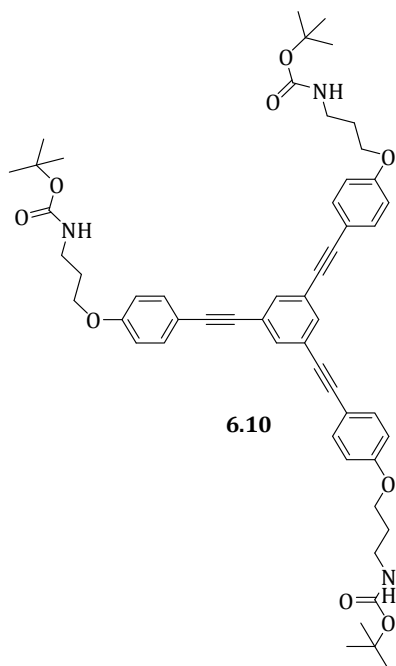
To a solution of 3-bromopropanamine hydrobromide (5 gr, 22.8 mmol) and NaOH (2.1 gr, 52 mmol) in water (50 ml) and tetrahydrofuran (50 ml) at 0-5°C, was slowly added a solution of di-tertbutyl-dicarbonate (5 gr, 22.8 mmol) in tetrahydrofuran (30 ml). The mixture was let to react for one hour at 0-5°C and for five hours at room temperature (22°C), then the organic phase was evaporated under reduced pressure. The aqueous phase was extracted with ethyl acetate (30 ml). The organic phase was washed with water (50 ml), a 10% solution of HCl down to pH=4 and water up to pH=6. The organic phase was recovered, dried on MgSO₄ and evaporated under reduced pressure to give the product as a yellow oil with a 90% yield, without any further purification. ¹H-NMR (300 MHz, CD₂Cl₂): δ (ppm) 4.81 (bs, 1H, -NH-), 3.45 (t, 2H, 6.6 Hz, NH-CH₂-), 3.45 (q, 2H, 6.3 Hz, NH-CH₂-), 2.03 (q, 2H, 6.6 Hz, -CH₂-), 1.42 (s, 27H, -O(CH₃)₃).¹³C-NMR (75 MHz, CD₂Cl₂): δ (ppm) 156.6 (C=O), 79.8 (C-O), 39.8, 33.7, 31.9, 28.9. MS (DCI/NH₃⁺): m/z 238.1 [M+H⁺] (calculated 238.0).

Rif. Bibl. : van Scherpenzeel, M. van den Berg, R. J.B.H.N., Donker-Koopman, W. E., Liskampa, R. M. J., Aertsc, J. M.F.G., Overkleeft, H. S., Pieters, R. J., *Bioorg. Med. Chem.*, **2010**, 18, 267-273.

Synthesis of tert-butyl 3-(4-iodophenoxy)propylcarbamate (6.11)



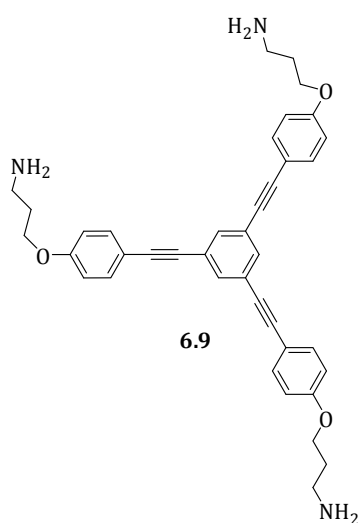
To a solution of p-iodophenol (2 gr, 9.1 mmol) and **6.13** (2.38 gr, 10 mmol) in dry acetonitrile (100 ml), were added Cs₂CO₃ (4.45 gr, 13.65 mmol) and NaI (0.34 gr, 2.28 mmol) and the mixture was let to react at 65°C for 5 hours. The inorganic salts were filtered away and the solvent evaporated under reduced pressure. The product, a light yellow solid, was purified by column chromatography on silica gel (pentane : diethyl ether 7:3, R_f 0.5) with a 83% yield. Melting point : 78-80°C. ¹H-NMR (300 MHz, CDCl₃): δ (ppm) 7.53 (dt, 2H, J₁=9 Hz, J₂=2.1 Hz, Ar-H(orto to O)), 6.69 (dt, 2H, J₁=9 Hz, J₂=2.1 Hz, Ar-H(orto to I)), 4.72 (bs, 1H, -NH-), 3.97 (t, 2H, J=6 Hz, -O-CH₂-), 3.31 (q, 2H, J=6 Hz, -NH-CH₂-), 1.96 (q, 2H, J=6.3 Hz, CH₂-CH₂-CH₂), 1.43 (s, 9H, -C(CH₃)₃).¹³C-NMR (75 MHz, CDCl₃): δ (ppm) 158.9, 156.3, 138.5, 117.2, 83.1, 66.2, 38.2, 29.8, 28.7. MS (DCI/NH₃⁺): 338.9 [M-C(CH₃)₃+H]⁺, 378.0 [M+H]⁺. HR MS (DCI CH₄⁺/TOF): m/z 377.0488 for C₁₄H₂₀INO₃ (calculated 377.0488) (13%); 278.0049 found for C₉H₁₃INO₃⁺ (calculated 278.0036) (100%).



Synthesis of tert-butyl 3,3',3''-(4,4',4''-(benzene-1,3,5-triyltris(ethyne-2,1-diyl))tris(benzene-4,1-diyl))tris(oxy)tris(propane-3,1-diyl)tricarbamate (**6.10**)

Procedure a): **6.11** (1.92 gr, 5.1 mmol) and 1,3,5-triethynylbenzene (**6.12**) (0.24 gr, 1.6 mmol) were dissolved in distilled tetrahydrofuran (25 ml) and triethylamine (7 ml). Argon was bubbled for 10 minutes then CuI (0.024 gr, 0.128 mmol) and Pd(PPh₃)₄ (0.074 gr, 0.064 mmol) were added and the mixture was let to react at room temperature (22°C) for 18 hours. The mixture was filtered on celite (washing with tetrahydrofuran) and the solvent evaporated under reduced pressure. The product (a yellow solid) was obtained pure by two column chromatographies on silica gel: 1) pentane : diethyl ether 6:4, then ethyl acetate; 2) pentane : ethyl acetate 6:4. (R_f = 0.3 in pentane:ethyl acetate 7:3). The yield was 24%-48%.

Procedure b): **6.11** (1.57 gr, 4.2 mmol) and 1,3,5-triethynylbenzene (**6.12**) (0.20 gr, 1.3 mmol) were dissolved in distilled tetrahydrofuran (20 ml) and dry diethylamine (13 ml). Argon was bubbled for 15 minutes then copper iodide (0.006 gr, 0.03 mmol) and bis(triphenylphosphine)palladium(II) dichloride (0.06 gr, 0.08 mmol) were added and the mixture was let to react at 45°C for 4 hours. The mixture was filtered on a silica pad (washing with ethyl acetate) and the solvent evaporated under reduced pressure. The product (a slightly yellow solid) was obtained pure by column chromatography on silica gel with cyclohexane : ethyl acetate 6:4 as eluent. (R_f = 0.35 in cyclohexane:ethyl acetate 6:4). The yield was 48%. Melting point : 104-106° C. ¹H-NMR (300 MHz, CD₂Cl₂) : δ (ppm) 7.59 (s, 3H, Ar-H), 7.49 (d, 6H, J=8.7 Hz, Ar-H), 6.91 (d, 6H, J=8.7 Hz, Ar-H), 4.82 (bs, 2.5H, -NHCO), 4.05 (t, 6H, J=6.3 Hz, CH₂), 3.31 (q, 6H, J=6.6 Hz, CH₂), 1.98 (q, 6H, J=6.6 Hz, CH₂), 1.44 (s, 27H, -CO(CH₃)₃). ¹³C-NMR (75 MHz, CD₂Cl₂): δ (ppm) 160.1 (-C=O), 156.6 (Ar-C), 134.1 (Ar-C), 134.0 (Ar-C), 125.1 (Ar-C), 115.6 (Ar-C), 115.4 (Ar-C), 91.2 (C-OR or C≡C), 87.3 (C≡C), 79.6 (C≡C), 66.7 (CH₂), 38.6 (CH₂), 30.4 (CH₂), 28.9 (-C(CH₃)₃). HR-MS (ESI⁺/TOF): 920.4 [M+Na]⁺ (calculated 920.4), 936.4 [M+K]⁺ (calculated 936.4).



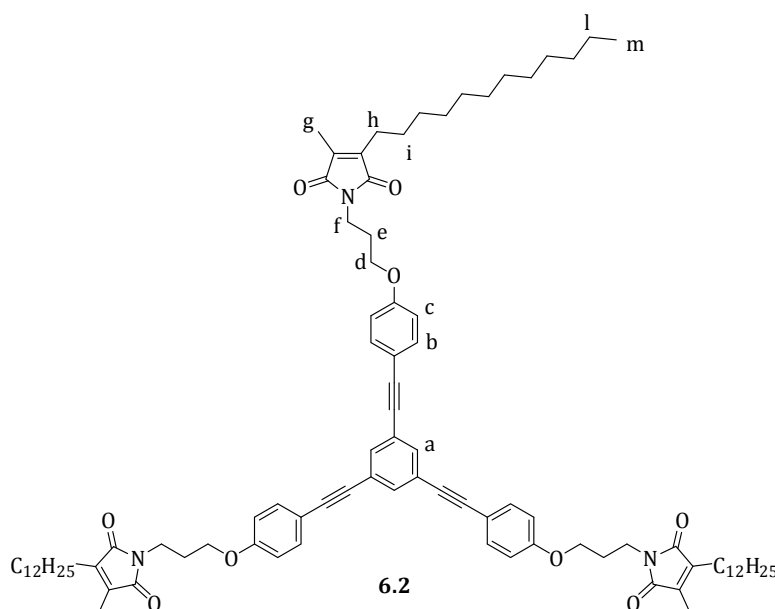
Synthesis of 3,3',3''-(4,4',4''-(benzene-1,3,5-triyltris(ethyne-2,1-diyl))tris(benzene-4,1-diyl))tris(oxy)tripropan-1-amine (**6.9**)

Procedure a) : In a microwave reactor equipped with a magnetic stirrer, **6.10** (0.105 gr, 0.12 mmol) was dissolved in 3 ml of dry dimethylformamide. The solution was warmed by microwave irradiation setting the parameters as to keep the temperature at 180°C for 10 minutes (PW 230 Watts). TLC analysis of the brown suspension revealed the disappearance of the reagent **6.10** and the appearance of a new spot characteristic of the desired product at R_f=0 (on SiO₂, with hexane : ethyl acetate 6:4 as eluent). After evaporation of the solvent under reduced pressure, a thick brown oil was obtained. The oil was washed twice with petroleum ether and used without any purification for the next step. The yield was quantitative.

Note: The product is only soluble in DMSO and sticks to the stationary phases for TLC (SiO₂, Al₂O₃ neutral), so it was directly used without any purification for the next step.

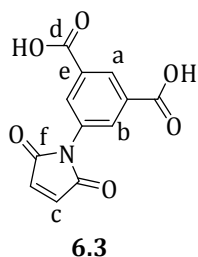
Procedure b): 6.10 (0.180 gr, 0.002 mmol) was dissolved in 10 ml of a solution 4 M of HCl in THF at 0°C. The mixture was stirred at 0°C for 10 minutes, then at room temperature (25°C) for 30 minutes. The solvent was evaporated under vacuum, then 10 ml of water were added, causing the precipitation of a white solid. The pH was basified at 14 by adding a solution of NaOH 0.01 M. The water phase was extracted with ethyl acetate (3 x 30 ml). The combined organic phases were dried on MgSO₄ and evaporated. Since NMR analysis revealed that the reagent was not completely deprotected, the reaction was restarted in the same conditions and let to stir at room temperature for 6 hours. The product was obtained with a 75% yield and used for the following reaction without further purification. (R_f=0 both on SiO₂ and Al₂O₃ neutral, with hexane : ethyl acetate 6:4 as eluent). ¹H-NMR (300 MHz, CD₂Cl₂): δ (ppm) 7.64 (s, 3H, Ar-H), 7.52 (d, 6H, J=8.7 Hz, Ar-H), 7.01 (d, 6H, J=8.7 Hz, Ar-H), 4.0-4.1 (m, 6H, CH₂), 2.7-2.9 (m, 6H, CH₂), 1.8-1.9 (m, 6H, CH₂).

Synthesis of 1,1',1''-(3,3',3''-(4,4',4''-(benzene-1,3,5-triyltris(ethyne-2,1-diyl))tris(benzene-4,1-diyl))tris(oxy)tris(propane-3,1-diyl))tris(3-dodecyl-4-methyl-1H-pyrrole-2,5-dione) (6.2)

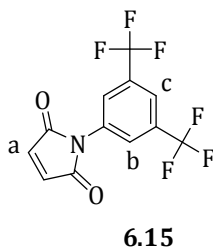


To the round bottom flask containing the triamine **6.9** (0.110 gr, 0.2 mmol), a solution of the alkylated maleic anhydride **6.4** (0.21 gr, 0.7 mmol) in 8 ml of dry toluene was added. The mixture was let to react at 111°C for 16 hours, giving a brown solution. Toluene was evaporated under reduced pressure. The obtained brown oil was re-dissolved in fresh dry toluene (6 ml) and transferred in a three necks flask, equipped with a dropping funnel

and argon entry. Zinc bromide (0.13 gr, 0.6 mmol) was added in one portion at room temperature, then the suspension was warmed at 80°C. It was added a solution of hexamethyldisilazane (0.15 gr, 0.19 ml, 0.9 mmol) in 2 ml of dry toluene drop by drop. It was let to react at 80°C for 5 hours then at room temperature (20-22°C) for 11 hours. The reaction was quenched by adding 25 ml of water. Ethyl acetate was added (30 ml), forming an emulsion. The emulsion was extracted with 2 x 30 ml of ethyl acetate, dried on MgSO₄ anhydrous and evaporated under reduced pressure. The product was obtained as an yellow oil by two column chromatography purifications on silica gel: 1) eluent hexane : ethyl acetate 6:4, allowed to recover clean the spots with R_f = 0.8 et 0.9; 2) this fraction was further chromatographed with eluent a) hexane : diethyl ether 95 : 5, then diethyl ether 100%, to recover the spot at R_f = 0. The yield was 20%. ¹H-NMR (500 MHz, CDCl₃): δ (ppm) 7.59 (s, 3H, Ar-H(a)), 7.48 (d, 6H, J=8.7 Hz, Ar-H(c)), 6.87 (d, 6H, J=8.7 Hz, Ar-H(b)), 4.00 (t, 6H, J=6 Hz, CH₂(f)), 3.68 (t, 6H, J=6.5 Hz, CH₂(d)), 2.36 (t, 6H, 7 Hz, CH₂(h)), 2.07 (m, 6H, CH₂(e)), 1.95 (s, 9H, CH₃(g)), 1.4-1.5 (m, 6 H, CH₂(i)), 1.2-1.3 (m, 54H, CH₂, chain), 0.88 (t, 9H, J=7Hz, CH₃(m)). ¹³C-NMR (125 MHz, CDCl₃): δ (ppm) 173.0, 172.7, 160.0, 141.9, 137.7, 134.0, 133.9, 125.1, 115.6, 115.3, 91.2, 87.3, 66.6, 35.8, 32.7, 30.1-30.4, 29.0, 28.9, 24.3, 23.4, 14.7, 9.2. HR-MS (MALDI, DCTB/TOF): m/z 1383.8790 found for C₉₀H₁₁₇N₃O₉, 1383.8790 calculated for C₉₀H₁₁₇N₃O₉.

Maleimide M3:**Synthesis of 5-(2,5-dioxo-2,5-dihydro-1H-pyrrol-1-yl) isophthalic acid (M3, 6.3)**

Maleic anhydride (1 gr, 10 mmol) and 5-amino isophthalic acid (1.81 gr, 10 mmol) were stirred at room temperature in 100 ml of THF for 3 hours. The solvent was evaporated under reduced pressure and the obtained maleanilic acid was dissolved in 100 ml of acetic anhydride. Sodium acetate (0.82 gr, 10 mmol) was added and it was let to react at 80°C for 3 hours. The solvent was partially removed (until about only 30 ml were left) under reduced pressure and ice-cold water (100 ml) was added to the mixture. The product, a yellow solid, precipitated after 1 hour and could be collected by filtration and washing with cold water and diethyl ether, with a yield of 50%. ¹H-NMR (300 MHz, CDCl₃): 8.4-8.5 (bs, 1H, Ar-H_a), 8.1-8.2 (m, 2H, Ar-H_b), 7.2-7.3 (bs, 2H, CH_c). ¹³C-NMR (75 MHz, CDCl₃): 169.6, 166.0, 134.9, 132.5, 132.1, 131.0, 128.6 (C_c). HR-MS (ESI-/TOF): m/z 260.0199 (found for C₁₂H₆NO₆), 260.0195 calculated for C₁₂H₆NO₆ [M-H]⁻. Melting point : decomposes before melting at 275°C (at air).

Maleimide MF (6.15):**Synthesis of 1-(3,5-bis(trifluoromethyl)phenyl)-1H-pyrrole-2,5-dione (MF, 6.15)**

3,5-Bis(trifluoromethyl)aniline (2.0 gr, 1.36 ml, 8.7 mmol) and maleic anhydride (0.85 gr, 8.7 mmol) were dissolved in 50 ml of dichloromethane and stirred for 2 hours at 50°C. It was obtained a white solid that was filtered, washed with dichloromethane and hexane and employed in the following step without any further purification.

The white salt dissolved in 40 ml of acetic anhydride and stirred for 16 hours at 120°C. Acetic anhydride was evaporated under reduced pressure. The product **6.15** was obtained pure as a white solid by sublimation at 66°C (-1 bar), with a global 77% yield. Melting Point: 83-85°C. ¹H-NMR (300 MHz, CDCl₃): δ (ppm) 7.95 (s, 2H, Ar-H(b)), 7.87 (s, 1H, Ar-H(c)), 6.94 (s, 2H, -CH-(a)). ¹³C-NMR (75 MHz, CDCl₃): δ (ppm) 168.7, 134.9, 133.3, 133.2, 132.7, 132.3, 125.8, 124.9, 121.3-121.5. ¹⁹F-NMR (282 MHz, CDCl₃): δ (ppm) -62.9.

Appendix A1

Scanning Tunnelling Microscopy (STM)

Scanning tunneling microscope has been invented in the early 1980s by G. Binnig and H. Rohrer¹, who were awarded the Nobel Prize in Physics in 1986 for their achievement. The operation principle relies on the quantum mechanical phenomenon known as “tunneling”. When a sharp metallic needle (tip) is placed at a short distance from a conducting material surface (sample) and a voltage is applied between them, the electrons can pass through the narrow vacuum barrier from the tip to the sample or vice versa, establishing a small tunneling current (I_t) (**Figure A1.1**). Due to the exponential dependence of the tunneling current value on the tip-sample distance, STM allows to image in the real space material surfaces with an atomic scale resolution ($I_t \propto U \cdot k_1 \cdot e^{-k_2 d}$, where I_t is the tunneling current, U is the potential applied to the sample, d is the tip-sample distance and k_1 and k_2 are constant factors).

The experiment consists in scanning the tip over a surface and can be run in one of two modes: *current control* and *voltage control*. In the *current control* mode, the electronic control system monitors the current between the sample and the tip and adjusts the voltage in order to keep the current value constant. The tip thus moves back and forth from the surface plane of the material and the recording of these little movements provides a map of the surface features. In the *voltage control* mode, the tip is held at a fixed distance from the surface and the variations in the current while scanning are measured. This signal can as well be employed in order to generate a map of the surface. The map does not reproduce the surface geometrical topography, but rather the conductance of the junctions tip-vacuum-adsorbate-surface.

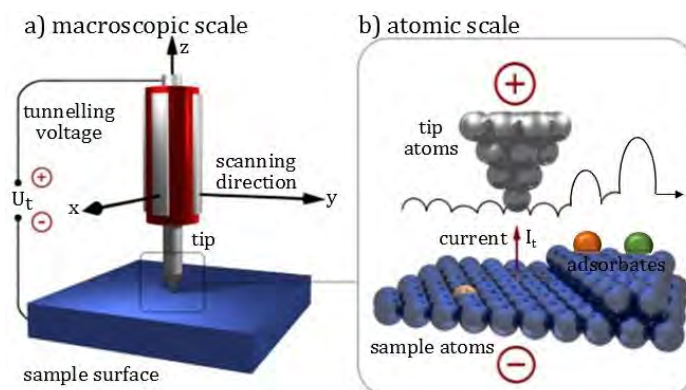


Figure A1.1 : Schematic representation of the working principle of Scanning Tunnelling Microscopy (STM) (picture adapted from: <http://www.ieap.uni-kiel.de/surface/ag-kipp/stm/stm.htm>).

STM can operate in a variety of environments: in ultra-high vacuum (UHV) (i.e. at pressures of the order of 10^{-10} - 10^{-11} torr), in air, or even at a solid-liquid interphase (i.e. the tip is immersed in a small drop of molecule-containing solution deposited on the surface).

The temperatures of the substrate can also be variable. It is possible to work at room temperature or to cool down the surface down to very low temperature values (for ex. 100 mK), or even to warm, typically up to 400-500K.

A1.1. STM as tool for molecular manipulation

STM can be employed not only for visualization, but also as a tool for molecular manipulation. STM-manipulations are based on different types of tip-sample interactions²:

1. Tip-sample mechanical interactions: rely on a physical action of the tip over the considered atom/molecule. They can be classified in:

- *lateral manipulations*: procedures allowing to relocate single atoms/molecules across a surface. Three modalities are possible: pushing (due to a repulsive tip-atom interaction), pulling (due to an attractive tip-atom interaction) and sliding (the atoms/molecules move together with the tip);

- *vertical manipulations*: involve the transfer of atoms/molecules between the tip and the surface. This kind of manipulation can be carried out also through an electrostatic interaction between tip/molecule.

2. Electric field between tip and sample: The atomic/molecular manipulation is carried on by applying a voltage between the tip and the sample. By changing the bias polarity, the atoms/molecules bearing a dipole can experience attractive or repulsive forces from the tip (biases inferior to 3 V are employed in order to avoid the breaking of chemical bonds), which can cause adsorption/desorption of atoms/molecules between tip and surface.

3. Inelastic tunneling electrons:

Low energy tunneling electrons or holes can be injected to a molecule on the surface by positioning the STM tip above it. By applying to the tip a selected potential and tunneling current value, for a certain time period (procedure defined as “pulse”), a quote of tunneling electrons (or holes) is transferred from the tip to the atom/molecule through a resonance state leading to various excitations (rotational, vibrational or electronic). By opportunely adjusting the potential (determining the energy of excitation) and the tunneling current values (determining the rate of excitation¹³, it is possible to bring a particular molecular bond to a certain excited state, that will

¹ As an indication, typical values for imaging on metallic surfaces are of the order of hundreds of mV for the potentials and currents ranging from 10 pA to 1 nA; typical values for the bias voltages are instead larger than ± 2 V and currents between 0.2 and 30 nA. In general, the typical electron/hole absorption yields are low and range between 10^{-11} to 10^{-6} events per electron (from reference³).

ultimately relax leading to a local warming (i.e. the energy is dissipated as heat) or to a precise chemical transformation (for ex. conformational changes, translations or even bond breaking/formation).

One example where different kinds of STM molecular manipulations are employed in order to drive an Ulmann reaction is reported in **Figure A1.2**⁴.

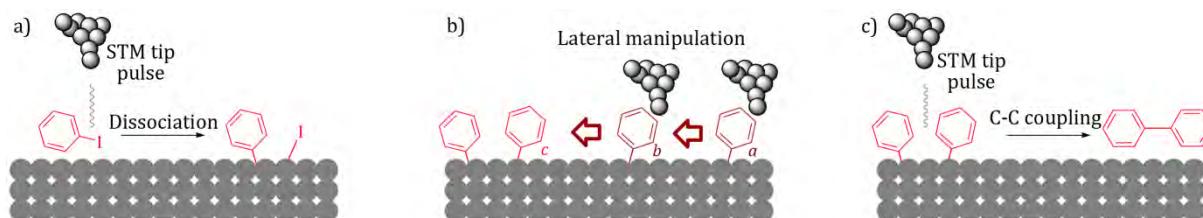


Figure A1.2: Examples of molecular manipulations involving inelastic electron tunnelling processes on a Cu(111) surface: a) C-I dissociation is induced by an STM-tip pulse (the radicals are stabilized by the formation of a carbon-metal and iodine-metal bonds); b) the aryls are brought closer by lateral manipulation; c) C-C coupling to yield a biphenyl is as well induced by a STM tip pulse (from reference 4).

A1.2. References

¹ Binnig, G., Rohrer, H., Gerber, Ch., Weibel, E., *Phys. Rev. Lett.*, **1982**, 49, 57.

² Hla, S.-W., *J. Vac. Sci. Tech. B*, **2005**, 23, 1351-1360.

³ Mayne, A. J., Dujardin, G., Comtet, G., Riedel, D., *Chem. Rev.*, **2006**, 106, 4355-4378.

⁴ Hla, S.-W., Bartels, L., Meyer, G., Rieder, K.-H., *Phys. Rev. Lett.*, **2000**, 85, 13, 2777-2780.

Appendix A2

The surfaces

A2.1 Epitaxial Graphene on Silicon Carbide (0001)

The term “epitaxy” (deriving from the Greek, “epi” = “upon”, and “taxis” = “arrangement”) refers to the process of growing a crystalline overlayer on top of another crystalline substrate, in conditions where the underlying crystal determines the new layer’s structure. The result is that in an epitaxial layer the atoms have a particular registry (i.e. location) relative to the underlying crystal.

Experimentally, the growth of epitaxial graphene on silicon carbide can be done both on the silicon-terminated or carbon-terminated face of the wafers. In general, the growth on carbon-terminated faces presents more difficulties related to the control of number of graphene layers produced¹. In our case, the graphene has been grown on a silicon terminated wafer face, and all through the manuscript the material will be indicated as G/SiC(0001) (more precisely, G/6H-SiC(0001)).

The reasons dictating the choice of silicon carbide wafer as supporting substrates are: a) the possibility of easier manipulation of supported graphene over free-standing graphene (i. e. without a substrate); b) silicon carbide semiconducting substrates appear as the most promising substrate in the aim of integration of graphene in electronic applications; c) the epitaxial G/SiC(0001) surface presents flat areas extended over hundreds of square nanometers and constitutes a very adapted substrate for the study of molecular self-assembly and STM imaging.

Experimentally, epitaxial growth of graphene can be carried out by a controlled thermal decomposition of silicon carbide, in UHV conditions or in an argon atmosphere, following a two steps procedure^{1, 2} (**Figure A2.1**):

1) *First annealing of SiC at high temperature (~1100°C)*: this procedure leads to the decomposition of SiC, with consequent evaporation of Si and accumulation of C atoms to form a carbon-rich surface layer, named as “carbon buffer layer” (or “carbon nanomesh”, or “interfacial graphene”);

2) *Second annealing at higher temperature (≥1200°C)*: the second annealing process determines the growth of the graphene layer over the buffer layer. In particular, depending on the annealing temperature and time, monolayer graphene (for eg. ~1200°C for 2 minutes), bilayer graphene (for eg. ~1250°C for 2 minutes), or trilayer graphene (for ex. > 1300°C, for 2 minutes) can be obtained.

By adapting the different combinations of time and temperature, substrates covered by different percentage areas of monolayer or bilayer graphene can be grown. Graphene mono and bi-layers are grown without discontinuities at the domain boundaries and uniformly cover the whole wafer surface (see **Figure A2.2c**).

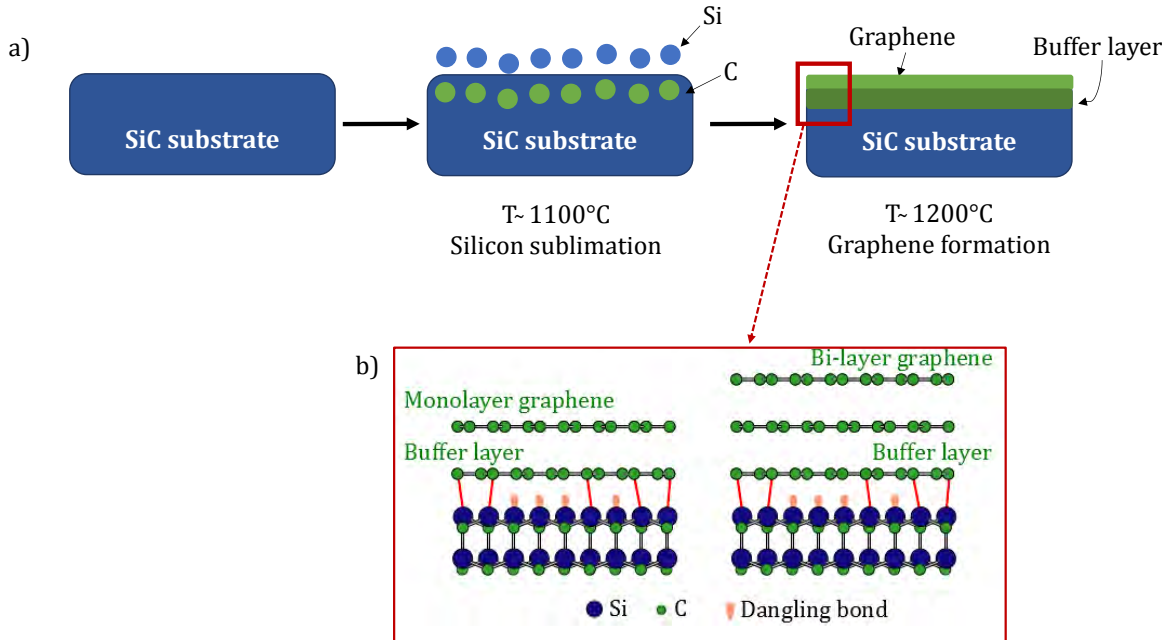


Figure A2.1 : a) Schematic representation of the mechanism of epitaxial graphene growth; b) schematic representation of the atomic structure of mono and bi-layer epitaxial graphene on silicon carbide (from reference 1).

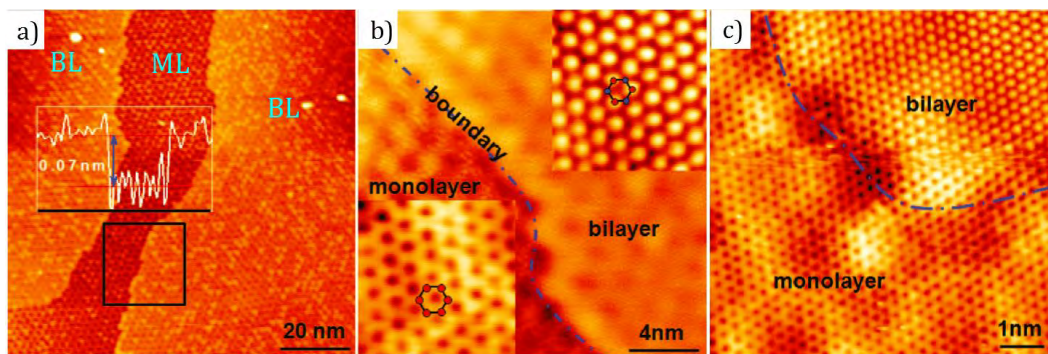


Figure A2.2 : Typical STM images of epitaxial graphene on SiC(0001) (from reference 1): a) topographic picture taken over a $100 \times 100 \text{ nm}^2$ area ($U_t = 1.78 \text{ V}$): in the image, two bright areas can be observed, separated by a darker one. The areas showing a brighter contrast are bilayer graphene (BL); the darker area is, instead, covered by a monolayer graphene (ML). The apparent height difference between the terraces is $0.07 \pm 0.01 \text{ nm}$; b) high-resolution STM image ($20 \times 20 \text{ nm}^2$, $U_t = 0.5 \text{ V}$). The insets show two atomic resolution pictures, of monolayer and bilayer graphene respectively. It can be noticed that in the case of monolayer graphene, it is possible to detect by STM all the atoms of the graphene unit cell, showing in the image a hexagonal lattice (underlined by the red hexagon superimposed in the picture). Bilayer graphene can instead be distinguished, since only one out of two carbon atoms can be detected by STM, like for HOPG.

The *buffer layer* is not eliminated during the graphene growth procedure and is visible as particular periodic pattern in STM images (period $\sim 2 \text{ nm}$), appearing for certain bias voltages

values (**Figure A2.2**). It is partially covalently bound to the underlying silicon carbide substrate, while graphene is interacting with it by van der Waals forces (**Figure A2.1**). As a consequence of the physical structure, G/SiC(0001) surface is extremely flat, without geometrical or electronic corrugations at the atomic level. This determines, as a first consequence, a high diffusivity of the molecules when deposited on the surface. From an electronic point of view, the presence of the buffer layer determines a n-doping of graphene, due to charge transfer, which may influence its chemical reactivity^{3,4}.

A2.2 Highly Oriented Pyrolytic Graphite (HOPG)

A highly pure 3D-ordered form of graphite, named after Highly Oriented Pyrolytic Graphite (HOPG), can be produced by annealing at high temperatures (above 3000°C) and high pressures pyrolytic carbon (i.e. obtained by pyrolysis of organic compounds). This material is characterized by the presence of large uniform and smooth terraces and pronounced chemical inertia and so is apt to being employed as substrate for molecular self-assembling studies and STM characterization, both in UHV⁵ and ambient conditions⁶.

The terraces are delimited by high step edges, constituted by dozens of carbon atoms sheets, superimposed in a “quasi perfect” lamellar structure, stacked in a ABABAB (Bernal) fashion. The Bernal stacking determines the possibility of detecting only one atom over two in the graphene hexagons by STM (**Figure A2.3**).

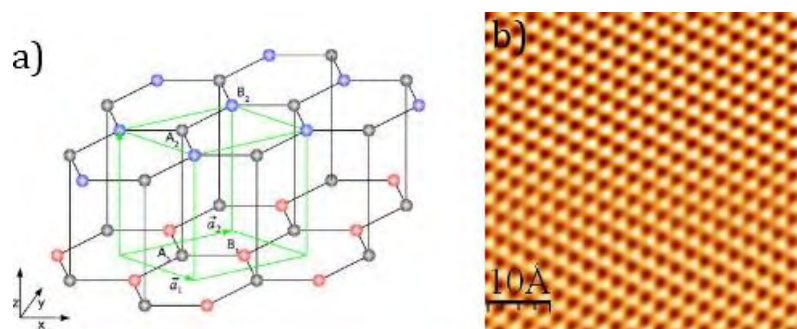


Figure A2.3: a) Bernal stacking(ABABAB...) between graphene layers in graphite; b) STM atomic resolution image of HOPG ($I_t=0.3$ nA, $U_t=-50$ mV).

A2.3 Mechanically exfoliated graphene on oxidized silicon

Graphene flakes of different thickness can be obtained through mechanical exfoliation (for ex. by employing scotch tape) from various graphitic materials, such as HOPG or natural graphite. The process takes benefit from the layered structure of graphite, characterized by weak interactions between the different layers.

Once produced, the thin graphite flakes and the graphene sheets can be deposited on oxidized silicon (SiO_2/Si) wafers. Generally the thickness of the SiO_2/Si substrate employed is ~ 300 nm and the area of the wafers 1×1 cm^2 .

Once deposited on the substrate, the obtained layers are initially observed under the optical microscope to identify single layer regions, from their characteristic colour and contrast against the oxidized silicon wafer (**Figure A2.4**). Further confirmations on the thickness are obtained by Raman spectroscopy and Atomic Force Microscopy (AFM) characterization.

Although by this methodology graphene of the highest quality is produced (i.e. characterized by the presence of the lowest density of defects), the method suffers of some limits, such as the lack of reproducibility and scalability. The sample to sample variability is high, both for the density of coverage of the wafer and the number and sizes of the different flakes. The density of coverage is generally rather small: only about the 10-15% of the surface is covered by graphite/graphene and for each sample 3-10 monolayer flakes of dimensions allowing Raman characterization (i.e. area larger than $4 \mu\text{m}^2$) are usually found. The distribution of areas of the monolayers is generally very broad, spanning from $\sim 0.5 \mu\text{m}^2$ to $\sim 1000 \mu\text{m}^2$.

The small flakes sizes determine a need for dedicated characterization (ex. micro-Raman, micro-XPS...).

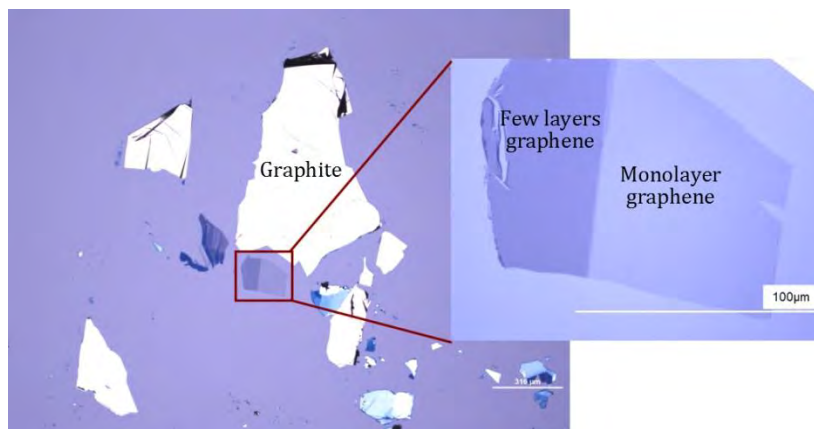


Figure A2.4: Optical image (white light) of the exfoliated graphene layers on 290 nm thick oxidized silicon wafers and enlarged view of single layer region, shown as inset (from reference 7).

A2.4 References

- ¹ Riedl, C., Coletti, C., Starke, U., *J. Phys. D: Appl. Phys.*, **2010**, *43*, 374009.
- ² Huang, H., Chen, W., Chen, S., Wee, A. T. S., *ACS Nano*, **2008**, *2*, 12, 2513-2518.
- ³ Wang, Y.-L., Ren, J., Song, C.-L., Jiang, Y.-P., Wang, L.-L., He, K., Chen, X., Jia, J.-F., Meng, S., Kaxiras, E., Xue, Q.-K., Ma, X.-C., *Phys. Rev. B*, **2010**, *82*, 245420, 1-5.
- ⁴ Paulus, G. L. C., Wang, Q. H., Strano, M. S., *Acc. Chem. Res.*, **2013**, *46*, 1, 160-170.
- ⁵ Ludwig, C., Gompf, B., Petersen, J., Strohmaier, R., Eisenmenger, W., *Z. Phys. B*, **1994**, *93*, 365-373.
- ⁶ Mali, K. S., Adisoejoso, J., Ghijsens, E., De Cat, I., De Feyter, S., *Acc. Chem. Res.*, **2012**, *45*, 8, 1309-1320.
- ⁷ Zan, R., Ramasse, Q. M., Jalil, R., Bangert, U., Atomic Structure of Graphene and h-BN Layers and Their Interactions with Metals, <http://dx.doi.org/10.5772/56640>.

Appendix A3

Conception, synthèse et études de molécules pour la fonctionnalisation du graphène

A3. 1 Introduction

Le graphène est un allotrope de carbone bidimensionnel où les atomes de carbone sont hybridés sp^2 et organisés dans un réseau en "nid d'abeille". Les études expérimentales ne sont devenues possibles que très récemment¹, après la première découverte d'une procédure facile et reproductible, permettant par exfoliation mécanique (i.e par des techniques utilisant la méthode "scotch-tape"ⁱ), d'obtenir des feuilles de graphène à partir de graphite.

Avant de pouvoir employer du graphène dans un certain nombre d'applications, trois problèmes doivent être surmontés : 1) les stratégies de production doivent être améliorées et standardisées afin de garantir des quantités de graphène adaptées à des applications industrielles^{2,3,4} ; 2) des méthodes reproductibles doivent être développées, à la fois pour la manipulation à large échelle du matériau, et permettre le contrôle de ses propriétés. En particulier, les propriétés électroniques doivent être adaptées aux fonctions désirées en fonction des dispositifs⁵. Un exemple consiste à permettre l'ouverture d'un gap entre les niveaux énergétiques pour transformer le graphène en semi-conducteur et pouvoir l'introduire dans une nouvelle génération des puces électroniques.

Dans ce contexte, différentes stratégies ont été envisagées. Il a été montré que celles utilisant des schémas de fonctionnalisation chimique covalente ou non-covalente, considérées comme extrêmement prometteuses⁶, pouvaient être viables. Cependant, de nombreuses questions restent encore ouvertes, concernant en particulier la possibilité de contrôler les sites de fonctionnalisation. En effet, si différentes méthodes permettant ce contrôle avec une précision nano or micrométrique⁷⁻¹¹ ont été proposées, il n'est pas encore possible de maîtriser la réactivité du graphène en dessous du nanomètre.

Ce travail de thèse se situe dans ce contexte. En particulier, la fonctionnalisation du graphène est envisagée à partir du point de vue de la chimie supramoléculaire de surface, où le microscope à effet tunnel, ou STM (Scanning Tunneling Microscope) peut être utilisé soit pour visualiser les atomes

ⁱ Des tentatives de croissance du graphène sur des surfaces cristallines ont commencé dès les années des années 1970, mais les interactions avec la surface étaient si fortes qu'il n'était pas possible de mesurer expérimentalement les propriétés du matériau.

et les molécules soit comme moyen d'activation des réactions chimiques. L'objectif général de cette thèse est de concevoir et de préparer des molécules permettant cette fonctionnalisation contrôlée du graphène (**Figure A3.1**).

Une partie des molécules synthétisées a été étudiée, ou est encore en cours d'étude, sur différentes surfaces de graphène, dans le cadre de collaborations avec plusieurs groupes en France et Chine.

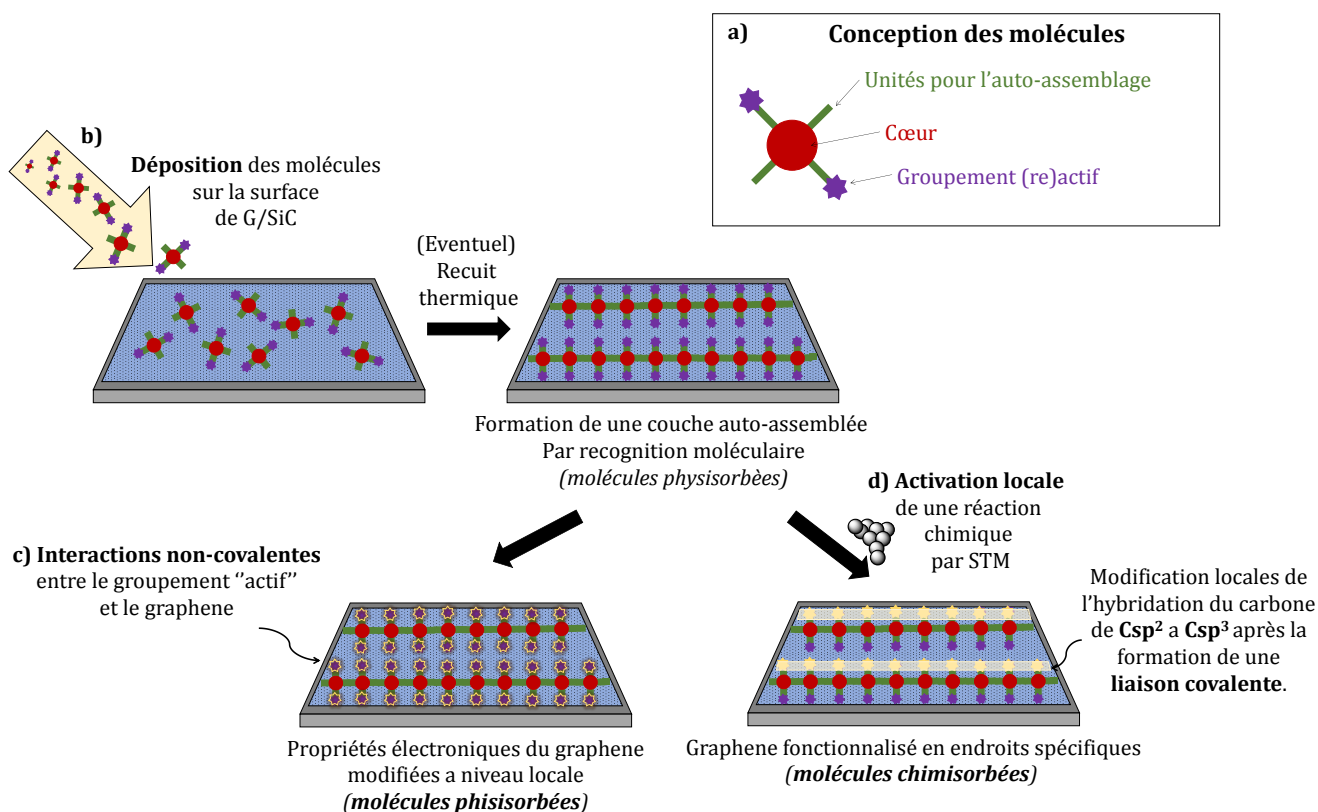


Figure A3.1: Objectif générale du projet.

Les molécules synthétisées présentent trois caractéristiques structurales communes (**Figure A3.1**):

- 1) un *cœur polyaromatique*, favorisant l'absorption des molécules sur le graphène, par interactions π - π ;
- 2) un *"groupe(m)nt actif"* capable d'interagir avec le graphène soit par transfert de charge soit par réaction chimique, conduisant à la formation d'une liaison covalente. Dans le deuxième cas, la réaction chimique doit être activée sous pointe STM, de manière de garantir la possibilité de choisir les sites de fonctionnalisation avec une précision atomique;
- 3) différents groupements permettant l'auto-assemblage et l'organisation des molécules sur la surface, de façon à limiter la diffusion moléculaire (généralement importante sur des surfaces de graphène épitaxie sur carbure de silicium, G/SiC) et aussi pour définir une organisation géométrique précise des groupements actifs sur la surface.

La conception des molécules devait aussi prendre en considération les différentes contraintes expérimentales liées à l'environnement ultravide. Le paramètre le plus importante était la stabilité thermique des fonctionnalités chimiques, de façon à permettre la sublimation sous UHV et le transfert des molécules sur la surface.

A partir de ces considérations et de la littérature existante, des solutions originales ont été proposées. Pour la fonctionnalisation *non-covalente* du graphène/SiC, nous avons synthétisé un dérivé de tetrathiafulvalene (**TTC₁₂-TTF**, **2.1**) (**Schéma A3.1**) et initié la synthèse d'un **hexaphenanthrocoronène** (**3.1**, **Schéma A3.2**). Pour ces deux molécules, les groupes d'autoassemblage sont des chaînes alkyles et les parties actives riches sont des composés planaires donneurs d'électrons.

A3. 2 Synthèse et études d'un dérivé de tetrathiafulvalene

Le tetrathiafulvalene^{12,13} (TTF) est un composé non-aromatique avec 14 électrons π , caractérisé par des propriétés de donneur d'électrons très intéressantes: la molécule possède, en effet, trois états d'oxydation stables, à des valeurs de potentiel relativement basses ($E_{1/2}^1 = 0.37$, $E_{1/2}^2 = 0.67$ vs SCE in CH_2Cl_2 ¹⁴). Le cœur TTF peut être fonctionnalisé de beaucoup des façons différentes, permettant de moduler son comportement électronique et lui donnant de nouvelles propriétés.

La molécule synthétisée est le **TTC₁₂-TTF 2.1**, **Schéma A3.1**. Le cœur est fonctionnalisé par quatre chaînes alkyles $-\text{C}_{12}\text{H}_{25}$. La présence des chaînes a pour but de: 1) favoriser l'adsorption des cœurs des molécules sur la surface; 2) favoriser l'organisation des TTFs en couche "non-compacte" sur la surface, permettant d'étudier leur interaction électronique avec le graphène.

La synthèse a été conduite en trois étapesⁱⁱ, avec un rendement global de 9% (**Schéma A3.1**).

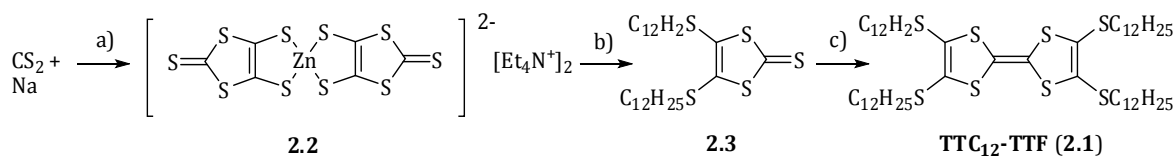


Schéma A3.1: Synthèse du dérivé **TTC₁₂-TTF (2.1)** : a) i) DMF anhydre, 0-25°C, 19h ; ii) ZnCl_2 , NH_3 aq. (28%), 30 mins.; iii) TEAB, H_2O , 18h, 25°C, 27% ; b) $\text{C}_{12}\text{H}_{25}\text{Br}$, acetone, 60°C, 18h, 100% ; c) $\text{P}(\text{OEt})_3$ anhydre, 130°, 6h, 32%.

Les propriétés d'auto-assemblage sur surface ont été étudiées par STM en UHV sur une surface de graphène épitaxie sur carbure de silicium et également à l'interface solide/liquide sur HOPG et graphène épitaxie sur carbure de siliciumⁱⁱⁱ.

ii La molécule a été synthétisée en suivant une procédure du Prof. M. Sallé (Université d'Angers, France).

Les études en UHV ont montré un réseau de molécules auto-assemblées très dense, avec une conformation *edge-on* des cœurs (dans une orientation "perpendiculaire" à la surface, **Figure A3.1**). Cette conformation originale, adoptée par ces dérivés en ultra-vide sur graphène/SiC, a été expliquée par un effet de «molecular fastener»¹⁵, induit par les chaînes alkyles. Les très fortes interactions de Van der Waals entre les chaînes, forcent les cœurs à interagir entre eux par interactions π - π , plutôt qu'avec le graphène. Ce type de mécanisme avait déjà été observé dans des cristaux, mais cette observation est la première au niveau moléculaire, où la conformation est induite par l'effet combiné de l'environnement ultra-vide et les interactions très faibles avec la surface du graphène.

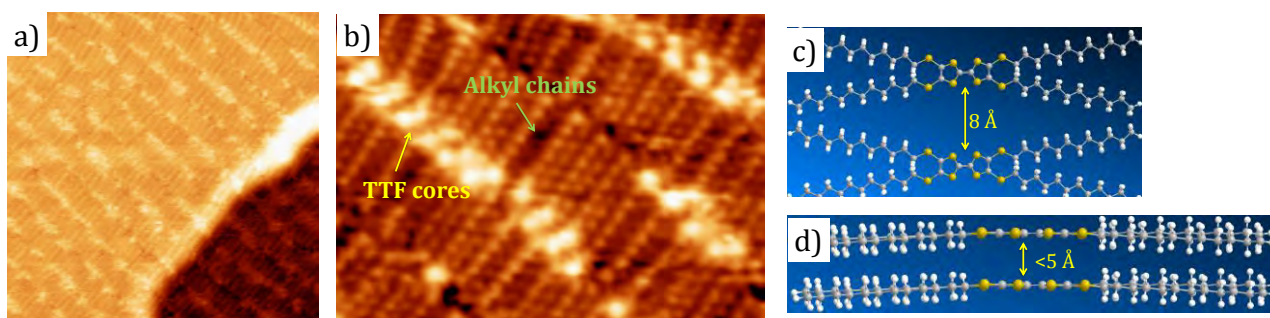


Figure A3. 1: a) Image STM de **TTC₁₂-TTF (2.1)** sur G/SiC en UHV ($U_t = -1.6$ V, 20×20 nm²) qui montre la continuité de l'assemblage moléculaire sur les bords de marche du graphène; b) zoom ($U_t = -1.6$ V, 6.4×6.4 nm²) qui montre la conformation *edge-on* adoptée par les molécules en UHV sur G/SiC; c et d) Model moléculaire de deux molécules de **TTC₁₂-TTF**: la distance entre les cœurs est de 8 Å quand ils sont planaires sur la surface (c), mais elle est inférieure à 5 Å si les molécules adoptent une conformation *edge-on* (d).

La structure électronique des molécules n'est pas perturbée après absorption sur le graphène. De plus la très faible distance entre les cœurs (< 5 Å) suggère une possibilité de conduction électronique par ces structures auto-assemblées¹⁶. Si un transfert de charge ne peut pas être mesuré entre les molécules et le graphène, par contre le substrat graphène/SiC en UHV paraît comme une surface idéale pour la génération de fils supramoléculaires de dérivés alkyles du TTF.

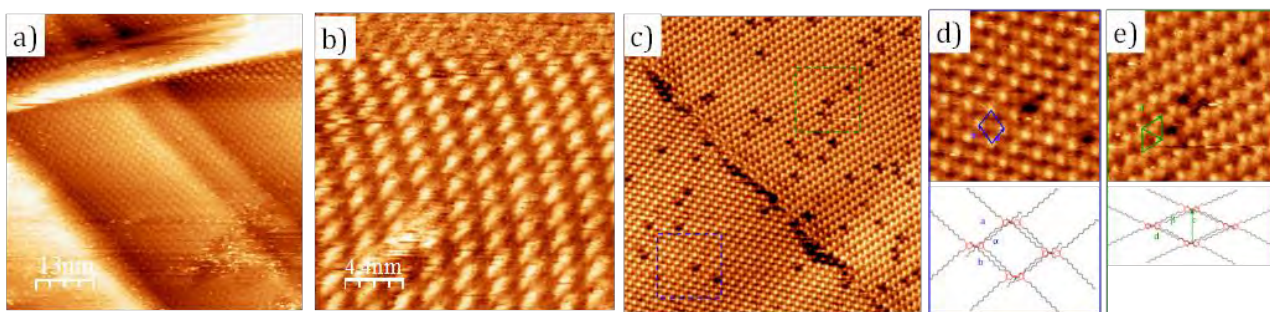


Figure A3.2: a et b) Images STM de **TTC₁₂-TTF (2.1)** sur G/SiC(0001) dans le 1-phenyloctane: a) $U_t = -1$ V, $I_t = 40$ pA, 66.4×66.4 nm²; b) $U_t = -1$ V, $I_t = 40$ pA, 22×22 nm². Les cœurs des molécules sont parallèles à surface ; c, d, e) Images STM de **TTC₁₂-TTF (2.1)** sur HOPG dans le 1-phenyloctane (solutions 2M): b) topographie ($U_t = -1.1$ V and

iii Les études STM en UHV et à l'interface liquide/solide ont été faites par le groupe de L. Simon à l'institut IS2M de Mulhouse (France). J'ai participé au le criblage initiale des conditions de mesure et en produisant les premières images STM à l'interface liquide/solide sur HOPG et G/SiC(0001).

$I_t = 7$ pA, $70 \times 70 \text{ nm}^2$); b) et c) zoom des domaines ($U_t = -1.1 \text{ V}$ and $I_t = 7$ pA, $15 \times 15 \text{ nm}^2$) and Schéma des assemblages moléculaires. Les cœurs des molécules sont planaires sur la surface. Paramètres des mailles : $a = 1.54 \pm 0.04$ nm, $b = 1.87 \pm 0.18$ nm et $\alpha = 73^\circ \pm 4^\circ$; $c = 1.55 \pm 0.03$ nm, $d = 1.90 \pm 0.20$ nm et $\beta = 65^\circ \pm 2^\circ$.

Les études à l'interface solide/liquide ont permis d'analyser le rôle des différents environnements (UHV ou liquide) et substrats (HOPG or G/SiC (0001)) dans la détermination de la conformation moléculaire après absorption. En particulier, sur HOPG et G/SiC(0001), dans le 1-phenyloctane, une géométrie d'absorption des cœurs parallèle à la surface a été observée, avec les cœurs en interaction π - π avec le graphène. Ce comportement a été expliqué en considérant le rôle du solvant dans la stabilisation de la structure poreuse et en empêchant l'interdigitation des chaînes alkyles.

A3. 3 Synthèse de un dérivé hexaphenanthrocoronène

Le **hexaphenanthrocoronène 3.1** est caractérisé par (**Schéma A3.2**):

1) 25 anneaux benzéniques fusionnés, pour un total de 78 atomes de carbone dans le cœur aromatique. Grace à sa structure, le cœur devrait donner un' interaction forte avec la surface ;

2) Six chaînes alkyles périphériques, avec deux fonctions :

a) elles doivent améliorer la solubilité des intermédiaires synthétiques, simplifiant les procédures de synthèse et purification. En fait, il est connu que les dérivés PAH (Hydrocarbures Aromatiques Polycycliques) sont très peu solubles, conséquence des interactions π - π entre les cœurs aromatiques et que de telles chaînes alkyles peuvent augmenter leur solubilité

b) elles sont censées diriger l'organisation moléculaire sur la surface de graphène, par interactions de van der Waals, de façon de laisser des zones non-fonctionnalisées sur la surface.

Le **hexaphenanthrocoronène 3.1** peut être obtenu à partir du précurseur hexabiphénylebenzène **HBB (3.2)** (**Schéma A3.2**).

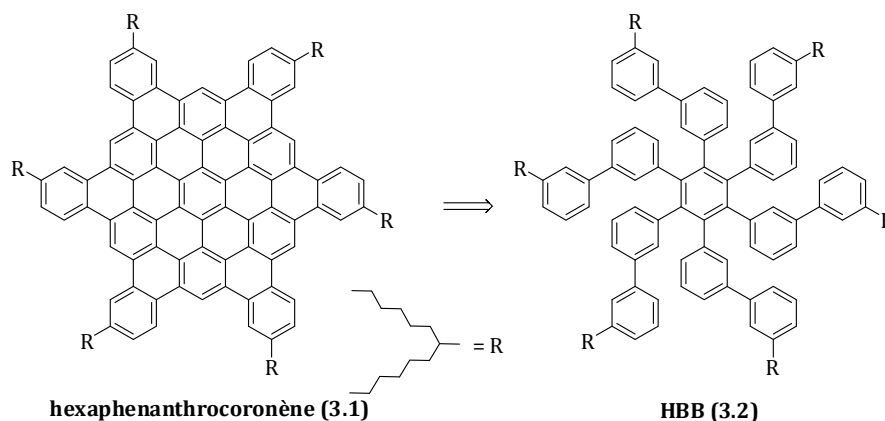


Schéma A3.2: Analyse rétro synthétique du **hexaphenanthrocoronène 3.1**.

Les étapes de synthèse sont décrites dans les **Schéma A3.4** et **Schéma A3.3**. Dans un premier temps, le précurseur **3.3** est synthétisé. Les différentes étapes comprennent : a) un homocouplage par cuprate de "Lipshutz" ou une réaction d'Ullmann; b) une lithiation, suivie de l'addition à du dihexylcétone; c) Une réduction de la fonction alcoolique par le triéthylsilane; d) Un échange bromo-iodure, par intermédiaire lithié ou par catalyse au cuivre ; e) Une double Sonogashira « one-pot ». L'alcyne **3.3** est ensuite cyclotrimerisé par catalyse au cobalt octa-carbonyle¹⁷ pour donner **HBB 3.2**. Le rendement de toutes ces étapes a été optimisé jusqu'à 19-26%.

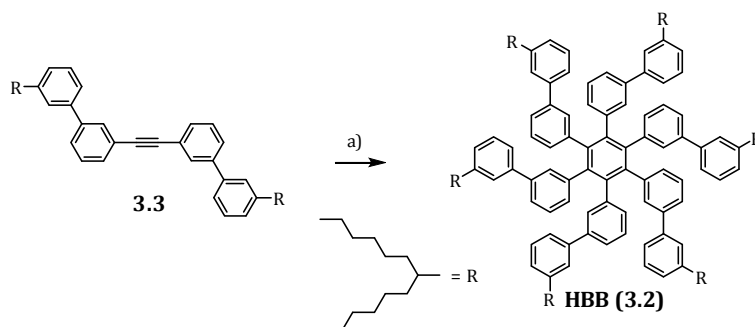


Schéma A3.3: Cyclotrimerisation conduisant au **HBB 3.2**. Conditions: a) $\text{Co}_2(\text{CO})_8$ (5%), dioxane anhydre, 111°C, 40h, 72%.

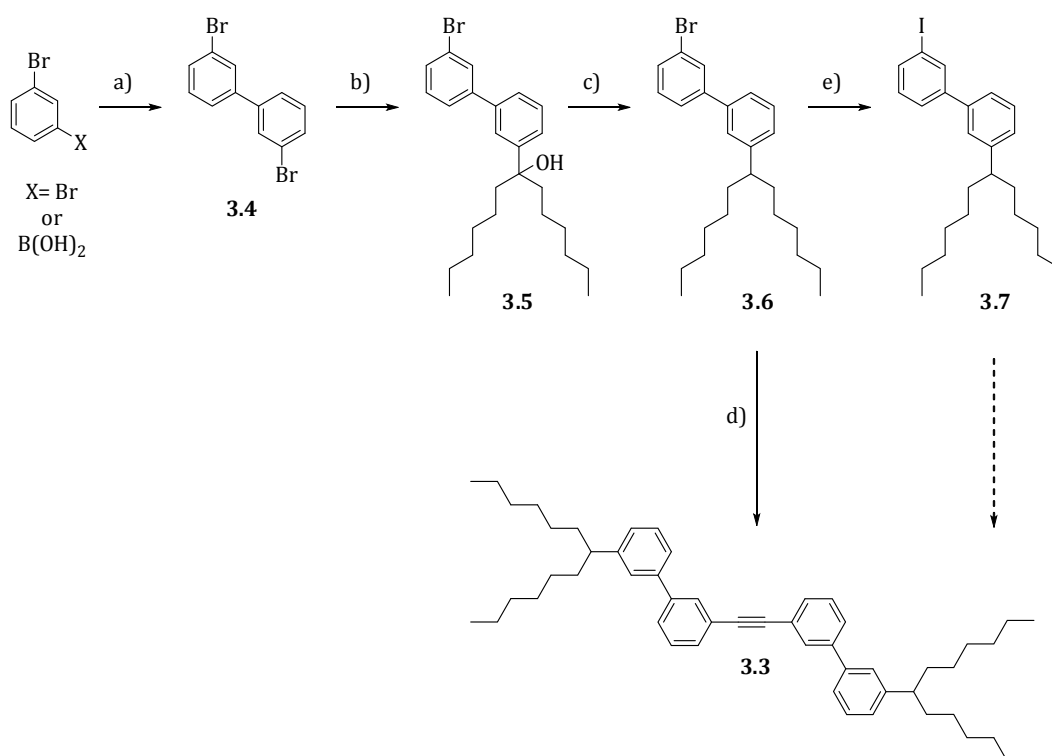


Schéma A3.4: Synthèse du précurseur **3.3**. Conditions: a) i: *t*-BuLi (1.1 eq.), Et₂O sec, -78°C, 1.5h; ii: CuCN (0.5 eq.), 22°C, 5 mins.; iii: tetraméthyl-*p*-benzoquinone (1.4 eq.), 23°C, 3h, 89% ou: a) CuCl (2%), MeOH, 19h, 21°C, 63%; b) i: *n*-BuLi (1 eq.), Et₂O sec, -78°C, 45 mins.; ii: dihexylcétone (1.05 eq.), Et₂O sec, -45°C -> 21°C, 17h, 69% wt/wt (impur à 5.4%); c) Et₃SiH (3 eq.), TFA (3 eq.), CH₂Cl₂ dry, -35°C-0°C, 3h, 78%; d) i: *n*-BuLi (1.1 eq.), THF distillé, -78°C, 1.5h; ii: I₂ (2 eq.), THF distillé, 22°C, 1 h, 11%; ou CuI (10%), NaI (2.5 eq.), (+/-)-trans-1,2-diaminocyclohexane (0.23 eq.), dioxane anhydre, 110°C, 70h, 89% wt/wt, 90% of **3.7**; e) TMSA (0.5 eq.), Pd(PPh₃)₂Cl₂ (6%), CuI (10%), DBU (6 eq.), H₂O (4 eq.), toluène anhydre, 80°C, 72h, 78%.

La dernière étape de cyclodehydrogénation oxydative a été faite en utilisant le couple DDQ/H⁺ comme système oxydant. A ce jour, le produit cible **hexaphenanthrocoronène 3.1** n'a pas encore été obtenu. En effet, les premiers essais ont montré que les conditions de cyclodehydrogénation conduisaient également à l'oxydation des carbones benzyliques pour donner des alcènes. Une seconde difficulté est due aux agrégations π - π intermoléculaires qui conduisent à des élargissements de pics en ¹H-NMR, même à température relativement élevée (pour un échantillon de concentration $\sim 8 \times 10^{-3}$ M) ce qui rend difficile leur caractérisation. La troisième difficulté tient au fait qu'une cyclodehydrogénation et une oxydation du carbone benzylique conduisent à deux produits de même poids moléculaires indiscernables par spectroscopie de masse. Les travaux en cours ont pour objectif d'accéder à notre molécule cible en passant par l'intermédiaire **hexaphenanthrocoronène-12H** (**Figure A3.4**), dont les positions benzyliques seront ensuite ré-hydrogénées

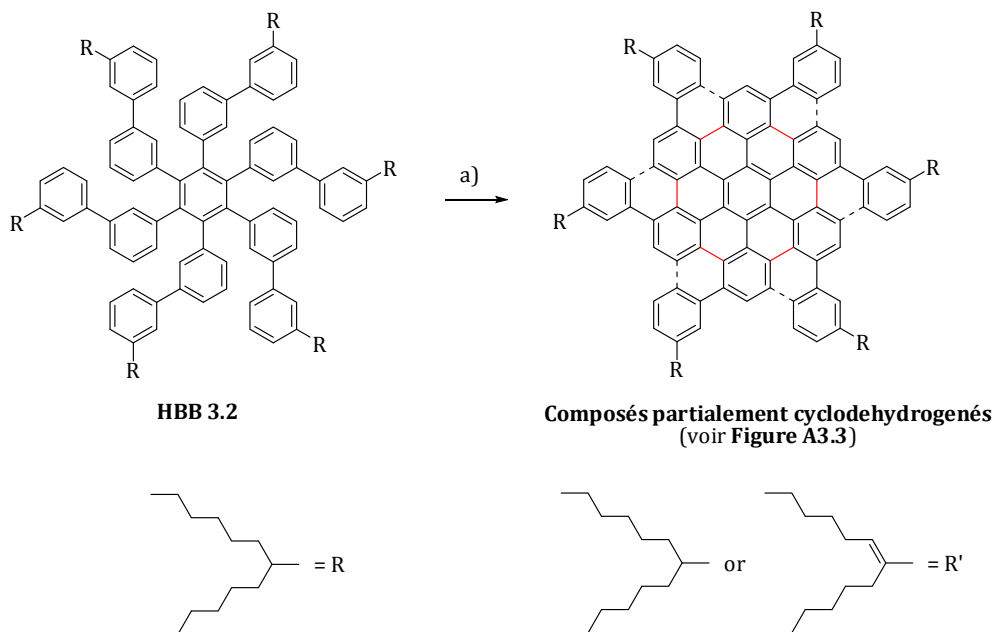


Schéma A3.5: Cyclodehydrogénation de **HBB 3.2** conduisant à des composés partialement cyclodéhydrogénés. Conditions: a) DDQ (12 eq.), acide triflique / CH₂Cl₂ 1:9, 0-5°C, 30 mins., 93%.

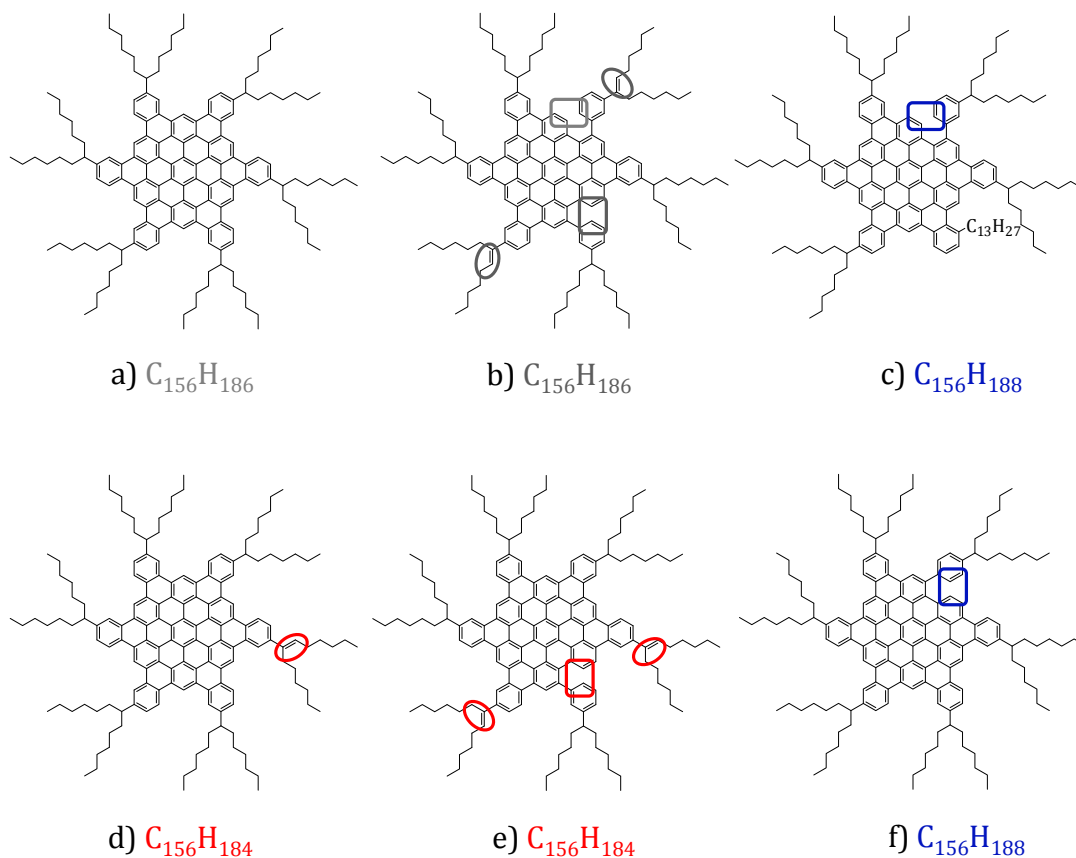
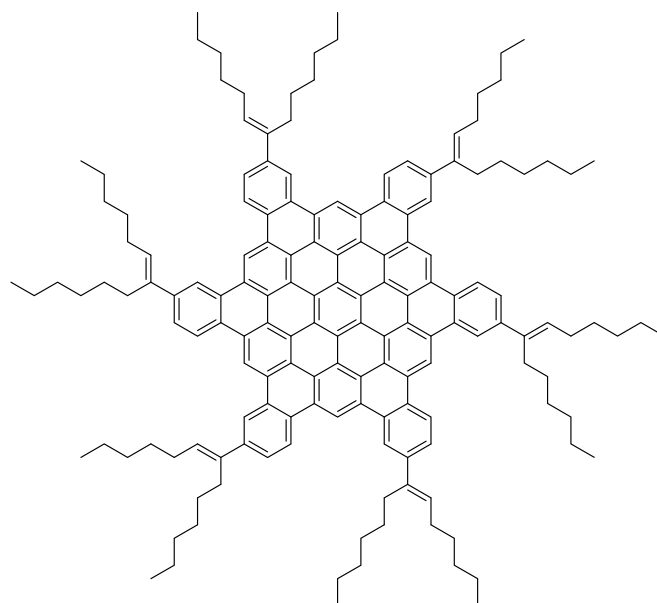


Figure A3.3: Possible isomères formés durant l'étape de cyclodehydrogenation oxydative: a) est l'isomère souhaité.



$C_{156}H_{174}$
hexaphenanthrocoronène-12H

Figure A3.4: Hexaphenanthrocoronène caractérisé par six positions benzyliques oxydés (**hexaphenanthrocoronène-12H**).

Dans une deuxième partie de la thèse, notre objectif a été d'employer les concepts de la chimie supramoléculaire sur surface pour diriger l'organisation des groupements fonctionnels sur une surface de graphène épitaxie sur carbure de silicium. Les molécules possèdent des groupements fonctionnels conçus pour interagir avec le graphène par formation d'une *liaison covalente*. Ces études ont été motivées par la possibilité de produire des modifications fortes des propriétés électroniques du matériau. En effet, la réaction covalente a comme objectif de modifier l'hybridation des atomes de carbone de sp^2 à sp^3 , et ainsi perturber localement le système π du matériau, et d'induire l'ouverture locale d'un gap entre les niveaux énergétiques^{10,18}.

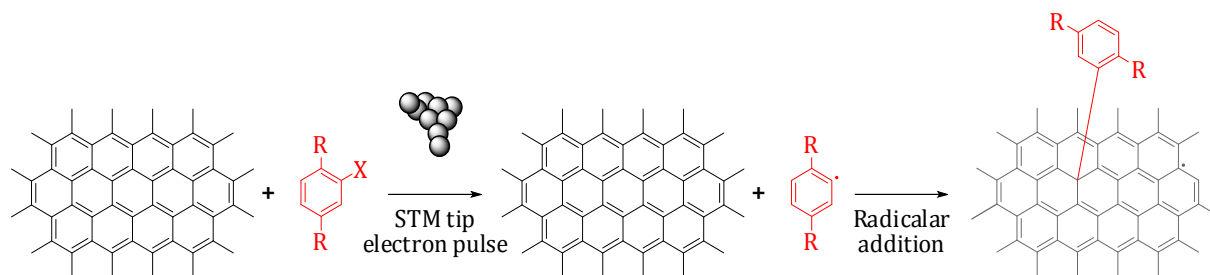
Une des difficultés principales était de trouver des groupements fonctionnels à la fois *réactifs* avec le graphène, un matériau relativement inerte, mais aussi assez *stables* pour permettre la sublimation sans dégradation de ces précurseurs en ultra-vide. En plus, les groupements devaient être réactifs avec le graphène par réaction activée sous pointe STM et la structure moléculaire devait être assez flexible pour permettre la formation d'une liaison covalente avec le graphène.

Dans ce contexte, nous avons proposé deux solutions différentes : 1) des précurseurs des espèces radicalaires bromés ; 2) des groupements réactifs avec le graphène par réaction de Diels-Alder.

A3. 4 Synthèse de précurseurs de espèces radicalaires

Les additions radicalaires sont les réactions les plus étudiées de la chimie du graphène. En particulier, les radicaux aryles, dérivés de la décomposition des sels de diazonium sont très souvent employés pour la fonctionnalisation de surfaces de graphène en solution¹⁹. Cependant l'utilisation de sels de diazonium thermiquement instable ne paraît pas adaptée à l'étape de sublimation nécessaire pour le transfert sous UHV de nos molécules.

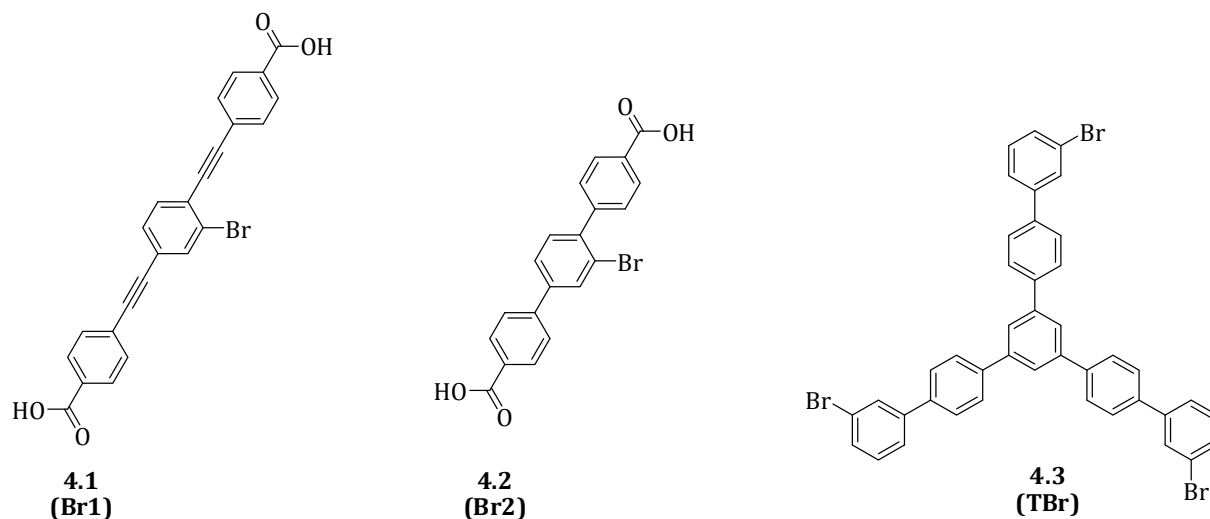
Notre objectif a donc été de synthétiser des molécules portant une fonction potentiellement réactive, qui pourrait amener à la formation d'un radical seulement après activation par la pointe d'un STM (**FigureA3. 5**). Le radical pourrait être généré par clivage homolytique d'une liaison particulière dans la molécule, par une "impulsion" STM. Après génération, le radical pourra réagir avec le graphène, conduisant à la formation d'une liaison covalente. Nos molécules cibles devaient aussi pouvoir s'organiser sur le graphène/SiC en couche auto-assemblée, de façon à définir une organisation spatiale des groupements réactifs sur la surface.



FigureA3. 5: Objectif général.

Dans ce contexte, nous avons conçu et synthétisé des molécules caractérisées par la présence d'un brome sur un des noyaux benzéniques. Après activation STM, la rupture homolytique de la liaison C-Br va générer l'espèce radicalaire centrée sur l'atome de carbone (C•).

Dans ce contexte, trois molécules sont été synthétisées : **Br1** (4.1), **Br2** (4.2), **TBr** (4.3) (Figure A3.6).

Figure A3.6: Structures des dérivés bromés **Br1** (4.1), **Br2** (4.2), **TBr** (4.3).

L'atome de brome est positionné en orto ou méta sur un/des noyaux benzénique. Ce choix est imposé par des raisons d'encombrement stérique. En effet, pour favoriser la réaction d'addition radicalaire, il semble nécessaire de permettre au carbone sp^2 du nouveau radical formé d'être perpendiculaire à la surface du graphène. Nous avons donc synthétisé des molécules pour lesquelles la rotation libre des phényles autour des liaisons σ peut, en principe, permettre au noyau aromatique une conformation perpendiculaire à la surface.

Les composées **4.1** et **4.2** ont été obtenus à partir des composées **4.4** et **4.8**, par déprotection de la fonction méthyle avec de l'hydroxyde de lithium (rendements de 30 et 60%).

L'ester **4.4** a été synthétisé par réaction de Sonogashira à partir du produit **4.6** (dérivé de 2-bromoaniline).

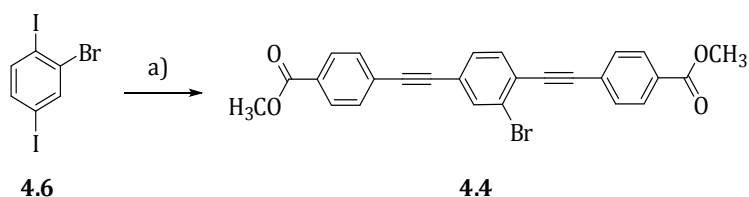


Schéma A3.6: Synthèse de **4.4**. Conditions : a) HCCPhCO₂Me, Pd(PPh₃)₂Cl₂ (6.7%), CuI (10%), DCM/Et₂NH, 18°C, 16h, 53%.

L'ester **4.8** a été synthétisé par réaction de Suzuki à partir du produit **4.6**.

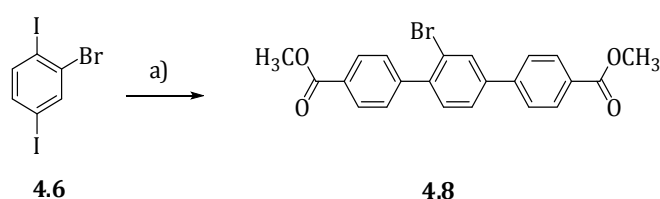


Schéma A3.7: Synthèse de **4.8**. Conditions: a) 4-méthoxycarbonyl-phenylboronic acide pinacol ester (2.05 eq.), Pd(PPh₃)₄ (6.8%), K₂CO₃ (6 eq.), dioxane/H₂O, 90°C, 18h, 55%.

Le produit **TBr** (**4.3**) a été obtenu par réaction de cyclotrimérisation aldolique à partir du précurseur **4.9**, lui-même synthétisé par réaction de Suzuki à partir du 3-bromo-1-iodobenzène.

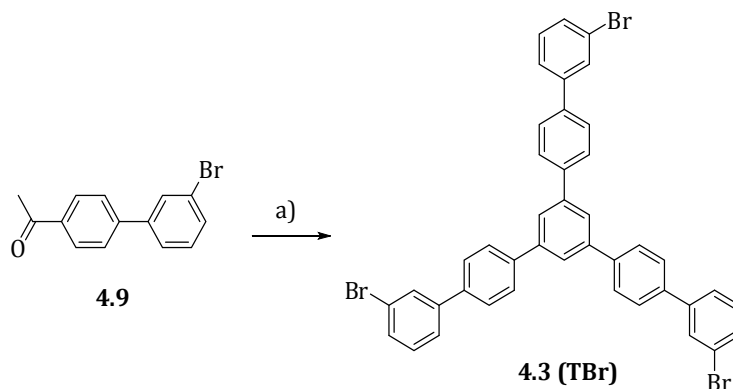


Schéma A3.8: Cyclotrimérisation aldolique permettant d'obtenir **4.3 (TBr)**. Conditions: a) SiCl₄ (10 eq.), éthanol /toluène anhydre, 18°C, 48h, 46%.

Au moment de la rédaction du manuscrit, les molécules n'avaient pas encore été étudiées sur surface. Les travaux sont en cours dans les groupes des Prof. Miao Yu (Harbin Institute of Technology (China)) et Laurent Simon (Institut des Science Moléculaires de Mulhouse (France)).

A3. 5 Synthèse de dérivées de l'anthracène pour des réactions de Diels-Alder

Les réactions de Diels-Alder présentent, par rapport à notre objectif d'étudier la réactivité avec la surface de graphène, un certain nombre d'avantages : a) une bonne stabilité thermique de beaucoup des réactifs ; b) pas de nécessité de catalyseurs; c) des réactions généralement réversibles (permettant une sorte de « correction des erreurs »). Parmi les nombreux réactifs de Diels-Alder existants, nous avons choisi d'employer pour nos études des anthracènes comme diènes et des maléimides comme dienophiles. Ce choix a été suggéré par la possibilité d'introduire différentes fonctionnalités sur le cœur réactif et également par la bonne stabilité thermique de ces composés.

La réactivité du graphène en réactions de Diels-Alder a été étudié pour la première fois par R. Haddon²⁰. Dans son travail Haddon a montré la possibilité de former des adduits de Diels-Alder entre le 9-methylanthracene et différents types de surfaces de graphène, comme l'HOPG ou le graphène exfolié en solution, à 130°C pendant 12 heures. La réaction est aussi réversible thermiquement à 160°C, ce qui permet d'enlever les "défauts sp³" introduits dans le matériau et de recouvrir le graphène non-fonctionnalisé. La formation d'une liaison covalente a été détectée par l'apparition d'une intense bande D (associée à l'introduction de carbones sp³ sur la surface). Cependant, il y a actuellement un débat très vif concernant la position de ces sites de fonctionnalisation par réaction de Diels-Alder soit sur tout le le plan du graphène ou seulement sur certaines zones, comme les bords de marche ou les défauts.

Dans ce contexte, il a apparu intéressant d'étudier la réactivité du plan du graphène en réactions de Diels-Alder directement par STM. En fait, les techniques STM permettent d'observer les molécules avec une résolution atomique, mais aussi de suivre le cours des réactions chimiques.

Le groupement anthracene est adapté à nos études pour différentes raisons : a) possibilité de s'absorber sur le graphène par interactions π - π ; b) bonne stabilité thermique.

Dans une première étape, il est nécessaire de favoriser la formation d'un réseau auto-assemblé de molécules sur la surface de graphène. Dans une deuxième étape, la possibilité d'induire la formation d'une liaison covalente peut être testée sous pointe STM (**Figure A3.7**).

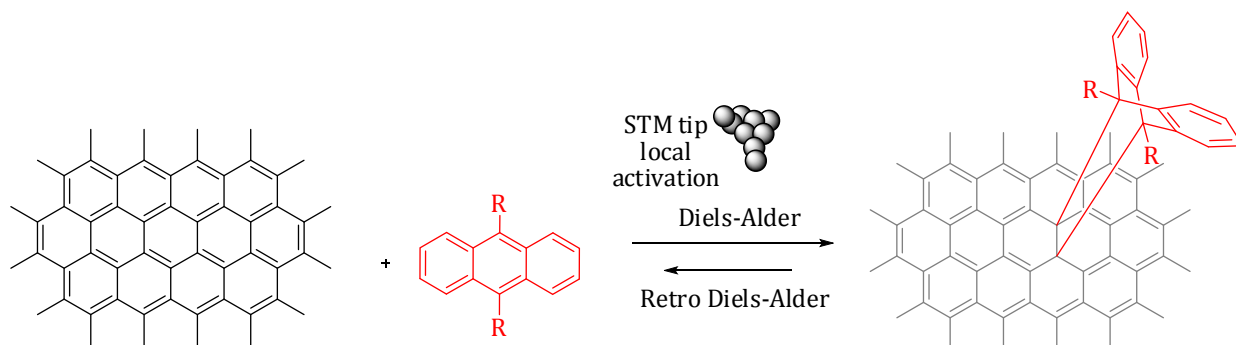


Figure A3.7: Objectif général.

Les molécules **A1 (5.1)** and **A2 (5.2)** qui ont été synthétisées, sont caractérisées par des éléments structuraux communs (Figure A3.8) :

- Une plateforme aromatique dérivée du phénylène-éthynylène ;
- Des chaînes alkyles, favorisant l'absorption des molécules sur le graphène/SiC et dirigeant l'organisation en un réseau auto-assemblé
- L'antracène **A2** est caractérisé par la présence de deux groupements carboxyliques additionnels, , pour favoriser l'organisation en chaînes par liaisons hydrogènes intermoléculaires.

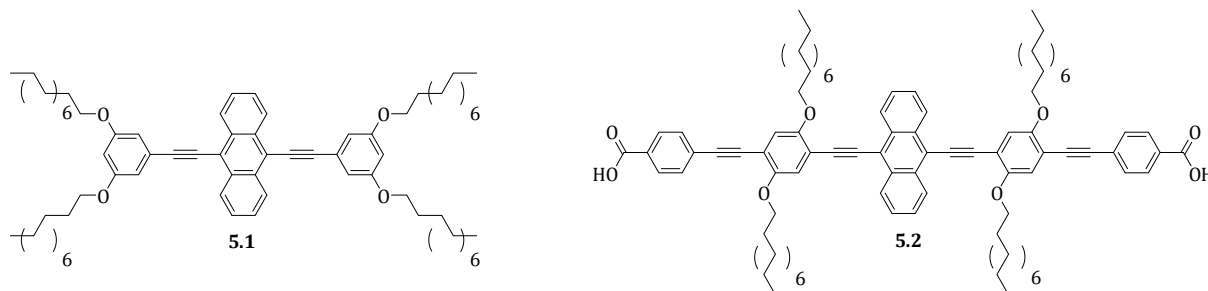


Figure A3.8: Structures chimiques des dérivés de l'antracène **A1 (5.1)** et **A2 (5.2)**.

La synthèse du composé **A1 (5.1)** été faite en suivant la procédure reportée sur le **Schéma A3.9**. Les étapes clés étaient a) la synthèse du groupement pour l'auto assemblage **5.7**, suivie par b) son introduction sur le cœur anthracène, soit par réaction de Sonogashira au 9,10-dibromoanthracene ou par addition aux carbonyles du 9,10-anthraquinone. La procédure d'addition sur l'anthraquinone s'est révélée la plus efficace et l'antracène **A1** a été obtenu avec un rendement global du 52%.

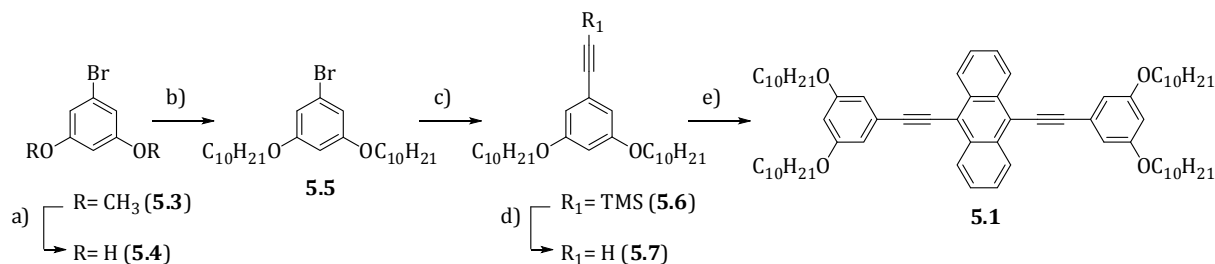


Schéma A3.9: Synthèse de l'antracène **5.1**. Conditions: a) HBr/AcOH, 110°C, 10h, 81%; b) 2.9 eq. C₁₀H₂₁Br, K₂CO₃, DMF, 65°C, 18h, 90%; c) TMSA, Pd(PPh₃)₄ (10%), CuI (1%), (iPr)₂NH, 100°C, 6h, 91%; d) CsF, MeOH/THF,

25°C, 4h, 96%; e) 1,9-anthraquinone, nBuLi, -78°C -> 20°C, 3h; SnCl₂, HCl, 25°C, 1h, 82% or 9,10-dibromoanthracene, Pd(PPh₃)₄ (4%), CuI (4%), (iPr)₂NH, Toluene/ACN ou THF, 100°C, 6h, 20-30%.

Pour la synthèse du composé **A2 (5.2)**, deux stratégies ont été comparées : a) le groupe pour l'auto-assemblage **5.10 ou 5.11** a été d'abord synthétisé et fait réagir dans un deuxième temps avec un cœur anthracène préalablement fonctionnalisé par des groupements alcyne ; b) ou bien, la fonctionnalité alcyne a été insérée sur le groupe possédant les longues chaînes alkyles et le composé **5.13** a été utilisé pour fonctionnaliser le 9,10-dibromoanthracene. Le produit **A2 (5.2)** a été obtenu par deprotection de fonctions méthyles des esters de **5.9**.

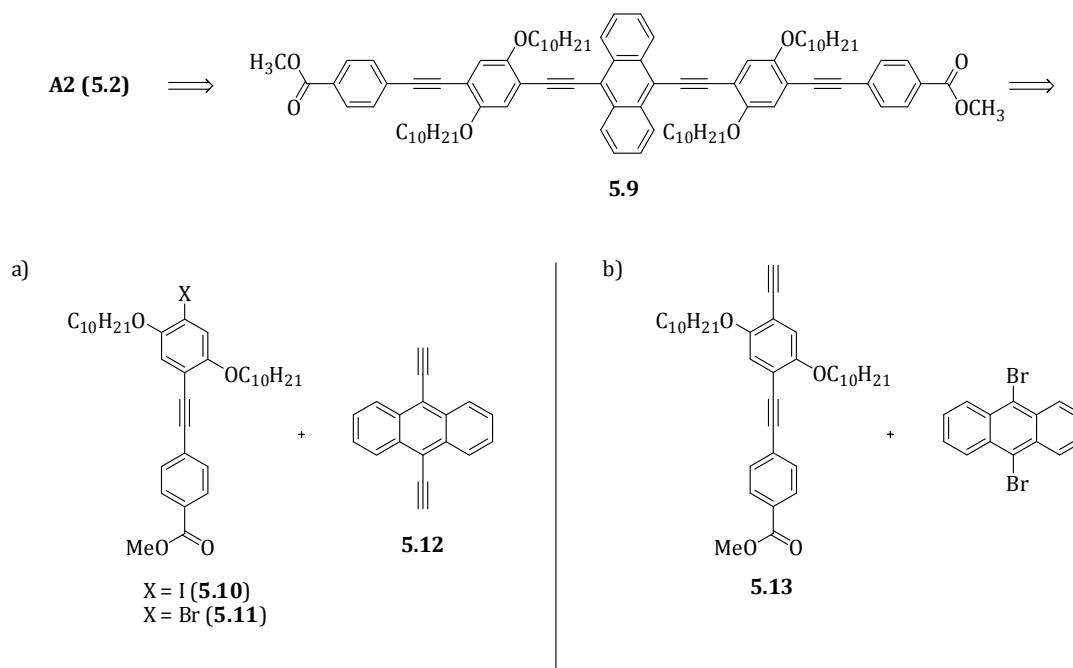


Schéma A3.10: Analyse retro-synthétique pour le dérivé de anthracene **A2 (5.2)**.

Ces molécules n'ont pas encore été étudiées sur surface au moment de l'écriture du manuscrit.

A3. 6 Synthèse et études de dérivées de maleimide pour réactions de Diels-Alder

Comme complément aux études de la réactivité du graphène comme diénophile, nous avons aussi envisagé d'étudier aussi la réactivité du graphène en tant que diène avec les diénophiles que sont les dérivés de maléimides.

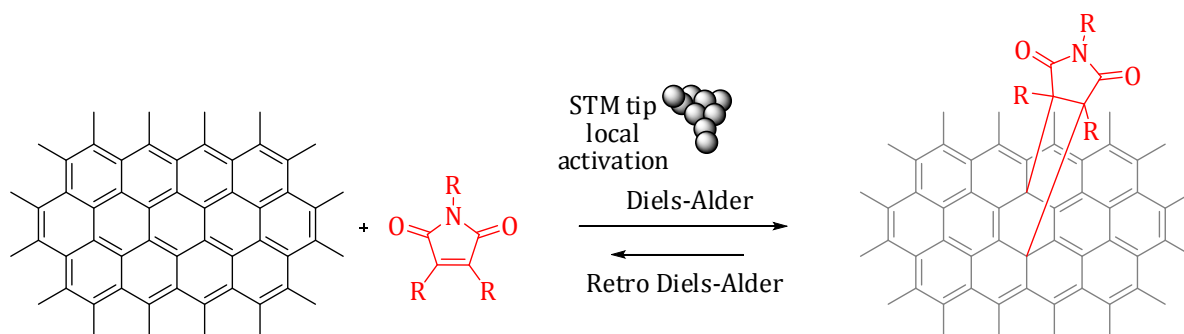


Figure A3.9: Objectif général.

La première étude de réactivité du graphène comme diène en Diels-Alder a été l'article de R. Haddon²⁰, qui a montré la réactivité de ce matériau avec l'anhydride maléique (à différentes températures selon le substrat : 70°C sur le graphène épitaxié sur carbure de silicium, 120°C sur HOPG et 130°C sur le graphène exfolié en solution). La réversibilité de la cycloaddition a aussi été démontrée et le même débat sur la faisabilité de la fonctionnalisation sur le plan ou juste sur les défauts/bords de marches est également en cours.

Trois molécules ont été synthétisées pour ces études. (**Figure A3.10**) : **M1**, **M2** et **M3**. **M1** et **M2** devraient s'organiser sur la surface par interactions de van der Waals entre les chaînes alkyles, **M3** par liaisons hydrogène entre les groupements carboxyliques.

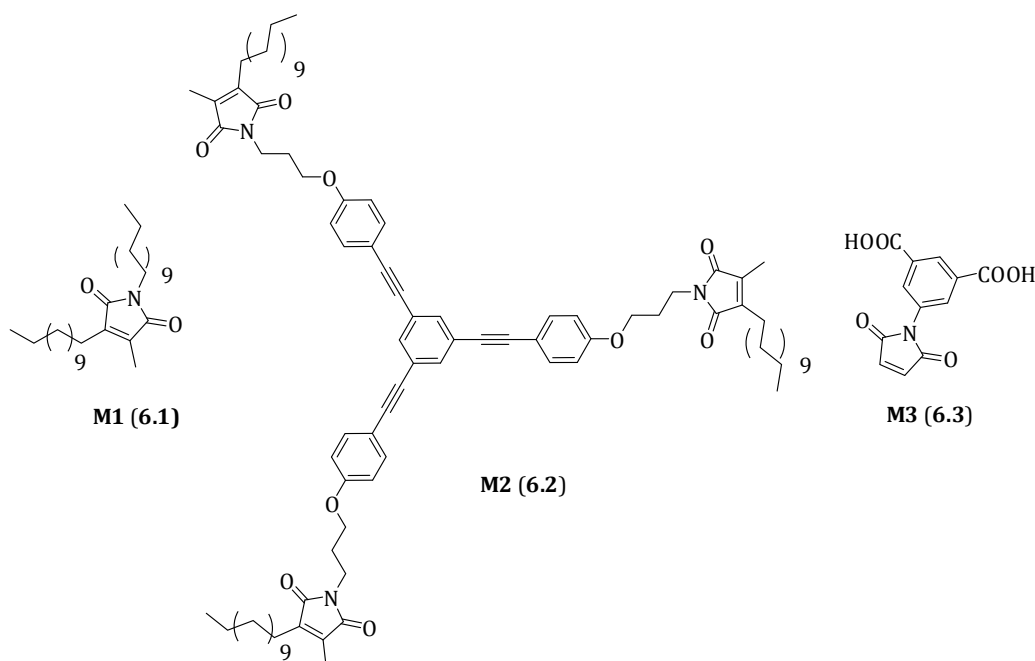


Figure A3.10: Structure chimique des dérivés de maléimide **M1**, **M2** et **M3**.

La synthèse des maléimides a été effectuée à partir des anhydrides correspondants fonctionnalisés.

L'anhydride maléique fonctionnalisé par une chaîne alkyle $-C_{12}H_{25}$ peut être synthétisé comme décrit sur le **Schéma A3.11**, en quatre étapes qui peuvent être faites de façon « one-pot », avec un rendement global de 27%.

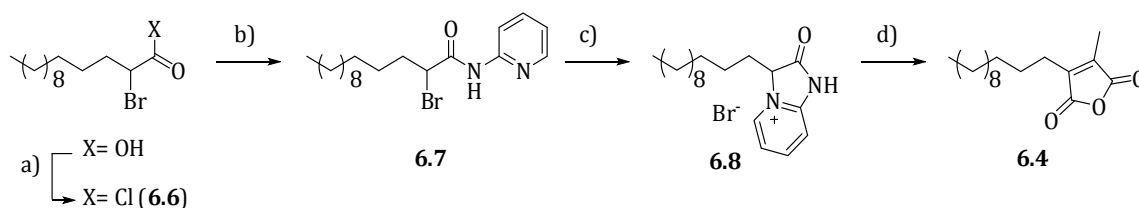


Schéma A3.11: Synthèse de l'anhydride maléique fonctionnalisé par une chaîne alkyle $-C_{12}H_{25}$ **6.4**. Conditions: a) chlorure d'oxalyle (1.6 eq.), DMF cat., toluène, 20°C, 2h; b) 2-aminopyridine (1 eq.), triéthylamine (1 eq.), diéthyl éther, 20°C, 3h; c) *tert*-butanol, 82°C, 18h; d) anhydride maléique (1 eq.), acétate de sodium (1 eq.), acide acétique, 120°C, 5h. Rendement sur les quatre étapes: 27%.

L'anhydride maléique fonctionnalisé **6.4** a ensuite été utilisé pour générer la maléimide **M1**, par réaction avec la 1-dodécylamine.

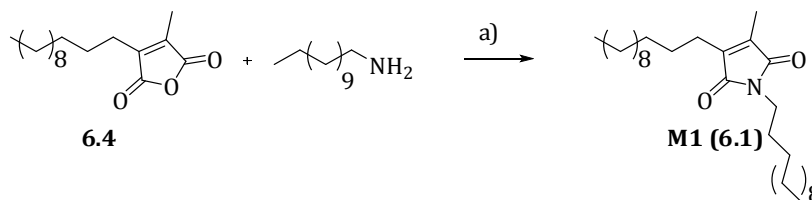


Schéma A3.12: Synthèse du dérivé de maléimide **M1** : a) 1-dodécylamine, $ZnBr_2$, HMDS, toluène anhydre, 80°C, 19h, 89%.

Dans la même logique, nous avons pu synthétiser le dérivé **M2** (**6.2**), en préparant tout d'abord le précurseur tri-amine **6.9**, dont ensuite on a fait réagir la fonction amine avec l'anhydride maléique **6.4**, pour générer la tri-maleimide **M2**.

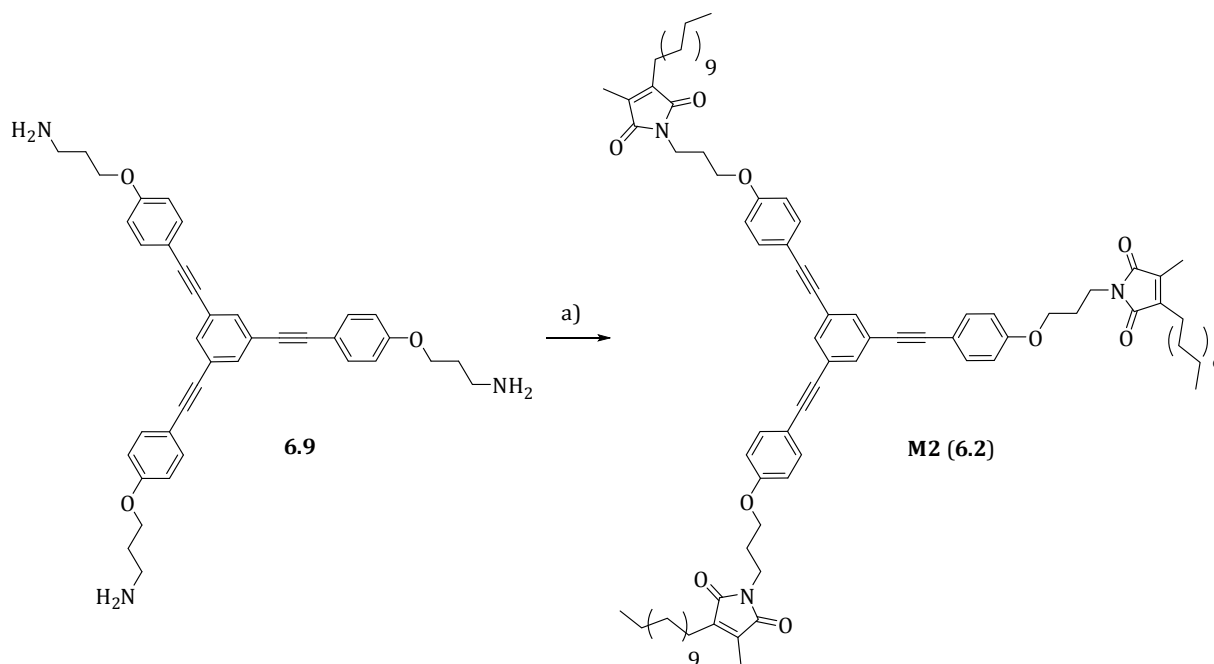


Schéma A3.13: Synthèse du dérivé de tri-maleimide **M2**: a) i: **6.4**, toluène anhydre, 111°C, 16h; ii: $ZnBr_2$, HMDS, 80°C, 5h, après 22°C, 11h, 20%.

M3 (6.3) a été synthétisé à partir d'anhydride maléique et l'acide 5-amino isophtalique. La synthèse en deux étapes a été faite one-pot.

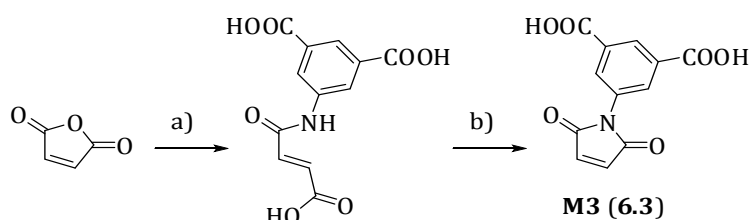


Schéma A3.14: Synthèse de la maleimide **M3**: a) i: acide 5-amino isophtalique, THF, 22°C, 3h; ii) Ac₂O, NaOAc, 16h, 80°C, 3h, 50%.

Comme complément aux tests de réactivité par STM, il a été envisagé de conduire des tests de réactivité l'interface solide/liquide par des moyens d'activation plus « classiques ». Pour ces expériences, nous avons choisi d'employer un dérivé de maleimide très réactif (**MF**, **6.15**).

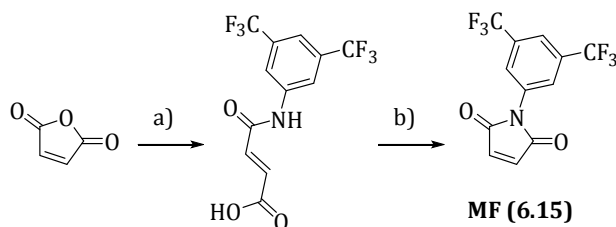


Schéma A3.15: Synthèse de la maleimide **MF (6.15)**: a) 3,5-bis(trifluorométhyl)aniline, DCM, 50°C, 19h; b) Ac₂O, 110°C, 1.5h, 77%.

La présence des groupements -CF₃ diminue la densité électronique sur la double liaison réactive de la maleimide et en augmente le caractère diénoophile.

Les tests de réactivité ont été effectués sur deux types de graphène (**Figure A3.11**), 1) du graphène exfolié mécaniquement et déposé sur oxyde de silicium et 2) du graphène épitaxié sur carbure de silicium^{iv}. La caractérisation a été faite par spectroscopies Raman, XPS et par analyse d'images STM.

La fonctionnalisation a été réalisée en trempant les échantillons de graphène dans des solutions 0.06 M de MF dans le toluène, suivi par des rinçages dans différents solvants. Des expériences de de-fonctionnalisation à haute température ont aussi été faites, de façon à déterminer la stabilité thermique des adduits obtenus.

^{iv} La préparation des échantillons de graphène exfolié et les expériences de fonctionnalisation et caractérisation Raman ont été faites par M. Rubio-Roy et E. Dujardin dans le groupe GNS. La préparation des échantillons de graphène/SiC et les études XPS et STM ont été faites par le groupe de L. Simon à l'Institut IS2M de Mulhouse.

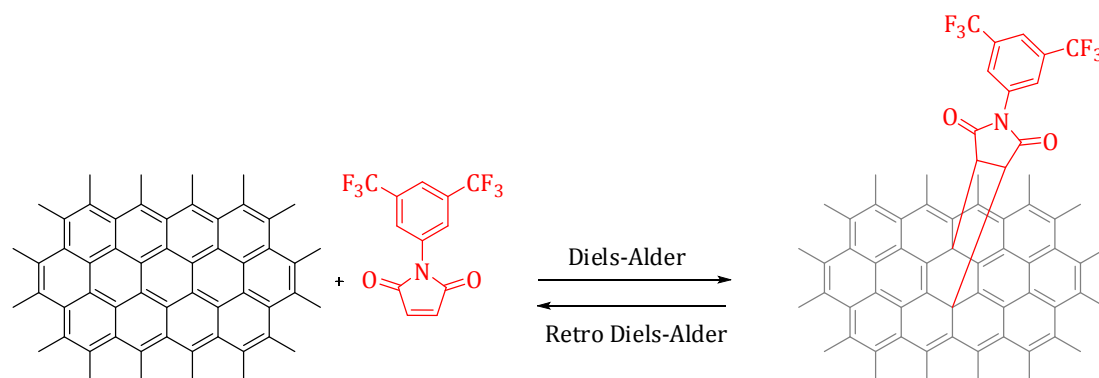


Figure A3.11: Objectif général: réaction de Diels-Alder entre la maleimide **MF** et le graphène.

Nous avons observé la formation d'adduits entre les deux typologies de graphène et la molécule **MF**. Les adduits présentent une forte stabilité thermique ($\sim 100^\circ\text{C}$). De plus, un changement de shift de la bande 2D du graphène a pu être observé ($\sim +7\text{ cm}^{-1}$) dans les spectres Raman. Ces observations peuvent indiquer une interaction forte entre les molécules et le graphène, ce qui est confirmée aussi par l'apparition d'ondes stationnaires autour des molécules dans les images STM. Cependant, il parait à ce stade difficile d'obtenir une preuve directe de la liaison covalente et la formation d'un complexe de transfert de charge très stable ne peut pas être exclue.

A3.7 References

- ¹ Novoselov, K. S., Geim, A. K., Morozov, S. V., Jiang, D., Zhang, Y., Dubonos, S. V., Grigorieva, I. V., Firsov, A. A., *Science*, **2004**, *306*, 666-669
- ² Bae, S., Kim, H., Lee, Y., Xu, X., Park, J.-S., Zheng, Y., Balakrishnan, J., Lei, T., Kim, H. R., Song, Y. II, Kim, Y.-J., Kim, K. S., Özyilmaz, B., Ahn, J.-H., Hong, B. H., Iijima, S., *Nature Nanotec.*, **2010**, *5*, 574-578.
- ³ Lee, J.-H., Lee, E. K., Joo, W.-J., Jang, Y., Kim, B.-S., Lim, J. Y., Choi, S.-H., Ahn, S. J., Ahn, J. R., Park, M.-H., Yang, C.-W., Choi, B. L., Hwang, S.-W., Whang, D., *Science*, **2014**, *344*, 6181, 286-289.
- ⁴ Paton, K. R., Varrla, E., Backes, C., Smith, R. J., Khan, U., O'Neill, A., Boland, C., Lotya, M., Istrate, O. M., King, P., Higgins, T., Barwich, S., May, P., Puczkarski, P., Ahmed, I., Moebius, M., Pettersson, H., Long, E., Coelho, J., O'Brien, S. E., McGuire, E. K., Sanchez, B. M., Duesberg, G. S., McEvoy, N., Pennycook, T. J., Downing, C., Crossley, A., Nicolosi, V., Coleman, J. N., *Nat. Mat.*, **2014**, DOI: 10.1038/nmat3944.
- ⁵ Novoselov, K. S., Falko, V. I., Colombo, L., Gellert, P. R., Schwab, M. G., Kim, K., *Nature*, **2012**, *490*, 192-200.
- ⁶ Georgakilas, V., Otyepka, M., Bourlinos, A. B., Chandra, V., Kim, N., Kemp, C. K., Hobza, P., Zboril, R., Kim, K. S., *Chem. Rev.*, **2012**, *112*, 6156-6214.
- ⁷ Sun, Z, Pint, C. L., Marcano, D. C., Zhang, C., Yao, J., Ruan, G., Yan, Z., Zhu, Y., Hauge, R. H., Tour, J. M., *Nature Comm.*, **2011**, *2*, 559, 1-5.
- ⁸ Sessi, P., Guest, J. R., Bode, M., Guisinger, N. P., *Nano Lett.*, **2009**, *9*, 12, 4343-4347.
- ⁹ Wang, Q. H., Hersam, M. C., *Nano Lett.*, **2011**, *11*, 589-593.
- ¹⁰ Balog, R., Jørgensen, B., Nilsson, L., Andersen, M., Rienks, E., Bianchi, M., Fanetti, M., Lægsgaard, E., Baraldi, A., Lizzit, S., Slijivancanin, Z., Besenbacher, F., Hammer, B., Pedersen, T. G., Hofmann, P., Hornekær, L., *Nature Mat.*, **2010**, *9*, 315-319.
- ¹¹ Bian, S., Scott, A. M., Cao, Y., Liang, Y., Osuna, S., Houk, K. N., Braunschweig, A. B., *J. Am. Chem. Soc.*, **2013**, *135*, 9240-9243.
- ¹² Segura, J. L., Martín, N., *Angew. Chem. Int. Ed.*, **2001**, *40*, 1372-1409.
- ¹³ Canevet, D., Sallé, M., Zhang, G., Zhang, D., Zhu, D., *Chem. Comm.*, **2009**, 2245-2269.
- ¹⁴ Garnier, J., Kennedy, A. R., Berlouis, L. E. A., Turner, A. T., Murphy, J. A., *Beilstein. J. Org. Chem.*, **2010**, *6*, 73.
- ¹⁵ Inokuchi, H., Saito, G., Wu, P., Seki, K., Tang, T. B., Mori, T., Imaeda, K., Enoki, T., Higuchi, Y., Inaka, K., Yasuoka, N., *Chem. Lett.* **1986**, *15* 1263-1266.
- ¹⁶ Puigmartí-Luis, J., Minoia, A., Lei, S., Geskin, V., Li, B., Lazzaroni, R., De Feyter, S., Amabilino, D. B., *Chem. Sci.*, **2011**, *2*, 1945-1951.
- ¹⁷ Baxter, R. J., Knox, G. R., Moir, J. H., Pauson, P. L., Spicer, M. D., *Organometallics*, **1999**, *18*, 2, 206-214.
- ¹⁸ Hossain, Z., Walsh, M. A., Hersam, M. C., *J. Am. Chem. Soc.*, **2010**, *132*, 43, 15399-15403.
- ¹⁹ a) Paulus, G. L. C., Wang, Q. H., Strano, M. S., *Acc. Chem. Res.*, **2013**, *46*, 1, 160-170; b) Koehler, F. M., Stark, W. J., *Acc. Chem. Res.*, **2013**, *46*, 10, 2297-2306.
- ²⁰ Sarkar, S, Bekyarova, E., Niyogi, S., Haddon, R. C., *J. Am. Chem. Soc.*, **2011**, *133*, 3324-3327.

Design, synthesis and study of molecules for graphene functionalization.

Getting a deeper insight into the controlled chemical functionalization of graphene represents a pre-requisite essential for fully exploiting all the promising properties of this material. The central objective of this thesis is to resort to self-assembly in order to achieve a precise spatial organization of "active" functional groups on the graphene surface. In particular, these functionalities are meant to interact with graphene either by strong non-covalent interactions, inducing a local doping, or by a Scanning Tunnelling Microscope (STM)-tip activated chemical reaction, driving to the formation of a covalent bond. In a first part, we synthesized a tetrathiafulvalene and a hexaphenanthrocoronene derivative, chosen because of their potential electron donor capabilities towards epitaxial graphene grown on silicon carbide. In a second part, we synthesized a series of poly-phenyl or poly-phenyl-ethynyl derivatives, designed to present a radicalar (i.e. brominated precursors) or Diels-Alder (i.e. maleimide or anthracene functional groups) reactivity with graphene, by STM activation. STM and Raman studies have allowed assessing the self-assembling behaviour and reactivity of some of the synthesized derivatives.

Keywords: Graphene, Diels-Alder, STM, functionalization, maleimide compounds, anthracene derivatives.

Conception, synthèse et étude de molécules pour la fonctionnalisation du graphène.

La compréhension du contrôle de la fonctionnalisation chimique du graphène est un prérequis essentiel pour pouvoir exploiter toutes les propriétés de ce matériau. L'objectif central de ces travaux de thèse est de recourir à l'auto-assemblage pour obtenir une organisation spatiale précise de groupements fonctionnels "actifs" avec une surface de graphène. En particulier, ces fonctionnalités chimiques doivent interagir avec le graphène soit par interaction non-covalente forte, amenant à un dopage local, ou par réaction activée sous pointe STM (Microscope à effet tunnel), amenant à la formation d'une liaison covalente. Dans une première partie, nous avons synthétisé un dérivé de tetrathiafulvalene et un hexaphenanthrocoronène, choisis pour leurs caractères donneurs d'électrons pour des surfaces de graphène épitaxié sur carbure de silicium. Dans la deuxième partie, nous présentons la synthèse de différents dérivés de polyphényles ou poly-phényléthynyles, conçus pour une réactivité avec le graphène de type radicalaire (dans le cas de précurseurs bromés) ou par réaction de Diels-Alder (par des fonctions maléimide ou anthracène). Des études STM et Raman ont permis de démontrer les propriétés d'auto-assemblage et la réactivité de certains de ces dérivés.

Mots clés: Graphène, Diels-Alder, STM, fonctionnalisation, dérivés de maléimide et anthracène.